

PETROGENESIS OF CARBONATITE AND ASSOCIATED ALKALINE ROCKS, PURULIA, W.B., INDIA

A THESIS

*Submitted in partial fulfilment of the
requirements for the award of the degree*

of

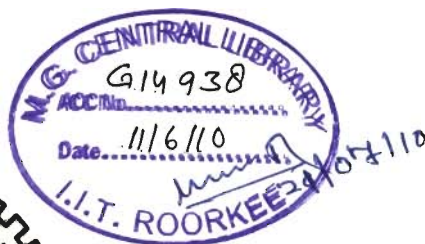
DOCTOR OF PHILOSOPHY

in

EARTH SCIENCES

by

ANIKET CHAKRABARTY



DEPARTMENT OF EARTH SCIENCES
INDIAN INSTITUTE OF TECHNOLOGY ROORKEE
ROORKEE - 247 667 (INDIA)

MAY. 2009

**©INDIAN INSTITUTE OF TECHNOLOGY ROORKEE, ROORKEE, 2009
ALL RIGHTS RESERVED**



INDIAN INSTITUTE OF TECHNOLOGY ROORKEE ROORKEE

CANDIDATE'S DECLARATION

I hereby certify that the work which is being presented in the thesis entitled **PETROGENESIS OF CARBONATITE AND ASSOCIATED ALKALINE ROCKS, PURULIA, W.B., INDIA** in partial fulfillment of the requirements for the award of the degree of Doctor of Philosophy and submitted in the Department of Earth Sciences of the Indian Institute of Technology Roorkee, Roorkee is an authentic record of my own work carried out during a period from July 2003 to May 2009 under the supervision of Dr. A. K. Sen, Associate Professor, Department of Earth Sciences, Indian Institute of Technology Roorkee, India and Prof. Christoph A. Heinrich, Institute of Isotope Geology and Mineral Resources, ETH Zurich, Switzerland.

The matter in this thesis has not been submitted by me for the award of any other degree of this or any other Institute.


(ANIKET CHAKRABARTY)


This is to certify that the above statement made by the candidate is correct to the best of my knowledge.

(Christoph A. Heinrich)
Supervisor




Date:

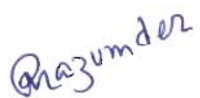
4.5.09


(A. K. Sen)
Supervisor

The Ph.D. Viva Voce examination of **Mr. Aniket Chakrabarty**, Research Scholar, has been held on 06.10.2009.



Signature of Supervisors



Signature of External Examiner

ABSTRACT

The carbonatite and other alkaline rocks are exposed at Sushina, Chirugora-Purdaha, Kutni-Dandodih-Gamardih, Mednitanr and Beldih from east to west along the Northern Shear Zone (NSZ). One of the study areas, Beldih (86°11'E to 86°23'E, 23°00'N to 23°07'N) is situated 38 Km south of the Purulia town, where the carbonatite-alkali-pyroxenite association occur within the host rock chlorite-phyllite and chlorite-schist. The other study area Sushina (22°57'N, 86°37'E) lies about 40 Km west of Beldih, where the varieties of nepheline-syenite is exposed along a lenticular-shaped NW-SE running hill.

Carbonatite around Beldih is essentially composed of calcite and minor apatite with amphibole, biotite and magnetite as common accessories. It is characterized by the presence of two varieties of amphibole: richterite and magnesiokatophorite, which are low-Al, sodic-calcic in composition. The amphiboles are characteristic of middle to late stage development of carbonatite. The co-existence of these two types of amphibole indicates rapid ascent of the carbonatite magma along NSZ. The *carbonatites* are found to be calico-carbonatite and enriched in Sr (8500-11200 ppm), Ba (797-1784 ppm) and Σ REE (1567-2114). The Nb and U concentrations are variable and primitive mantle normalized plot reveals that the Purulia carbonatite is relatively poorer in Rb (0.30 times), Zr (0.40 times) and Hf (0.80 times) while enriched in Sr (500 times), La (600 times), Ce (500 times) and Sm (150 times) and Nb (13 times for two samples and about 100 times for other two). However, Nb shows prominent negative anomaly when it is compared to average carbonatite and the pattern is characteristics of Precambrian carbonatites. Based on low HFSE content a carbothermal fluid derivation could be postulated. The Grenvillian metamorphic event resulted post-magmatic changes in the carbonatite as reflected from their bulk rock (Rb-Sr) isotopic studies. This shows that the measured $^{87}\text{Sr}/^{86}\text{Sr}$ ratio of the bulk rock and apatite (0.70340) is well within

the range of mantle values. The present study rather support genesis of Purulia carbonatite from a parent primary carbonatitic magma than genesis from a carbothermal fluid. Moreover the $^{87}\text{Sr}/^{86}\text{Sr}$ ratio suggests that the existence of long-lived heterogeneity in the mantle during the time of formation of these rocks which is well in accord with the world-wide mantle heterogeneity during 2800 to 1000 Ma period. Pb-Pb model age suggest that the Purulia carbonatite is at least ≥ 1.37 Ga of age.

The *alkali-pyroxenite*, associated with the carbonatite had undergone extensive alkali-metasomatism during carbonatite intrusion. Such alkali-metasomatism is exemplified by two major changes: *alteration of the primary mineral assemblages* and *formation of a vein-filling assemblage*. The *alteration process* of the primary magmatic assemblage resulted transformation of pyroxene to amphibole (taramite/katophorite) and biotite respectively. The *vein-filling assemblage* is dominated by the calcite and apatite. Along with the apatite and calcite, albite is also found within the vein filling assemblage indicating dominance of sodic metasomatism. On the other had introduction of K resulted transformation of pyroxene and amphibole to biotite. The alteration process was accompanied by the introduction of incompatible element, including REE, in the system. The role of fluoride complexing was dominant as evident from the higher concentration of Y, REE in the apatite of the *alkali-pyroxenite*. The overall pressure is estimated to be around 2-3 kbar or less with temperature ranging around 400-450°C. The $f\text{O}_2$ -condition was low and suppressed by presence of CO_2 and alkalis.

Two varieties of *under-saturated syenite* (banded and massive syenite) are found in the Sushina area. Based on the intensity of banding, the banded syenite can further be subdivided into two sub categories: poorly and strongly banded syenite gneiss. Both the varieties of *banded syenite* are essentially composed of albite, orthoclase, nepheline and aegirine. The *strongly banded syenite gneiss* characterized by the presence eudialyte and complex sodium-zirconium silicates. The

massive syenite is characterized by the complete absence of mafic constituents except few late stage Mn-rich biotites. Pure end member compositions of the feldspars along with the nepheline compositions converging towards the Morozewicz-Buerger field of plutonic/metamorphic-metasomatic assemblage suggest that the banded variety of syenite represent a recrystallized mineral assemblage and can be best termed as *nepheline gneisses*. Textural and mineralogical study reveals that these rocks of miaskitic character were originally emplaced under plutonic condition and pervasive subsolidus or deuteritic alteration related to autometasomatism changed the original miaskitic composition towards the agpaitic one. The metamorphic effect is also evident by the preferential partitioning of Al in the octahedral coordination in pyroxene of the banded variety of syenite. The metasomatic effect and subsequent change in the alkalinity (pH) is best exemplified by the apatite group of minerals. The maximum alkalinity stage is represented by the Sr-LREE enriched apatite of the banded syenite. Maximum alkalinity stage resulted formation of eudialyte and complex sodium-zirconium (Na-Zr) bearing silicate, partial replacement of nepheline by sodalite, analcime. However the effect of deuteritic alteration in the massive syenite is somewhat less which can be attributed by the presence of Sr-Na-LREE apatite which indicates a lower/decreasing alkalinity stage of the deuteritic fluid. The dissolution of zircon at the maximum alkalinity stage is evident by the absence of zircon in the strongly banded syenite gneiss. However, Pb mobility is observed in one of the studied sample of banded syenite reflecting dissolution and re-precipitation of the zircon which yields an age of 877 ± 52 Ma. Zircons from the poorly banded syenite gneiss give an age range of 1.3-0.96 Ga indicating a complex poly-phase metamorphic activity of Grenvillian metamorphic event under amphibolite to greenschist facies condition. The 1.51 Ga zircon age of the massive syenite is somewhat similar to the intrusive age of the near by Bengal anorthosite, indicating at least ≥ 1.51 Ga age of the Sushina nepheline syenites.

There is no conclusive evidence to support consanguineous relation between carbonatite-pyroxenite of Beldih and nepheline syenite of Sushina. The present study proposes mantle derivation of these rocks under similar geodynamic conditions controlled by NSZ.

ACKNOWLEDGEMENT

First of all, without His will; this would not have been possible. I wish to thank the **ALMIGHTY GOD** for giving me the *strength, health and determination* to carry out this research work through His divine grace.

Today, undergoing retrospection, I recall many people who had contributed in their own ways throughout the entire period in the completion of this work. Penning down all the names is definitely not possible, but it is indeed my proud privilege to thank all those who have directly or indirectly helped and influenced in the completion of my thesis work.

First and foremost, I owe my profound gratitude and sincere thank to my supervisors **Dr. A.K. Sen (Sen Sir)** and **Prof. Christoph A. Heinrich (Stoeff)**. I am extremely thankful to **Sen Sir** for his perennial inspiring guidance and encouragement during the entire period of the work. I consider myself fortunate to have had the opportunity to work under his supervision. Throughout the work, his stimulating discussions, cogent arguments and ever-lasting encouragement were of immense help to me. His clarity of thoughts, creativity and his vast knowledge of different scientific fields has been a great source of inspirations. His total devotion for teaching and research has been influential throughout this work and will continue to exert great influence in my future work also. The mental support provided by him is a lesson for me which helped me a lot during my struggling periods. His innate goodness, humanistic enthusiasm has unerringly steered the work on smooth and steady course. His constant support by all means is an asset to me and to him I remain professionally as well as emotionally indebted.

I am sort of word in expressing my humble and sincere thank to **Stoeff**, who helped me in every possible way during my stay at Zurich. His able guidance and methodical approach towards the scientific problems always influenced me to carry out my work with more enthusiasm and sincerity. I recall back the days of Zurich and our discussion on the snow laden way to the morning class in the chilling winter and his words of inspiration “*a good mentor/teacher should not look for what you have not done, rather what can be done up to the optimum keeping all the limitations in mind*”. I humbly acknowledge a lifetime’s gratitude to him.

I am extremely thankful to **Prof. Albrecht von Quadt (Albrecht)** for his immense help during my stay at ETH Zurich. His helping attitude and tireless effort in helping me out of the mystery and miseries of analytical work and endless argument helped in understanding the basics of *zirconology*, the most difficult part of my thesis.

I am thankful to **Prof. R. P. Gupta, Head of the Department of Earth Sciences, IIT Roorkee**, for providing me with all the facilities during my entire span of work.

I express my sincere gratitude to **Prof. D. K. Mukhopadhyay (DKM Sir)** and **Prof. V. N. Singh (V. N. Singh Sir)**, for their constant encouragement and cooperation during the entire course of my thesis work. Special mention must be made for those *witty* comments by *DKM Sir*, particularly during the heated arguments between me and *Sen Sir* and helped us to back into normalcy with LOL (Laughing Out Loudly). Constant inspiration by *DKM Sir* motivated me to overcome all the barriers I have faced during the entire period of this work.

I would like to express my profound gratitude to **Dr. Tamal Kanti Ghosh (Tamal Da)** for his untiring help during the EPMA analysis and guiding me for betterment everyway of life. My special thanks goes to **Mr. Basab Chattopadhyay (GSI, Kolkata)** for his help in the analyzing some typical minerals in a very short notice.

I am extremely thankful to my lab mates of ETH Zurich: **Svetlo, Caroline, Caludia and Ramon**. My special thanks to **Britt**, for her whole hearted help and support during and after my stay at Zurich.

I am extremely thankful to my batch mates and friends **Bati, Biswajayee, Debapratim, Antara, Nishant, Ashis (Mishra ji), Satya, Gargi, Puru, Aparna** for providing me the mental support during this work.

My special thank goes to my former teachers and/or would be colleague **Supratim Da, Nilanjan Da, Samiran Da, Sandeep Da, Biplab Da, and Subhajit Da**. I also owe my sincere gratitude to **Dr. S. S. Ray (SSR Sir), Head of the Department, Durgapur Govt. College**, for his constant help and encouragement particularly during the end of my thesis work.

I am very much thankful to my seniors **Partho Da, Rajeev Sir, Dulu Da** and **Ashish Da** for their help and support during the entire period of my work.

My sincere gratitude goes to **Ravikant Sir** and **Pruseth Sir** for their constant support and encouragement, particularly during the end phase of my thesis work.

I am short of appropriate words to express my feelings for my dearest junior and younger brother **Dhruba** for being such a wonderful and caring, who stood beside and supported me at the time of rough weather. I proudly remember those eventful days of highs and lows that we faced and shared together during last ten years or so. He stood behind me during the toughest period of my life and gave me strength to come out of the phase and also motivated me towards my work. *His friendship is treasure to me.* A special mentioned must be made for **Moti** whose caring attitude made the things easy and smooth during the end of my thesis work.

I am extremely thankful to my juniors **Rupam, Palash, Anindya, Bhombol, Suman (one and only the great BEGUN), Atanu and Rajib** for their auspicious, prompt and punctual assistance whenever I needed the most. Special mention must be made for **Palash and Rupam** for their endless help in the last few days in making the earlier version of this thesis. My special thanks go to **BEGUN** for his constant help and support, particularly during the crucial periods of my thesis.

I am extremely thankful to **Ashok Bhaiya, Nair Ji and Rakesh Ji** for their heartfelt love and affection they bestowed on me and helped in every way during my entire stay at Roorkee.

Special thanks to **Kakima (Mrs. Sen) and Bucho (Motu) (Master Sen)** who had spared their invaluable time to Sen Sir from their family hours especially in the second stage of my thesis work. Motherly affection of **Kakima** never let me feel that I am far away from my home and parents.

The faith, aspirations and confidence that my family members and friends have shown in me have sustained me to achieve this coveted academic endeavor at this Institute.

At the end, I am short of words to express my feelings for my parents (*Ma-Baba*); to them I will always remain grateful throughout my life. They stood beside me throughout all the hardship that I have faced. They taught me to dream and reach out dreams.

CONTENTS

	PAGE NO.
ABSTRACT	i
ACKNOWLEDGEMENT	v
CONTENTS	ix
LIST OF FIGURES	xiii
LIST OF TABLES	xxiii
CHAPTER 1	
INTRODUCTION	1
1.1 INDIAN CARBONATITES: AN OVERVIEW	3
1.2 PROBLEM DEFINED	4
1.3 OBJECTIVES	8
1.4 METHODOLOGY	10
CHAPTER 2	
PREVIOUS WORK AND REGIONAL GEOLOGY	17
2.1 GEOLOGY OF THE SINGHBHUM CRATON	18
2.1.1 ARCHEAN NUCLEUS	23
2.1.2 NORTH SINGHBHUM FOLDED BELT (NSFB)	27
2.1.3 CHOTANAGPUR GRANITIC GNEISSIC COMPLEX (CGGC)	31
2.2 GEOLOGY OF THE STUDY AREA	31
CHAPTER 3	
PETROGRAPHY AND MINERALOGY	49
3.1 ANALYTICAL TECHNIQUE	49
3.2 CARBONATITE	50
3.3 ALKALI-PYROXENITE	58
3.3.1 PRIMARY MINERAL ASSEMBLAGES	63
3.3.2 SECONDARY MINERAL ASSEMBLAGES	64

3.4 APATITE MAGNETITE ROCK	77
3.5 NEPHELINE SYENITE	78
3.6 SUMMARY	126
CHAPTER 4	
GEOCHEMISTRY	159
4.1 ANALYTICAL TECHNIQUE	159
4.2 CARBONATITE	160
4.3 ALKALI-PYROXENITE	171
4.4 NEPHELINE SYENITE	178
4.5 SUMMARY OF BULK ROCK CHEMISTRY	187
4.6 MINERAL CHEMISTRY	191
4.6.1 ANALYTICAL PROCEDURE	192
4.6.2 APATITE AND CALCITE FROM THE CARBONATITE	193
4.6.3 APATITE FROM THE ALAKLI-PYROXENITE	203
4.6.4 APATITE FROM THE NEPHELINE SYENITE	204
4.6.5 SUMMARY OF THE APATITE MINERAL CHEMISTRY	210
CHAPTER 5	
ISOTOPE GEOLOGY AND GEOCHRONOLOGY	233
5.1 ANALYTICAL TECHNIQUE	233
5.2 CARBONATITE	235
5.3 ALKALI-PYROXENITE	241
5.4 NEPHELINE SYENITE	241
5.4.1 ZIRCON DATING (U-Pb) OF NEPHELINE SYENITES	242
5.5 SUMMARY	251
CHAPTER 6	
DISCUSSIONS	263
6.1 CARBONATITE AND PYROXENITE ASSOCIATION	264
6.1.1 FIELD AND PETROGRAPHIC SIGNATURES	264
6.1.2 AMPHIBOLE AS A PETROGENETIC INDICATOR IN	

CARBONATITE AND ASSOCIATED ROCKS	265
6.1.3 EFFECT OF ALKALI-METASOMATISM IN ALKALI-PYROXENITE	273
6.1.4 GEOCHEMICAL SIGNATURES	285
6.1.5 APATITE AND CALCITE AS PETROGENETIC INDICATORS	292
6.1.6 ISOTOPIC STUDIES	294
6.1.7 PETROGENETIC MODEL	298
6.2 NEPHELINE SYENITES	301
6.2.1 FIELD AND PETROGRAPHIC SIGNATURES	301
6.2.1.1 FELDSPAR AND NEPHELINE PARAGENESIS	302
6.2.1.2 BEHAVIOUR OF PYROXENE IN RESPONSE TO METAMORPHISM	306
6.2.1.3 BIOTITE AND OTHER MINERAL PARAGENESIS	313
6.2.2 GEOCHEMICAL SIGNATURES	317
6.2.3 APATITE AND OTHER ACCESSORY COMPOSITION AND THEIR PARAGENESIS-A POSSIBLE 'pH' INDICATOR?	318
6.2.4 GEOCHRONOLOGICAL STATUS OF THE NEPHELINE SYENITE AND REGIONAL GEOLOGY	322
6.3 GENETIC LINEAGE (?) BETWEEN THE STUDIED ROCKS	330
CHAPTER 7	
CONCLUSIONS	337
REFERENCES	341

LIST OF FIGURES

Figure No	CAPTION	Page No
1.1	Carbonatites of occurrences of India along with the study area.	5
1.2	Flow chart of the methodology applied in the present study	11
2.1	Crustal provinces of Peninsular India. During the Precambrian time (c. 2.0Ga) Indian was mainly divided into two major blocks: North Indian Block (NIB) and South Indian Block (SIB) and they were separated by Central Indian Tectonic Zone. Singhbhum carton were grouped along with the SIB and considered to be the oldest cratonic province in Indian Peninsula (Eriksson et al., 2006).	19
2.2	Generalized geological map of the Singhbhum area with three petro-tectonic zones and different litho-units present within this Proterozoic cratonic province.	21
2.3	Revised chronostratigraphic succession of the Singhbhum-Chotanagpur area.	25
2.4	Regional geological map of the Purulia along the Northern Shear Zone (NSZ). Localities: B- Beldih, M- Mednitandr, K- Kutni, C- Chirugora and S- Sushina.	33
2.5	The lineament map of the Purulia area showing the major lineament (NSZ) along with the others and the alkaline-carbonatite complex is located at the intersection between the WNW and ESE lineaments.	35
2.6	Different rock type present at Beldih area. (a) Chlorite-phyllite host rock for carbonatite and alkaline-ultramafic rocks; (b) Quartzite making a part of the country rock and (c) late stage quartz vein intruded the country rock and the area is covered mostly by lateritic soil cover.	39
2.7	Carbonatite exposure at Beldih. (a) and (b) showing that the exposure is affected by the meteoric water action. (c) Fresh exposures are found at depth and (d) fresh surface of the carbonatite which is devoid of weathering.	41
2.8	Exposures of alkaline-pyroxenite at Beldih (a & b). The white portion is dominated by the felsic minerals. (c) Contact between carbonatite and alkali-pyroxenite.	43
2.9	Different varieties of syenite exposed at Sushina Hill. (a) Poorly banded syenite gneiss. The large plagioclase laths are visible in the exposure itself. (b) Strongly banded syenite gneiss. The banding is made by the alternating bands of mafic and felsic minerals. (c) Pink coloured eudialyte grains are present in the strongly banded syenite gneiss. (d) Massive syenite.	45
3.1	(a) Hand specimen of the Purulia Carbonatite. (b) Apatite within calcite matrix. Calcite grains are defining the mosaic texture of carbonatite. (c) Well developed subhedral crystal of magnesiokatophorite in polygonal calcitic matrix along with	51

apatite and magnetite. (d) BSE image of magnesiokatophorite with calcite inclusion within calcitic matrix. (e) Richterite in polygonal calcitic matrix. (f) BSE image of richterite within calcite matrix which is highly fractured. (MK: *Magnesiokatophorite*; R: *Richterite*; Cal: *Calcite*; Apt: *Apatite and Magnetite*; Mt)

- 3.2 Classification of the sodic-calcic amphiboles from carbonatite as per IMA norm (Leake et al., 1997). Diagram parameters: $(Na+K)_A \geq 0.50$; $(Ca+Na_B) \geq 1.00$; $0.50 < Na_B < 1.50$. R – Richterite, MK – Magnesiokatophorite, MT – Magnesio-taramite, FR – Ferro-richterite, K – Katophorite, T – Taramite. Composition of amphiboles from Purulia carbonatite falls in R and MK fields. Amphibole composition (Hogarth, 1989) from Iron Hill (IH), Colorado; Gatineau, Quebec; Homa Bay (HB), Kenya; Turii peninsula (TP), Russia and Goldray (GR), Ontario are also plotted for the comparison with the studied amphibole. **55**
- 3.3 (a) v_{IR}^{3+} v $R^{+}+R^{2+}$ plot of low-Al amphiboles (Hogarth, 1989) from Purulia carbonatite. Composition of the amphibole from the study area cluster between MA and R. (b) $Ca+v_{IV}Al$ v. $Si+Na+K$ plot of amphiboles (Fabries, 1978) from the Purulia carbonatite. Composition of amphibole from the study area falls on the line joining R and MK. MR – Magnesio-riebeckite, MA – Magnesio-arfvedsonite, R – Richterite, T – Tremolite, FW – Ferri-winchite, H – Hal, MH – Magnesio-hastingsite, E – Edenite, MK – Magnesiokatophorite, R – Richterite, W – Winchite, T – Tremolite, I – High Al field, II – Low Al field. Symbols used for the other reported amphibole composition (Hogarth, 1989) as in the Figure 3.2 except for G1 and G2 representing Gatineau, Quebec. **59**
- 3.4 (a) Altered alkali-pyroxenite with calcite veins. (b) A part of the calcite vein along with other mineral constituents. (c) Primary magmatic amphibole (Amph-I) represented by magnesiokatophorite (d) Subhedral to euhedral crystals of calcite within calcite veins. (e) Development of dark green amphibole (Amph-II) at the expense of brown pyroxene. (Inset: Apatite within carbonatite) (f) Alteration of pyroxene to biotite. (MK: *Magnesiokatophorite*; K-T: *Katophorite Taramite*; Ab: *Albite*; Bt: *Biotite*; Cpx: *Clinopyroxene*; C: *Calcite*; Apt: *Apatite and Mt*; Magnetite) **61**
- 3.5 Composition of the pyroxene (Alkali-pyroxenite: thick red line) from alkali-pyroxenite of the study area compared with pyroxene compositional trends of different alkaline rocks (Mitchell, 1980). A. Fen, damkjernite-vibetite trend; B. Fen, acmite-hedenbergite trend; C. Fen, acmite trend; 1, Morotu (Yagi, 1953); 2. Uganda (Tyler and King, 1967); 3. Itapirapua (Gomes et al., 1970); 4. South Qôroq (Stephenson, 1972); 5. Pantellerite (Nicholls and Carmichael, 1969); 6. Nandewar (Abbott, 1969); 7. Illimaussaq (Larsen, 1976); 8. Coldwell Complex (Mitchell and Platt, 1978); 9. Turja (Mitchell unpublished data); 10. Iron Hill (Nash, 1972); P_{W1} , P_{W2} , P_E and P_B are Alnö trends for the western, eastern and Barang sectors respectively (Morogan and Woolley, 1988). **65**
- 3.6 Classification of sodic-calcic amphiboles from alkaline-ultramafic rock as per IMA norm (Leake et al., 1997). Diagram parameters: $(Na+K)_A \geq 0.50$; **67**

$(Ca+Na_B) \geq 1.00$; $0.50 < Na_B < 1.50$. R – Richterite, MK – Magnesiokatophorite, MT – Magnesio-taramite, FR – Ferro-richterite, K – Katophorite, T – Taramite. Composition of amphiboles from Purulia carbonatite falls in R and MK fields. Amphibole composition (Hogarth, 1989) from Iron Hill (IH), Colorado; Gatineau, Quebec; Homa Bay (HB), Kenya; Turii peninsula (TP), Russia and Goldray (GR), Ontario are also plotted for the comparison with the studied amphibole.

- 3.7 (a) $v_I R^{3+}$ v $R^+ + R^{2+}$ plot of low-Al amphiboles (Hogarth, 1989) from alkaline-ultramafic rock. Composition of these amphiboles cluster between MA and E i.e. they are moving from low-Al to high-Al field (b) $Ca + vAl$ v. $Si + Na + K$ plot of amphiboles (Fabries, 1978) from the Purulia carbonatite. Composition of amphibole from the study area falls on the line joining R and MK. MR – Magnesio-riebeckite, MA – Magnesio-arfvedsonite, R – Richterite, T – Tremolite, FW – Ferri-winchite, H – Hal, MH – Magnesio-hastingsite, E – Edenite, MK – Magnesiokatophorite, R – Richterite, W – Winchite, T – Tremolite, I – High Al field, II – Low Al field. Symbols used for the other reported amphibole composition (Hogarth, 1989) as in the Figure 3.2 except for G1 and G2 representing Gatineau, Quebec. **69**
- 3.8 Classification diagram for micas (apfu) from alkali-pyroxenite, after Rieder et al. (1998). Most of the analyzed grains are falling well within the biotite field while only three are plotted close to the biotite-phlogopite boundary. **73**
- 3.9 Composition of plagioclase feldspar from alkaline-pyroxenite. The feldspars are found to be pure albite and developed during fenitization or alkali-metasomatism. **75**
- 3.10 (a) Apatite magnetite rock in hand specimen showing alteration due to meteoric water actions. (b) Hexagonal prismatic apatite crystal in apatite-magnetite rock. (c) Cross fractures in apatite crystals. (d) Yellow colour silicate phase along the periphery of the apatite crystal. **79**
- 3.11 Lithological map of the Sushina Hill region showing different varieties of syenites. The area is dominantly consists of banded syenite followed by massive syenites. **81**
- 3.12 (a) Hand specimen of poorly banded syenite gneiss showing alternating banding of mafic and felsic minerals. Large plagioclase crystals are also visible. (b) and (c) Dominant mineral constituents of poorly banded syenite gneiss defining the porphyritic texture. (d) Large megacrysts of albite. (e) Alternating banding of mafic (aegirine) and felsic (feldspars and nepheline) minerals (f) Perthite texture in poorly banded syenite gneiss. (g) Microcline in poorly banded syenite gneiss showing cross-hatched twinning (h) Thick rimming of albite by late stage metasomatic alterations. (i) Large nepheline enclosed (poikilitically) within large albite megacrysts. Alteration of nepheline to sodalite at places is clearly visible. (j) Eudialyte replacing nepheline along the periphery which is enclosed within albite megacrysts. (k) and (l) large aegirine grains sometimes misleads to amphiboles. (*Ae: Aegirine, Ab: Albite, Or: Orthoclase, Ne: nepheline, Eud: Eudialyte, Sod: Sodalite, Anl: Analcime*) **85**

- 3.13 Compositions of feldspars from different varieties of nepheline-syenites. The feldspars are found to be pure albite and orthoclase. **89**
- 3.14 (a) Compositional variation of nepheline from nepheline syenite gneiss and massive syenite in terms of Ne-Ks-Qtz. (b) Nepheline composition from the other occurrences are given for comparison (after Mitchell and Liferovich, 2006; Mitchell and Platt, 1979; Woolley and Platt, 1986; Wilkinson and Hensel, 1994; Coulson, 1997; Markl and Baumgartner, 2002; Marks and Markl, 2003). The dashed line drawn from the Ne-Ks line (“Barth join”) denotes the Dollase-Thomas compositional trend fro natural nephelines (Dollase and Thomas, 1978); the dashed lines with temperature notations denotes the Morozewicz (M)-Buerger(B) convergence field (Hamilton, 1961; Wilkinson and Hensel, 1994). **93**
- 3.15 Comparison between the nepheline composition from the studied nepheline syenite gneiss and massive syenite with the nepheline from the other reported nepheline syenite gneiss. The data sets used for comparison are taken from Tilley (1954). In all the cases nepheline is associated with albite±microcline assemblage. Studied nephelines along with other reported nephelines are plotted close to ideal Morozewicz composition ($Ne_{75.0}Ks_{20.5}Qtz_{4.5}$). **97**
- 3.16 Classification of pyroxene different varieties of nepheline-syenites. (a) Q-J Diagram and (b) (Wo–En–Fs)-Jd-Ae ternary plot for Ca-Na pyroxenes (Classification based on Morimoto et al., 1988). **99**
- 3.17 Post magmatic changes of poorly banded syenite by hydrothermal/deuteric fluid. (a) Granulation of the constituent grains during fluid migration. (b) Veinform nepheline within megacrysts of albite. (c) and (d) Fluid entering the rock and giving rise to new minerals mainly eudialyte. **103**
- 3.18 (a) and (b) Eudialyte (Eud-I) replacing aegirine. Relatively larger grains are formed at the first stage while that of the smaller eudialyte crystals formed at late stage (Eud-II) present within the orthoclase, albite as tiny inclusion. **105**
- 3.19 (a) Hand specimen of strongly banded syenite gneiss showing alternating banding of mafic and felsic minerals. (b) The rock dominantly consists of euhedral to subhedral albite. (c) Eudialyte-NZS-aegirine assemblage. (d) Aggregates of aegirine (lower right with higher order interference colour) are consistently present throughout the rock defining strong band of this mineral. (*Ab: Albite, Ae: Aegirine, NZS: Na-Zr silicates*) **109**
- 3.20 (a) Complex zoning of eudialyte-Na-Zr silicates (NZS) replacing albite (Ab) and aegirine (Ae). BSE image of (a) showing the similar mineralogy. (c) Similar assemblages of eudialyte and corresponding BSE image (d). In this case eudialyte is replacing albite. (e) BSE image of the eudialyte and NZS. Some unidentified (U) REE, Nb, Y, Zr, Na and Cl bearing phase is also identified. (f) Inclusion like eudialyte (Eud-II) present within all the constituent minerals. Perthite is also observed in this variety of syenite gneiss. **111**

- 3.21 (a) and (b) Compositions of eudialyte, NZS and some other unidentified phase analyzed by SEM-EDAX and Raman Spectroscopy respectively. For details see text (Post Magmatic Alterations of Strongly Banded Syenite Gneiss). 115
- 3.22 (a) Hand specimen of poorly banded syenite showing alternating banding of mafic and felsic minerals. Large plagioclase crystals are also visible. (b) and (c) Dominant mineral constituents of poorly banded syenite (for abbreviations see below) defining the porphyritic texture. (d) Large megacrysts of albite. (e) Alternating banding of mafic (aegirine) and felsic (feldspars and nepheline) minerals (f) Perthite texture in poorly banded syenite. (*Ab: Albite, Or: Orthoclase, Ne: nepheline, Ae: Aegirine*) 117
- 3.23 (a) Microcline grains indicative of low temperature recrystallization of the early formed orthoclase. (b) Late stage biotite grains are terminating at the grain boundaries. (c) and (d) Post magmatic alterations by deuteritic fluid resulting formation of eudialyte as well as some complex Na-Zr bearing silicates. 119
- 3.24 (a) Composition of late stage biotites from massive syenite. (b) Comparison of the biotite on Mg - Al+Fe³⁺+Ti - Fe³⁺ (Mn²⁺) (after Foster, 1960) diagram from the studied massive syenite with the other well known nepheline syenite gneiss from Bigwood and Blue Mountain Complex of Ontario, Canada. The diagram shows the close proximity of the biotite with that of the Blue Mountain Amphibolites and Big Wood Syenites gneiss indicating formation of biotite during metamorphism. 123
- 3.25 The composition of biotite from massive syenite in terms of Fe³⁺ - Fe²⁺ -Mg. Lines representing oxygen fugacity buffers are from Wones and Eugster (1965). MH: magnetite-hematite, NNO: nickel-nickel oxide, QFM: quartz-fyallite-magnetite. The studied biotites are falling close to the MH buffer. 127
- 3.26 Photomicrograph showing post magmatic alteration by hydrothermal/deuteritic fluid. (a) Fracture filling by late stage mineral phase formed from the deuteritic fluid (pink to violet colour) in apatite of carbonatite. (b) The same mineral is also present as small inclusion within the calcite grains (in carbonatite). (c) and (d) Prominent pink to violet colour mineral present in albite and biotite grains in alkali-pyroxenite. (e) Replacement of pyroxene (aegirine) by eudialyte the late stage deuteritic fluid in poorly banded syenite gneiss. The other constituent grains (orthoclase-albite) are also carrying tiny grains of eudialyte. (d) Replace of aegirine by eudialyte and further formation of complex Na-Zr bearing silicates in poorly banded syenite gneiss. In all the photomicrograph the zone marked by the circle indicates pronounced effect of late stage alteration by deuteritic fluid. (*Ae: Aegirine; Amph: Amphibole; Apt: Apatite; Ab: Albite; Bt: Biotite; Cal: Calcite; Di: Diopside; Eud: Eudialyte; Mt: Magnetite; NZS: Na-Zr Silicates*) 129
- 3.27 Composition of nephelines and feldspars from nepheline syenite gneisses of the Sushina area plotted on the system NaAlSiO₄ (Ne)-KAlSiO₄ (Ks)-SiO₂ (Qtz). The studied nepheline syenite gneisses are similar to the nepheline syenite gneisses of the Bigwood and Blue Mountain Complex (cf. Duke and Edgar, 1977). 133

4.1	Schematic diagram showing steps of bulk rock analysis by XRF.	161
4.2	Plots of range of oxides (Wt%) for carbonatite, metasomatized or altered alkali-pyroxenite, alkali-pyroxenite and nepheline syenite. (Harker variation diagrams). Considerable scatter is observed for CaO, Al ₂ O ₃ , Na ₂ O, K ₂ O, Fe ₂ O ₃ and MgO (For detailed descriptions see text under the corresponding sections)	163
4.3	Chemical classification of Purulia carbonatite in a CaO-(FeO+Fe ₂ O ₃ +MnO)-MgO ternary plot (Weight percent of oxides) (after Le Bas and Streckeisen, 1991)	167
4.4	(a) Primitive mantle normalized spider diagram for carbonatite. The Purulia carbonatites are compared with the average calico-carbonatite values given by Woolley and Kempe (1989). (b) Chondrite normalized REE plot of Purulia carbonatite. In this plot similar symbols are used as that of the spider diagram. Normalizing values are from Sun and McDonough (1989).	169
4.5	Total Alkali versus Silica (TAS) plot of the silicate rocks viz. metasomatized alkali-pyroxenite (alkali-pyroxenite in the figure) and nepheline-syenites. One sample is showing higher amount of alkalis.	173
4.6	(a) and (b) Graphical representation of the elementary loss and gain of elements between the alkali-pyroxenite (igneous) and altered alkali-pyroxenite (metasomatized alkali-pyroxenite) during alkali-metasomatism.	175
4.7	(a) Primitive mantle normalized spider diagram for alkali-pyroxenite. (b) Chondrite normalized REE plot of fenitized alkali-pyroxenite (alkaline-ultramafic). Normalizing values are from Sun and McDonough (1989).	179
4.8	BSE image showing presence of nioborutile in alkali-pyroxenite. These grains were analyzed by SEM-EDAX. (Nb-Rtl: Nioborutile; Cpx: Clinopyroxene; Apt: Apatite; Bt: Biotite, MK: Magnesiokatophorite)	181
4.9	(a) Primitive mantle normalized spider diagram of nepheline-syenites (ANK 2, 6, 7, 8 are poorly banded syenite gneiss and ANK 9 is massive syenite) from Sushina. (b) Chondrite normalized REE plot of nepheline-syenites. Normalizing values are from Sun and McDonough (1989).	185
4.10	(a) Primitive mantle normalized spider diagram of three different rocks viz. carbonatite, alkali-pyroxenite and all varieties of nepheline syenites. (b) Chondrite normalized REE plot of the above mentioned rocks. Normalizing values are from Sun and McDonough (1989).	189
4.11	(a) and (b) Ramon spectral response curve of apatite and calcite from carbonatite. 97% match with the standard is noticed. (c) and (d) Ramon spectral response curve of apatites separated from alkali-pyroxenite and nepheline syenites respectively.	195

4.12	Primitive mantle normalized spider diagram (column 1) and chondrite normalized REE plot (column 2) of the apatite and calcite separated from the Purulia carbonatite. Normalizing values are from Sun and McDonough (1989).	199
4.13	(a) Primitive mantle normalized spider diagram of average calcite, apatite along with the whole rock from which these mineral grains were separated. (b) Chondrite normalized REE plot of average calcite, apatite along with the whole rock from which these mineral grains were separated. Normalizing values are from Sun and McDonough (1989).	201
4.14	Primitive mantle normalized spider diagram (column 2) and chondrite normalized REE plot (column 1) of the apatite separated from the alkali-pyroxenite. Normalizing values are from Sun and McDonough (1989).	205
4.15	(a) Primitive mantle normalized spider diagram of average apatite from the alkali-pyroxenite along with the whole rock. (b) Chondrite normalized REE plot of the same. Normalizing values are from Sun and McDonough (1989).	207
4.16	Primitive mantle normalized spider diagram (column 2) and chondrite normalized REE plot (column 1) of the apatites separated from the nepheline-syenites (ANK 8: poorly banded syenite gneiss; ANK 9: Massive syenite). Normalizing values are from Sun and McDonough (1989).	211
4.17	(a) Primitive mantle normalized spider diagram of average apatite along with the whole rock from the nepheline-syenites. (b) Chondrite normalized REE plot of average apatite along with the whole rock from the nepheline-syenites (ANK8: poorly banded syenite gneiss, ANK9: Massive syenite). Normalizing values are from Sun and McDonough (1989).	213
4.18	(a) Primitive mantle normalized spider diagram of average apatite from the carbonatite and alkali-pyroxenite along with the respective whole rocks. (b) Chondrite normalized REE plot of average apatite of these rocks along with the respective whole rocks. Normalizing values are from Sun and McDonough (1989).	215
4.19	(a) Primitive mantle normalized spider diagram of average apatite from the different varieties of nepheline syenites. (b) Chondrite normalized REE plot of average apatite of syenites. Normalizing values are from Sun and McDonough (1989).	219
5.1	$^{87}\text{Rb}/^{86}\text{Sr}$ vs. $^{87}\text{Sr}/^{86}\text{Sr}$ plot of carbonatites as well as mineral separates viz. calcite and apatite. No correlation has been noticed between the bulk rocks as well as for the minerals.	237
5.2	$^{206}\text{Pb}/^{204}\text{Pb}$ - $^{207}\text{Pb}/^{204}\text{Pb}$ isochron (pseudo-isochron) for the carbonatites showing an age of about 1370 ± 39 Ma.	239
5.3	$^{87}\text{Rb}/^{86}\text{Sr}$ vs. $^{87}\text{Sr}/^{86}\text{Sr}$ plot of whole rock nepheline-syenites. No correlation has	243

been noticed between the bulk rock samples.

5.4	$^{206}\text{Pb}/^{204}\text{Pb}$ vs. $^{207}\text{Pb}/^{204}\text{Pb}$ plot of whole rock nepheline-syenites. Linear correlation has been found between the bulk rock samples. ANK 2 showing evidences of Pb-mobility.	245
5.5	U-Pb Concordia diagram of poorly banded syenite gneiss (ANK 7).	247
5.6	Monte Carlo Simulation histogram for two samples of poorly banded syenites: ANK 2 and ANK 7 respectively.	249
5.7	U-Pb Concordia diagram of banded syenite sample ANK 8. (a) Both the air abraded and non abraded grains are together giving an age of about 934 Ma while a much more precise age is given by three point isochron with low MSWD and gives an age of ~960 Ma.	253
5.8	U-Pb Concordia diagram of poorly banded syenite gneiss (ANK 2).	255
5.9	U-Pb Concordia diagram of massive syenite sample ANK 9.	257
6.1	(a) $_{\text{IV}}\text{Al}-\text{Ti}^{4+}$. (b) $_{\text{IV}}\text{Al}-\text{Fe}^{3+}$ and (c) $_{\text{IV}}\text{Al}-\text{Mg}$ plots of the amphibole from the Purulia carbonatite. $_{\text{IV}}\text{Al}$ shows positive correlation with Ti^{4+} (a) and Fe^{3+} (b) and negative correlation with Mg (c) in richterite and magnesiokatophorite species. For comparisons the amphibole composition (Hogarth, 1989) from Iron Hill, Colorado; Homa Bay, Kenya; Turii Peninsula, Russia and Goldray, Ontario.	267
6.2	(a) $(\text{Si}^{4+}+\text{Na}^+_{\text{B}})-(\text{Al}^{3+}_{\text{T}}+\text{Ca}_{\text{B}})$ plot for the two varieties of amphibole – richterite and magnesiokatophorite. There are two distinct fields of these two types of amphibole with correlation coefficient of -0.9652 and -0.9805 for richterite and magnesiokatophorite, respectively. b. $\text{Na}_{\text{B}}-\text{Ca}_{\text{B}}$ plot of richterite and magnesiokatophorite, showing strong negative correlation between them in B – site.	269
6.3	$(\text{Na}+\text{K})/(\text{Na}+\text{K}+\text{Ca})$ vs. $\text{Mg}/(\text{Mg}+\text{Fe}^{\text{T}}+\text{Mn})$ plot of pyroxene, Amph-II and biotite shows that the Mg released during the pyroxene alteration to the amphibole (Amph-II) was later introduced into the biotite. Also note the substantial increase in alkalinity $(\text{Na}+\text{K})/(\text{Na}+\text{K}+\text{Ca})$ during biotite formation.	275
6.4	REE plots of the metasomatized and unaltered alkali-pyroxenite. Please note the lower level of REE enrichment in the unaltered alkali-pyroxenite compared to the altered equivalent, suggesting introduction of REE during metasomatism. Normalizing values are from Sun and McDonough (1989).	279
6.5	Y-Sr (a), Y-(Nd/Ho) _{cn} (b) and Y-(Nd/Yb) _{cn} (c) plots of apatite from the metasomatized alkali-pyroxenite and carbonatite. See text for detail explanations.	281
6.6	$\text{Fe}^{3+}/(\text{Fe}^{3+}+\text{Fe}^{2+})$ (oxidation ratio) vs. $(\text{Na}+\text{K})/(\text{Na}+\text{K}+\text{Ca})$ (alkalinity) plot of pyroxene, Amph-II and biotite from the alkali-pyroxenite. The oxidation ratio is	283

lower during alteration of pyroxene to Amph-II. The ratio was highest during formation of the biotite.

- 6.7 Generalized sequence of formation of different mineral assemblages in the alkali-pyroxenite during metasomatic alteration. **287**
- 6.8 Bivariant plot (whole rock samples) of different trace elements (a) Ba-Sr, (b) Nb-Ta and (c) Ba-Nb. **289**
- 6.9 Different bivariant plot of the apatite grains separated from the carbonatite and metasomatized alkali-pyroxenite. **295**
- 6.10 $^{87}\text{Sr}/^{86}\text{Sr}$ growth lines for bulk Earth are contained within hatched envelope, the line shown is the best estimate for the depleted mantle source (Bell et al., 1982). The data of the Purulia carbonatite falls close to the hatched envelope. The age of the carbonatite (1.37 Ga) indicates the existence of long-lived mantle heterogeneity during this period of time. **299**
- 6.11 Feldspar thermometry (of Fuhrman and Lindsley, 1988) used for banded syenite (poorly banded syenite gneiss) showing equilibration temperature of 500°C for albite and orthoclase. **303**
- 6.12 Feldspar thermometry (of Fuhrman and Lindsley, 1988) used for massive syenite showing equilibration temperature of 200°C for albite and orthoclase. **307**
- 6.13 Pyroxene from the banded syenite on (Na-Mg) vs. Al (a) and [$^{\text{VI}}\text{Al}/(^{\text{VI}}\text{Al}+\text{Fe}^{3+})$] vs. [$\text{Na}/(\text{Na}+\text{Ca})$] (b) plots respectively showing their response in relation to the metamorphism. The pyroxene from this variety of syenite is compared with the NNAP pyroxenes of Woolley et al. (1996). **309**
- 6.14 Pyroxene from the banded syenite on a $^{\text{VI}}\text{Al}$ vs. (Na- Fe^{3+}) plot showing their response in relation to the metamorphism. The pyroxene from this variety of syenite is compared with the NNAP pyroxenes of Woolley et al. (1996). Analyzed pyroxenes are showing enrichment of $^{\text{VI}}\text{Al}$ and plotted in the field of metamorphic pyroxenes along with the Kasungu and Chipala pyroxenes (a). They are showing a transition between igneous and metamorphic pyroxenes when compare with the Ilomba pyroxenes. **311**
- 6.15 Plot of [$^{\text{VI}}\text{Al}/(^{\text{VI}}\text{Al}+\text{Fe}^{3+})$] vs. [$\text{Na}/(\text{Na}+\text{Ca})$] (after Woolley et al. 1996) for pyroxenes from metamorphosed alkaline rocks including Red Wine, Labrador (Curtis and Gittins, 1979), Ghana (Holm, 1971), Nkonglong, Cameroon (Kornprobst et al., 1976), Norra Kärr, Sweden (Adamson, 1944), Japan (Iwasaki, 1960) and Ontario (Lumbers, 1976). The pyroxenes from the banded variety of syenite falls with thin the metamorphosed alkaline rock of Red Wine complex. **315**
- 6.16 Apatite from banded syenites (poorly banded syenite gneiss) in terms of Na_2O - REE_2O_3 - SrO ternary diagram. The apatites from the banded syenite were formed under maximum alkalinity and that of apatites of massive syenite at relatively low **323**

alkalinity.

- 6.17 Generalized schematic chronostratigraphic map of the study area along with the data set obtained in the present study. Geochronological data obtained from the near by Saltora area by Maji et al. (2008) and Chatterjee et al. (2008) is also included for ready reference. **325**
- 6.18 Range of metamorphic ages obtained from the poorly banded syenite gneiss reflecting Grenvillian metamorphism affected the pre existing nepheline syenites. **327**
- 6.19 Selected paired trace element ratios for carbonatite and nepheline syenites to find out the genetic link between these rocks. No common trend is observed. The bloc arrow indicates where the hypothetical immiscible carbonate magmas (a, b) and carbothermal fluids (c). **333**

LIST OF TABLES

TABLE NO	CAPTION	PGE NO.
Table 1.1	Occurrences of Indian carbonatites (as in Fig. 1.1), Associated Rock types and types of Fenitization present (after Krishnamurthy, 1988).	14
Table 1.2	Selected Geochronological data from Indian Carbonatite Complexes	15
Table 3.1a	Composition of calcite in carbonatite	136
Table 3.1b	Composition of opaque in carbonatite	136
Table 3.2	Composition of apatite from carbonatite	137
Table 3.3	Composition of amphibole from carbonatite	139
Table 3.4	Composition of clinopyroxene from alkali-pyroxenite	142
Table 3.5	Composition of amphibole from alkali-pyroxenite	143
Table 3.6	Composition of biotite from the alkali-pyroxenite	145
Table 3.7	Composition of plagioclase feldspar in alkali-pyroxenite	146
Table 3.8	Composition of calcite from the alkali-pyroxenite	147
Table 3.9	Composition of apatite, ilmenite and magnetite from the alkali-pyroxenite	147
Table 3.10	Composition of orthoclase from poorly banded syenite gneiss	148
Table 3.11	Composition of albite from poorly banded syenite gneiss	149
Table 3.12	Composition of nepheline from poorly banded syenite gneiss	150
Table 3.13	Composition of pyroxene from poorly banded syenite gneiss	151
Table 3.14	Compositions of nepheline and its' alteration to sodalite from the poorly banded syenite gneiss. Two examples of replacement of nepheline by analcime are also shown.	152
Table 3.15	Composition of albite from strongly banded syenite gneiss	153
Table 3.16	Composition of pyroxene from strongly banded syenite gneiss	154
Table 3.17	Composition of eudialyte and Na-Zr bearing silicates from strongly banded syenite gneiss	155
Table 3.18	Composition of feldspars from massive syenite	156
Table 3.19	Composition of nepheline from massive syenite	157
Table 3.20	Composition of mica from massive syenite	157
Table 4.1	Whole rock analyses (major and trace elements) of representative carbonatites, syenites and alkali-pyroxenite (AP)	221
Table 4.2	Norm data for different varieties of syenite and alkali-pyroxenite	224
Table 4.3	Mass balancing between the unaltered and the metasomatized alkali-pyroxenite	226
Table 4.4	Trace element composition of apatite and calcite in the carbonatite	227
Table 4.5	Trace elemental composition of apatite from alkali-pyroxenite	229
Table 4.6	Trace element composition of apatite in nepheline-syenites	231
Table 5.1	Sr-Pb data from the carbonatite, nepheline-syenite and alkali-pyroxenite	261
Table 5.2	U-Pb isotope data for zircons from two varieties of nepheline syenites	262
Table 6.1	Element averages (from Table 4.4) and partitioning coefficients between apatite & calcite (vice versa) of carbonatite	336

INTRODUCTION

Carbonatite is a magmatic rock which contains more than 50 modal percent primary (i.e., magmatic) carbonate and represents very small volume of the total igneous rock in the earth crust. It is commonly associated with alkaline, alkaline-ultramafic rocks like syenites, ijolites, etc. The nomenclature of carbonatite depends upon the dominant carbonate species like calcite (calcite carbonatite), dolomite (dolomite carbonatite), ankerite (ankerite carbonatite) etc. (Woolley & Kempe, 1989). In addition to carbonates, numbers of other minerals may also be present in this rock. Common accessory minerals are apatite, monazite, magnetite, pyrochlore, pyroxene (sodic-calcic), olivine (forsterite), mica (phlogopite, vermiculite), amphibole (sodic), etc. (Hogarth, 1989). The other reported rare accessories are nepheline, zircon, strontianite, garnet (pyrope), rutile etc. (Hogarth, 1989). The carbonatite is commonly associated with extensional tectonic regime and typically found in the rifted continental margins e.g. carbonatite occurrences of East African Rift forming a broad zone trending southwards from Kenya through Mozambique. It is also found near the plate margins and may be linked with plate separation or orogenic activity. Though intrusive carbonatite complexes are common, extrusive varieties are reported from different parts of the world. Woolley and Church (2005) listed about 50 known localities of extrusive carbonatite, out of which 35% are located within the African continent.

The first detailed compilation on world carbonatite and the associated rocks are available in two books by Heinrich (1966) and Tuttle & Gittins (1966). Le Bas (1977) gave very detailed account East African carbonatite complexes. Kapustin (1980) proposed classification of carbonatite based on their mineralogical association and stages of development. Woolley and Kempe (1989) suggested a carbonatite nomenclature which is very similar to the IUGS system (Streckeisen,

1980) along with some changes of the early suggested classification by Woolley (1982). The details of carbonatite genesis and its evolution are discussed in depth by Bell (1989).

The petrogenesis of carbonatite is still a debatable issue. There is no single mechanism which can successfully explain the formation of the carbonatitic melt. The presence of carbonatitic magma was established long back in the 1960s but there was much debate since then as to whether carbonatite magma is developed directly by partial melting of mantle peridotite or by modification within the crust and hence at much lower pressure, of a mantle derived magma by fractional crystallization or liquid immiscibility (Gittins, 1988). Much of these controversies are summarized by LeBas (1987), Twyman (1987) and Gittins (1987). Melting studies reveals there are three possibilities by which carbonatite can be formed, (1) direct partial melting of a metasomatized mantle (Wyllie & Hung, 1975; Wallace & Green, 1988; Wyllie & Lee, 1998); (2) immiscible separation at low or high pressure from carbonated silicate melts e.g. carbonated nephelinite (Koster van Groos & Wyllie, 1963; Le Bas, 1977; Kjarsgaard et al., 1995; Brooker, 1998) and (3) crystal fractionation of a carbonated alkali silicate melt (King; 1949; Veksler et al., 1998).

Recently, Mitchell (2005) proposed a mineralogical-genetic approach in classifying the carbonatites in terms of the 'petrological clan'. Two major groups of carbonatite can be classified on the basis of their petrological clan; these are (1) calcite or dolomite carbonatite (or both), these are primary carbonatites and genetically related to nephelinite, melilitite, kimberlite and other mantle-derived magmas. (2) carbothermal residua derived from a wide variety of magmas. Carbothermal refers to the low-temperature fluids derived from a fractionated magma dominated by CO₂ also containing fluorine and H₂O in variable proportions.

In recent years the work on carbonatite achieved a new dimension as isotopic study of carbonatite is helpful in understanding the nature of the sub-continental mantle over a long period of time starting from Precambrian to most recent.

1.1 INDIAN CARBONATITES: AN OVERVIEW

Occurrence of carbonatite in India was first come in early 1960's with significant discoveries of fluorite and conspicuous radioactivity in and around Ambadongar Chhota Udaipur, Baroda district, Gujarat (Sukeswala & Udas, 1963; Subramaniam & Parimoo, 1963; Bose, 1884). Later on significant discovery was made in late 70's at Sung Valley, Meghalaya (Yusuf and Saraswat, 1977), which opened a new chapter in Indian Carbonatites.

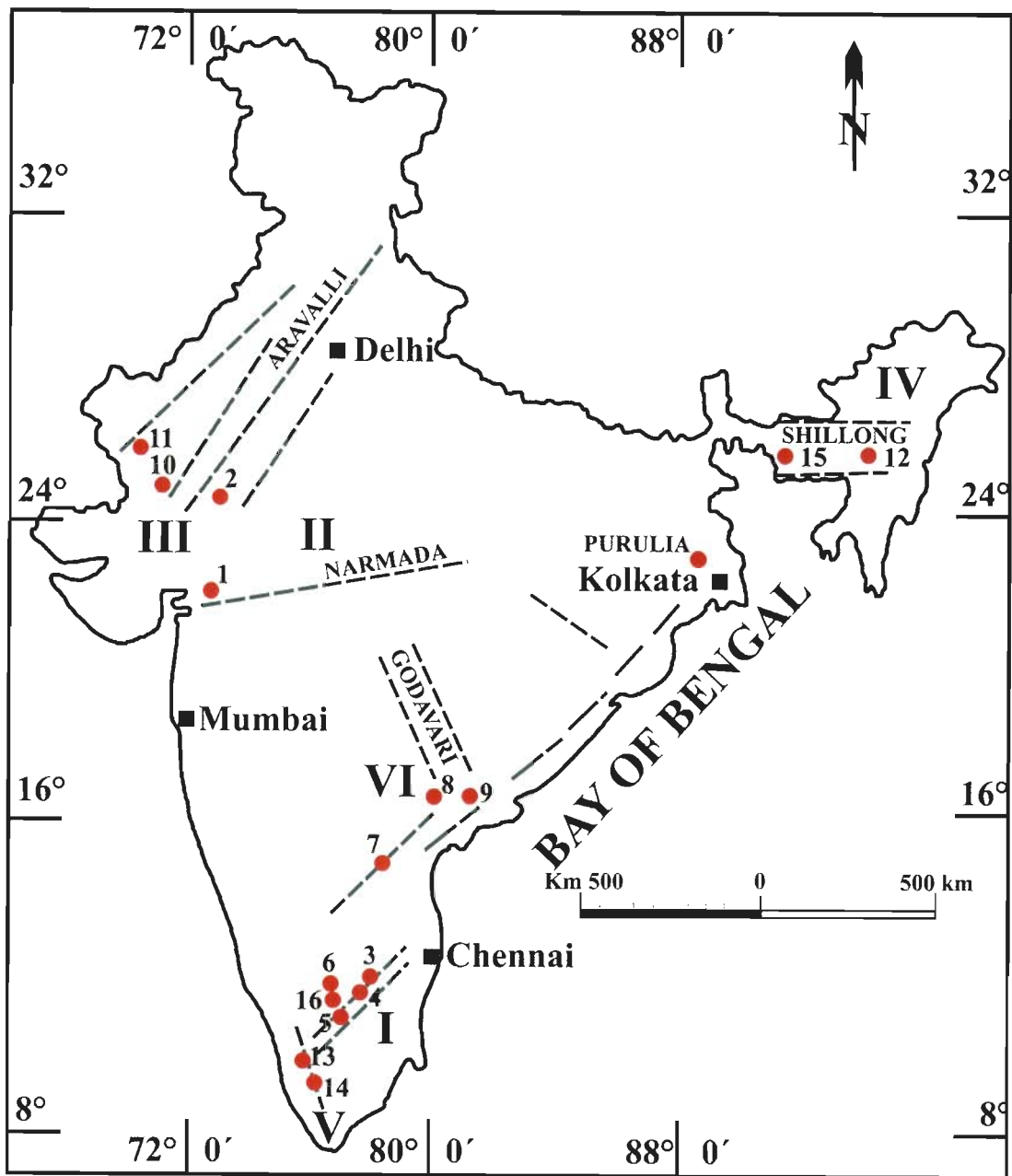
So far, around twenty carbonatite complexes have been reported in India. These carbonatite occurrences are associated with some well-defined geological environments and structural set-up (Fig. 1.1 & Table 1.1) and belong to two major age groups. Those are associated with the Eastern Ghat, Cuddapah, Aravalli and Western Ghat faults are of Meso/Neoproterozoic age. On the other hand, those are associated with Narmada and trans-Aravalli rifts and Meghalaya plateau are of Late Mesozoic to Early Cenozoic age. Four major carbonatite complexes represent the older group and the areas are Borra (A.P.), Chelima (A.P.), Sevattur, Samalpatti, Hognekal (Tamil Nadu) and Newania (Rajasthan.). Newania, Mesoproterozoic in age, is the oldest carbonatite in India so far. Both Borra and Chelima carbonatites are also of Mesoproterozoic age but are slightly younger than Newania and the Sevattur carbonatite is Neoproterozoic in age. The carbonatites from Meghalaya are of Early Cretaceous age whereas Amba Dongar represents age of Late Cretaceous-Early Tertiary. Out of these carbonatite complexes only 6-7 carbonatites have been dated by different radiometric dating methods (Table 1.2). Correlation of the Amba Dongar carbonatite intrusion with Deccan volcanism vis-à-vis Reunion hotspot activity (Basu et al., 1993) is well accepted. Both carbonatite and basaltic magmatism is caused during movement of Indian plate over the Reunion hotspot (Neil et al., 2003). Similarly, Rajmahal-Syllhet volcanics and carbonatite of Assam-Meghalaya are related to Kerguelen hotspot (Baksi 1995; Kent, 2002). Interestingly, the Newania carbonatite which lies within the area affected by the Deccan magmatism and north of Amba

Dongar, is much older and Meso-Proterozoic in age. Such close association of two carbonatite complexes of contrasting age is very much possible in the same segment of the earth, e.g. West and South Greenland where carbonatites were emplaced during four periods extending over 2500 Ma (Woolley, 1989). Presence of Alkaline-Carbonatite Complex (ACC) is also reported within the oldest Precambrian group i.e. Singhbhum group of rocks in Purulia, West Bengal (Basu, 1993; 2005). A small body of carbonatite along with alkaline ultramafics, nepheline syenites etc. are found at isolated places along Northern Shear Zone (NSZ), which defines the contact between two oldest group of rocks of Indian subcontinent i.e. Singhbhum Group and Chotanagpur Granitic Gneissic Complex (CGGC). This shear zone marks the southern boundary of the CGGC and northern extremity of Singhbhum Group of rocks hence termed as South Purulia Shear Zone or Northern Shear Zone respectively (NSZ).

In brief, carbonatites are associated with major faulting and rifting, related to doming or upper mantle related hotspot activity, within continental shield areas. The carbonatite magmatism has also significantly increased with time. It is also possible that the carbonatite magmatism can be repeated in the same segment of the earth over a large span of geological time.

1.2 PROBLEM DEFINED

The proposed study area lies about forty kilometers south of Purulia town, West Bengal along NSZ. The NSZ marks the contact between Singhbhum Group of rocks and CGGC and extends for about 100 Km through Beldih, Medinitanr, Kutni, and Chirugora in WNW-ESE direction (Bhattyacharya, et al., 1991). Carbonatite (Beldih), apatite-magnetite (Beldih), alkali-pyroxenite (Beldih) and nepheline syenite (Sushina) are found at different locations along this shear zone within the Singhbhum Group of rocks (Basu, 1993, 2005).



(Modified after Krishnamurthy, 1988)

**I Eastern Ghat Belt; II. Narmada; III. Aravalli;
IV. Assam-Meghalaya Plateau; V. Western Ghat
Faluts; VI. Cuddapah-Godavari rifts.**

**Fig. 1.1 Carbonatite of occurrences of India along with the study area.
(For location details please refer to section 1.1)**

Two major gaps exist in understanding the implication of carbonatite clan of rocks in this area. The very first problem is to characterize and correlate these rocks which are scattered along a linear zone stretching for forty kilometers. Detailed geological mapping along with petrological, geochemical and isotopic studies are necessary to know the magma source, its generation and subsequent differentiation which may generate the carbonatite and associated rocks. However, scanty surface exposure with intense weathering hinders the investigation. Once the carbonatite and the associated rocks are properly characterized, their importance in tectono-magmatic evolution of this part of Indian shield is the other major gap. The tectono-magmatic evolution of the area started during 1700 Ma. At this time, the Singhbhum micro-plate started moving towards north to collide with Chotanagpur micro-plate. These two micro-plates were then separated by ocean where parent sediments and volcanics for the Singhbhum Group of rocks were accumulated. Gradually these micro-plates came closer to each other and finally joined with each other around 850 Ma (Sarkar, 1982). The present day Singhbhum Shear Zone (SSZ) may be the remnant of an old subduction zone along which Singhbhum micro-plate subducted with Chotanagpur micro-plate. On the other hand, NSZ, lie north of the SSZ, represents the contact between Chotanagpur micro-plate with the Singhbhum Group of rocks. This shear zone, NSZ, might have developed during or after collision of the Singhbhum micro-continent with the Chotanagpur. One of the possibilities is that the carbonatite magmatism took place close to this time marking (?) the end of Singhbhum orogeny. Recently, Chatterjee, et al. (2008) reported presence of 1500 Ma anorthosite intrusion in the Bankura District, West Bengal which lies further east of the study area.

Further, this area was reactivated during the formation of Gondwana rift valley during the end of Paleozoic Era. The Gondwana sediments were accumulated till Jurassic and then Rajmahal volcanics were erupted. Eruption of Rajmahal volcanics is also intimately related with upper mantle activities and presence of lamprophyres in the coalfields is a major evidence for the same.

The relation of carbonatite and alkaline rocks along the NSZ with the Gondwana rifting is also a reasonable possibility. The culmination of this tectonic activity is the break up of Indian Shield from Antarctica. So the carbonatite-alkaline rocks of Purulia can either be Meso/Neoproterozoic or Late Cretaceous. Thus detailed study of petrology and geochemistry will help in characterizing and deciphering the genesis of these rocks. The isotopic data can be very useful for petrogenesis and also to predict the nature of the sub continental mantle beneath at the time of their formation. Proper age determination of these rocks will reveal the time of emplacement of these rocks along the shear zone. Thus the petrology, geochemistry and isotopic studies altogether may help in finding out the tectono-magmatic evolution of this area in relation to these intrusives and their relation to the major tectonic events of East Indian shield like Singhbhum orogeny or Gondwana rifting.

1.3 OBJECTIVES

The present study area lies along the NSZ; marking the contact between the rocks of Singhbhum Group and Chotanagpur Granitic Gneissic Complex and lies north of the SSZ. Carbonatite, alkali-pyroxenite, nepheline syenite etc. are present as intrusives along NSZ. Earlier, extensive works were carried out on mineralogy, petrology, geochemistry, geochronology and mineralization for both Singhbhum Group of rocks and CGGC. In comparison, very little works were so far done along NSZ. Hence detailed petrology and geochemistry of these intrusive along NSZ i.e. carbonatite, fenitized alkali-pyroxenite and nepheline syenite is yet to be carried out. Moreover, carbonatite mostly occurs in association with rocks like peridotite, pyroxenites, dunite, ijolite, nepheline syenite, etc. and indicates an extensional tectonic regime. Though the previous workers like Basu (1993, 2005) reported the presence of an alkaline carbonatite complex (ACC) but the genetic relationship between these rocks is still enigmatic; as these rocks are present at distant

places from each other. Carbonatite is reported from Beldih and Kutni along with apatite-magnetite and alkali-pyroxenite while nepheline-syenite is exposed around forty kilometers away at Sushina. So, detailed petrological and geochemical work may help in establishing the genetic relationship between these rocks of this alkaline complex. Moreover different isotopic signatures of these rocks will further strengthen establishing the co-genetic relationship between these rocks, if any.

Geochemical along with isotopic data of these rocks can provide valuable insight into the nature of the sub-continental mantle beneath at the time of their formation

- *Detailed petrological and geochemical characterization of these rocks, both bulk rock and mineral chemistry, is necessary to get an overview of their genesis.*
- *Isotopic studies will help to solve the enigma of the co-genetic (?) relationship between these rocks.*
- *Application of geochemical and isotopic data for determining the nature of the sub-continental mantle during magma generation.*

Close association of the Purulia carbonatite and related rocks along the contact (NSZ?) of the Singhbhum Group of rocks and CGGC, indicates their age could probably be Meso/Neoproterozoic. However, the possibility of much later origin of these intrusives i.e. Mesozoic, particularly for carbonatite can not be ruled out as the study area lies in the close proximity of the Gondwana formations which also bears the evidence of upper mantle activity by the presence of lamprophyres in the coal fields. This part of the Indian shield reactivated during Gondwana rifting i.e. the final break up of Indian shield from Antarctica, resulted the formation of Rajmahal-Syllhet trap (basalt) due to plume activity (Kerguelen) of mid-Cretaceous age. Sung Valley carbonatite complex (Meghalaya) is believed to be formed at the same time due to same Kerguelen plume activity. So, the correct age determination of these rocks is very much essential

in order to correlate these rocks with major orogenic events like Singhbhum orogeny or Gondwana rifting. An attempt has been made to find out the age of these rocks.

- *Age determination of carbonatite and associated rocks to know their time of emplacement.*

Petrological, geochemical and isotopic data along with age of these rocks can help in developing the petrogenetic modeling.

- *Petrogenetic modeling of the carbonatite and associated rocks.*

1.4 METHODOLOGY

The present study is divided into three main parts i.e. petrology, geochemistry and isotope geology and then further subdivided into number sub categories (Fig. 1.2). Initially detailed field work and sampling were carried out in and around the study area.

- *Detailed field work and sampling.*
- *Selection of the rock types. In this study three main rock types are selected namely Carbonatite, Alkali-pyroxenite and Nepheline Syenite for further analysis.*

Thin sections of the selected rock samples were prepared and studied in details under the microscope followed by the EPMA.

Microscopic studies were carried out and number of minerals selected for SEM and EPMA studies.

- *SEM and EPMA study of the selected mineral grains were carried out for knowing about the internal structures like zoning, inclusions, etc. particularly from the BSE images and to find out the chemical compositions of the constituting minerals.*

Geochemical studies are divided into two parts i.e. bulk rock geochemistry and mineral geochemistry.

- *Whole rock geochemistry of the selected rock samples using XRF (Major elements) and LA-ICP MS (Trace elements).*

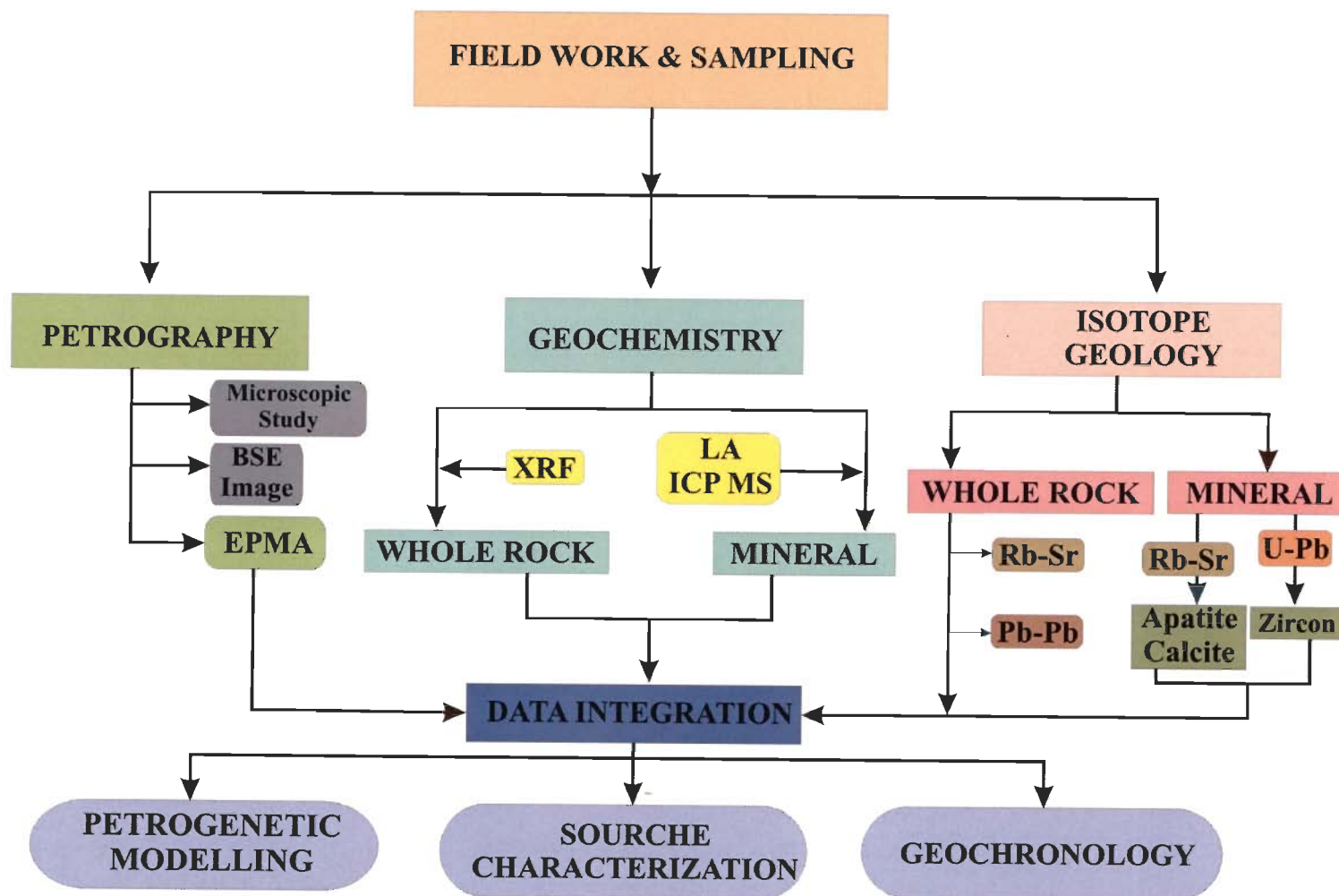


Fig. 1.2 Flow chart of the methodology applied in the present study.

- *Mineral (Apatite) chemistry from all three rock types by LA-ICP MS.*

Isotopic studies also divided into two parts i.e. whole rock and mineral isotopic analysis and were carried out using TIMS (Thermal Ionization Mass Spectrometer). Whole rock isotopic studies (Rb-Sr & Pb-Pb systematics) were carried out using representative rock samples. The mineral isotopic studies (Rb-Sr systematic) were carried out for apatite-calcite pair, separated from carbonatite. Zircon grains are separated from nepheline syenite and U-Pb dating method is applied.

- *Whole rock isotopic analysis of selected rock samples by Rb-Sr and Pb-Pb systematics.*
- *Apatite and calcite grains from carbonatite are studied by Rb-Sr method.*
- *U-Pb (ID-TIMS) dating of zircon grains from nepheline syenites.*

All these data set were synthesized to achieve the objectives of the present study.

- *Integration of the data acquired by petrological, geochemical and isotopic studies for understanding the magma generation process(es), source of the parent magma, fractionation of the magma and finding out the age of the rocks.*

Table 1.1: Occurrences of Indian carbonatites (as in Fig. 1), Associated Rock types and types of Fenitization present (after Krishnamurthy, 1988).

Number	Locality	Associated Rocks	Fenitization
1	Amba Dongar, Gujarat	Nephelinite-phonolitic-nephelinite	Sodic, sodic-potassic, potassic
2	Newania, Rajasthan	None	Sodic
3	Sevattur (also known as Koratti), T.N.	Pyroxenite-syenite	Sodic, sodic-potassic
4	Samalpatti Complex (Also includes Karapattu, Jogipatti etc.), T.N.	Dunite-pyroxenite-syenite	Sodic, sodic-potassic
5	Pakkanadu –Mulakkadu, T.N.	Dunite-pyroxenite-syenite	Sodic
6	Hogenakal, T.N.	Pyroxenite-syenite	Sodic
7	Chelima, A.P.	Kimberlite	
8	Elchuru, A.P.	Alkali granite-syenite	
9	Kunavaram, A.P.	Nepheline syenite-syenite	
10	Mer-Mundwara, Rajasthan	Theralite-melteigite-pyroxenite-syenite	
11	Sarnu-Dandeli, Rajasthan	Tinguaite-phonolite-techenite-syenite	
12	Sung Valley, Meghalaya	Alkali peridotite-alkali pyroxenite-ijolite-uncompahgrite	Sodic, sodic-potassic, potassic
13	Munnar, Kerlala	Alkali granite-syenite	
14	Khambammettu, T.N.	None	
15	Swangkre, Meghalaya	Ijolite-lamprophyre	
16	Kollegal, Karnataka	Pyroxenite-syenite	
17	Purulia, West Bengal	Pyroxenite (alkaline ultramafite)	

T.N. – Tamil Nadu, A.P. – Andhra Pradesh

Table 1.2: Selected Geochronological data from Indian Carbonatite Complexes

Carbonatite Complex	Associated Rock(s)	Mineral/ Whole rock Dated	Dating Method	Age (Ma)
MAJOR MIDDLE TO LATE PROTEROZOIC CARBONATITE COMPLEXES OF INDIA				
<i>Borra, AP</i> Venkatasubramaniam and Krishnan, 1960	Pyroxenite-Syenite	Phlogopite	Rb	1490
<i>Chelima, AP</i> Crawford, 1969	Kimberlite	Whole Rock	Rb-Sr	1340
<i>Sevattur, TN</i> Deans and Powell, 1968	Pyroxenite-Syenite	Biotite from Pyroxenite	K-Ar	720±30
Moralev et al., 1975		Pyrochlore From Carbonatite	Pb-Pb	840-845
Parthasarathy and Sankardas, 1976		Zircon from Carbonatite	U-Pb	600
Nagpaul and Mehta, 1975		Zircon From Carbonatite	Fission Track	1330±40
Nagpaul and Mehta, 1975		Apatite from Carbonatite	Fission Track	690±50
Schleicher et al., 1998		Whole Rock (Ankeritic carbonatite)	Pb-Pb	801±11
<i>Newania, Rajasthan</i> Deans and Powell, 1968		Intrusive within Granite gneiss	Alkali amphibole from Carbonatite	K-Ar
Schleicher et al., 1998	Whole Rock		Pb-Pb	1551±46

Table 1.2 (continued)

Carbonatite Complex	Associated Rock(s)	Mineral/ Whole rock Dated	Dating Method	Age (Ma)
MAJOR LATE MESOZOIC TO CENOZOIC CARBONATITE COMPLEXES OF INDIA				
<i>Amba Dongar, Gujarat</i> Deans et al., 1973	Nephelinite-phonolitic-nephelinite	Pyroxene from nephelinite intruding the carbonatite	K-Ar	37.5±2.5
Deans et al., 1973		Feldspar from Potash fenite	K-Ar	61±2 76±2
Ray and Pande, 1999		Whole Rock	⁴⁰ Ar- ³⁹ Ar	65
<i>Sung Valley, Meghalaya</i> Chattopadhyay and Hashimi, 1984	Peridotite Pyroxenite Melilitolite Ijolite Nepheline-Syenite	Apatite from Carbonatite	Fission Track	84±13 to 90±10
Ray and Pande, 2001		Phlogopite from Carbonatite	K-Ar	149±5
		Whole Rock Carbonatite	Pb-Pb	134±20
		Phlogopite from Carbonatite	Rb-Sr	106±11
		Whole Rock + Phlogopite from Carbonatite	⁴⁰ Ar- ³⁹ Ar	107.2±0.8
Srivastava et. al., 2005	Pervoskite	U-Pb	115.1±5.1	

PREVIOUS WORK AND REGIONAL GEOLOGY

The present Indian subcontinent was believed to be divided into two major blocks, the North Indian Block (NIB) and the South Indian Block (SIB); by c. 2.0 Ga, which were then amalgamated along the Central Indian Tectonic Zone (CITZ) to give rise the single large cratonic plate i.e., Indian craton (e.g., Rogers, 1996; Eriksson et al., 1999 & 2006; Mazumder et al., 2000, Mazumder, 2005) (Fig. 2.1). The CITZ is considered to be the product of plate collision and composed of platformal sediments metamorphosed to lower greenschist to upper amphibolite-facies, along with gneiss, bordered on both northern and southern sides by granulites (Mazumder et al., 2000). Dharwar, Bastar and Singhbhum cratons, together comprises the South Indian Block (SIB) while the North Indian Block (NIB) was composed of Aravalli-Bundelkhand cratonic province (Fig. 2.1). NIB and SIB together with CITZ, constituted the major Indian Precambrian landmass, but there are other two smaller provinces also existed at that time was Eastern Ghats and the other one was accreted on to the northwestern margin of the Aravalli-Bundelkhand Province (Fig. 2.1) (Mazumder et al., 2000). Among these cratonic provinces the most debatable one is the Singhbhum; both in terms of its geodynamic evolution and the relative stratigraphic positions of the individual units (Groups and/or Formations), representing this part of the Indian shield. Lack of fossil records, except few rare organo-sedimentary structures, stromatolites constraints its proper age determination. The same is solely dependant on isotopic studies of the individual rock units constituting the Singhbhum crustal province. Isotopic studies suggest a range of age starting from 3500 Ma to 1400 Ma. for formation of Singhbhum craton (Sharma et al., 1994; Goswami et al., 1995; Mishra et al., 1999; Sengupta and Mukhopadhaya, 2000; Mukhopadhaya, 2001). The present study area lies along the Northern Shear Zone (NSZ) or South Purulia Shear Zone (SPSZ) which marks the contact between Chotanagpur Granitic Gneissic Complex (CGGC) in the

north and rocks of North Singhbhum Folded Belt (NSFB) (also called North Singhbhum Mobile Belt: NSMB) in the south (Fig. 2.2). Numbers of alkaline intrusive rocks like carbonatite, pyroxenite (alkaline-ultramafic), nepheline syenite and apatite-magnetite, are present along this shear zone representing a prevalence of extensional tectonic regime during the intrusion of these rocks. It is therefore important to understand the Singhbhum geology in brief and then its relation to the present study area.

2.1 GEOLOGY OF THE SINGHBHUM CRATON

Singhbhum cratonic province is one of the few in the world which bears the evidence of both sedimentation and volcanism at the Archean-Proterozoic boundary (Acharyya, 1993, 2003a,b; Sengupta et al., 1997; Eriksson et al., 1999; Mazumder et al., 2000; Sengupta and Mukhopadhaya, 2000; Mazumder, 2002, 2003; Mazumder and Arima, 2004). It has been established by the earlier workers that the Singhbhum crustal province is broadly classified into three distinct petrotectonic zones (Fig. 2.2) (Bose and Chakraborty, 1994; Sarkar et al., 1992; Blackburn and Srivastava, 1994). Starting from south to north (Fig. 2.3) these zones are: (1) the Southern Archean granite-greenstone terrain (Acharyya, 1993; Sengupta et al., 1997; Mukhopadhaya, 2001), commonly known as 'Singhbhum Granite Craton or Archean Nucleus, (2) 200 km long North Singhbhum Folded Belt (NFSB) or North Singhbhum Mobile Belt (NSMB) comprising the Dhanjori, Chaibasa, Dhalbhum, Dalma and Chandil Formations (Gupta and Basu, 1991, Acharyya, 2003a,b; Ray et al., 1996), and (3) the extensive granite-gneiss and migmatite terrain in the north known as Chotanagpur Granitic Gneissic Complex (CGGC).

A highly deformed sheared zone which marks the contact between zone 1 and 2, is termed as Singhbhum Shear Zone (SSZ) or Copper Belt Thrust (Mukhopadhaya et al., 1975; Mukhopadhaya, 1984; Ghosh et al., 1985; Saha, 1994; Bhattacharya, 1992). The SSZ is characterized by the presence of crushed rocks which has suffered retrograde metamorphism.

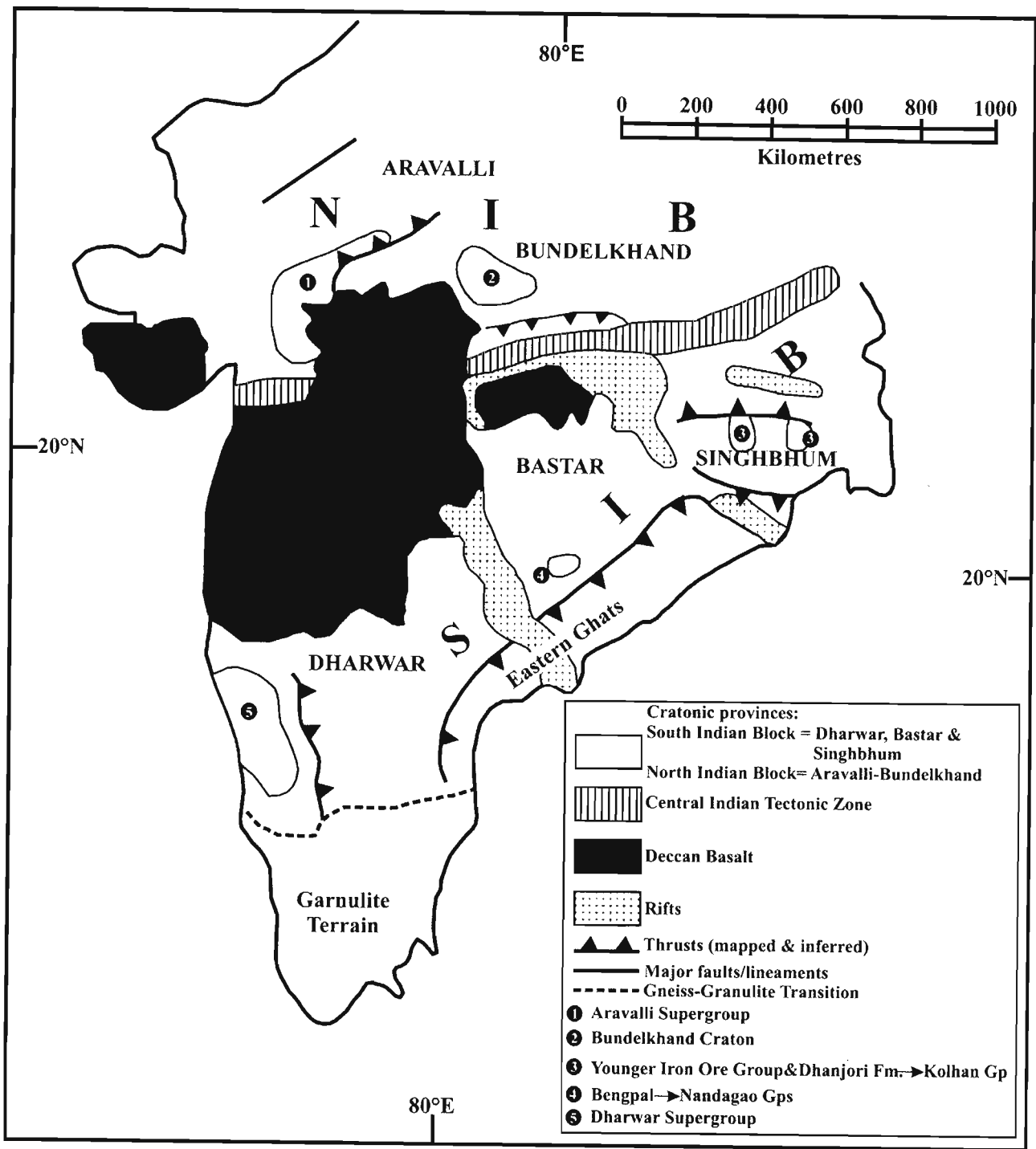
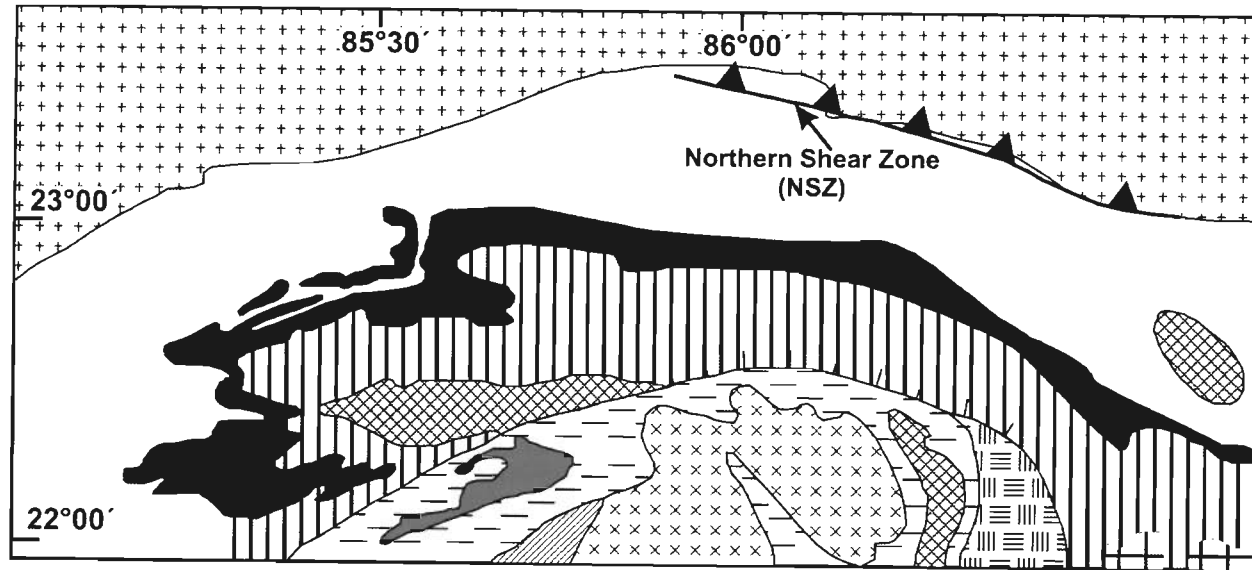


Fig. 2.1 Crustal provinces of Peninsular India. During the Precambrian time (c. 2.0Ga) Indian was mainly divided into two major blocks: North Indian Block (NIB) and South Indian Block (SIB) and they were separated by Central Indian Tectonic Zone. Singhbhum craton were grouped along with the SIB and considered to be the oldest cratonic province in Indian Peninsula (Eriksson et al., 2006).



(after Majumder, 2005) with the inclusion of NSZ

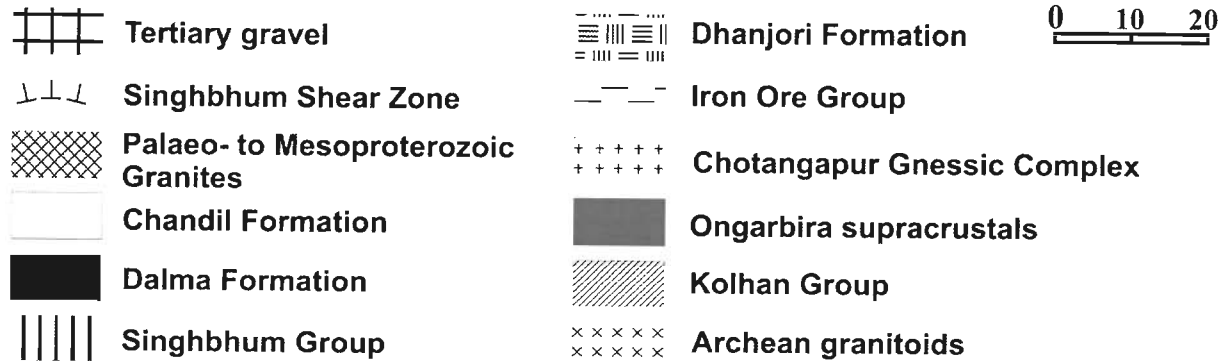


Fig. 2.2 Generalized geological map of the Singhbhum area with three petrotectonic zones and different litho-units present within this Proterozoic cratonic province.

The rocks on either side of the SSZ are also distinguished by contrasting metamorphic facies. It is an arcuate belt of high strain characterize by multi-phase deformation, intense ductile shearing (Mahadevan, 2002). Some granite intrusive (Arkasani granophyre and soda granite) are present as small linear bodies along SSZ, which gives an age of about 1600 Ma. This age reflects the age of metamorphism of the sediments and of thrusting along the SSZ (Sarkar et al., 1986; Sengupta and Mukhopadhaya, 2000; Mazumder and Sarkar, 2004).

This part of the Indian shield, i.e. Singbhum craton, is being studied extensively by the geoscientists over more than few decades, starting from Dunn (1929). Several stratigraphic models have been proposed on the Singbhum area. In recent years the stratigraphy of the Singbhum craton has been revised and modified substantially with the availability of new isotopic data from different stratigraphic units. Further, sedimentological evidences (e.g. facies analysis, sedimentary structural analysis), and a new 'freeboard concept' based on sea level changes (Eriksson et al., 1999 & 2006), enabled us to draw a more precise stratigraphic succession of the area. The stratigraphic succession of the Singbhum craton is given in Fig. 2.3 and the individual units are described in brief below.

2.1.1 ARCHEAN NUCLEUS

The Archean Nucleus is represented by Older Metamorphic Group, Iron Ore Group, and Singbhum Granite. The basement is a matter of debate and it is believed that the basement is still unknown.

- a) **Older Metamorphic Group:** This group is the oldest unit (also called 'Archean Cratonic Core Region' i.e. ACCR) and consists of Older Metamorphic Gneiss (OMG) and Older Metamorphic Tonalitic Gneiss (OMTG) units. This group occurs as enclaves and the major enclave is exposed around Champua, which is the type area for OMG and OMTG. The other exposures are found at Bahalda, Haludpukhur and around Seraikela (Mahadevan, 2002). The OMG is comprised of paragneiss, quartzites, varieties of mica-

schist, calc-silicates (marbles) and amphibolites. These rocks are metamorphosed to upper amphibolite facies and later intruded by OMTG (Tonalitic-trondhjemitic-granodioritic gneiss also called: TTG) (Zhao et al., 2003). The $^{207}\text{Pb}/^{206}\text{Pb}$ isotopic data produced an age of 3.6 Ga to 3.55Ga for OMTG (Saha et al., 1984; Bhattacharya, 1998; Goswami et al., 1995; Mishra et al., 1999), while microprobe dating of zircon ($^{207}\text{Pb}/^{206}\text{Pb}$) from OMTG yielded an age of 3437 ± 9 Ma (Mishra et al., 1999).

b) Iron Ore Group (IOG): Iron Ore Group includes the following three major basins occurring along the fringes of the ACCR.

- i)** The Gorumahisani-Badampahar (GB) basin, on the eastern part of the ACCR (Fig 2.2).
- ii)** The Daiteri-Pala Lahara (DPL) basin, along the southern part of the ACCR.
- iii)** The extensive West Singhbhum-Keonjhar (WSK) basin, on the western flank of the ACCR.

There exists two school of thoughts regarding the IOG of rocks; one group believes that the IOG is evolved as a single unit in the above mentioned basins and they are interconnected to form a large basin (Jones, 1934; Dunn, 1929; Dunn and Dey, 1942; Sarkar and Saha, 1983; Chakraborty, 1996) and later on was intruded by Singhbhum Granite (SG); while the other group believes that the IOG evolved in two phases and termed as Older IOG (GB) and Younger OIG (DLP, WSK) (Iyengar & Banerjee, 1964, Iyengar & Murthy, 1982). Banerjee (1974) supported the later view and suggested that the Noamundi basin (equivalent to WSK) and GB-DLP basins, the stratigraphically distinct and older, have evolved by independent cycles of deformation, metamorphism and igneous activity. These basins later on welded to the the Singhbhum Granite Platform. However, the Older IOG (<3.3 Ga to >3.1 Ga, Singh, 1998) originally consists of chemical sedimentary rocks, with minor clastic lithologies and synsedimentary volcanics represented mainly by pillow basalts and these rocks later on suffered greenschist facies of metamorphism; while the Younger IOG (>2.55 Ga to <3.0 Ga,

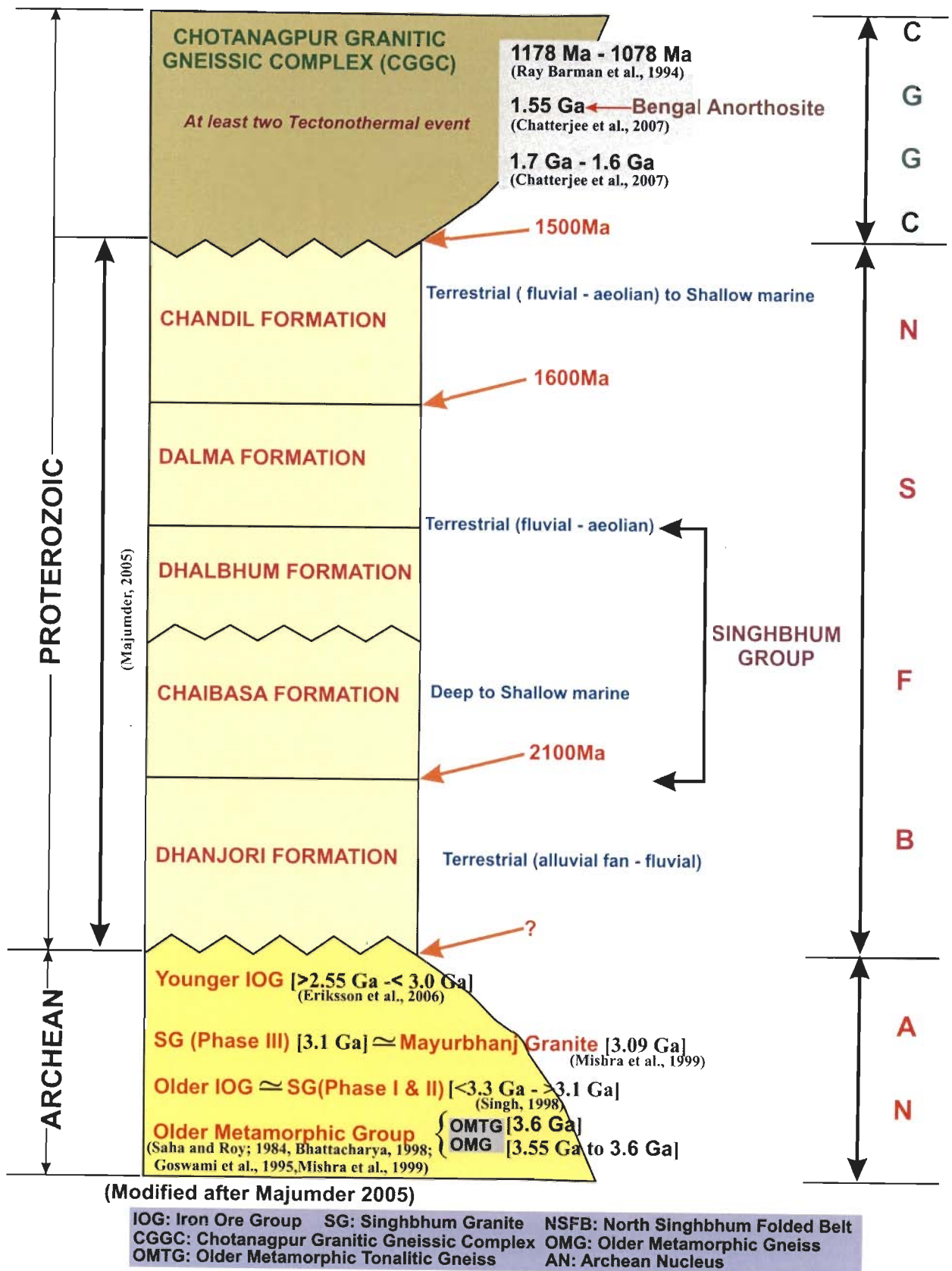


Fig. 2.3 Revised chronostratigraphic succession of the Singhbhum-Chotanagpur area.

Eriksson et al., 2006) is characterized by the presence of low-grade metamorphic equivalent of shale, sandstone, hematite-bearing BIF and Mn-bearing shale-dolomite-chert (Singh, 1998).

a) Singhbhum Granite: The Singhbhum Granite (SG) intruded into the IOG in three phases (I: oldest, II, and III: youngest). The older SG i.e. Phase I and Phase II (3.3 Ga, Mishra et al., 1999; Moorbath et al., 1986) is considered to be equivalent of Older IOG. The emplacement of final phase (Phase III) at 3.1 Ga is related and approximately equivalent to Mayurbhanj Granite (3.09 Ga, Mishra et al., 1999; Eriksson et al., 2006). The SG of Phase I is K-poor granodiorite-trondhjemite and Phase II and III granites are granodioritic grading into adamellite. The trace element geochemistry of these three granites suggests that Phase I and Phase II granites are comparable to each other and may be grouped together into Type A while the Phase III is significantly different from the other two types and grouped into Type B granites (Mahadevan, 2002).

2.1.2 NORTH SINGHBHUM FOLDED BELT (NSFB)

This is an arcuate belt of volcano-sedimentary succession of Palaeo- to Meso-proterozoic age, surrounding IOG on the east, north, and northwest is known as North Singhbhum Folded Belt (NFSB) or North Singhbhum Mobile Belt (NSMB). The southern boundary of the NFSB is marked by the SSZ, while, the northern boundary is marked by another shear zone known as the Northern Shear Zone (NSZ) or the South Purulia Shear Zone (SPSZ), defining the contact (?) with the vast terrain of CGGC. The present study was carried out on different alkaline intrusives occurring along NSZ. Therefore, the geology and geodynamic evolution of NFSB is of immense importance in relation to the present study and described in the later part of this chapter. This belt suffered intense multi-phase-deformation and also metamorphism under greenschist facies (at places amphibolite facies) at around 1600Ma (Naha, 1965; Saha, 1994; Acharyya, 2003; Mazumder, 2005). NFSB includes the rocks of Dhanjori, Chaibasa, Dhalbhum, Dalma and Chandil Formations and described briefly below.

a) ***Dhanjori Formation***: The main Dhanjori basin is situated in the NE part of the Archean Nucleus and north of the SSZ, and unconformably rests over the Archean Nucleus, divided into an upper and a lower member, respectively. The lower member mostly comprise phyllites, quartzites and thin conglomerate, while, the upper member exhibits a volcano-sedimentary assemblage (Mazumder, 2005). Overall, the lower member exhibits a fining upward sequence (Mazumder and Sarkar, 2004; Mazumder, 2005), while the upper volcano-sedimentary assemblage include ultramafic to mafic rocks with rare presence of acidic lava flows (Gupta et al., 1985; Gupta and Basu, 1991, 2000; Singh, 1998). The chemistry and micro-spinifex texture points towards komatiitic affinity for these ultramafic rocks (Gupta et al., 1985; Gupta and Basu, 2000). The representative mafic volcanics are basaltic in composition. The Sm-Nd isotopic analysis of these rocks yielded 2072 ± 106 Ma age (Roy et al., 2002a). The age data from the lower member of the Formation is yet to be available but the minimum age for the upper member of the Dhanjori Formation can be considered as at least 2.0 Ga.

b) ***Singhbhum Group (Chaibasa and Dhalbhum Formations)***: The upper volcano-sedimentary succession of Dhanjori Formation is conformably overlain by the psammopelitic and pelitic rocks Singhbhum Group (Mazumder, 2005). The Singhbhum Group is represented by lower Chaibasa and upper Dhalbhum Formations, separated by an unconformity (Sarkar and Saha, 1962; Eriksson et al., 1999; Mazumder et al., 2000; Mazumder, 2005). At places the Singhbhum Group directly overly the Dhanjori Formation while it rests on the Archean Nucleus elsewhere. The Chaibasa Formation is characterized by the interbedding of sandstone, shale and a heterolithic (very fine sandstone/silt stone-mudstone) with minor mafic volcanics (Mazumder, 2005) now metamorphosed to garnet-kyanite-staurolite-schist, quartzite and ortho and para hornblende schist (Saha, 1994). The Dhalbhum Formation is divided into upper and lower part by the difference in their lithological character. The lower part is represented

by the alternative phyllites and quartzite sequence while the upper part is characterized by the extensive development of tuffaceous rocks (Gupta et al., 1980, 1982; Mazumder, 2005). The basal sedimentary sequence contains mafic-ultramafic intrusives (peridotites and serpentinites) and number of thin lava flows are also found to be interlayered with sediments and tuffaceous members of the Dhalbhum Formation, having different petrochemical characters (tholeiites, felspathoidal basalts and basaltic komatiites) (Gupta et al., 1980, 1982). The tuffaceous member from the upper part of the Dhalbhum Formation is represented by high-magnesian vitric tuffs metamorphosed to tremolitic schists. These tuffaceous member are then intruded by comagmatic intrusives having very similar character that of peridotitic-pyroxenitic komatiites of Archean greenstone belts (Gupta et al., 1980).

- c) ***Dalma Formation:*** The Dalma formation, which conformably overlying the Dhalbhum Formation is one of the most debatable volcanic belts within NSFB. The Dalma volcanic belt occurs centrally within the NSFB and represented by thick sequence of mafic-ultramafic volcanic rocks with lenses of basic agglomerates (Gupta et al., 1980; Chakraborti, 1980; Chakraborti and Bose, 1985; Bose, 1994; Singh, 1997, 1998; Sengupta et al., 2000). The volcanic sequence is characterized by a lower unit of high-magnesian basic ultrabasics followed upward by the mafic lavas (Saha, 1994). The origin of Dalma volcanics is still a matter of controversy. Earlier it was postulated that the Dalma mafics are solely of continental origin (Dunn and Dey, 1942; De, 1964) while Naha and Ghosh (1960) postulated that the island arc environment for the same. Bose et al. (1989) and Bose (1994) considered that the Dalma volcanics (basalts) are the representative of N-type MORB and therefore a close relation to the basalts formed under back-arc basin setting i.e. supra-subduction zone environment. A different model of mantle plume activity related to ensialic evolutionary model (Gupta et al., 1980; Mukhopadhyaya, 1984, Roy et al., 2002a) is also postulated for the genesis of Dalma

volcanics. However, another model of converging microplates and collision (Sarkar, 1982, 1988) consider that the Dalma volcanics are largely ophiolitic in nature and marks the collision zone with the Singhbhum microplate in the south subducting underneath the Chotanagpur block in the north. An Rb-Sr whole rock isochron of gabbro-pyroxenite, intrusive of the Dalma volcanic belt gives an age of 1619 ± 38 Ma (~ 1.6 Ga) which may be related to the global thermal anomaly around 1.6 Ga (Roy et al., 2002b).

d) Chandil Formation: The metasedimentary and metavolcanic rocks lying inbetween CGGC and Dalma Formation includes quartzites, mica schists, carbonaceous phyllite, weakly metamorphosed acid volcanic and volcanoclastic rocks (including vitric and lithic tuffs), and amphibolites (Bhattacharya, 1992; Bose, 1994; Ray et al., 1996; Singh, 1997, 1998; Sengupta et al., 2000; Acharyya, 2003b). The nomenclature of Chandil Formation for these above rocks was given by Ray et al. 1996. A large portion of the Chandil Formation is represented by porphyritic, banded tuffaceous rocks (Ray et al., 1996; Sengupta et al., 2000). These rocks are rhyolitic to dacite in composition and have comparable major and trace elemental characteristics similar to the ash flow tuffs from the other part of the world (Ray et al., 1996). A number of minor alkaline intrusives such as carbonatite, apatite-magnetite rock, pyroxenite (alkaline-ultramafic) and nepheline syenite occur between Sushina and Balarampur within the Chandil Formation (Singh et al., 1977; Bhattacharya and Chaudhuri, 1986; Ghoshroy and Sengupta, 1988; Basu, 1993, 2005; Chakrabarty, 2002, 2005; Chakrabarty and Sen, 2004, 2007). The similarity in trace elemental signature with the other Proterozoic carbonatites of India, points towards a possible Meso or Neoproterozoic age of emplacement for the carbonatite (Chakrabarty, 2005).

2.1.3 CHOTANAGPUR GRANITIC GNEISSIC COMPLEX (CGGC)

The Chotanagpur Granitic Gneissic Complex (CGGC) is predominantly a complex collage of high-grade granitic gneiss, migmatites, and metasedimentary enclaves showing wide variations in structure, texture, and mineralogy. The sedimentary component includes quartzite, psammopelitic, and pelitic rocks with local psammitic and calc-magnesian variants. CGGC is intruded by numerous metabasic, anorthositic and granitic plutons (Mahadevan, 2002). Younger mafic, ultramafic and alkaline (sodic and ultra potassic) intrusives of early Tertiary age are also present within CGGC (Chatterjee et al., 2008). The oldest age data obtained from the whole rock Rb-Sr isochron method from three different parts of the CGGC viz. gneiss from the central part yield an age of 1717 ± 102 Ma (Mallik et al., 1991), granite from the western (1741 ± 65 Ma, Ray Barman and Bishui, 1994) and northern (1590 ± 30 Ma, Pandey et al., 1986) parts suggesting a major tectonothermal event took place in the CGGC around ca. 1.7-1.6 Ga (Chatterjee et al., 2008). A second tectonothermal event is recorded in the southern granulite domain where migmatite and hypersthene granite yielded Rb-Sr whole rock age of 1071-1178 Ma (Ray Barman et al., 1994). Thus it can be concluded that the CGGC suffered at least two major tectonothermal events, the first during Palaeoproterozoic and the second during Mesoproterozoic (Chatterjee et al., 2008). The different parts of the CGGC show a wide range of age variation between 900 ± 200 Ma (Pb-isotope and K-Ar dates, Holmes, 1950, 1955; Vinogradov et al., 1964; Sarkar, 1968; Ghose et al., 1973). A recent study of the Saltora anorthosite, which is intrusive to the CGGC yielded an age of 1.55 Ga (Chatterjee et al., 2008) suggesting the age of CGGC older than 1.55 Ga.

2.2 GEOLOGY OF THE STUDY AREA

The SPZS (termed also as Tamar-Porapahar Shear Zone, Dasgupta and Bhattacharya, 1992) or NSZ (Saha, 1994) is a discontinuous, 100 Km. long zone located along the contact between southern border of the CGGC and the margin of the NSFB. The rocks of Chandil Formation

(Roy et al., 1996) (part of the NSFB) and the CGGC are in contact along this tectonically disturbed zone. The NSZ has been traced from Katra (22°59'N, 86°52'E) in the Bankura district, West Bengal to Tamar (23°03'N, 86°40'E) in Jharkhand. This zone hosts alkaline-carbonatite rocks and also mineralization of apatite-magnetite, Rare Earth, Nb and base metal. Sushina, Chirugora, Purdaha, Kutni, Dandodih, Gamardih, Mednitanr, Beldih and Tamakhun (Kumar et al., 1985) are the important localities for investigation of alkaline-carbonatite rocks and related mineralization. The WNW–ESE trending NSZ passes through Precambrian rocks composed mainly of quartzites, phyllites, mica schists, and phlogopite-amphibolites. The carbonatite, alkaline-ultramafic, alkali-syenite and apatite-magnetite bodies are reported from Sushina (alkali syenite), Chirugora-Purdaha, Kutni-Dandodih-Gamardih (carbonatite), Mednitanr (carbonatite), and Beldih (carbonatite, alkaline-ultramafic and apatite-magnetite rock) (Basu, 1993) from east to west (Fig 2.4). The LANDSAT satellite imagery and aerial photos points to the presence of two sets of lineaments: the WNW–ESE lineament represents SPSZ or NSZ and the other one is NW–SE trending. The alkaline-carbonatite bodies occur at the intersection of the above two sets of lineaments (Fig 2.5). Ghosh Roy and Sengupta (1988) also stated that the alkaline carbonatite intrusions happen to occur at the intersection of three lineaments. The present study is carried out on the alkaline intrusives along NSZ, which are met at centres like Beldih (carbonatite, alkaline-ultramafic and apatite-magnetite rock) and different alkali syenites of Sushina (Fig 2.4).

The country rocks (phyllite, quartzite and schists) trend E–W to ESE–WNW and the dip of the foliation is very steep, 65° to 85° northerly, or southerly or even vertical at places. The earliest deformational structure recognized is a set of mesoscopic, reclined to steeply inclined isoclinal folds with E–W trending axial traces (F_1). These are dominantly preserved in the fine-grained schistose rocks. Next event was the development of asymmetrical sinistral folds with non-plunging to gently plunging E–W trending axial traces (F_2) and sub vertical axial planes. This

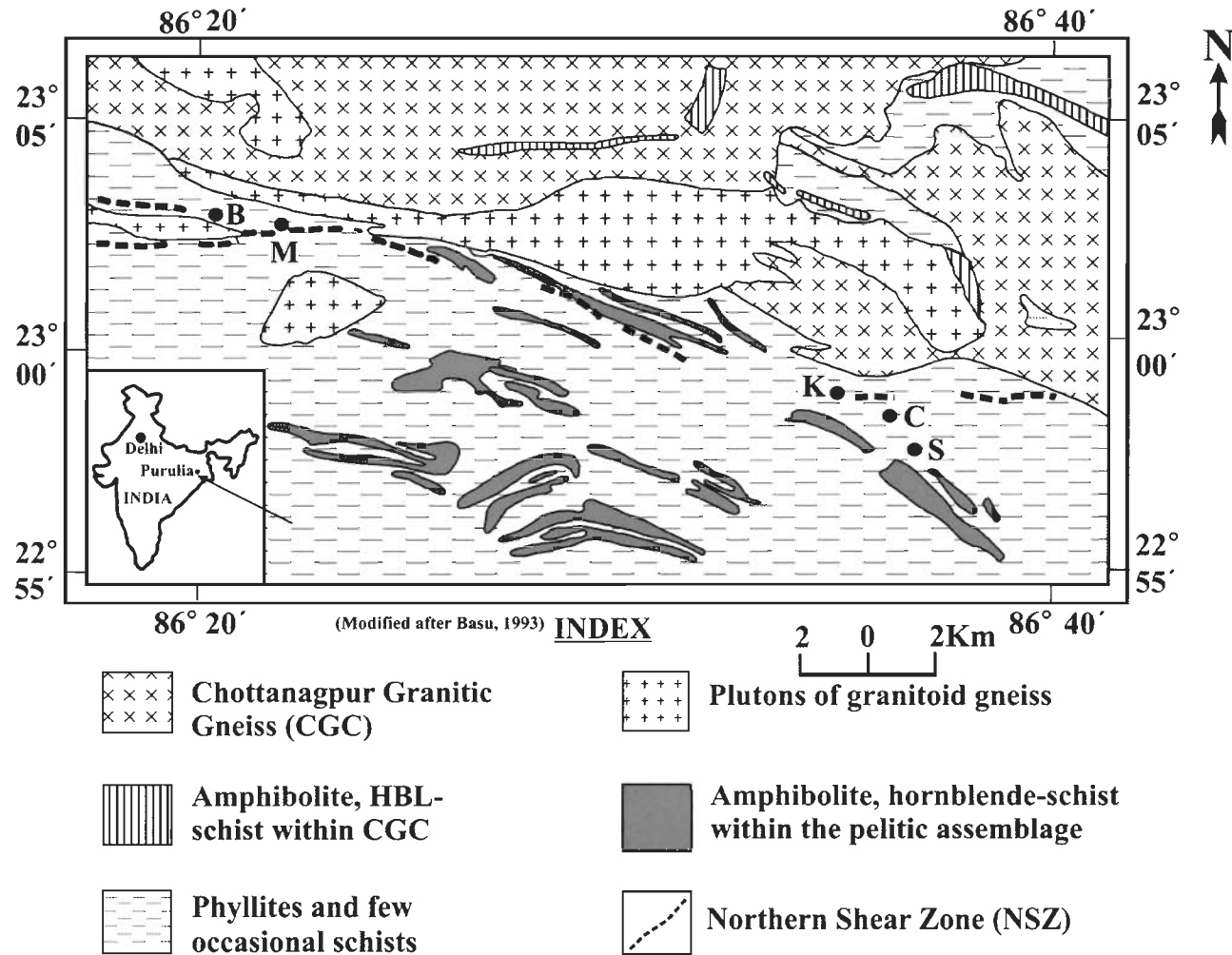
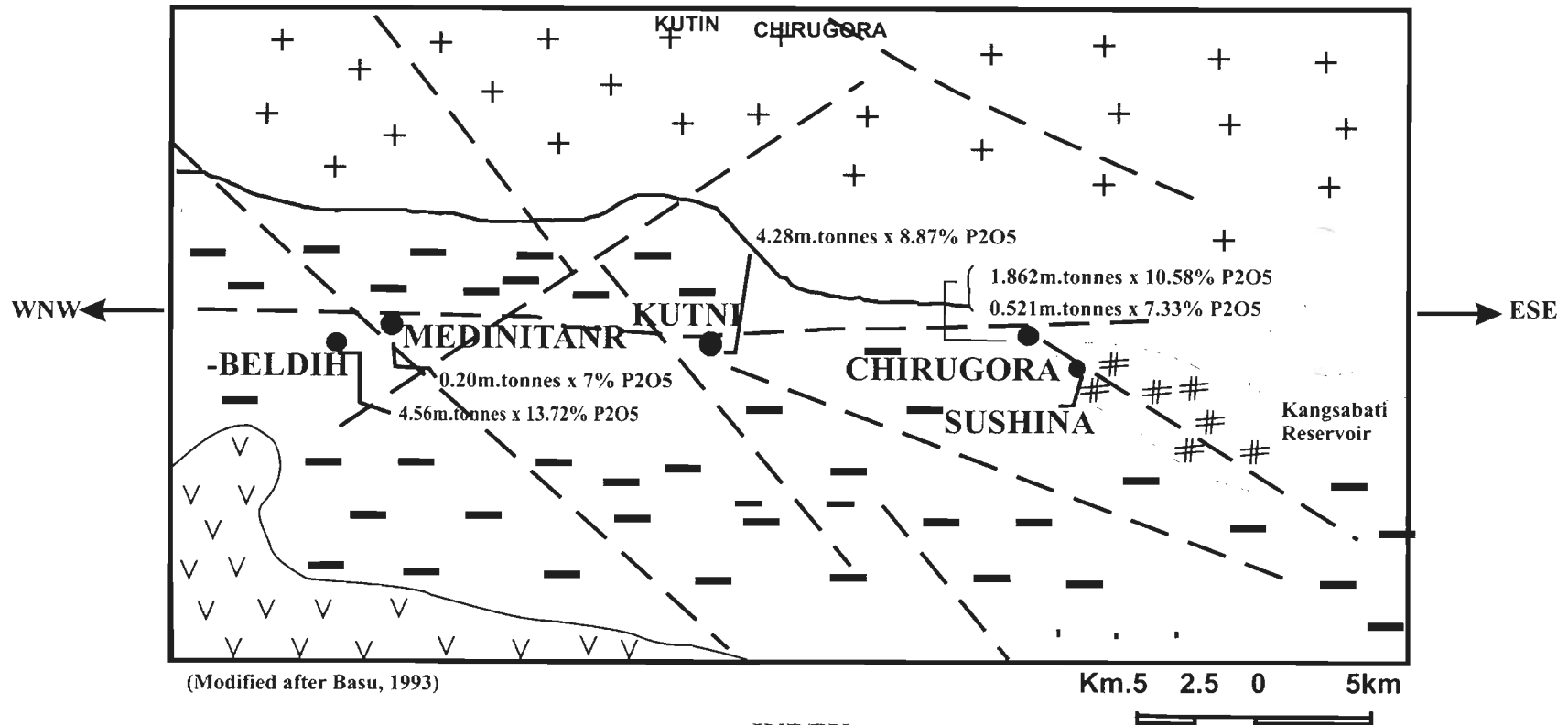


Fig. 2.4 Regional geological map of the Purulia along the Northern Shear Zone (NSZ).
Localities: B- Beldih, M- Mednitanr, K- Kutni, C- Chirugora and S- Sushina.



INDEX


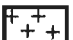



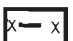

- | | | |
|--|---|---|
|  Ultrabasic Rocks |  Chhotanagpur Granite Gneiss |  Trend of Lineaments |
|  Dalma Volcanics |  Chamdil Formation |  Northern Shear Zone |
|  Apatite Deposits | | |

Fig. 2.5 The lineament map of the Purulia area showing the major lineament (NSZ) along with the others and the alkaline-carbonatite complex is located at the intersection between the WNW and ESE lineaments.

particular fold geometry was responsible for the long linear E-W trend of the lithostratigraphic units exposed in the area (Basu, 1993).

The study area around Beldih ($86^{\circ}11'E$ to $86^{\circ}23'E$, $23^{\circ}00'N$ to $23^{\circ}07'N$) is now considered to be part of the Chandil Formation and is situated 38 Km. south of the Purulia town of West Bengal (Roy et al., 1996; Mazumder, 2005). Though some earlier workers proposed that the Beldih is a part of the CGGC (Dasgupta and Bhattacharya, 1992; Bhattacharya and Dasgupta, 1992), later this area is included within the Chandil Formation (Roy et al., 1996). Along the NSZ carbonatite, alkaline-ultramafic and magnetite-apatite rocks occur within the host rock chlorite-phyllite (Fig. 2.6a) which grades into chlorite-schist (Bhattacharya and Dasgupta, 1992). Quartzite (Fig. 2.6b) and mica-schists also form the part of the country rock. The area is later intruded by number of quartz vein (Fig. 2.6c). Dun and Dey (1942) were the first to report the occurrences of uraniferous apatite bodies along the NSZ. Singh et al., (1977), Ghosh Roy and Sengupta (1988), Basu (1988, 1989, and 1990) worked on different geological aspects of the alkali carbonatitic magmatism along this shear zone. A detailed work on the petrology and geochemistry of the carbonatite, alkaline-ultramafic and apatite-magnetite rocks of Beldih area suggests a possible co-genetic relationship between them (Chakrabarty, 2002; Basu, 2005). Chakrbarty and Sen (2007) suggested that the amphibole present in the carbonatite is characteristic of the middle to late stage development of carbonatite and postulated shallow depth of intrusion for the carbonatite.

The area is mostly covered by the lateritic soil cover with very scanty exposures. Furthermore the carbonatite (Fig. 2.7) and alkaline-ultramafic rock (Fig. 2.8a,b) exposure is greatly affected by weathering and erosion. However, the contact between carbonatite and alkaline-ultramafic rock is very sharp (Fig. 2.8c) and can easily be marked in the field. Beldih area is also well known for apatite deposit, presently mined by the West Bengal Mineral Development and Trading Corporation and is known as 'Purulia Phos' (Bhattacharya, Chakraborty and Banerjee, 1991).

The varieties of alkali syenites are reported from the Sushina hill (Fig. 2.4) lies about 750 meters SW from the Sushina village (22°57'N, 86°37'E). This is a lenticular hill running NW-SE and essentially composed of different varieties of syenites with minor sodic schists (Bhattacharya and Chaudhuri, 1986). Earlier these alkali syenites were described as the 'albite' composed dominantly of albite with minor amounts of microperthite, allanite and piedmontite and quartz (Dunn and Dey, 1942). However later Bhattacharya and Chaudhuri (1986) renamed them as albite-acmite-nepheline syenite gneiss and albite-acmite-sodalite syenite gneiss. Three varieties of alkali syenites are reported from this area namely: albite-acmite-nepheline syenite, albite-biotite-acmite nepheline syenite and albite-acmite-sodalite syenite (Bhattacharya and Chaudhuri, 1986). The present study classified these varieties broadly into two categories (banded syenite and massive syenite) based on their field occurrence and later on detailed petrographic studies are carried out on them to find out the exact mineralogical composition of these varieties. On the basis of the incipient banding, the banded syenite can further be subdivided into two sub groups: poorly banded syenite and strongly banded syenite. The poorly banded syenite is characterized by the large laths of plagioclase feldspars with discontinuous bands of mafic minerals (Fig. 2.9a,b). The rock at places resembles to augen gneiss. The strongly banded syenite on the other hand is characterized by the alternating banding of mafic and felsic minerals (Fig. 2.9b,c). The massive syenite is dominantly consists of alkali feldspar and appears to be cloudy and creamy appearance in the field (Fig. 2.9d). Though more than one variety of syenite is present in Sushina area, no contact relationship among these varieties is seen in the field. So, it is difficult to ascertain the relative ages and the genetic relationship between them based on field observations.

It is evident that the carbonatite and syenite are present along NSZ but the exposures are separated by about 40 Km. This spatial isolation on the ground raises doubt on their genetic connection at depth. This gap in understanding the mutual relationship can be bridged by

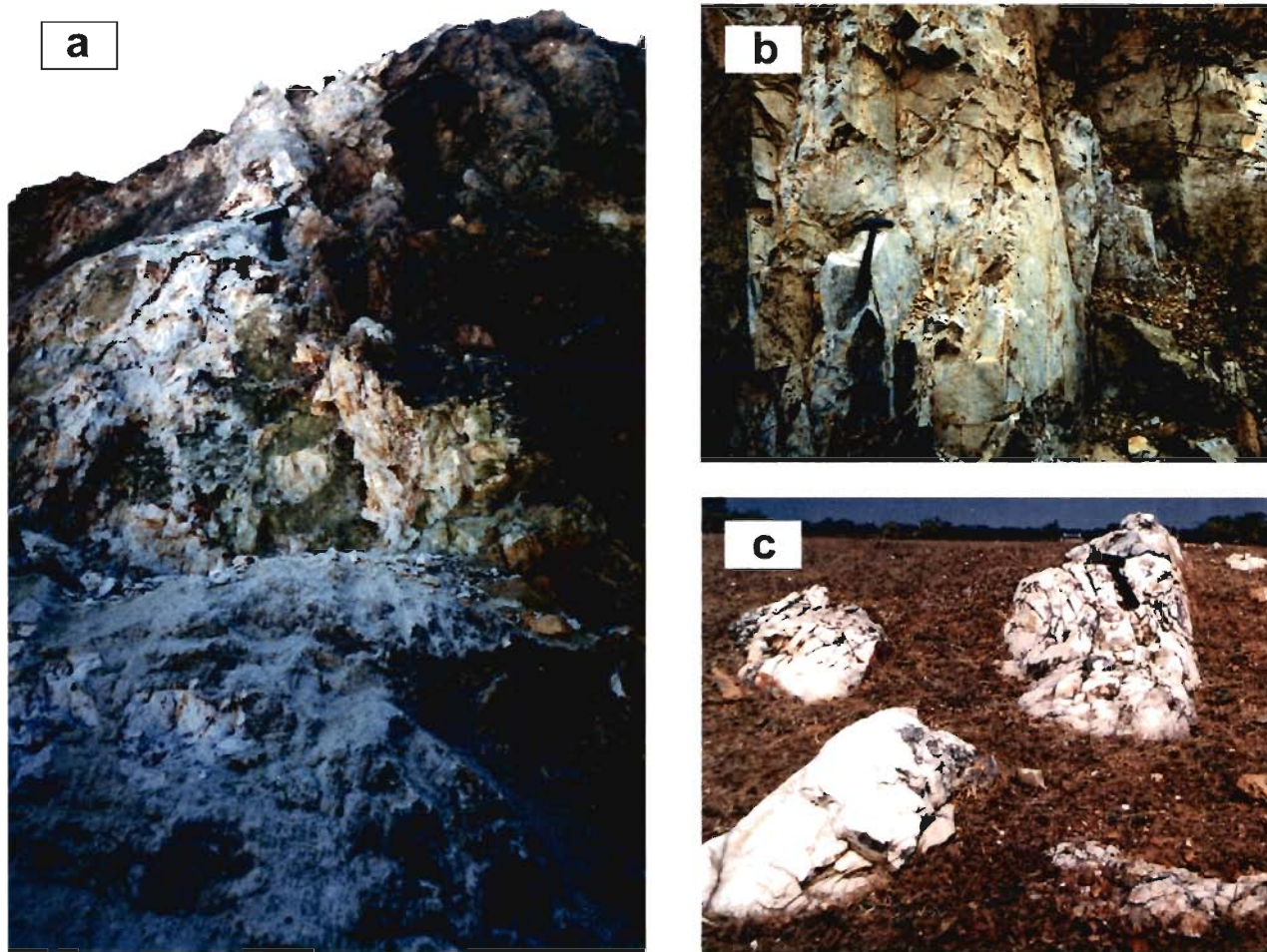


Fig. 2.6 Different rock type present at Beldih area. (a) Chlorite-phyllite host rock for carbonatite and alkaline-ultramafic rocks; (b) Quartzite making a part of the country rock and (c) late stage quartz vein intruded the country rock and the area is covered mostly by lateritic soil cover.

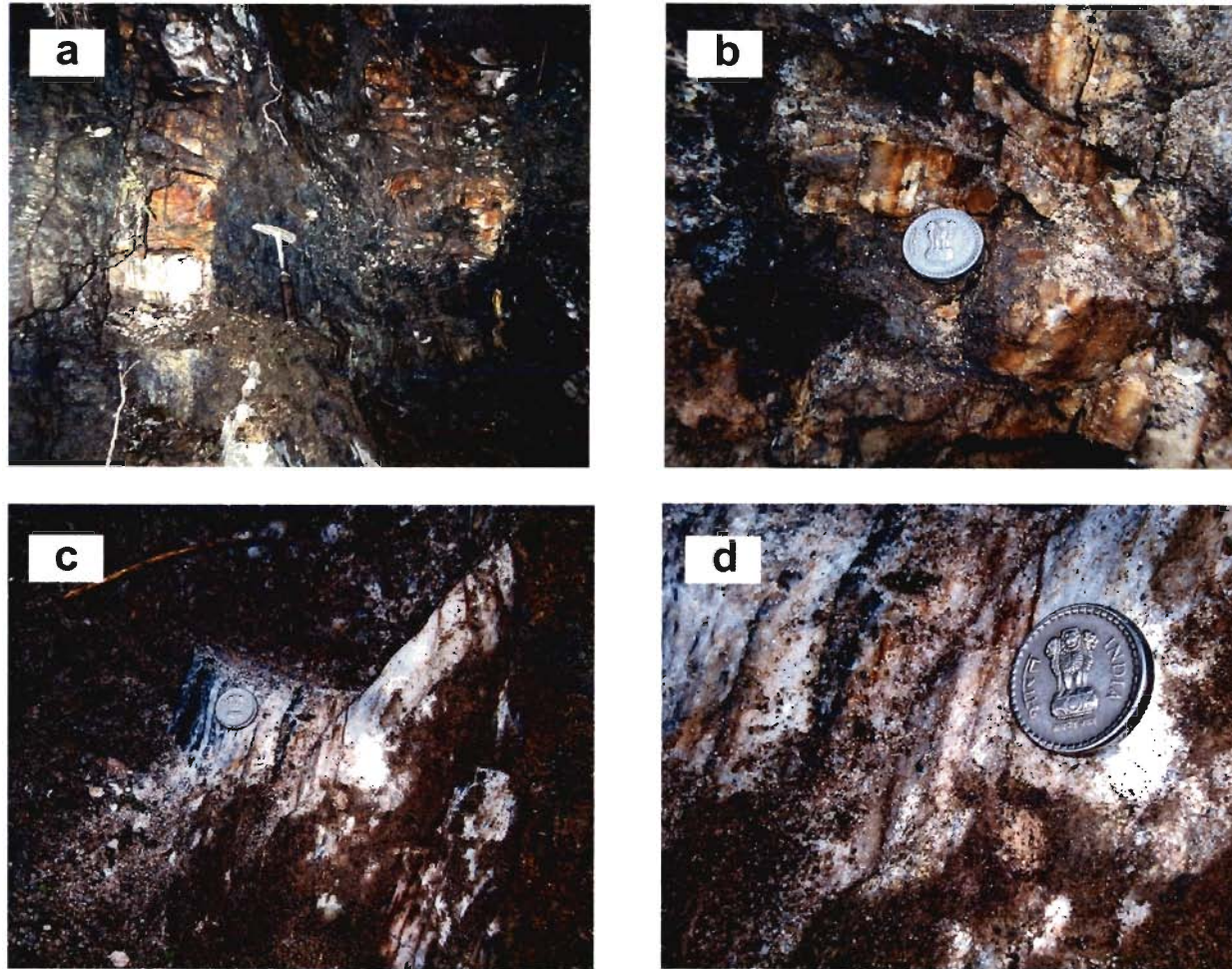


Fig. 2.7 Carbonatite exposures at Beldih. (a) and (b) showing that the exposure is greatly affected by the meteoric water action. (c) Comparatively fresh exposures are found at depth and (d) fresh surface of the carbonatite which is devoid of weathering.

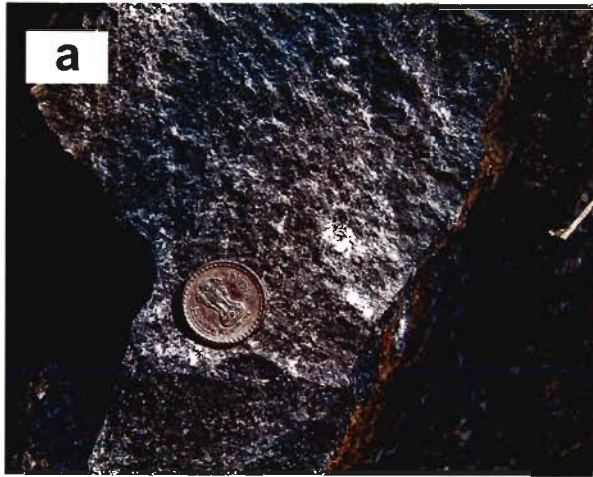


Fig. 2.8 Exposures of alkaline-pyroxenite rocks at Beldih (a & b). The white portion is dominated by the felsic minerals. (c) Contact between carbonatite and alkaline-ultramafic rock in Beldih area.

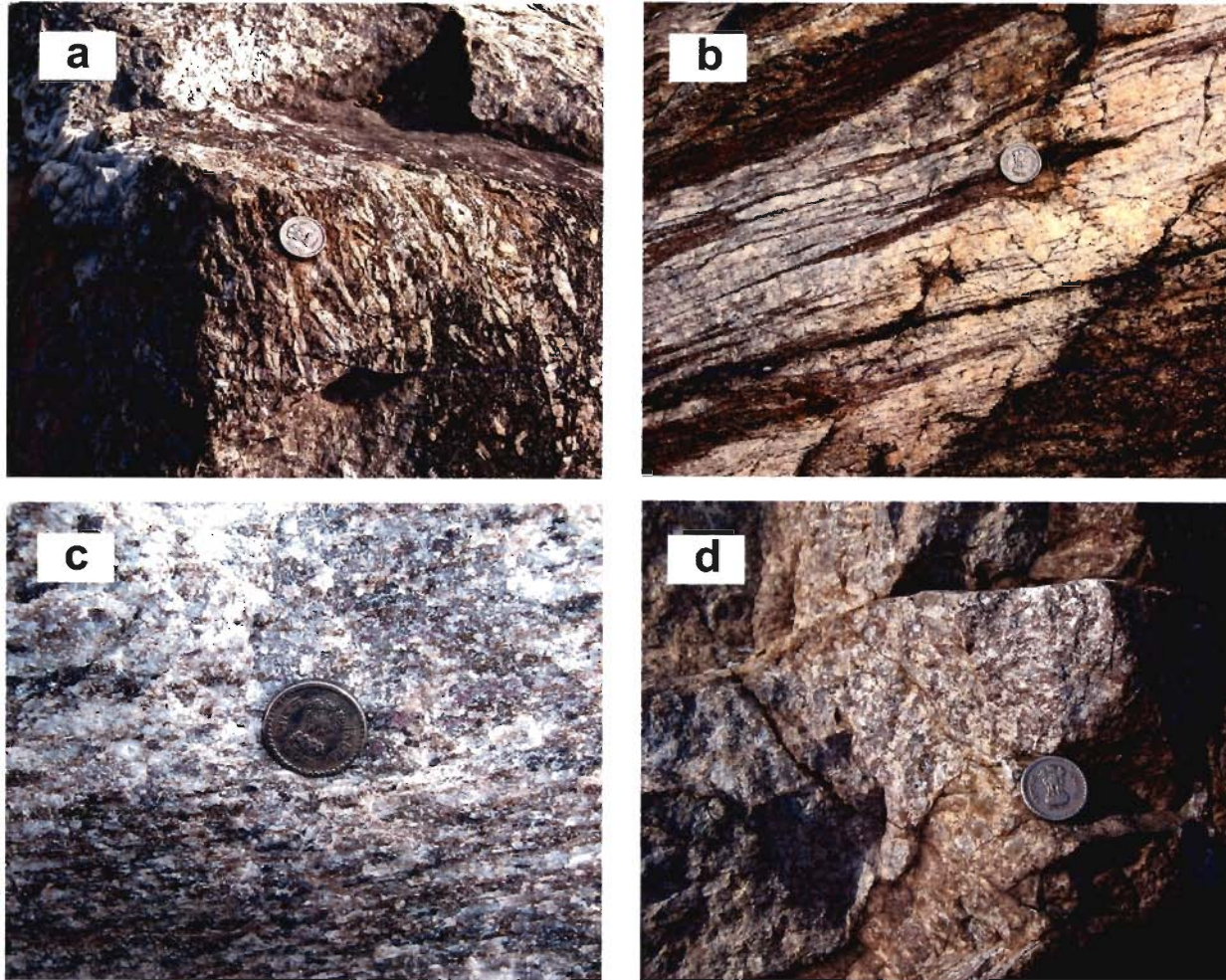


Fig. 2.9 Different varieties of syenite exposed at Sushina Hill. (a) Poorly banded syenite. The large plagioclase laths are visible in the exposure itself. (b) Strongly banded syenite. The banding is made by the alternating bands of mafic and felsic minerals. (c) Pink coloured cancrinite grains are present in the strongly banded variety of syenite. (d) Massive syenite.

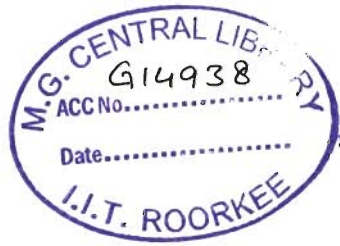
proper mineralogical, geochemical and isotopic data from both Beldih and Sushina areas. The present study aims to reduce this disparity in knowledge by systematic and thorough investigation of these rocks using above approach. In addition, petrogenesis of these rocks can help in a better way in understanding the geodynamic evolution of this part of the Indian shield.

PETROGRAPHY AND MINERALOGY

The rock samples for detailed petrographic studies were collected from two areas: Beldih and Sushina (Fig. 2.5). In Beldih area, the carbonatite is associated with alkali-pyroxenite and apatite-magnetite rocks whereas different varieties of syenite are present in Sushina. Petrographic study of the carbonatite-alkali-pyroxenite association at Beldih is described in the first part of the chapter followed by description of Sushina syenites. The petrographic investigations, based on the study of hand specimen and thin section, were followed up by EPMA studies of carbonatite, alkali-pyroxenite and syenite. During the EPMA examination emphasis has been given on some key minerals including accessory ones e.g. apatite, amphibole, pyroxene etc. The apatite-magnetite rock was omitted for EPMA study as this rock has suffered very extensive surficial alterations. The results of the petrographic studies were subsequently used for choosing samples for further geochemical and geochronological investigations.

3.1 ANALYTICAL TECHNIQUE

The EPMA-WDS analysis was performed on the polished thin sections. The samples were chosen after careful and detailed mineralogical and textural studies. The EPMA study was done using JEOL 8600M Superprobe, at the Institute Instrumentation Centre (IIC), IIT Roorkee, India. Simulated analytical conditions included: 15kV acceleration voltage, 50nA beam current (cup) and point beam mode with 2 μ m probe diameter. Calibration of the instrument was done using well-characterized silicate and oxide standards (multistandard), supplied by SPI Supplies Division of Structure Probe Inc., Canada. Analytical precision of the data was based on replicate analysis of the standards and was much less than $\pm 1\%$. Matrix corrections were performed with the JEOL



8600 ZAF (oxide method) software. During the amphibole analysis the total-Fe is calculated as FeO and later converted into FeO and Fe₂O₃ using AX Mineral End-Member Activity Models as given by Holland and Blundy (1994). The conversions of total FeO to FeO and Fe₂O₃ for pyroxenes were carried out by the formula given by Droop (1987) using PX-NOM spreadsheet programme (Sturm, 2002). Some of the analysis, specially all the apatite analysis, was done using CAMECA SX 100 at the Wadia Institute of Himalayan Geology (WIHG), Dehra Dun. The simulation analytical condition was kept same except the beam size, instead of 2µm; here 1µm probe diameter was used.

3.2 CARBONATITE

The Purulia carbonatite is a light coloured, medium-grained and incipiently banded rock (Fig 3.1a), composed essentially of calcite (Fig. 3.1b) (about 90-95%, by volume) with appreciable amount (about 2-5%, by volume) of apatite (fluor-apatite) (Fig. 3.1b). Other accessories (max. 2-5%, by volume) present are amphibole (Fig. 3.1c-f), phlogopite, biotite, magnetite and ilmenite. Clustering of biotite and phlogopite flakes at places is also observed. Magnetite and ilmenite are evenly distributed throughout the rock. At places, dark green colour bands, continuous or discontinuous, are formed due to higher concentration of ferro-magnesian minerals such as, phlogopite, biotite and amphibole. The rock exhibit mosaic texture (Fig. 3.1b). The chemical composition of the amphibole has been carried out thoroughly. The results are used extensively to infer the petrogenesis of the Purulia carbonatite and described in the later part of this Chapter. The detailed results of mineralogical studies are described below:

Calcite: The carbonate species in the Purulia carbonatite is calcite which is characterized by the presence of perfect rhombohedral cleavage. In thin sections it is colourless and appears to be cloudy with pearl grey to first order grey interference colour. These are also

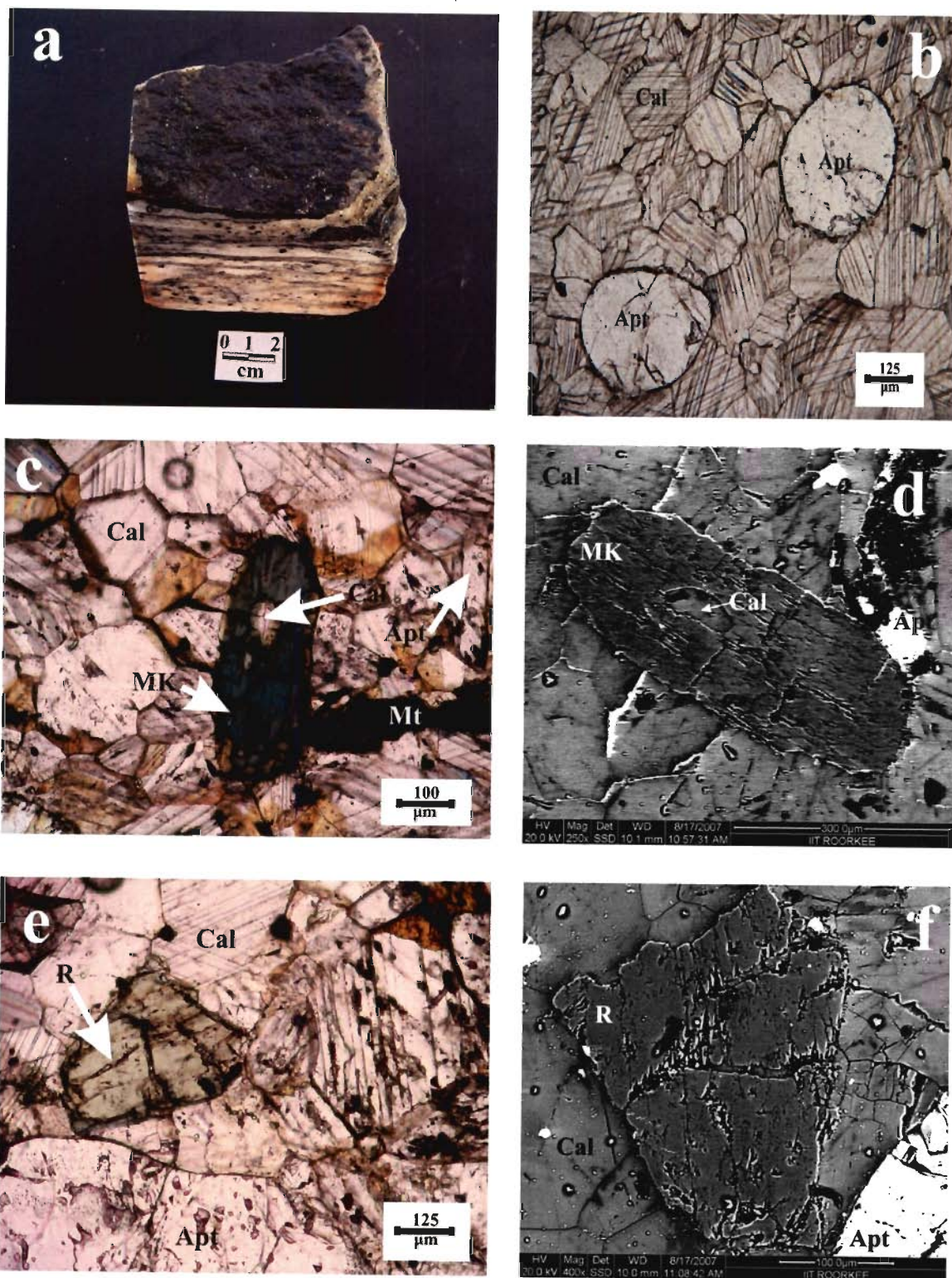


Figure 3.1 (a) Hand specimen of the Purulia Carbonatite. (b) Apatite within calcite matrix. Calcite grains are defining the mosaic texture of carbonatite. (c) Well developed subhedral crystal of magnesiokatophorite in polygonal calcitic matrix along with apatite and magnetite. (d) BSE image of magnesiokatophorite with calcite inclusion within calcitic matrix. (e) Richterite in polygonal calcitic matrix. (f) BSE image of richterite within calcite matrix which is highly fractured.

(MK: Magnesiokatophorite; R: Richterite; Cal: Calcite; Apt: Apatite and Magnetite: Mt)

characterized by the occurrence of prominent polysynthetic twinning. The twin lamellae are mostly parallel to the long diagonal direction, but the oblique intersections have also been observed. The calcite grains are mostly polygonal in shape (Fig. 3.1b). The calcite is found to be almost pure (Table 3.1a) with small amount of FeO (0.30-1.3%), MgO (0.28-1.13%) and MnO (0.14-0.44%), together constituting about 1-3.0 wt%. Random check shows that the Sr-content of the calcite is about 0.8-1.0%.

Apatite: The apatite grains are colourless with higher relief compared to the calcite. They are the second abundant mineral after calcite. These are mostly subhedral (Fig. 3.1b) and elliptical in shape with parallel extinction. The grains are identified by its parallel extinction with second order grey interference colour. EPMA study of apatite grains reveal that these are mostly fluor-apatite (Table 3.2) variety. The P₂O₅ content is very consistent (~41%) along with CaO (~53%) in apatite. The CaO and P₂O₅ together constitute about 95% of the major oxides. Random analysis for F in few apatite grains reveals high F content (2.5 to 4.5%). A special emphasis has been given to study trace element composition of apatite grains and the results are presented in the next chapter (Chapter 4).

Magnetite and Ilmenite: Opaques are mostly ilmenite and evenly distributed throughout the rock. The ilmenite contains very small quantity of MgO and MnO, the two constituents making upto 1.5-2.0 wt%. Overall MgO:MnO ratio calculates at about 2:1 (Table 3.1b). In addition to ilmenite magnetite is also present. As the magnetite crystals are mostly altered to hematite due to surficial alterations, detailed EPMA study was not carried out on them.

Amphibole: The amount of amphibole in carbonatite rarely exceeds 1-2%, by volume, but it can easily be distinguished by the green colour in a white calcite matrix. Detailed mineralogical study allows division of the amphibole into two groups: (1) dark green variety (Fig. 3.1c) with pleochroism into dark brown. Its BSE image (Fig. 3.1d) shows

absence of zoning but presence of the inclusions of the apatite and the calcite and (2) light green amphibole (Fig. 3.1e) with pale-green to light green pleochroism. The BSE image of this type of amphibole (Fig. 3.1f) is marked by the presence of relatively fewer inclusions. The first variety of amphibole is coarser and more crystalline compared to the second one. Both varieties of amphibole, however, show extinction angle between 20° to 35° . Presence of corroded boundary of both the types of amphibole crystals is suggestive of possible post-crystallization reaction with the carbonate melt.

Members of the amphibole family are represented by a common formula $A_0-1B_2^{VI}C_5^{IV}T_8O_{22}(OH)_2$. The nomenclature and cationic distribution of this mineral group is carried out as per recommendation of IMA (Leake, 1978, Leake, et al., 1997, 2004). Three varieties of amphibole – calcic, sodic-calcic and sodic, are generally reported from carbonatite and a comprehensive review of their mineralogy and the composition of these is given by Hogarth (1989). Pioneer work on amphibole from carbonatite was, however, carried out by Bulakh (1965), Samoylov et al., (1974), Samoylov & Gormasheva (1975), Samoylov (1977), Fabriés (1978) and Kapustin (1980). Giret, et al., (1980) and Mitchel (1990) have also affirmed that there are marked compositional variations among the minerals of amphibole group that are present in different types of alkaline rocks.

The amphibole composition of the Purulia carbonatite (Table 3.3) falls within the broad group of sodic-calcic amphibole. This group is defined as monoclinic amphibole with $(Ca+Na)_B \geq 1.00$ and $0.50 < Na_B < 1.50$ and further classified into two sub categories: $(Na+K)_A > 0.50$ and $(Na+K)_A < 0.50$ based on $(Na+K)$ in A site i.e. $(Na+K)_A$. The amphibole composition of the Purulia carbonatite in a $ivSi-Mg/(Mg+Fe^{2+})$ plot (Leake, 1997) falls in the first group (Fig.3.2) and is represented by magnesiokatophorite (Fig.3.1c,d) and richterite (Fig.3.1e,f) varieties. The magnesiokatophorite variety with dark green to dark

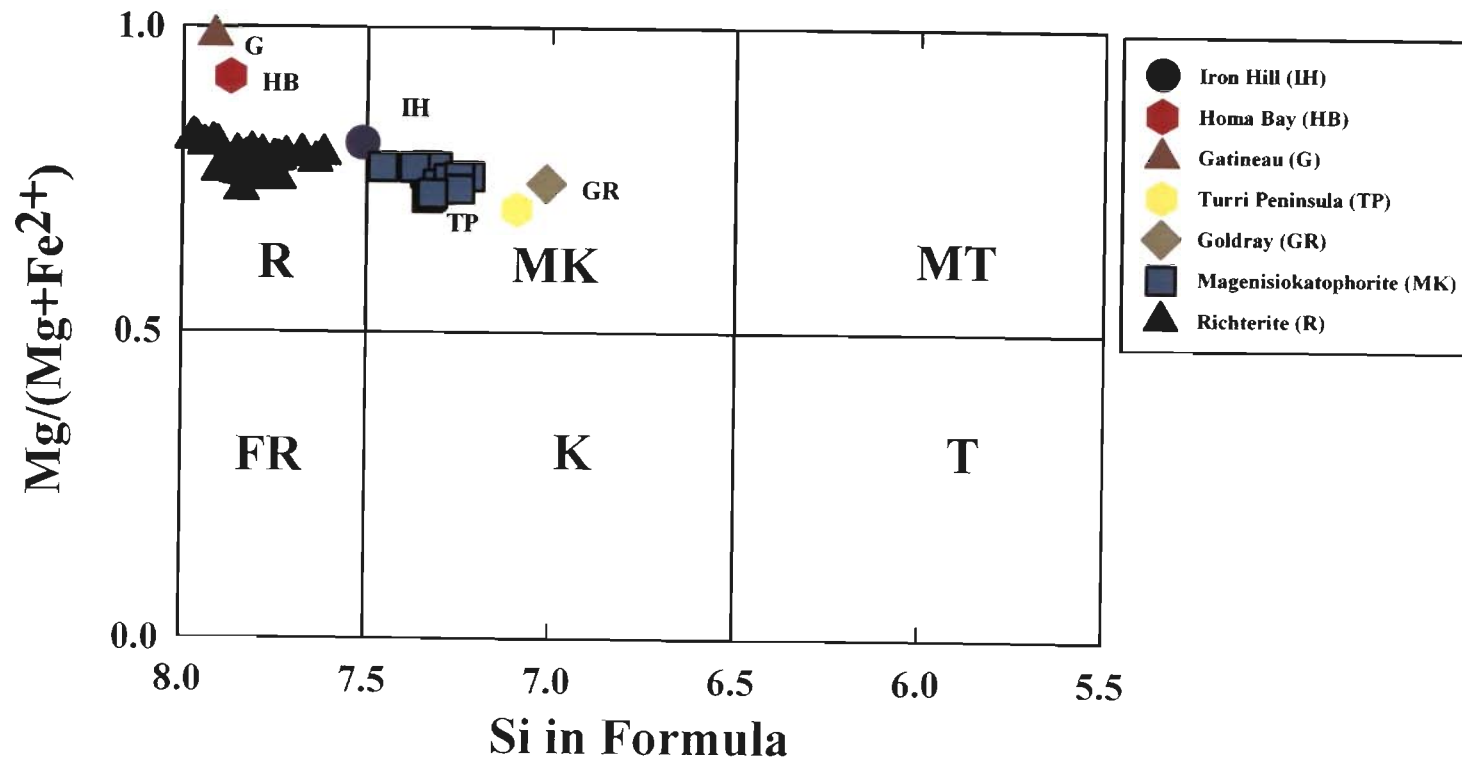


Figure 3.2 Classification of the sodic-calcic amphiboles from carbonatite as per IMA norm (Leake et al., 1997). Diagram parameters: $(Na+K)_A \geq 0.50$; $(Ca+Na_B) \geq 1.00$; $0.50 < Na_B < 1.50$. R – Richterite, MK – Magnesiokatophorite, MT – Magnesio-taramite, FR – Ferro-richterite, K – Katophorite, T – Taramite. Composition of amphiboles from Purulia carbonatite falls in R and MK fields. Amphibole composition (Hogarth, 1989) from Iron Hill (IH), Colorado; Gatineau, Quebec; Homa Bay (HB), Kenya; Turri peninsula (TP), Russia and Goldray (GR), Ontario are also plotted for the comparison with the studied amphibole.

brown pleochroism is more crystalline and in general smaller in size. Richterite grains with greenish to pale greenish pleochroism are subhedral in nature and shows clear evidence of reaction with the surrounding calcite crystals. Reaction between magnesiokatophorite grains with calcite is comparatively less pronounced.

EPMA study reveals a minor but distinctive difference in chemical composition of the two mineralogical varieties of amphibole. Compared to richterite, the magnesiokatophorite is relatively SiO₂ (49.4-51.9%), MgO (14.9-15.8%) poor, but enriched in Al₂O₃ (3.4-4.3%), TiO₂ (0.66-0.42%) and CaO (5.0-5.5%). The reverse trend is, however, noticed in the richterite variety, which is characterized by relatively higher SiO₂ (52.7-55.1%) and MgO (15.7-17.2%) but low values of Al₂O₃ (1.3-2.1%), CaO (3.4-3.7%) and TiO₂ (0.09-0.50%). The total iron, as FeO, does not show any significant variation. The amounts of Na₂O and K₂O are very much similar in both the varieties ranging from 6.9 to 8.1% and 0.42 to 0.66% respectively. The total alkali (Na₂O+K₂O) content is, nevertheless, slightly higher in richterite. As mentioned earlier that the amphibole composition of the Purulia carbonatite is sodic-calcic, represented by the magnesiokatophorite (Fig. 3.1c,d) and richterite (Fig. 3.1d,e) varieties (Fig. 3.2), which are in parity to other well known carbonatite complexes of the world such as Iron Hill (IH), Colorado; Gatineau (G), Quebec; Homa Bay (HB), Kenya; Turii Peninsula (TP), Russia and Goldray (GR), Ontario (Hogarth, 1989). Moreover, it is also low-Al amphibole (Fig.3.3a) when plotted in a $v_1R^{3+}-R^++R^{2+}$ diagram (Fabriés, 1978). Similarly, the amphibole compositions in the (Ca+_{IV}Al)–(Si+Na+K) plot (Fabriés, 1978) falls between richterite and magnesiokatophorite lying in low-Al amphibole field (Fig.3.3b). Thus the middle to late stage formation of the Purulia carbonatite in hypabyssal condition is evidenced by the presence of low Al-amphibole, magnetite as a common accessory mineral (Kapustin, 1973) and further supported by mode of occurrence

as dyke and its texture. More elaborate interpretation based on amphibole composition is presented in Chapter 6 i.e. Discussions.

3.3 ALKALI-PYROXENITE

Alkali-pyroxenite is a dark coloured medium grained rock, juxtaposed with the carbonatite dyke. In the first look it appears to be an ultramafic rock containing only ferro-magnesian minerals (Fig. 3.4a) which at later stage transected by numerous light coloured veins. The dark coloured minerals are clinopyroxene, alkali-amphibole and biotite. The light coloured ones, mostly of secondary origin and vein-filling within the parent alkali-pyroxenite, are calcite, apatite and albite (Fig. 3.4b-f). The rock shows hypidiomorphic texture and consists primarily of subhedral clinopyroxene (Fig. 3.4b) with rare euhedral primary amphibole (Amph-I) characterized by two sets of cleavage at 120° angle (Fig. 3.4c). The secondary amphibole (Amph-II), altered from pyroxene, is common and constitute more than two-third of the bulk mineralogy. The biotitization of primary alkali-pyroxene is prominent and biotites flakes can be identified very easily even in the hand specimen (Fig. 3.4a). The calcite (euhedral to subhedral) and apatite (subhedral) grains within the vein-fillings showing mosaic texture. The minerals, dominated by calcite, apatite and albite, were introduced at later stage into the system and paragenetically secondary in nature. The rock was originally alkali-pyroxenite, which was later affected by alkali-metasomatism during the carbonatite injection. Depending on the mineral paragenesis, three distinct assemblages: primary (orthomagmatic), secondary (altered) and vein-fillings, are observed and described below. The primary mineral assemblages referred the minerals that are formed during magmatic process and thus can also be termed as orthomagmatic mineral assemblage. On the other hand the post

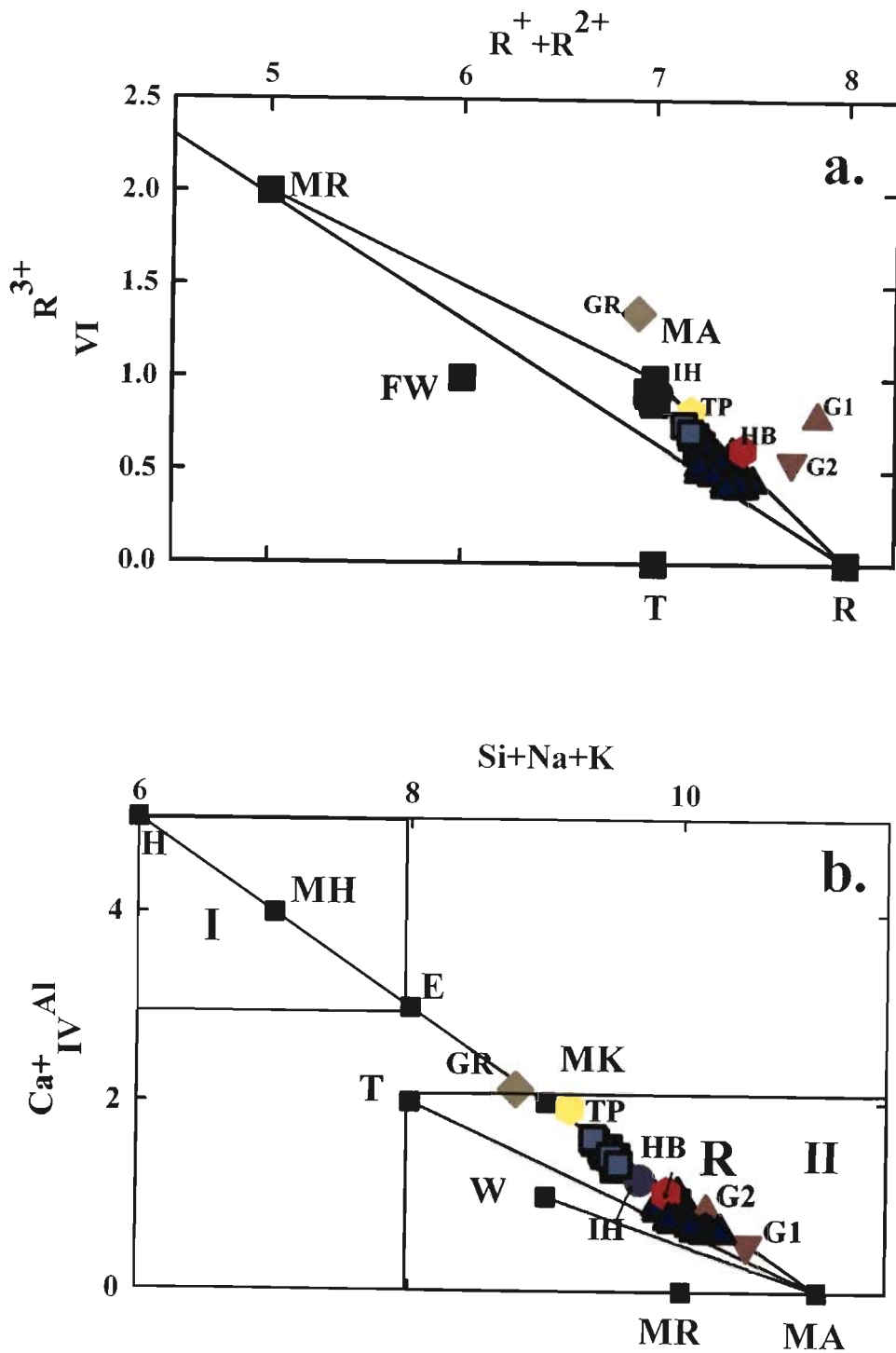


Figure 3.3 (a) $VI R^{3+}$ v $R^{+} + R^{2+}$ plot of low-Al amphiboles (Hogarth, 1989) from Purulia carbonatite. Composition of the amphibole from the study area cluster between MA and R. (b) $Ca + IVAl$ v. $Si + Na + K$ plot of amphiboles (Fabries, 1978) from the Purulia carbonatite. Composition of amphibole from the study area falls on the line joining R and MK. MR – Magnesio-riebeckite, MA – Magnesio-arfvedsonite, R – Richterite, T – Tremolite, FW – Ferri-winchite, H – Hal, MH – Magnesio-hastingsite, E – Edenite, MK – Magnesiokatophorite, R – Richterite, W – Winchite, T – Tremolite, I – High Al field, II – Low Al field. Symbols used for the other reported amphibole composition (Hogarth, 1989) as in the Figure 3.2 except for G1 and G2 representing Gatineau, Quebec.

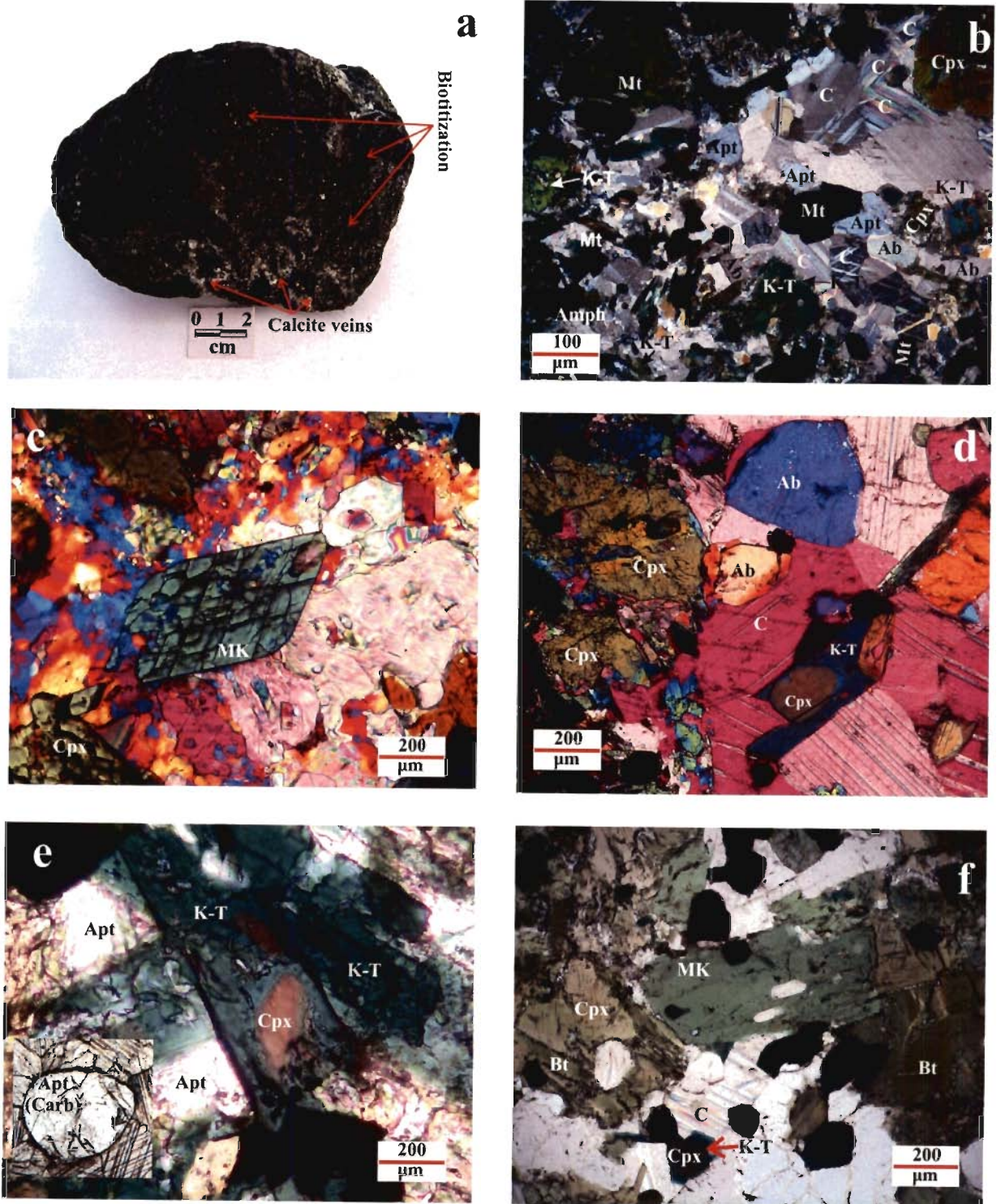


Fig. 3.4 (a) Altered alkali-pyroxenite with calcite veins. (b) A part of the calcite vein along with other mineral constituents. (c) Primary magmatic amphibole (Amph-I) represented by magnesiokatophorite (d) Subhedral to euhedral crystals of calcite within calcite veins. (e) Development of dark green amphibole (Amph-II) at the expense of brown pyroxene. (Inset: Apatite within carbonatite) (f) Alteration of pyroxene to biotite.

(MK: Magnesiokatophorite; K-T: Katophorite Taramite; Ab: Albite; Bt: Biotite; Cpx: Clinopyroxene; C: Calcite; Apt: Apatite and Mt: Magnetite)

magmatic alteration of primary minerals give rise to secondary mineral assemblage as evidenced by the alteration of pyroxene to amphibole (Amph-II) and to biotite. As described above this rock is intersected by numerous late stage apatite-calcite veins, albite these are termed here as vein-filling mineral assemblage as the textural evidences points that these minerals were formed at the last stage of postmagmatic alteration probably by the fluid expelled out from the associated carbonatite.

3.3.1 PRIMARY MINERAL ASSEMBLAGES

Pyroxene: The pyroxene grains are euhedral to subhedral in shape and at places pristine prismatic crystals are still preserved (Fig. 3.4b,d). It shows lemon green to yellow pleochroism with extinction angle lying between 14° to 40° and higher order interference colour. Majority of the pyroxene grains have undergone post crystallization alteration, evident by the corroded margins and replacement by the alkali-amphibole along the grain boundaries and fractures. The pyroxene grains are composed of SiO_2 (53.58-53.92%), Al_2O_3 (1.70-1.91%), FeO (12.01-13.42%), CaO (16.22-17.27%), MgO (7.64-8.08%) and appreciable amount of Na_2O (3.96-4.43%) and diopsidic in composition. In the present study, the scheme given by Larsen (1976) has been adopted for the classification and nomenclature which is normally followed for the pyroxenes from the alkaline rocks (Mitchell, 1980) (Table 3.4). In terms of the three end-member system i.e. Ac (Acmite)-Hedenbergite (Hd)-Diopside (Di), the representative pyroxenes are quite evolved and mostly in $\text{Ac}_{34.42-37.29}\text{-Hd}_{12.67-13.32}\text{-Di}_{52.91-49.39}$ in composition (Table 3.4). Similar observations have also been reported from many other alkaline complexes (Fig. 3.5). The pyroxene here follows the acmite compositional trend similar to the pyroxene from melane-pheline syenites at Turja (Mitchell, 1980).

Amphibole (Amph-I): The primary amphibole (Amph-I) grains are euhedral in shape (Fig. 3.4c) and characterized by pale green to dark brown pleochroism. Composition of this variety of amphibole (Fig. 3.4c) is shown in Table 3.5 and it is magnesiokatophorite in a Si-Mg/(Mg+Fe²⁺) plot (Fig. 3.6) (Leake et al. 1997). This amphibole is found to be low-Al type when plotted in a R^{3+VI}-R⁺+R²⁺ (Fig. 3.7a) and Ca+Al^{IV}-Si+Na+K (Fig. 3.7b) diagrams (Fabriés, 1978). This type of amphibole is similar to that of the magnesiokatophorite reported from the associated carbonatite (Chakrabarty et al. 2009).

3.3.2 SECONDARY MINERAL ASSEMBLAGES

The secondary mineral assemblages are mainly dominated by the amphibole and biotite along with other vein filling minerals like calcite, apatite, albite and magnetite-ilmenite. The vein filling minerals are similar to that of the associated carbonatite dyke which is dominantly composed of calcite (> 90%, by volume) and fluor-apatite (2-5% by volume) with amphibole, phlogopite, biotite, magnetite, ilmenite as other accessory minerals (Chakrabarty et al. 2009).

I. Altered minerals

Amphibole (Amph-II): This variety amphibole is dark green in colour (Fig. 3.4b,e). Both the grain size and shape, is highly variable. The Amph-II is clearly distinguished with Amph-I by relatively low SiO₂, MgO and TiO₂ and higher Al₂O₃ and FeO contents (Table 3.5). The Si-Mg/(Mg+Fe²⁺) plot (Fig. 3.6) (Leake et al., 1997) characterizes Amph-II as katophorite/taramite (Fig. 3.4e) and lying in the low-Al amphibole field (Fig. 3.7a) but leading towards the high-Al amphibole (Fig. 3.7b). Moreover such a high Al₂O₃ content of katophorite/taramite is very unusual and only found in schists like gedrite, aluminotschermakite (Deer et al., 1992). Thus the role of metasomatism can only be the possible cause for such a high-Al₂O₃ katophorite/taramite. The composition Amph-II is sodic-calcic

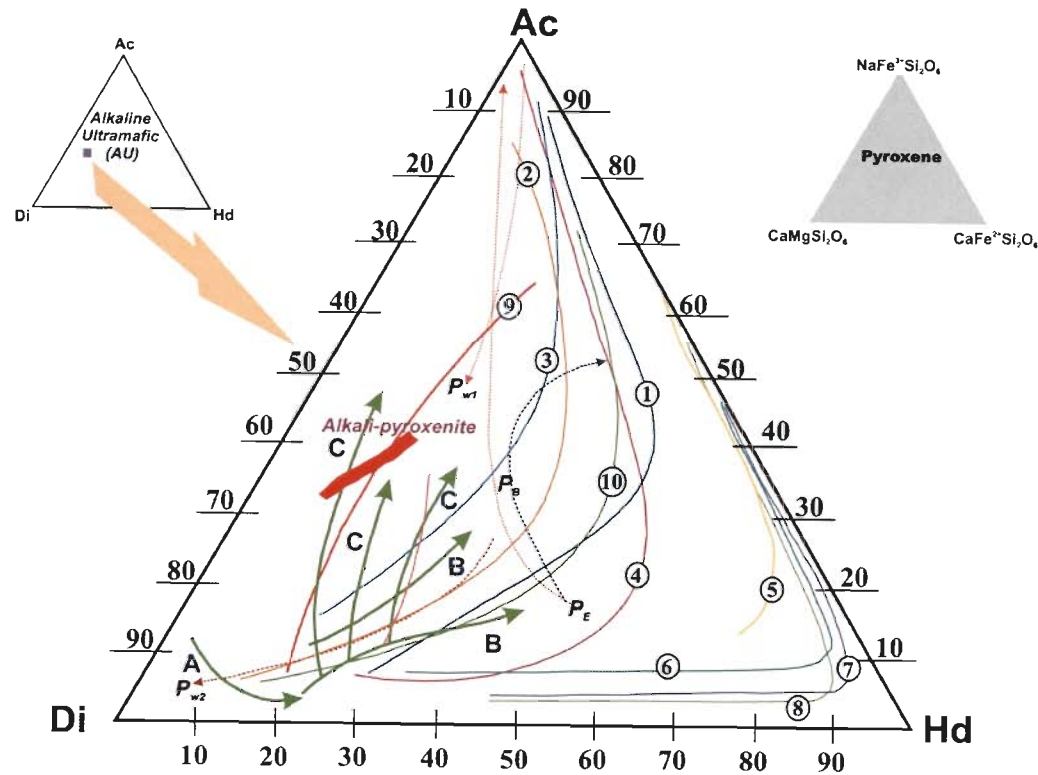


Fig. 3.5 Composition of the pyroxene (Alkali-pyroxenite: thick red line) from alkali-pyroxenite of the study area compared with pyroxene compositional trends of different alkaline rocks (Mitchell, 1980). A. Fen, damkjernite-vibetoite trend; B. Fen, acmite-hedenbergite trend; C. Fen, acmite trend; 1, Morotu (Yagi, 1953); 2, Uganda (Tyler and King, 1967); 3, Itapirapua (Gomes et al., 1970); 4, South Qôroq (Stephenson, 1972); 5, Pantellerite (Nicholls and Carmichael, 1969); 6, Nandewar (Abbott, 1969); 7, Illimaussaq (Larsen, 1976); 8, Coldwell Complex (Mitchell and Platt, 1978); 9, Turja (Mitchell unpublished data); 10, Iron Hill (Nash, 1972); P_{W1} , P_{W2} , P_E and P_B are Alnö trends for the western, eastern and Barang sectors respectively (Morogan and Woolley, 1988).

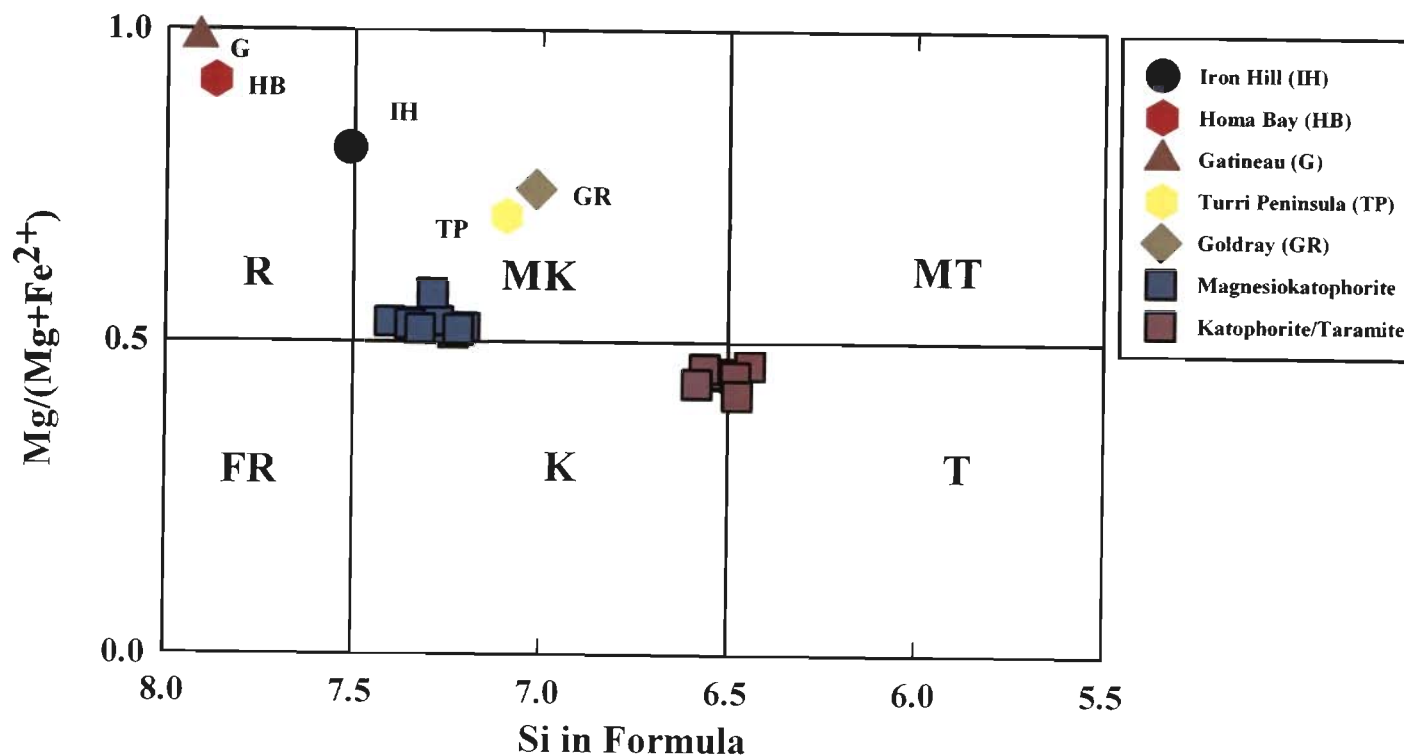


Figure 3.6 Classification of sodic-calcic amphiboles from alkaline-ultramafic rock as per IMA norm (Leake et al., 1997). Diagram parameters: $(Na+K)_A \geq 0.50$; $(Ca+Na_B) \geq 1.00$; $0.50 < Na_B < 1.50$. R – Richterite, MK – Magnesiokatophorite, MT – Magnesio-taramite, FR – Ferro-richterite, K – Katophorite, T – Taramite. Composition of amphiboles from Purulia carbonatite falls in R and MK fields. Amphibole composition (Hogarth, 1989) from Iron Hill (IH), Colorado; Gatineau, Quebec; Homa Bay (HB), Kenya; Turri peninsula (TP), Russia and Goldray (GR), Ontario are also plotted for the comparison with the studied amphibole.

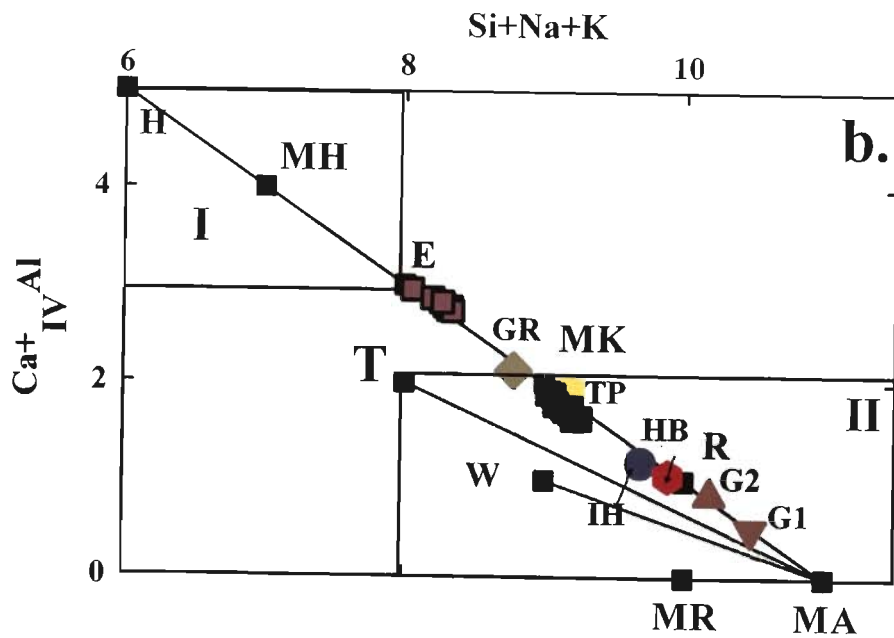
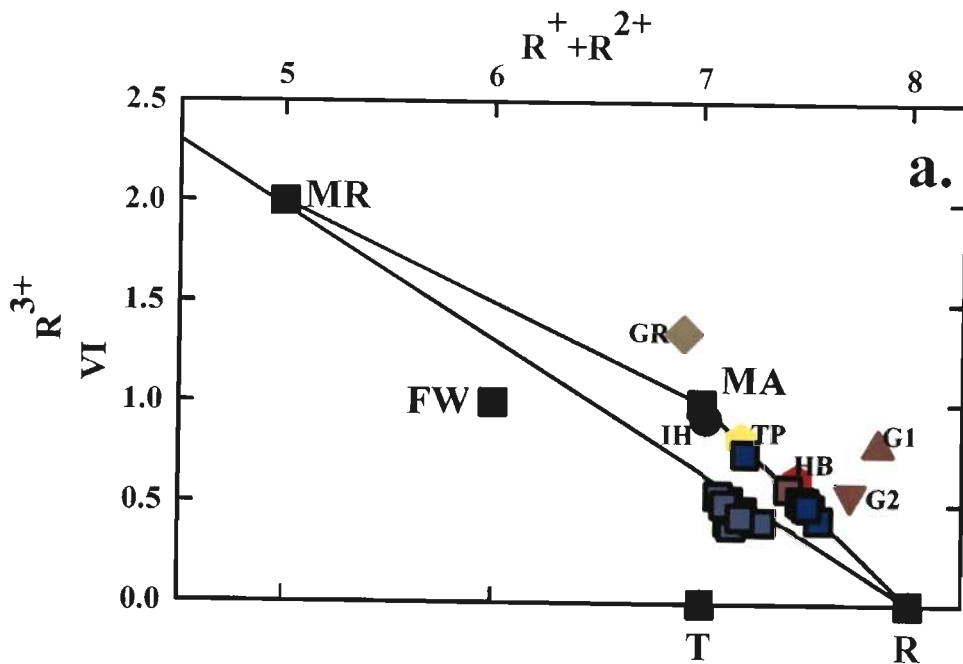


Figure 3.7 (a) $VI R^{3+}$ v $R^{3+} + R^{2+}$ plot of low-Al amphiboles (Hogarth, 1989) from alkaline-ultramafic rock. Composition of these amphiboles cluster between MA and E i.e. they are moving from low-Al to high-Al field (b) $Ca + IV Al$ v. $Si + Na + K$ plot of amphiboles (Fabries, 1978) from the Purulia carbonatite. Composition of amphibole from the study area falls on the line joining R and MK. MR – Magnesio-riebeckite, MA – Magnesio-arfvedsonite, R – Richterite, T – Tremolite, FW – Ferri-winchite, H – Hal, MH – Magnesio-hastingsite, E – Edenite, MK – Magnesiokataphorite, R – Richterite, W – Winchite, T – Tremolite, I – High Al field, II – Low Al field. Symbols used for the other reported amphibole composition (Hogarth, 1989) as in the Figure 3.2 except for G1 and G2 representing Gatineau, Quebec.

and controlled by the parent clinopyroxene which is made up of diopside-hedenbergite with approximately 35% acmite-component (Table 3.4).

Biotite: Biotite grains are highly altered and irregular in shape (Fig. 3.4f). They are identified in the hand specimen by their typical reddish brown colour. In thin section they are showing yellowish brown to brown pleochroism with higher order interference colour and sometimes second order red interference colour in highly altered grain. Extinction angle is highly variable as some of the grains are showing straight extinction whereas majority is characterized by mottled extinction with a crinkly effect typical of biotite. The composition of biotite is shown in Table 3.6. Most of the analyzed grains are falling within the biotite grains with two very close to the biotite-phlogopite boundary (Fig. 3.8). Higher concentration of Fe^{2+} relative to Mg indicates late magmatic or alteration phenomenon was responsible for these biotite formations.

II. Vein-filling minerals

Feldspar: Subhedral to euhedral shaped feldspars are present along the white coloured vein (Fig. 3.4d) in the rock. These grains are colourless under plane polarized light but under crossed polar they are showing polysynthetic twining of albite type. These plagioclase grains are showing first order grey interference colour. The grain size is highly variable. Chemically these are pure albite with average composition of $\text{Ab}_{99.05}\text{Or}_{0.12}\text{An}_{0.83}$ (Fig. 3.9; Table 3.7).

Calcite: Calcite grains colourless and appear to be cloudy with pearl grey to first order grey interference colour (Fig. 3.4b, d). They are also characterized by the prominent polysynthetic twining and the twin lamellae are mostly parallel to the long diagonal, but they also intersected obliquely. The calcite grains are subhedral to euhedral, in shape. The

chemical composition of calcite grains, both from the veins and the adjacent carbonatite dike, is similar (Table 3.8).

Apatite: The apatite grains are anhedral in shape with cloudy appearance and identified by its parallel extinction with second order grey interference colour (Fig. 3.4b). The apatite crystals from the adjacent carbonatite are subhedral and relatively larger in size. The composition of apatite is given in Table 3.7. The random checks show presence of 2.5-3.0 wt.% F in apatite. More details on apatites are discussed in the Chapter 4 (see section 4.6.4).

Ilmenite and Magnetite: These two minerals are common in the vein-filling. The ilmenite and magnetite can be distinguished by dark brown and black colours respectively. Ilmenite crystals, at places, alter to yellowish leucosene (?). Composition of these minerals is given in Table 3.9. It may be noted that ilmenite is MnO (3.2-3.7 wt.%) rich and on the other hand TiO₂ content of magnetite is very low (<0.5 wt.%) indicating low-temperature hydrothermal assemblage.

The overall mineralogy indicates a mixed composition of the rock which has undergone alkali-metasomatism, evident by its texture and composition. Presence of alkali-pyroxene, alkali-amphibole, albite and biotite points towards a mixed composition for this rock. The evidence of biotitization and formation of albite is a strong indication of intense alkali-metasomatism which this rock has suffered (Kapustin, 1980) probably during carbonatite intrusion. Such alkali-metasomatism of the country rock associated with carbonatite intrusion is commonly known as fenitization. In this case the effect of metasomatism is only noticed in the alkali-pyroxenite, not within the country rock and hence the term 'metasomatism' is more appropriate than fenitization. Such alkali metasomatism resulted enrichment of alkalis (Na+K) and alumina as evidenced by the

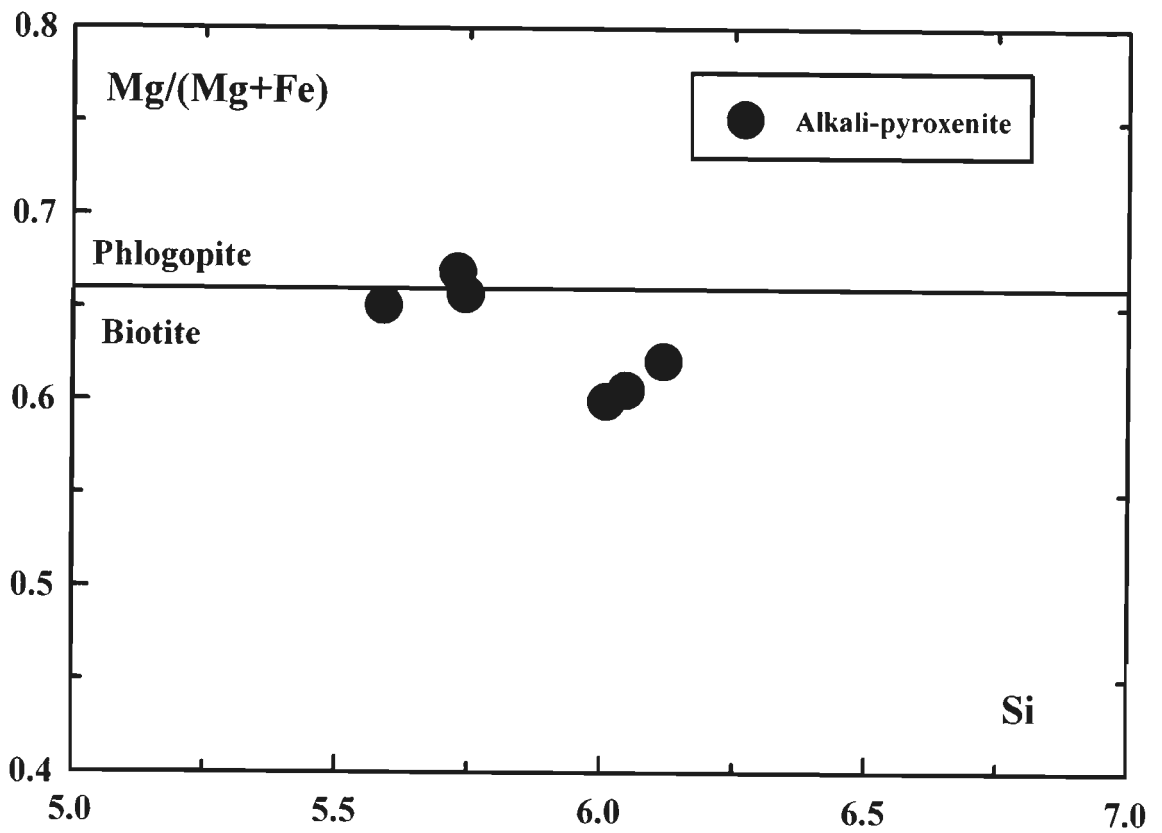


Fig. 3.8 Classification diagram for micas (apfu) from alkali-pyroxenite, after Rieder et al. (1998). Most of the analyzed grains are falling well within the biotite field while only three are plotted close to the biotite-phlogopite boundary.

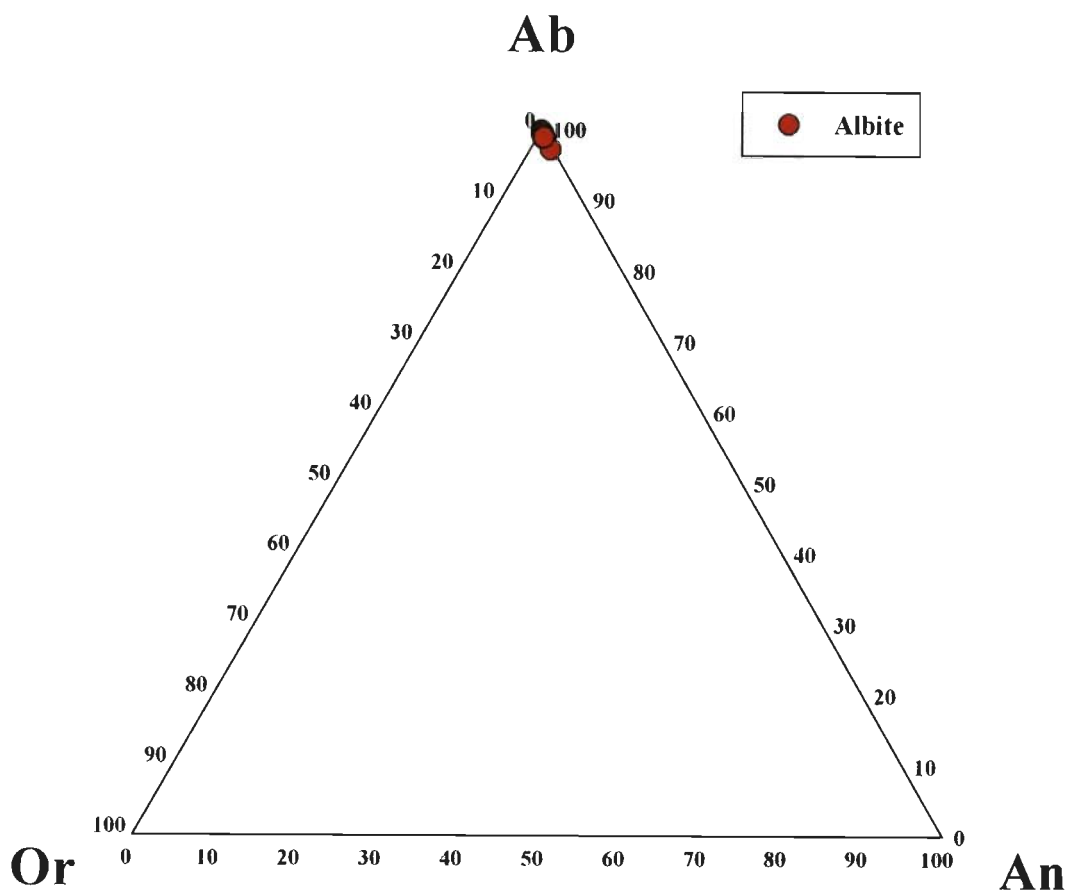


Fig. 3.9 Composition of plagioclase feldspar from alkaline-pyroxenite. The feldspars are found to be pure albite and developed during fenitization or alkali-metasomatism.

late stage formation of biotite, albite, Al-rich amphibole (Amph-II) in the original alkali-pyroxenite and also lost most of its original magmatic texture and structure.

3.4 APATITE MAGNETITE ROCK

A strike length of about 300meters of apatite bearing rocks has been proved with a maximum width of about 58meters tapering towards east and west in the Beldih area. Numbers of apatite-magnetite lenses of variable dimensions have been reported along NSZ. These lenses are intruded within the country rock represented by mica schist, calc-silicate, metabasite, quartzite and biotite gneiss which are often sheared. Clayey alterations around the apatite-magnetite lenses are very common. In general composite lenses of apatite-magnetite with several offshoots and stringers are separated by phyllite partings varying in thickness from 1 to 12 meters. These offshoots and stringers run for some distance either north or south of the main ore body. The rock is light colored (Fig. 3.10a) and dominantly composed of apatite (Fig. 3.10b). Surficial alterations have severely affected the apatite crystals. However, at places remnant apatite grains under microscope are colorless and showing parallel extinction with imperfect basal cleavage which appears to be cross fractured (Fig. 3.10c). The shape of the apatite crystals or pseudomorphs is highly variable from elliptical to hexagonal prismatic (Fig. 3.10b). At places marginal overgrowth of the apatite grains are marked yellow colour under the microscope. Other than apatite and magnetite some silicate phase is also noticed within the rock (Fig. 3.10d). In Beldih area, the apatite-magnetite rock is extensively affected by the surficial alterations due to meteoric water action. In many places the meteoric water reacted and subsequently dissolved the apatite grains. Further, there are evidences of re-precipitation of secondary apatite giving rise to colloform texture (Fig. 3.10d). As this rock has undergone severe alteration as mentioned above, it is therefore not considered for further chemical analysis as well as for isotopic studies.

3.5 NEPHELINE SYENITE

The exposures of nepheline syenite have been found in Sushina hill, lying about 40Km east of the Beldih village. Two varieties of nepheline syenite were identified in the field namely: a) banded syenite and b) massive syenite and is shown in the lithological map (Fig. 3.11). Most of the mapped area is covered by banded syenite while the southern part is covered by almost pure massive variety. The banded varieties of syenites are foliated and characterized by the alternating banding of mafic and felsic minerals (described in details below) and hence it is more appropriate to termed them as *nepheline syenite gneisses* or *nepheline gneisses* as described and reported by the many other workers across the world e.g. Blue Mountain Complex, Methuen Township and Bigwood Complex (Sudbury) of Canada (Duke and Edgar, 1977). Banded syenite can further be divided in to two subgroups: poorly banded syenite gneiss and strongly banded syenite gneiss. The banding is very prominent in the central part of the mapped area which is flanked by poorly banded syenite. The poorly banded syenite gneiss is characterized by the presence of large lath shaped plagioclase grain and the banding is not continuous or persistent throughout the rock. On the other hand the strongly banded syenite gneiss is showing prominent alternating banding of mafic and felsic minerals. The massive syenite is devoid of planar structure like banding and dominantly consists of orthoclase. In general the banded variety is dominant over the massive syenite. The exposures of syenites are dispersed over an area of about 1500 square meters but the contact with the invaded rock is not exposed. During field investigation and sample collection, the whole area was divided into ten 15m×10m grids each covering approximately 150 m² aerial extents (Fig. 3.11). About one hundred samples in total were collected from all the grids. After careful examination with the naked eye, fresh samples were chosen initially for microscopic studies followed by EPMA and subsequently for the geochemical and isotopic studies. The different varieties of syenite are described below.

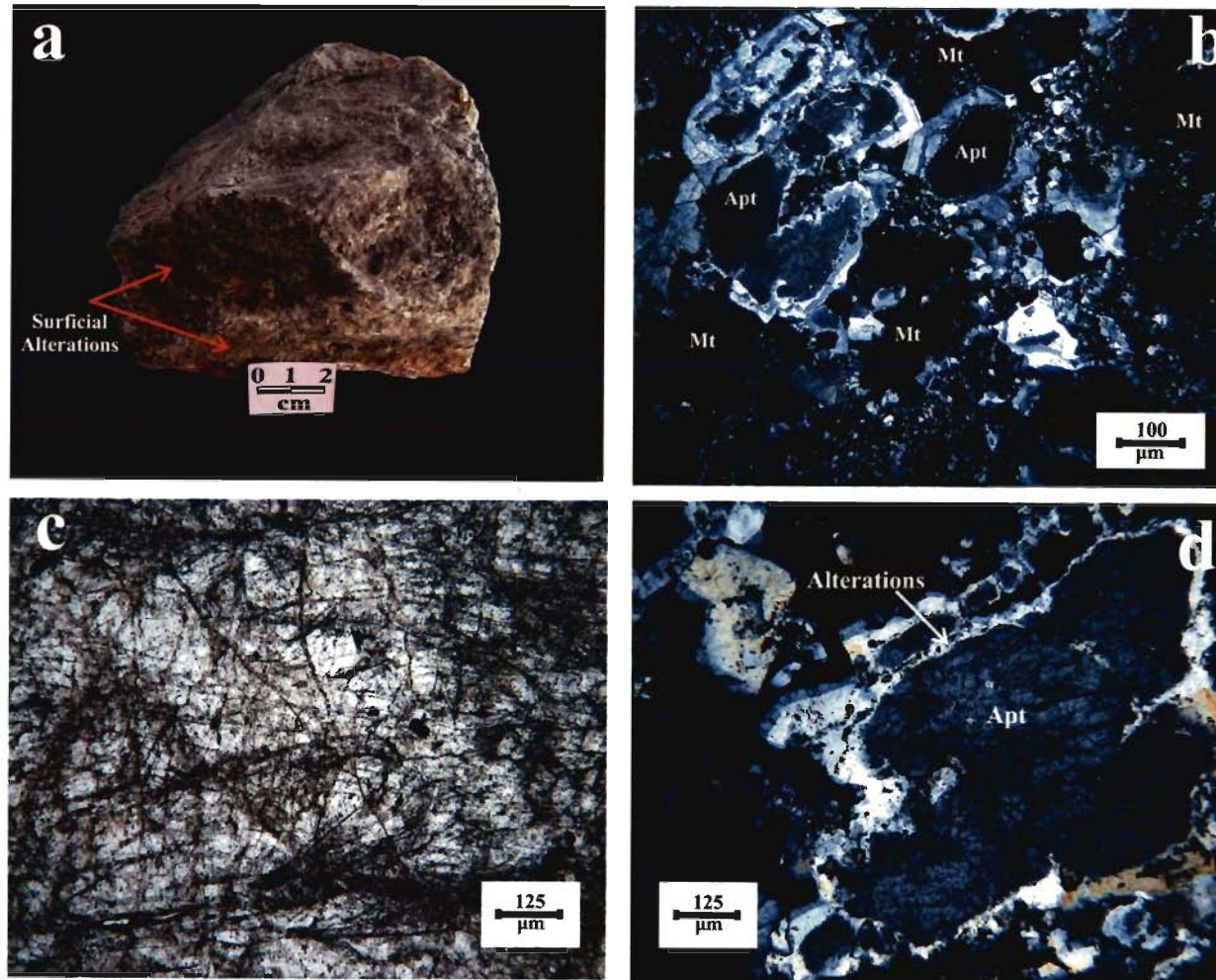


Fig. 3.10 (a) Apatite magnetite rock in hand specimen showing alteration due to meteoric water actions. (b) Hexagonal prismatic apatite crystal in apatite-magnetite rock. (c) Cross fractures in apatite crystals. (d) Yellow colour silicate phase along the periphery of the apatite crystal.

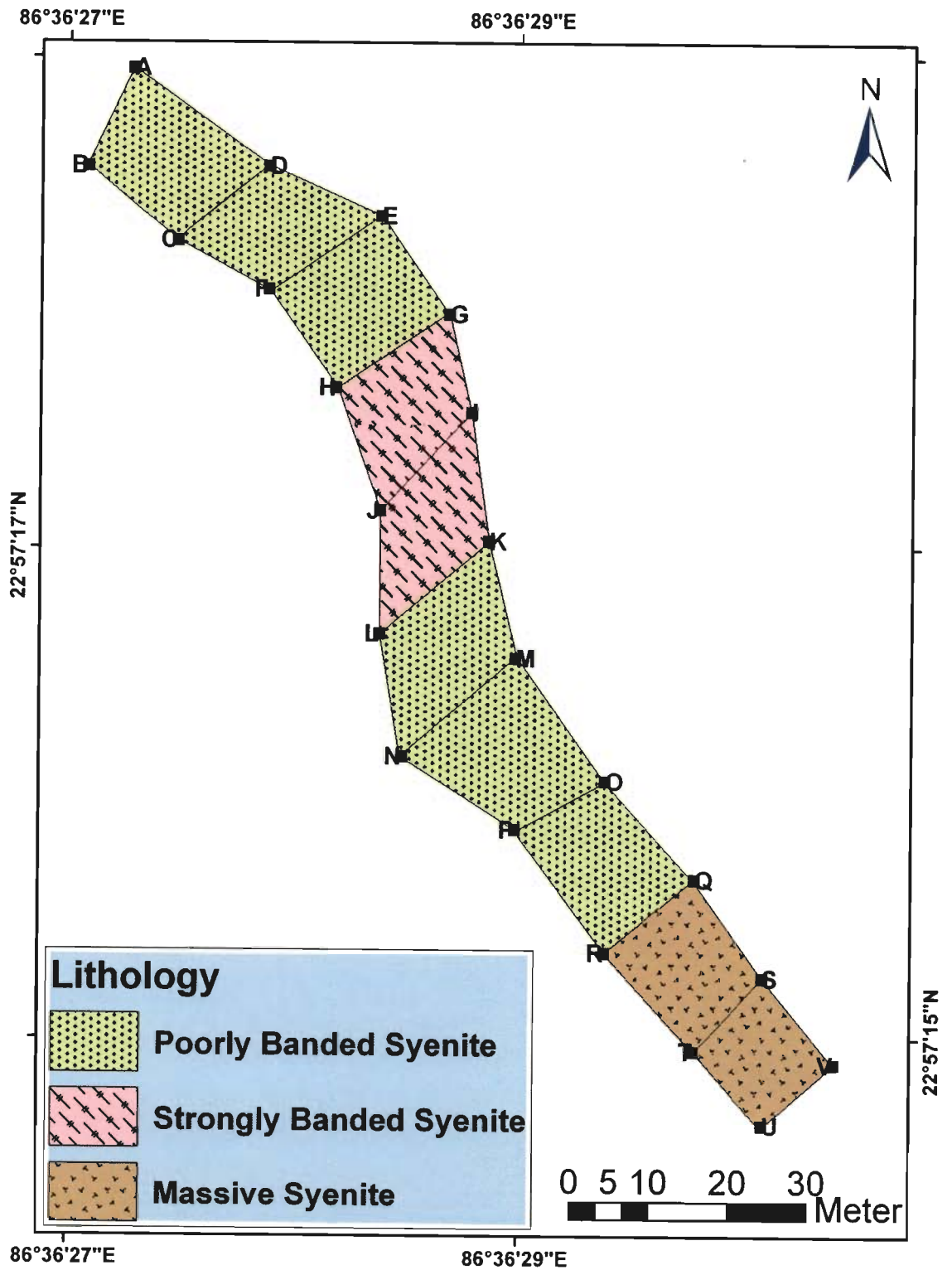


Fig. 3.11 Lithological map of the Sushina Hill region showing different varieties of syenites. The area is dominantly consists of banded syenite followed by massive syenites.

A. BANDED SYENITE

A.1. POORLY BANDED SYENITE GNEISS

This variety of syenite gneiss (Fig. 3.12a) is medium grained and is essentially composed of plagioclase, orthoclase and mafic minerals (Fig. 3.12b, c). The plagioclase grains, mostly albite, are long tabular or laths shaped and are large enough to identify in hand specimen and can be termed as “megacrysts” (Fig. 3.12d). Orthoclase grains are mostly coarse and clouded in appearance. The most striking feature of this variety of syenite is their compositional layering due to varying proportions of nepheline, feldspar and ferromagnesian minerals in the adjacent bands (Fig. 3.12a, e). Within these bands the mafic minerals tend to coalesce and cluster, giving rise to gneissic texture as well as knotted or mottled appearance. In thin section, the rock dominantly consists of felsic minerals: orthoclase, plagioclase (albite), nepheline (Fig. 3.11b, c) and perthite (Fig. 3.12f). Interlayering of polygonal feldspar and nepheline with dimensionally oriented aegirine and/or amphibole produces platy granoblastic texture at places (Fig. 3.12c). At places equilibrium textures are best developed in the monomineralic aggregates with 120° interfacial angles at their triple points (Fig. 3.12b). The mafic mineral is represented by clinopyroxene (aegirine) (Fig. 3.12e) which commonly occurs as discontinuous bands or as clusters (Fig. 3.12d). Well developed porphyritic texture is exhibited by the presence of large phenocryst of orthoclase and albite embedded within the relatively finer groundmass of orthoclase, albite and nepheline. The overall size of the constituent mineral grains is highly variable and they are exhibiting the sign of deformation and recrystallization. This feature is most prominent within the large laths shaped albite crystals which are broken down and recrystallized along the periphery (Fig. 3.12d). The similar feature is observed in case of aegirine grains too. Textural features in this variety of syenite gneiss suggest more than one generation of minerals. The first generation or orthomagmatic mineral assemblage is represented by the orthoclase, albite, nepheline and smaller aegirine

embedded within large albite laths. The second generation or post magmatic mineral assemblage formed during deformation and/or recrystallization resulting the primary orthomagmatic minerals' granulations and preferred orientation of the mafic minerals resulting development of incipient gneissic texture throughout the rock. Moreover, very late stage replacement of aegirine by eudialyte and development of Na-Zr silicate indicates that the rock has experienced late stage metasomatic alteration by deuteric/hydrothermal fluid. The detailed mineralogy and texture of the rock is described below.

Orthoclase: Orthoclase is found to be the dominant felsic mineral in this variety of syenite and making up to 60% by volume. In thin section, they are colourless but cloudy in appearance (Fig. 3.12b, c). They are present both as phenocryst (>2cm. in diameter) as well as in the groundmass (~ few mm. to 0.5cm.) giving rise to a porphyritic texture of the rock (Fig. 3.12d). Orthoclase grains are mostly subhedral to anhedral in shape and characterized by first order grey interference colour and parallel extinction. As mentioned earlier, the size of the orthoclase grain is highly variable. The smaller grains are formed by recrystallization along the periphery of the larger grain. The smaller orthoclase grains are devoid of inclusions and appear to be less altered than the phenocryst. The large orthoclase grains are frequently carrying inclusions of aegirine and magnetite. They are often cut by the aegirine grain. Analyses of the orthoclase reveal that they are almost pure (Table 3.10) and composed mainly of SiO₂ (65.55-66.22%), Al₂O₃ (17.80-18.24%) and K₂O (14.10-14.88%) with negligible Na₂O (0.41-0.65%), MnO (0.02-0.06%), MgO (0.01-0.03%) and FeO (0.01-0.14%). CaO is almost absent in orthoclase. The composition of orthoclase from this variety of syenite occupies the orthoclase (Or) vertex in Ab-Or-An ternary diagram (Fig. 3.13a) indicating that they are almost pure orthoclase. Presence of large grains of microcline (Fig. 3.12g) indicates that the recrystallization was taken place at relatively

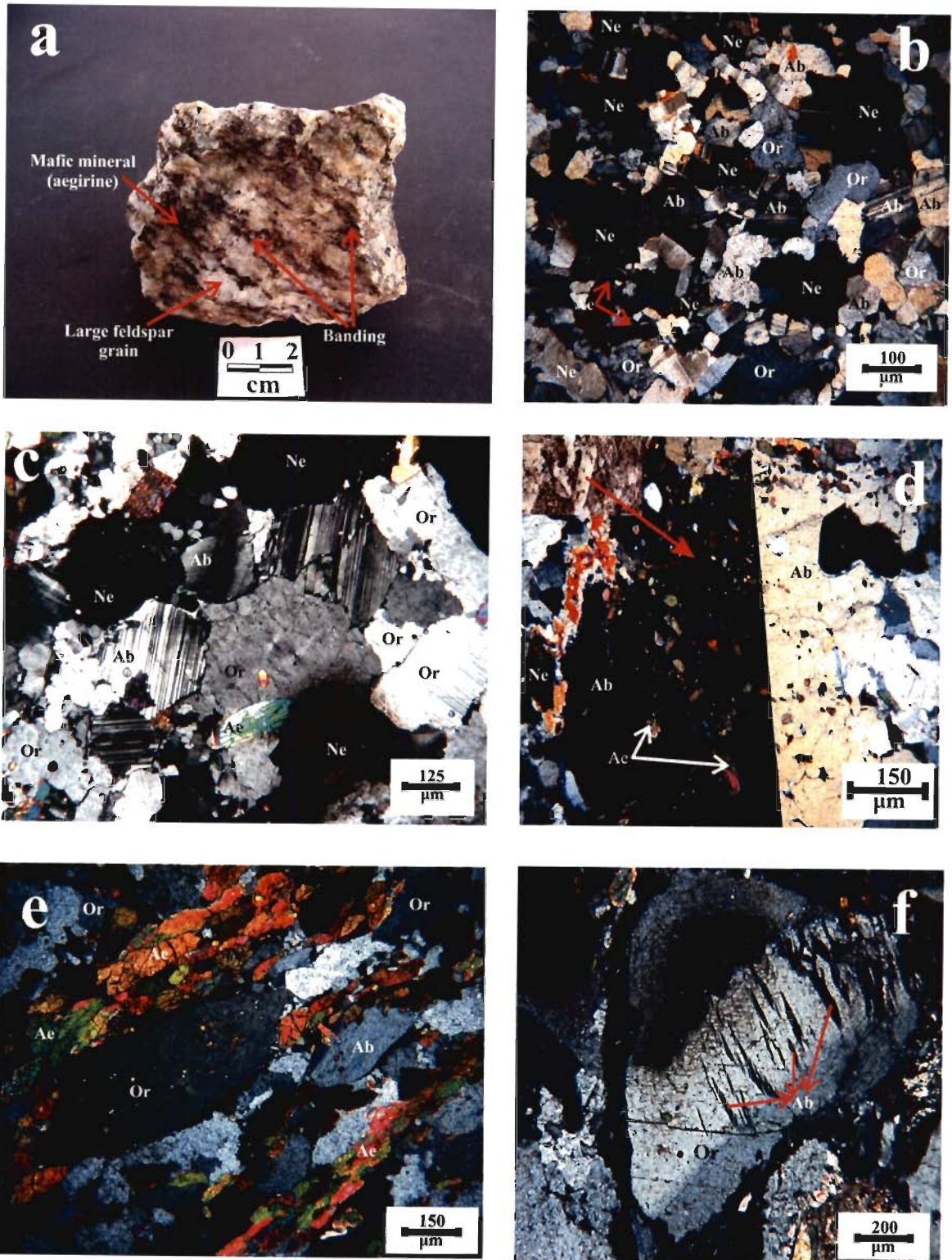


Figure 3.12 (a) Hand specimen of poorly banded syenite gneiss showing alternating banding of mafic and felsic minerals. Large plagioclase crystals are also visible. (b) and (c) Dominant mineral constituents of poorly banded syenite gneiss defining the porphyritic texture. (d) Large megacrysts of albite. (e) Alternating banding of mafic (aegirine) and felsic (feldspars and nepheline) minerals (f) Perthite texture in poorly banded syenite gneiss.

(Ab: Albite, Or: Orthoclase, Ne: nepheline, Ae: Aegirine)

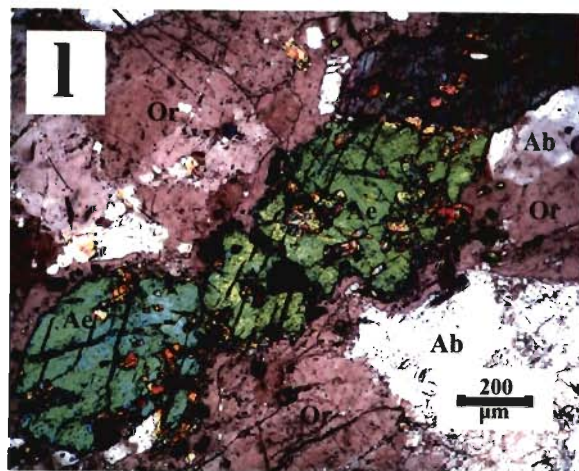
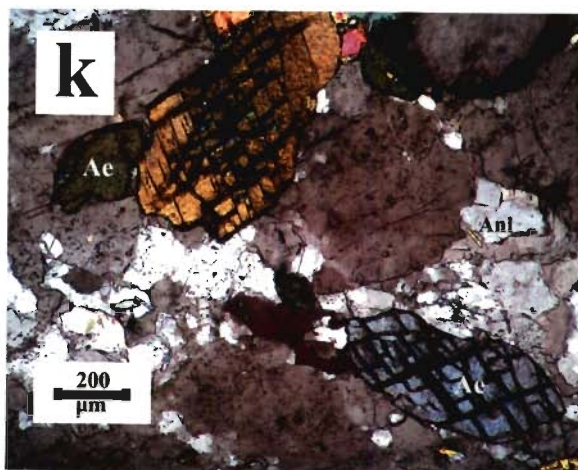
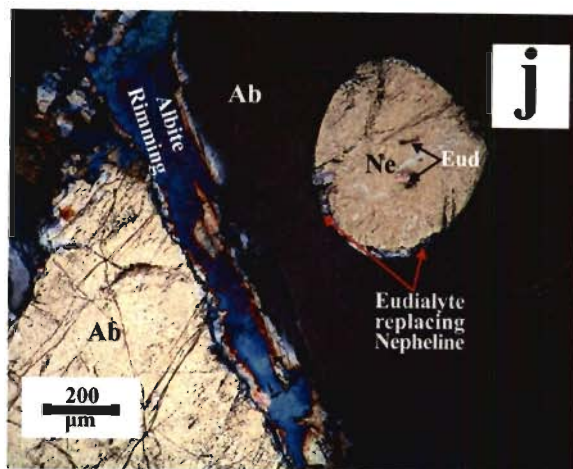
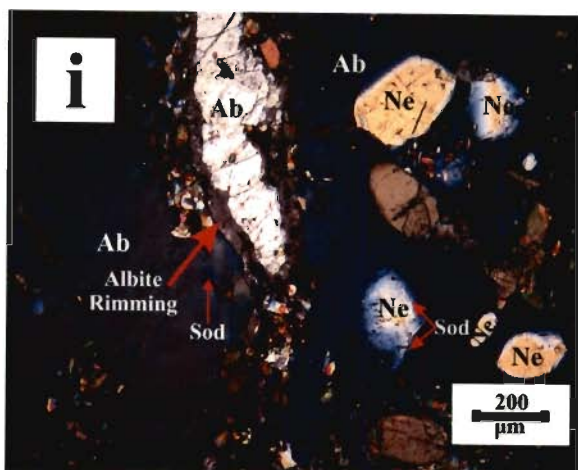
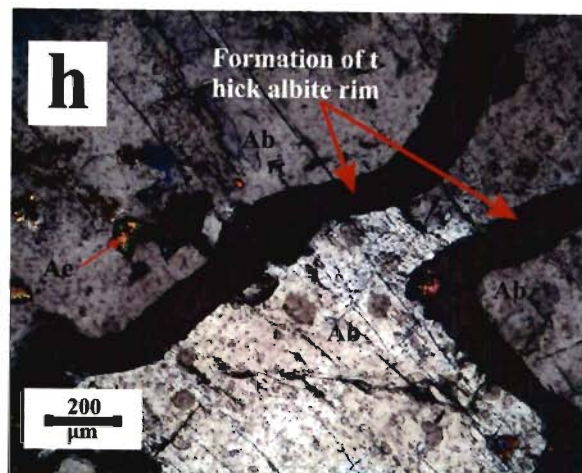
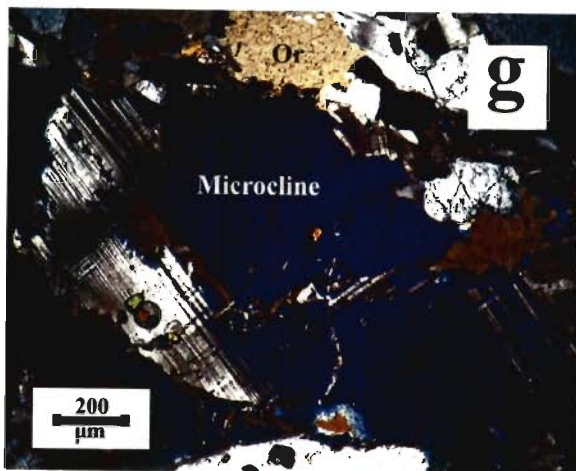


Figure 3.12 (g) Microcline in poorly banded syenite gneiss showing cross-hatched twinning (h) Thick rimming of albite by late stage metasomatic alterations. (i) Large nepheline enclosed (poikilitically) within large albite megacrysts. Alteration of nepheline to sodalite at places is clearly visible. (j) Eudialyte replacing nepheline along the periphery which is enclosed within albite megacrysts. (k) and (l) large aegirine grains sometimes misleads to amphiboles.

(Ab: Albite, Or: Orthoclase, Ne: nepheline, Ae: Aegirine, Eud: Eudialyte, Sod: Sodalite, Anl: Analcime, Ne: Nepheline)

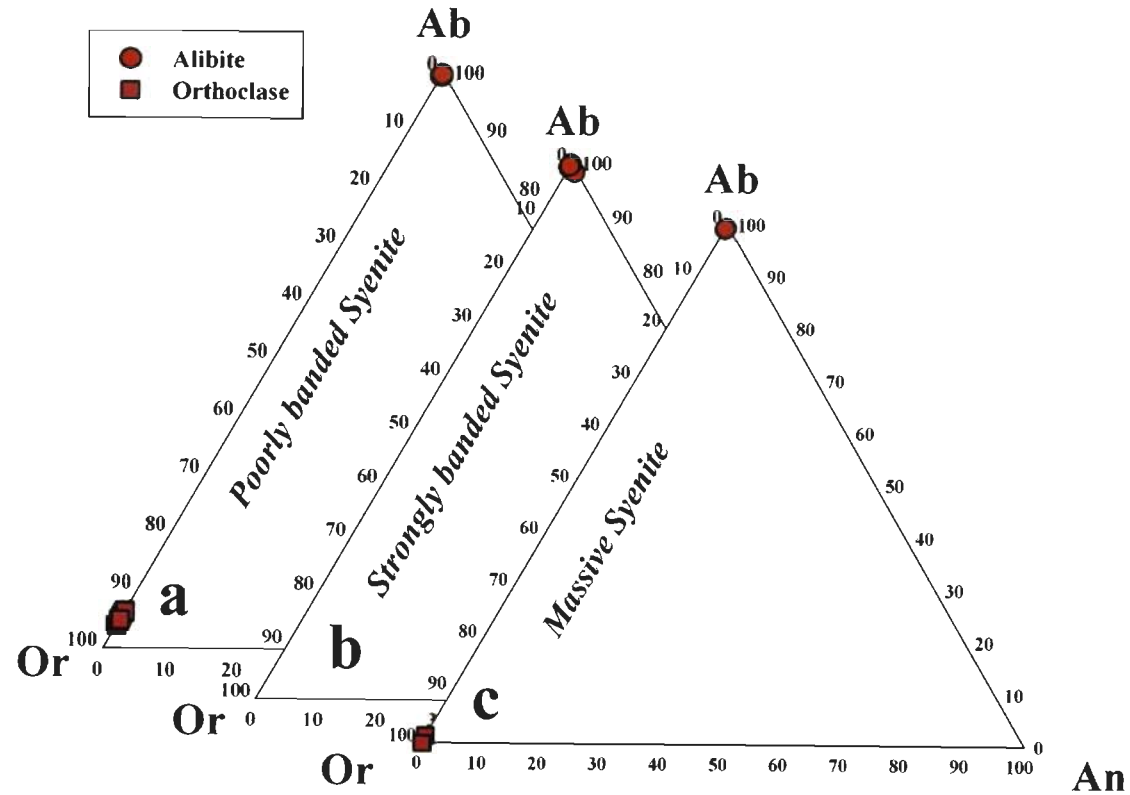


Fig. 3.12 Compositions of feldspars from different varieties of nepheline-syenites. The feldspars are found to be pure albite and orthoclase (for detail discussions see text).

lower temperature resulting triclinicity of the monoclinic orthoclase and subsequently readjustment into microcline structure. Such recrystallization of nepheline syenites have also been reported from the number of areas like Haliburton-Bancroft area of Ontario (Appleyard, 1969; Duke and Edgar, 1977), Mt. Copeland (Currie, 1976) and Norra Kärr, Sweden (Adamson, 1944).

Albite: Next to orthoclase albite is the most dominant felsic found in the rock making up to 20-25% by volume. The albite grains are colourless in thin section under plane polarized light but under crossed polar they are showing polysynthetic twinning of albite type. They are showing first order grey interference colour. As mentioned earlier the albite grains are excessively large (more than 3cm. long grains have been observed in hand specimen) hence can be termed as megacrysts (Fig. 3.12d). The most striking feature is the presence of needle shaped aegirine inclusions in these large albite megacrysts. The aegirine grains are poikilitically embedded within the large albite grains (Fig.3.12d). Such features indicate that the mafic minerals crystallize first which is basically a characteristic of miaskitic nepheline syenite (Sørensen, 1974). In general in miaskitic rocks mafic minerals crystallize earlier than the felsic one, but the pyroxene, alkali feldspar and nepheline appear within an interval of 30-40°C below the liquidus (Sørensen, 1974). Like orthoclase these grains are also showing the evidence of deformation and recrystallization which is evident from their variable grain size distribution. The continuity of the albite twin lamellae with that of the grid twinning (cross-hatched twinning) has been observed. Thick layer of albite at margin is developed towards the rim of the larger albite grain clearly indicate late stage or post magmatic alteration of albite by fluid or metasomatic activity (Fig. 3.12h). Large nepheline grains associated with albite show diffuse margins at their contact (Fig. 3.12i). At places even larger nepheline is found to be poikilitically embedded within the albite megacrysts

(Fig. 3.12j). The large albite laths are often broken and carrying inclusions of aegirine, magnetite and nepheline. Perthite texture is also observed rarely, the host orthoclase is carrying albite inclusions (Fig. 3.12f). The association of albite with orthoclase and microcline probably point towards the fact that these are low albite. The EPMA analyses of albite grains reveal that they are pure albite (Table 3.11) and occupy the albite (Ab) corner of the Ab-Or-An ternary diagram (Fig. 3.13a). The albite grains are composed of SiO₂ (>69.00%), Al₂O₃ (19.00%) and Na₂O (10.90-11.20%). The K₂O is absent or negligible. They are devoid of FeO, MnO and contain insignificant amount of MgO and CaO.

Nepheline: Nepheline content is about 5-10% by volume and the grains are subhedral to anhedral in shape (Fig. 3.12b, c). They are colourless under plane polarized light and carry numbers of inclusions within them. They are showing first order grey interference color. Like other felsic minerals, nepheline has highly variable grain size. At places these grains show patchy in appearances (Fig. 3.12k). Nepheline occurs as both inclusion within aegirine as well as a separate mineral in association with albite and orthoclase. The chemical composition of nepheline is highly consistent and is as follows: SiO₂ (42.70-43.25%), Al₂O₃ (33.03-33.97%), Na₂O (16.49-16.89%) and K₂O (6.09-6.69%) (Table 3.12). The K/(Na+K) (atomic proportions) of nepheline varies from 19-21 with majority of 20 indicates that these nepheline grains are plutonic in origin (Tröger, 1969). The composition of nepheline when expressed in terms of Nepheline (Ne: NaAlSiO₄)-Kalsilite (Ks: KAlSiO₄)-Silica (Qtz: SiO₂) is very useful in deciphering the temperature condition under which they have crystallized/recrystallized. The nepheline composition varies from Ne_{74.5}Ks_{19.8}Qtz_{5.7} to Ne_{76.1}Ks_{19.5}Qtz_{4.4} (Table 3.12) and falling within the Morozewicz-Buerger convergence field of plutonic nepheline (Fig. 3.14a), suggesting equilibration temperatures were in the range of 500-600°C. Composition of the nepheline when

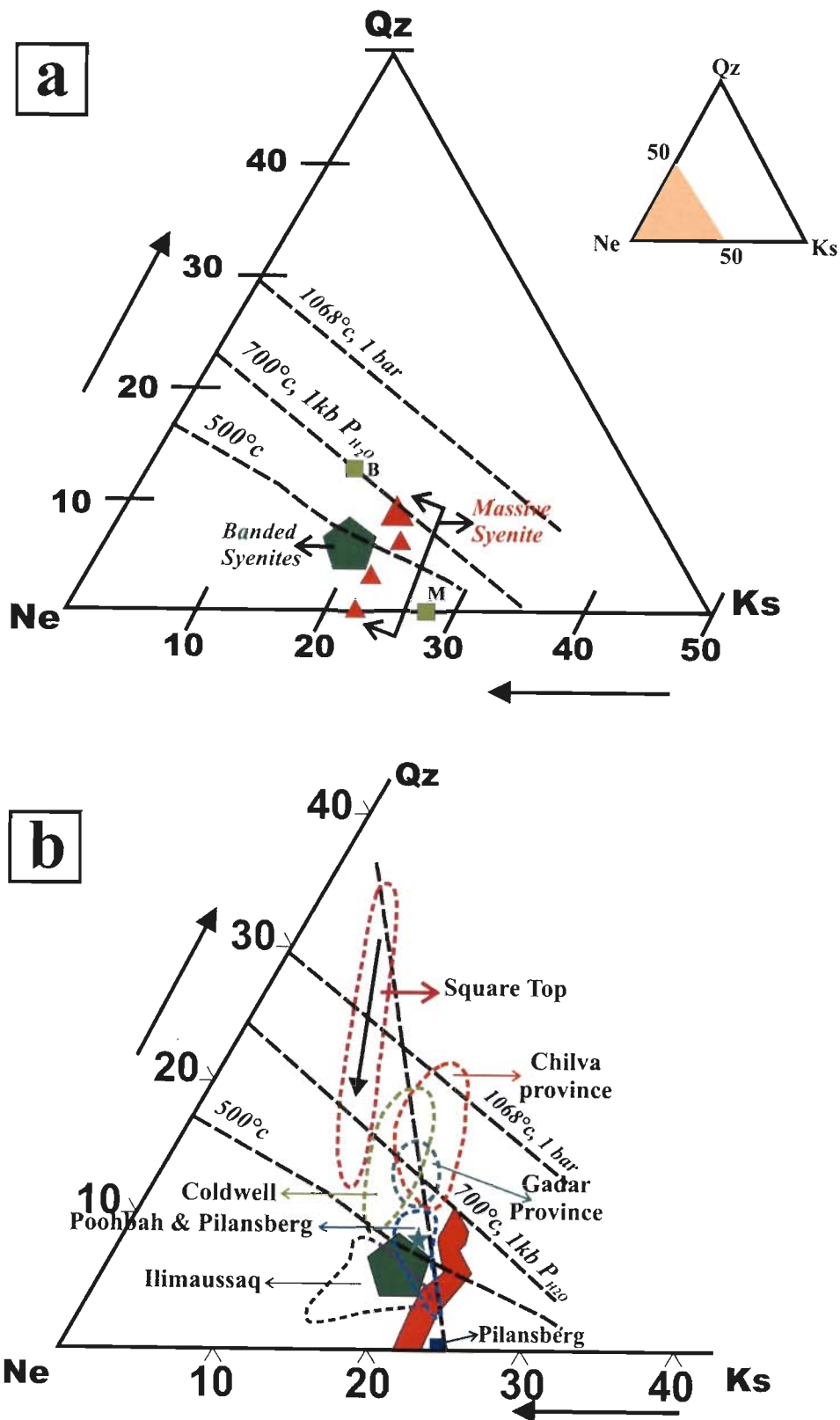


Fig. 3.14 (a) Compositional variation of nepheline from nepheline syenite gneiss and massive syenite in terms of Ne-Ks-Qtz. (b) Nepheline composition from the other occurrences are given for comparison (after Mitchell and Liferovich, 2006; Mitchell and Platt, 1979; Woolley and Platt, 1986; Wilkinson and Hensel, 1994; Coulson, 1997; Markl and Baumgartner, 2002; Marks and Markl, 2003). The dashed line drawn from the Ne-Ks line ("Barth join") denotes the Dollase-Thomas compositional trend for natural nephelines (Dollase and Thomas, 1978); the dashed lines with temperature notations denote the Morozewicz (M)-Buerger (B) convergence field (Hamilton, 1961; Wilkinson and Hensel, 1994).

compared with the other reported nepheline-syenite world-wide (Fig. 31.14b) it has been noticed that they are remarkably similar to the Ilimaussaq alkaline complex of South Greenland, Pilansberg alkaline complex of South Africa. The close proximity of this nepheline towards ideal Morozewicz composition ($Ne_{75.0}Ks_{20.5}Qtz_{4.5}$) along with the presence of albite and microcline assemblage indicates that they are formed by either plutonic or metamorphic environment (Tilley, 1954, 1957). Considering the textural evidences i.e. megacrysts of albite, orthoclase and nepheline phenocrysts, gneissic banding, and recrystallization of the albite grains it is evident that the nepheline was formed under plutonic condition and latter subjected to the metamorphism and as a consequence they are showing convergence within the Morozewicz-Buerger field. The same is also evident when the nepheline composition of the studied poorly banded nepheline syenite gneiss are plotted with nepheline compositions of other known nepheline syenites gneiss as that of the Haliburton-Bancroft area, York river, Blue Mountain (Tilley, 1954) and all are found to be plotted within the Morozewicz-Buerger field of convergence (Fig. 3.15). At places alteration of nepheline to sodalite and analcime is evident and such post magmatic alteration feature is discussed later.

Aegirine: The mafic silicate mineral in the rock is represented by aegirine (10-15% by volume). They are green and yellowish green under plane polarized light (Fig. 3.12e), strongly pleochroic and showing green to dark green pleochroism with very low extinction angle (2° - 8°) and having strong higher order interference colour. They are present as long prismatic crystals (Fig. 3.12c, e). The aegirine grains are present in two distinct modes. The early formed aegirine grains are poikilitically embedded within the large albite grains (Ae-I) while the grains that are formed at late stage (Ae-II) are cutting across all the other constituting minerals like albite, orthoclase and nepheline and relatively long prismatic in

shape. Later on during deformation they oriented along the main stress directions to form the banding (Fig. 3.12e) giving rise to gneissic texture. The aegirine grains are composed of SiO_2 (53.60-54.24%), FeO (23.13-25.48%) and Na_2O (13.24-13.65%) (Table 3.13) with Al_2O_3 (2.43-2.90%), MgO (0.06-0.39%), CaO (0.04-0.95%) and MnO (0.02-0.32%). The K_2O content is extremely low and lying within the range of 0.01-0.03%. Such higher content of Na_2O is usually characteristic of the sodic pyroxene. The clinopyroxene grains also have very small amount of TiO_2 (0.68-0.80%) and MnO (0.16-0.28%). The higher proportion of Na compared to the Fe in these pyroxenes constrains the Larsen (1976) classification scheme as applied to the pyroxenes of alkali-pyroxenite. The nomenclature of the pyroxene is determined by the procedure given by Morimoto et al. (1988) and then plotted in Q-J diagram (Fig. 3.16a). It has been found that they are dominantly Na-pyroxene. In a Q (Wo: Wollastonite, En: Enstatite, Fs: Ferrosilite)- $\text{NaFe}^{3+}\text{Si}_2\text{O}_6$ (Aegirine)- $\text{NaAlSi}_2\text{O}_6$ (Jadeite) ternary diagram (Fig. 3.16b) they are essentially found to be Na-pyroxene field and represented by aegirine.

POST MAGMATIC ALTERATIONS

Post magmatic alterations are evident throughout the rock. The alterations are mainly two fold: the one by metamorphism as evidenced by the gneissic texture, recrystallization of albite megacrysts and the second one by the hydrothermal fluid (internal or external) i.e. metasomatic alteration. The metasomatic alteration of nepheline syenite is well known from many places around the world e.g. Pilansberg alkaline complex of South Africa where late stage deuteric fluid derived from the magma itself caused autometasomatism of the nepheline syenite (Olivo and Jones, 1999; Mitchell and Liferovich, 2006). The fluid which is responsible for late stage metasomatic alteration also caused granulation and recrystallization of the constituting minerals particularly feldspars and

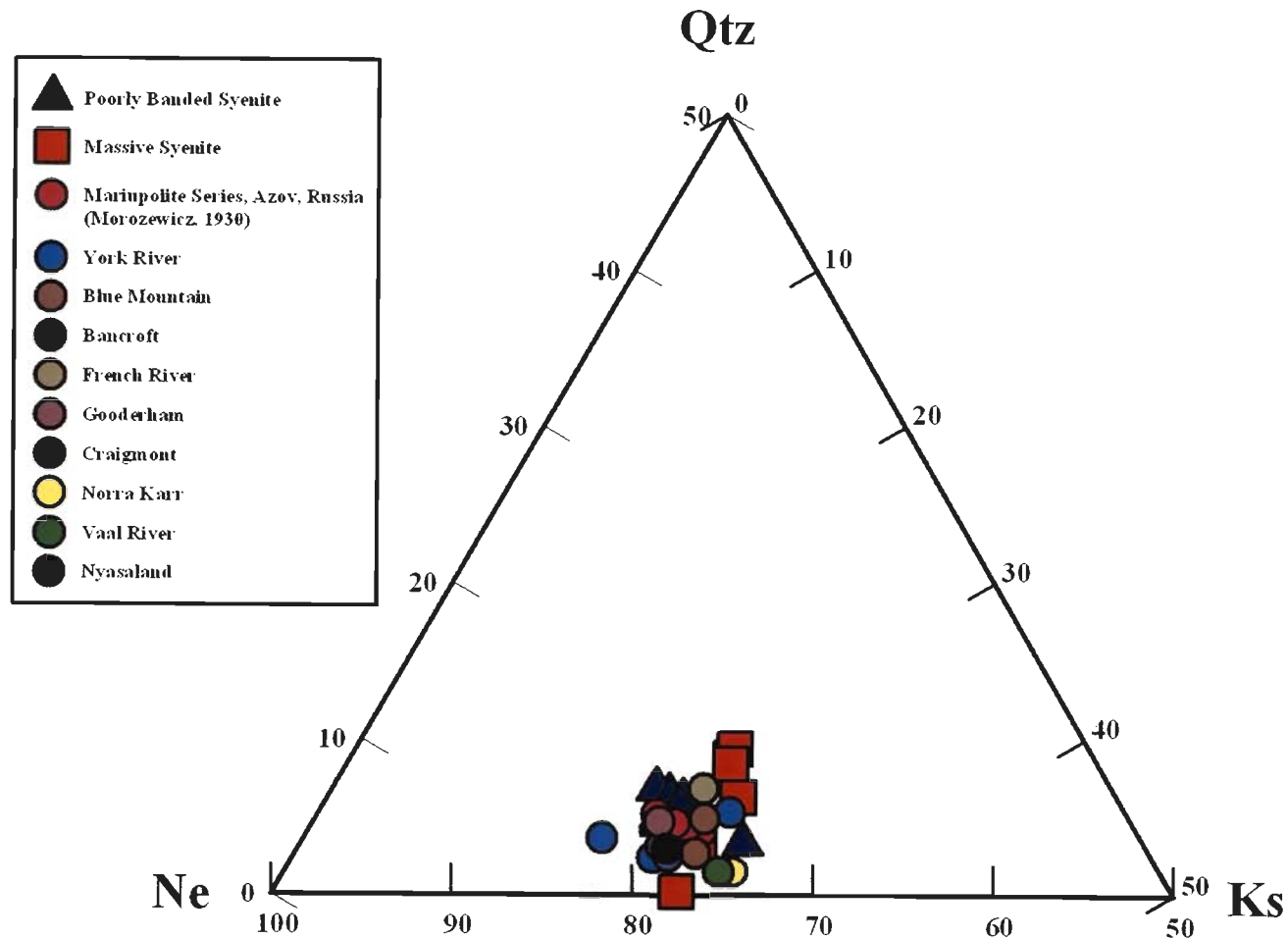


Fig. 3.15 Comparison between the nepheline composition from the studied nepheline syenite gneiss and massive syenite with the nepheline from the other reported nepheline syenite gneiss. The data sets used for comparison are taken from Tilley (1954). In all the cases nepheline is associated with albite±microcline assemblage. Studied nephelines along with other reported nephelines are plotted close to ideal Morozewicz composition ($\text{Ne}_{75.0}\text{Ks}_{20.5}\text{Qtz}_{4.5}$).

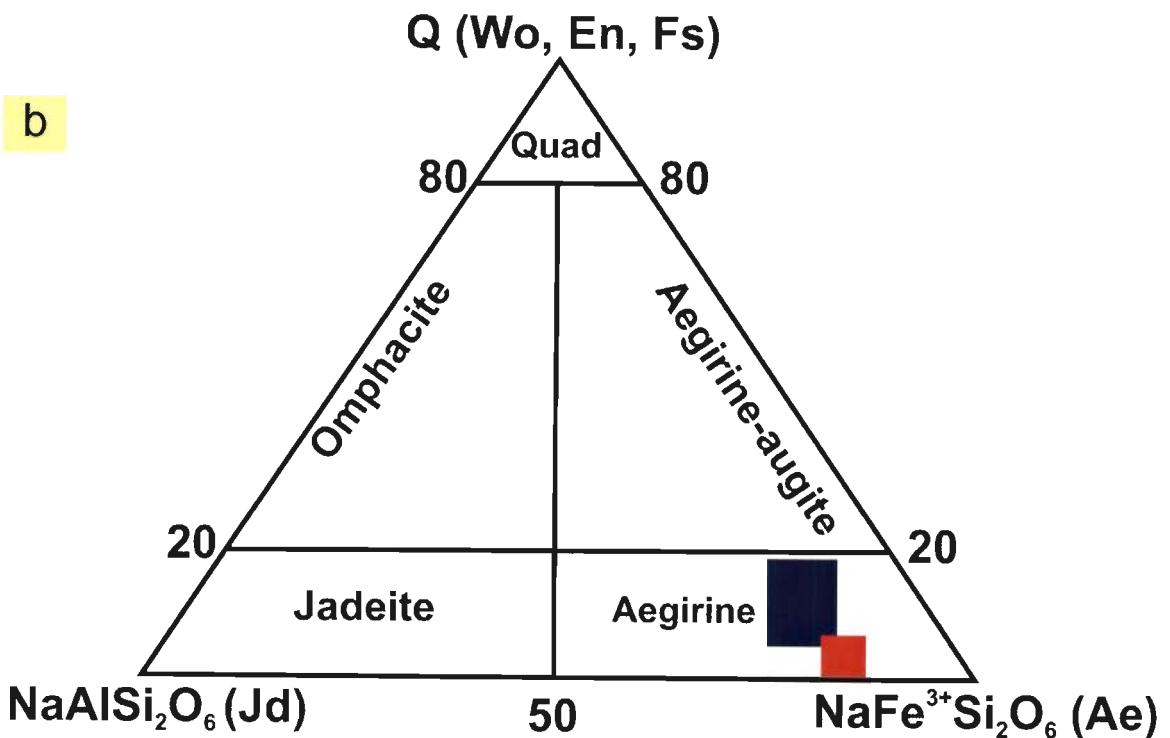
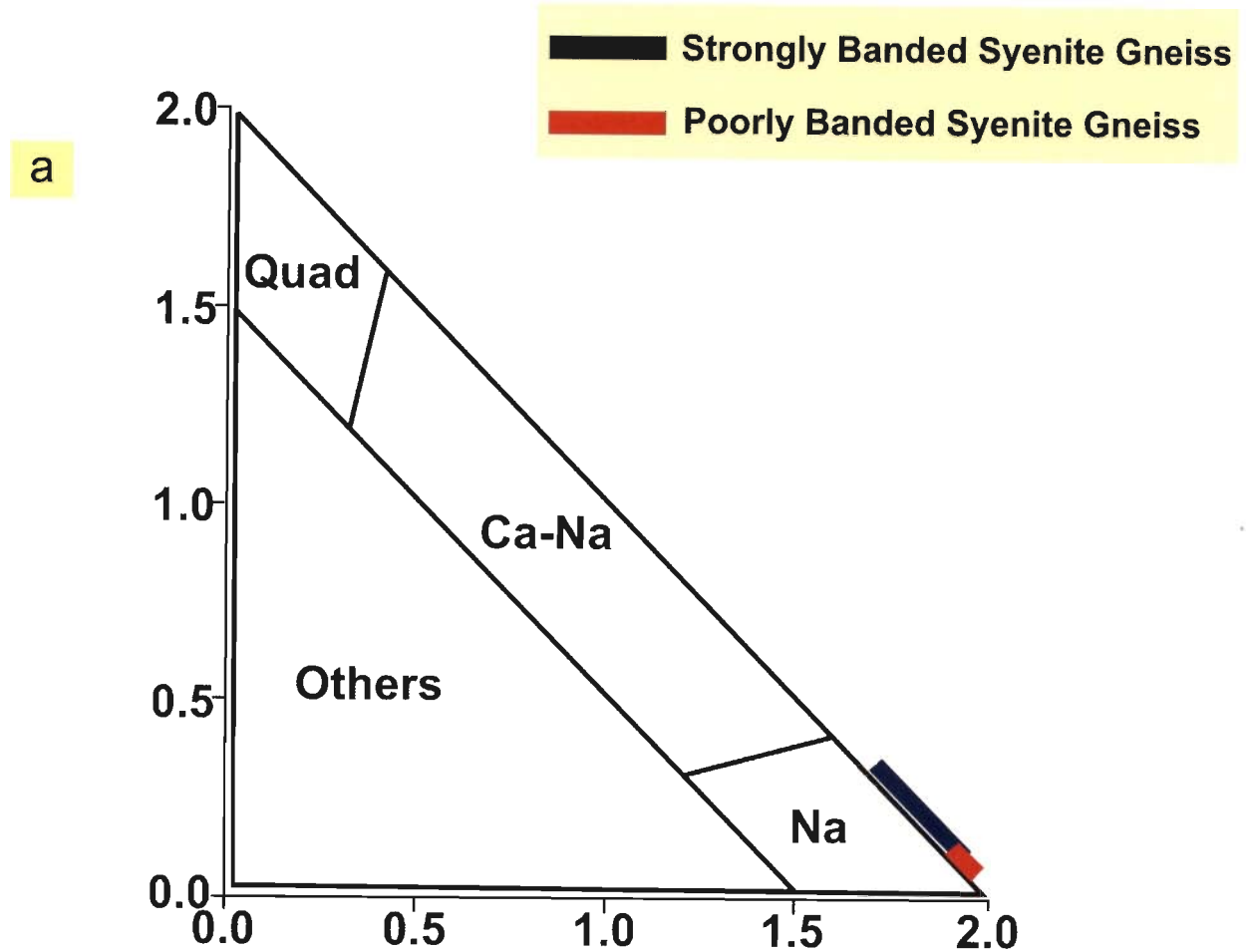


Fig. 3.16 Classification of pyroxene different varieties of nepheline-syenites. (a) Q-J Diagram and (b) (Wo-En-Fs)-Jd-Ae ternary plot for Ca-Na pyroxenes (Classification based on Morimoto et al., 1988).

nepheline (Fig. 3.17a). Some of the analyzed nepheline along this zone is found to be approaching towards the ideal nepheline composition indicating recrystallization and alteration of either early formed nepheline or metasomatically formed from the plagioclase. Nepheline can form metasomatically by the reaction between early formed plagioclase and a chloride solution and reported from the nepheline syenite of Eastern Ghat (Rao and Murthy, 1974). Prominent bands of nepheline and its alteration to sodalite and analcime (Table 3.14) is also observed along the fluid migration path (Fig. 3.17a). The large albite grains are transected by the very fine and thin veinlets of nepheline (Fig. 3.17b). Moreover as mentioned earlier the development of thick rim of albite (Fig. 3.12h) certainly point towards metasomatic alteration and recrystallization of early formed albite grains. At places direct evidences of fluid which in turn giving rise to new minerals is also evident (Fig. 3.17c, d). These new minerals are highly irregular in shape (ant-shaped as shown in Fig. 3.17d) and dispersed throughout the rock. The most notable feature of alterations is the replacement of primary aegirine and albite by eudialyte and described below.

Eudialyte: Eudialyte grains are typically pleochroic (pink) and usually replacing early formed aegirine and albite (Fig. 3.18a). The eudialyte grains are complexly zoned which making up to few centimeters in diameter. Textural appearances of eudialyte suggest two distinct modes of occurrences: the one which forms the large crystals (Eud-I, Fig. 3.18a, b) and usually replacing aegirine and albite. The other mode is the replacement of all (Eud-II, Fig. 3.18a) the early formed minerals through outer zones (along the rim, Fig. 3.12j, in this case nepheline is replaced by eudialyte from the periphery) and fills the fractures, partings of the constituting minerals. Such fracture filling may indicate that the metasomatic alteration or such late phase eudialyte development took place preferably after metamorphism. The eudialyte formation is more prominent in the strongly banded variety and described in the next section. However the textural evidences cited above are clearly

indicates that this phase formed late, replacing most of the magmatic silicates. Similar, feature is also described by Olivo and Jones (1999) from the Pilansberg alkaline complex of South Africa (cf. FIG. 3A to 3F, Olivo and Jones, 1999). However the presence of late stage eudialyte certainly points towards the fact that the fluid was essentially enriched in Na-Cl. Such fluid (deuteric fluid) and subsequent alteration of the mineralogy of the original lujavrite is also reported by Mitchell and Liferovich (2006) from Pilansberg alkaline complex.

In general, the gneissic texture and recrystallization of orthoclase (microcline), albite etc. indicates that the rock has suffered low temperature recrystallization. Moreover the presence of felsic minerals like orthoclase, albite and nepheline suggest the rock was crystallized from an undersaturated melt. Presence typically agpaitic mineral like eudialyte along with orthoclase, albite, nepheline and aegirine points towards agpaitic nature of the parent igneous nepheline syenite which in turn metamorphosed and metasomatically altered by low temperature deuteric fluid and presently resembling nepheline syenite gneiss similar to the other nepheline syenite occurrences as in Haliburton-Bancroft area, Canada; Sørøy, Norway; Kishangarh, India. The crystallization of mafic minerals prior to the felsic one along with the presence of apatite, zircon (described in the Chapter 4) is characteristic of the miaskitic nepheline syenite (Sørensen, 1974; Heinrich; 1966). On the other hand presence of late stage eudialyte is characteristic of agpaitic nepheline syenite (Sørensen, 1997). So, from the mineralogical and textural evidences described above it is evident that the poorly banded syenite gneiss was originally of miaskitic character and undergone metamorphism as well as subsolidus deuteric/hydrothermal alteration. In its present form the rock resembles nepheline syenite gneiss of agpaitic/intermediate character.

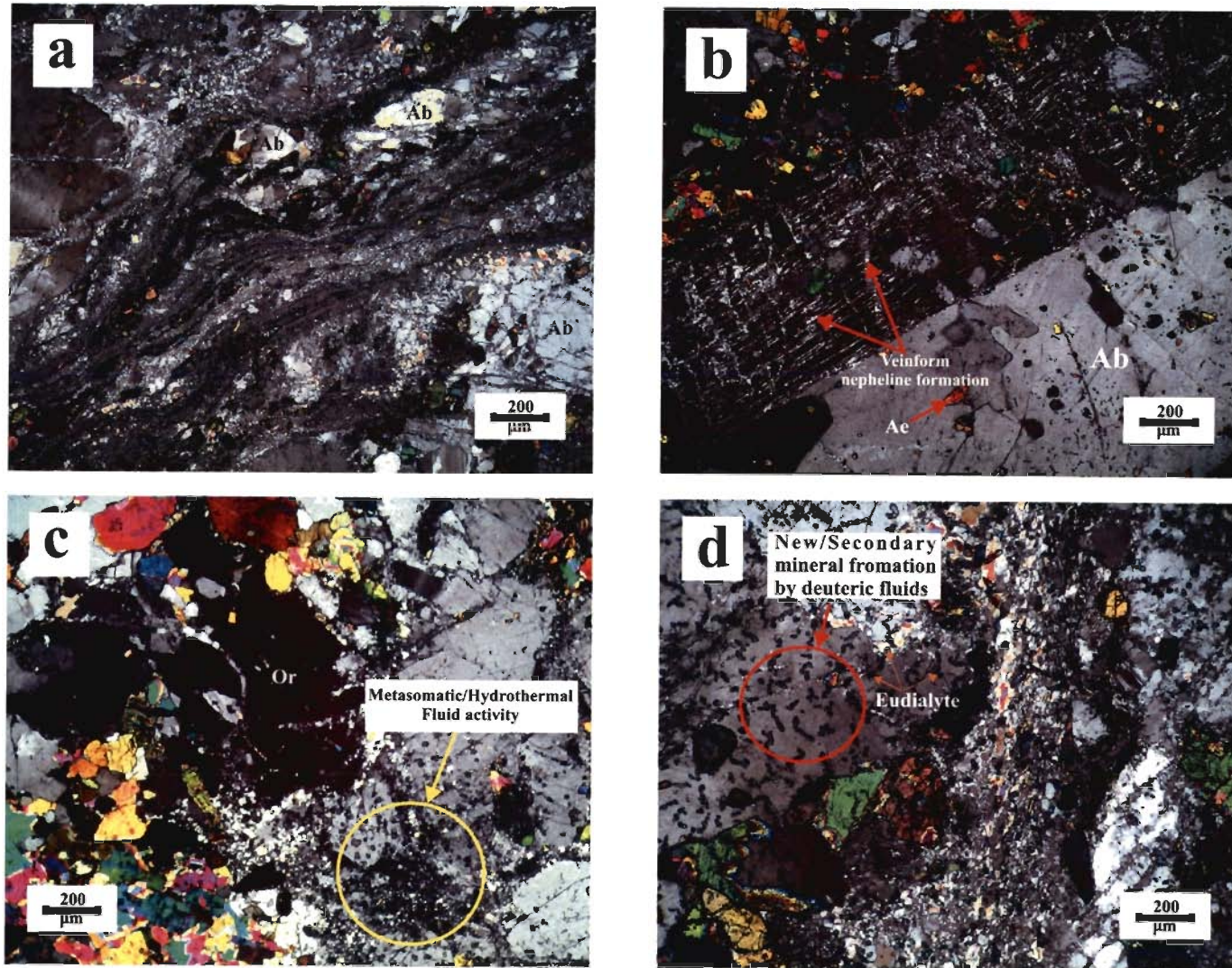


Fig. 3.17 Post magmatic changes of poorly banded syenite by hydrothermal/deuteritic fluid. (a) Granulation of the constituent grains during fluid migration. (b) Veiniform nepheline within megacrysts of albite. (c) and (d) Fluid entering the rock and giving rise to new minerals mainly eudialyte.

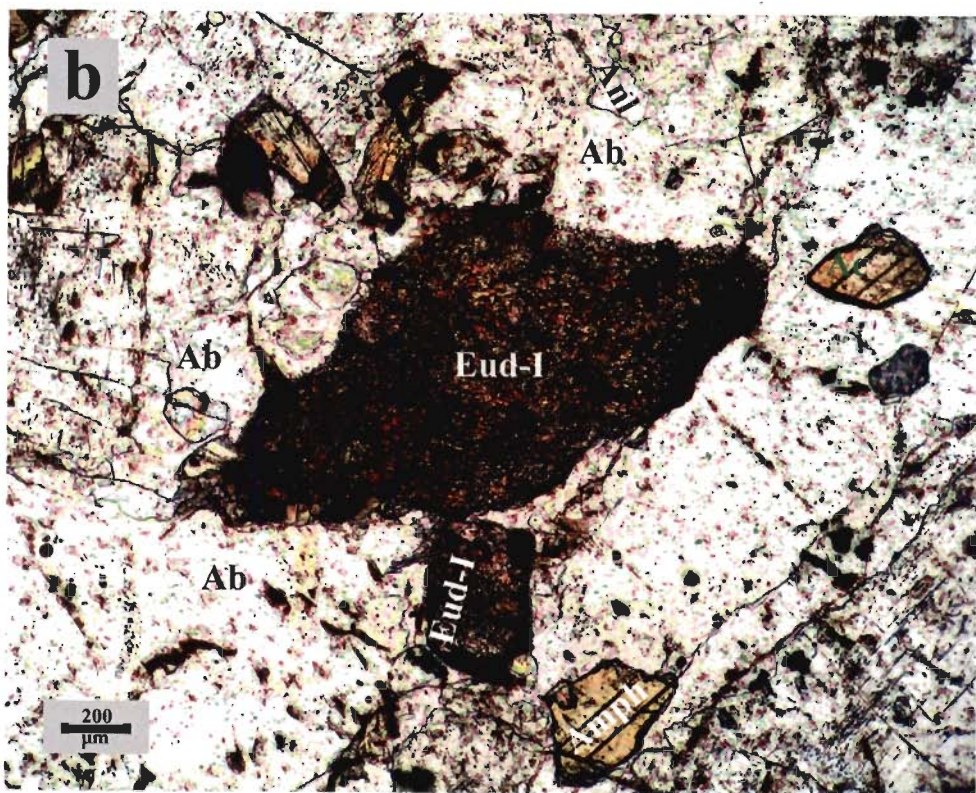
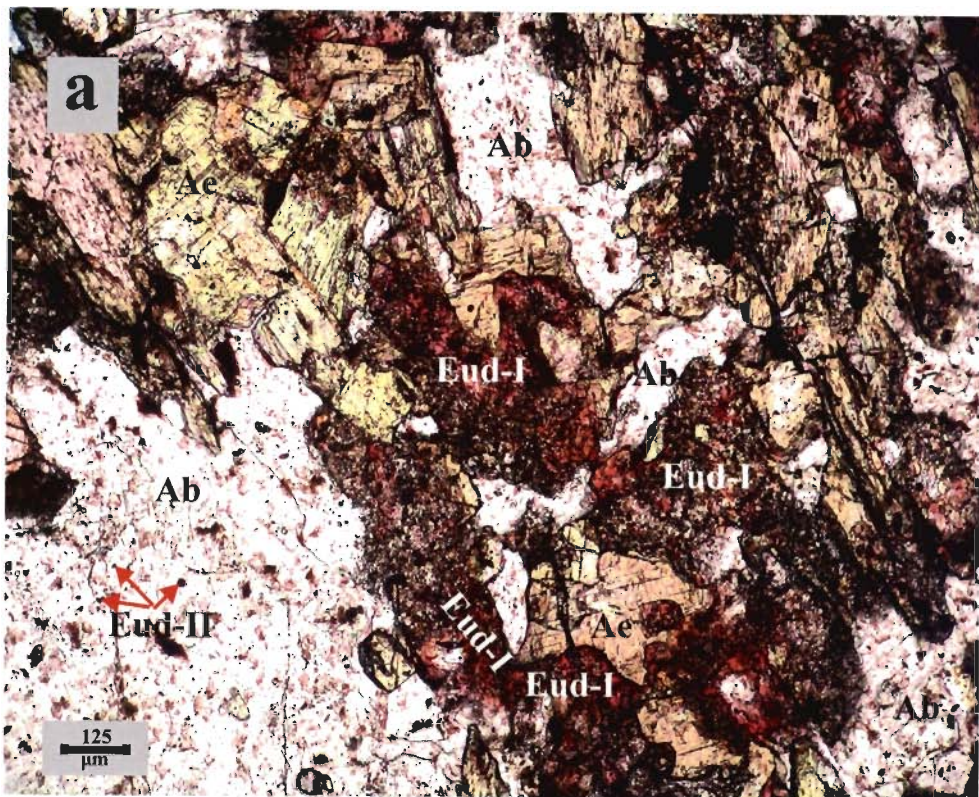


Fig. 3.18 (a) and (b) Eudialyte (Eud-I) replacing aegirine. Relatively larger grains are formed at the first stage while that of the smaller eudialyte crystals formed at late stage (Eud-II) present within the orthoclase, albite as tiny inclusion.

A.2. STRONGLY BANDED SYENITE GNEISS

This rock is the other variant of the poorly banded syenite gneiss with pronounced alternating banding of mafic and felsic minerals. The rock is medium grained (Fig. 3.19a-d) and finer in comparison to the poorly banded variety. It is essentially composed of plagioclase with appreciable amount of mafic minerals in comparison to the previous type. Nephelines are present as inclusions within the aegirine grains (Fig. 3.19d, inset). Nepheline grains are smaller and the modal percentage of nepheline is also less compared to the other variety of syenite gneiss. Eudialyte is consistently present throughout the rock (Fig. 3.20a-e) and appears to be fresh and more crystalline compared to the poorly banded syenite gneiss. They are mostly found to be associated with the felsic minerals and at places formed prominent banding. Some micaceous minerals are also present. In thin section dominant felsic mineral is albite and the mafic mineral is aegirine and eudialyte. Alternating bands of albite-rich felsic and aegirine-eudialyte rich mafic is present throughout the rock which is giving rise to a gneissic appearance of this variety of syenite. The eudialyte is formed at late stage replacing albite and pyroxene (aegirine) as described in the earlier variety of syenite gneiss.

Albite: The albite grains are euhedral to subhedral in shape and showing typical albite twinning combined with carlsbad twinning (Fig. 3.19b-d). They are making up to 75% by volume. The albite grains are fairly large (~200 μ m) and giving first order grey interference colour. The albite grains are devoid of any inclusions and there is no evidence of recrystallization is noticed. Compositionally these are pure albite and composed of SiO₂ (69.10-69.69.81%), Al₂O₃ (18.14-19.07%) and Na₂O (11.95-12.41%) (Table 3.15). The other constituents: K₂O, FeO MgO, CaO and MnO are almost below the detection limits and if present is very low in content. In the Ab-Or-An ternary plot (Fig. 3.13b) they occupy the albite (Ab) end indicating that they are almost pure albite.

Microcline and Orthoclase: Occasional microcline is found mingled with albite (Fig. 3.19d, lower left). At places orthoclase is present as perthite (3.20f). The orthoclase is found to be pure as in poorly banded syenite gneiss. However, the modal proportion of orthoclase is very low compared to the poorly banded syenite gneiss.

Aegirine: The aegirine grains are very similar to that of the previous variety of syenite and showing similar optical properties. They are characterized by the typical green and pleochroic from green to dark green with higher order interference colour. They constitute about 25% of the rock by volume. Analyses of these pyroxene (Table 3.16) reveals that they are composed mainly of SiO₂ (53.78-54.27%), FeO (22.18-24.62%) and Na₂O (11.55-13.01%) with small amount of Al₂O₃ (2.33-2.89%), CaO (1.24-3.34%), MgO (1.25-2.17%), MnO (0.18-0.88%) and TiO₂ (0.24-0.34%). When plotted in a Q-J diagram they are found to be Na-pyroxene and represented by aegirine (Fig. 3.16).

POST MAGMATIC ALTERATIONS

Post magmatic alterations are evident by the presence of pink colored eudialyte which is replacing early formed albite and aegirine. The eudialyte grains are relatively fresh compared to the previous variety of syenite gneiss and typically pleochroic pink in colour (Fig. 3.20a-c). Complex zoning observed within the eudialyte-albite-aegirine assemblages. Detail description of the eudialyte is described below.

Eudialyte: On the basis of textural relationship three distinct mode of eudialyte has been identified. First type is described earlier in the poorly banded syenite and referred as Eudialyte-I (Eud-I). The Eud-I is essentially replacing albite and aegirine. This is comparable with the miaskitic paragenesis described by Khomyakov (1995). The other variety is observed is the replacement of complex deuteric Na-Zr (NZS in Fig. 3.20a-f;

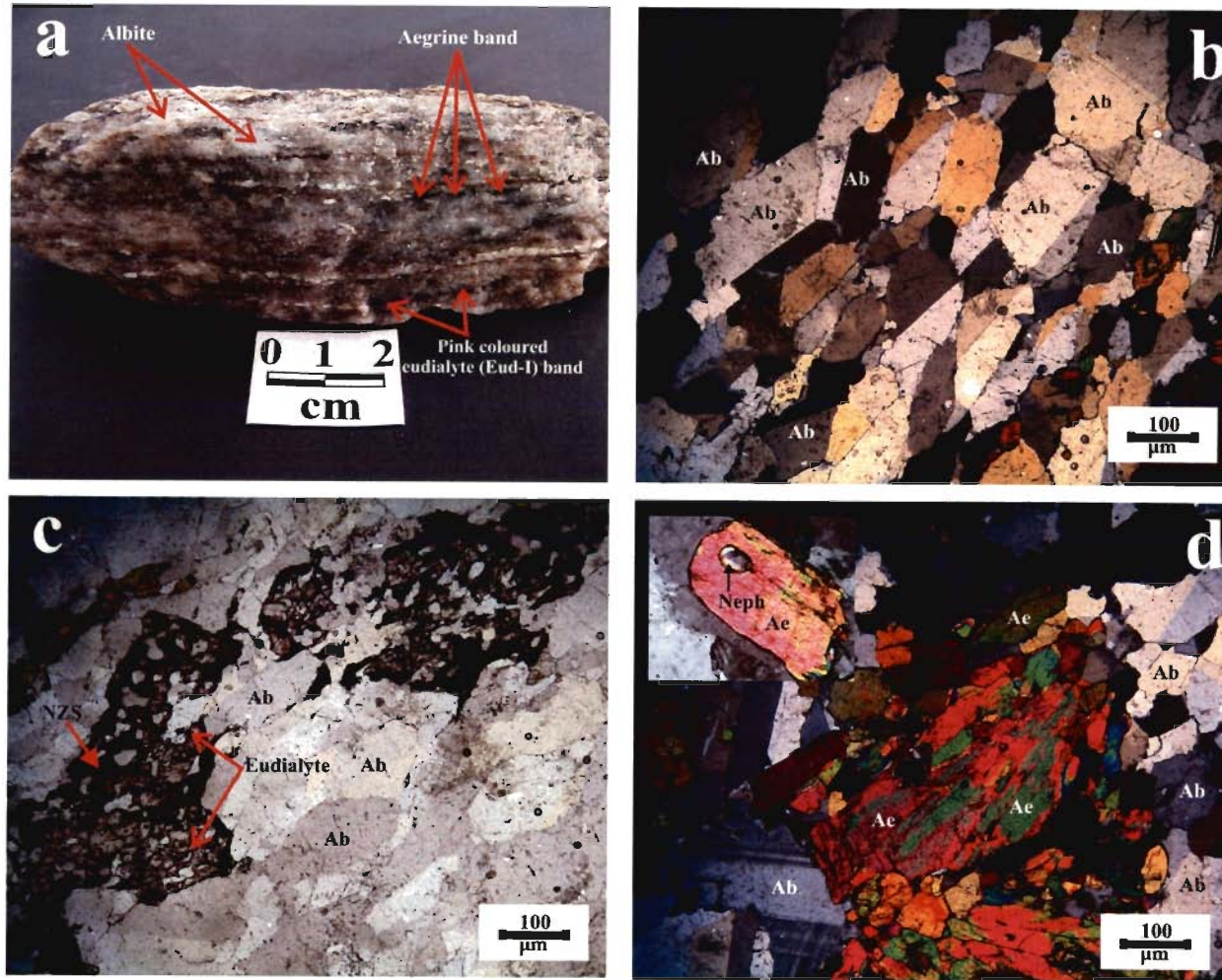


Figure 3.19 (a) Hand specimen of strongly banded syenite gneiss showing alternating banding of mafic and felsic minerals. (b) The rock dominantly consists of euhedral to subhedral albite. (c) Eudialyte-NZS-aegirine assemblage. (d) Aggregates of aegirine (lower right with higher order interference colour) are consistently present throughout the rock defining strong band of this mineral. (*Ab*: Albite, *Ae*: Aegirine, *NZS*: Na-Zr silicates)

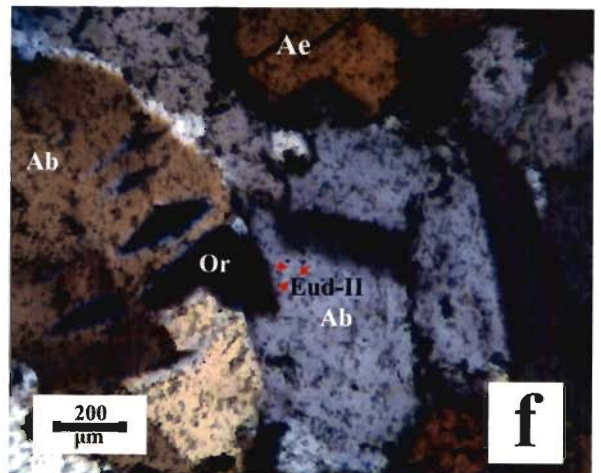
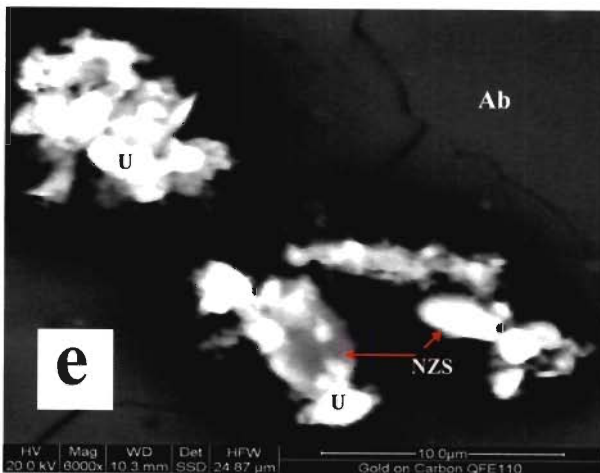
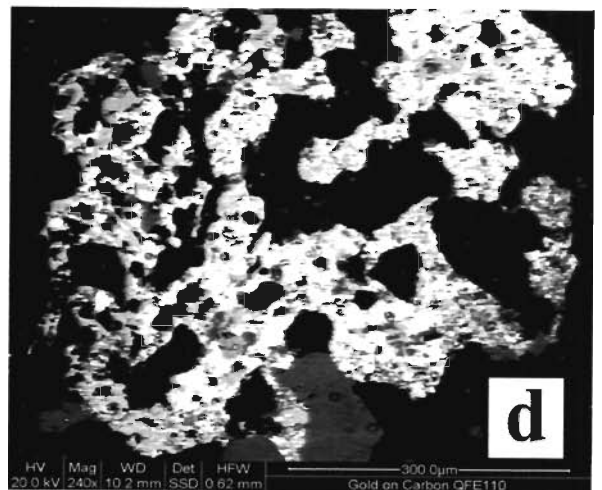
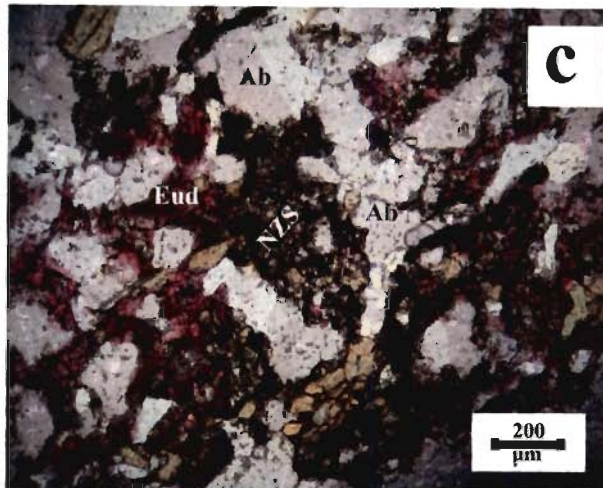
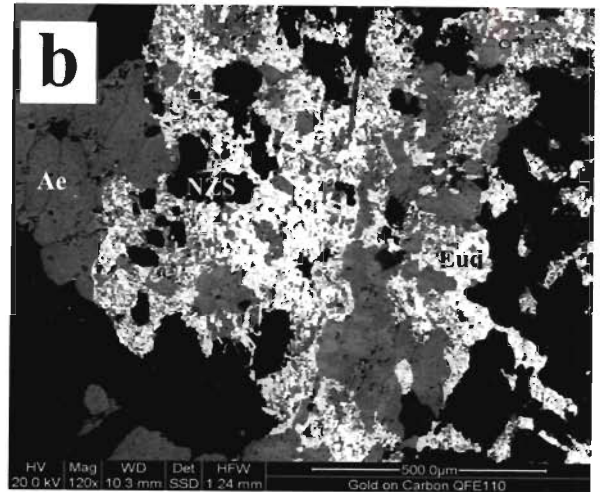
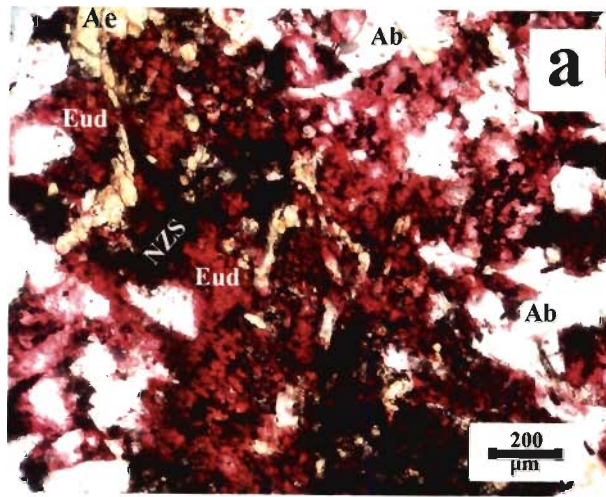


Fig. 3.20 (a) Complex zoning of eudialyte-Na-Zr silicates (NZS) replacing albite (Ab) and aegirine (Ae). BSE image of (a) showing the similar mineralogy. (c) Similar assemblages of eudialyte and corresponding BSE image (d). In this case eudialyte is replacing albite. (e) BSE image of the eudialyte and NZS. Some unidentified (U) REE, Nb, Y, Zr, Na and Cl bearing phase is also identified. (f) Inclusion like eudialyte (Eud-II) present within all the constituent minerals. Perthite is also observed in this variety of syenite gneiss.

Table 3.17) silicates which is mainly associated with the Eud-I and probably formed from the interaction of deuteritic fluid with the eudialyte-I. Such assemblage is comparable to the agpaitic to hyperagpaitic assemblage of Khomyakov (1995). The third variety is the last stage eudialyte formation (Eud-II) as fracture and parting fillings as described earlier. The determination of eudialyte composition by EPMA is not simple one. Lack of proper standard particularly standards for the determination of REE_2O_3 and Nb_2O_5 was not available and hence proper composition determination as described by Johnsen and Grice (1999) was not carried out for the present study. Only ZrO_2 along with the other major oxides were determined and presented in Table 3.17. The ZrO_2 content for the analyzed eudialyte is found to be ranging from 9.53 to 11.94 wt% along with higher Na_2O (7.40-8.36 wt%) and CaO (10.16-13.48 wt%). The associated Na-Zr silicates are characterized by higher concentration of ZrO_2 (~35 wt%). In addition to the EPMA detailed SEM-EDAX (FEI: Quanta 200F) and Raman Spectroscopic analysis were carried out on the polished thin sections of the same eudialyte grains and shown in Fig. 3.21. The simulated working condition was kept at 20Kv with spot size of $3\mu\text{m}$. The analyzed eudialyte is found to be essentially containing Zr, Nb and Y (atomic %) (Fig. 3.21a). Along with the eudialyte some Ca-Nb-Y-Zr-Na-Cl bearing silicate phase is also identified (Fig. 3.21b). Increase of Nb, Zr is observed towards the eudialyte and its complex assemblage with albite and aegirine (Fig. 3.21b). It is evident from the texture that the eudialyte is formed at late stage replacing early formed albite and aegirine. Complex zoning and subsequent transformation to Na-Zr bearing silicate phases point towards change in alkalinity of the deuteritic fluid which caused extensive metasomatism of the syenite gneiss.

Overall the rock is showing gneissic texture and essentially composed of albite, aegirine and eudialyte. Perthite is seen at places (Fig. 3.20f) and nephelines are mostly present as inclusions

within aegirine (Fig. 3.19d, inset figure). This variety of syenite differs from the earlier variety of syenite with increasing amount of mafic mineral i.e. aegirine. Presence of more pristine eudialyte along with the presence of complex Na-Zr and an unidentified Ca-Nb-Zr-Y-Na-Cl silicate may be attributed to the very late stage formation of this variety of syenite gneiss. However the mineral paragenesis described above is somewhat indicative of more agpaitic nature of this variety of syenite and simply other variant of poorly banded syenite.

B. MASSIVE SYENITE

This variety of syenite is also a medium grained (Fig 3.22a) with massive appearance and devoid of any visible banding. The amount of mafic mineral is very low compared to other varieties of syenite gneiss described above. The felsic minerals in the rock are represented by the orthoclase, albite and nepheline. The main mafic mineral is mica with rare presence of aegirine and both are randomly distributed within the rock. The dominant minerals in this variety of syenite are orthoclase which is making up to 75% by volume and then albite (15-20%). The nepheline is making maximum up to 5% by volume in the rock. The rock, in general, shows equigranular granulo texture (Fig. 3.22b) and relatively pristine in nature.

Orthoclase: This is the most dominant mineral found in this rock (Fig. 3.22a-d). Orthoclase grains are smaller in size (~1cm in diameter) in comparison to the other two variety of syenite gneiss. The grains are mostly subhedral to anhedral in shape and characterized by first order grey interference colour and shows parallel extinction. They are showing evidences of low temperature recrystallization or deformation as evidenced by the presence of microcline (Fig. 3.23a). Compositionally they are pure potash feldspar and contain 17.01-17.76% K₂O (Table 3.18). The other important constituents are SiO₂ (63.56-64.87%) and Al₂O₃ (17.20-17.63%). The Na₂O is almost absent. In the Ab-Or-An ternary plot (Fig.

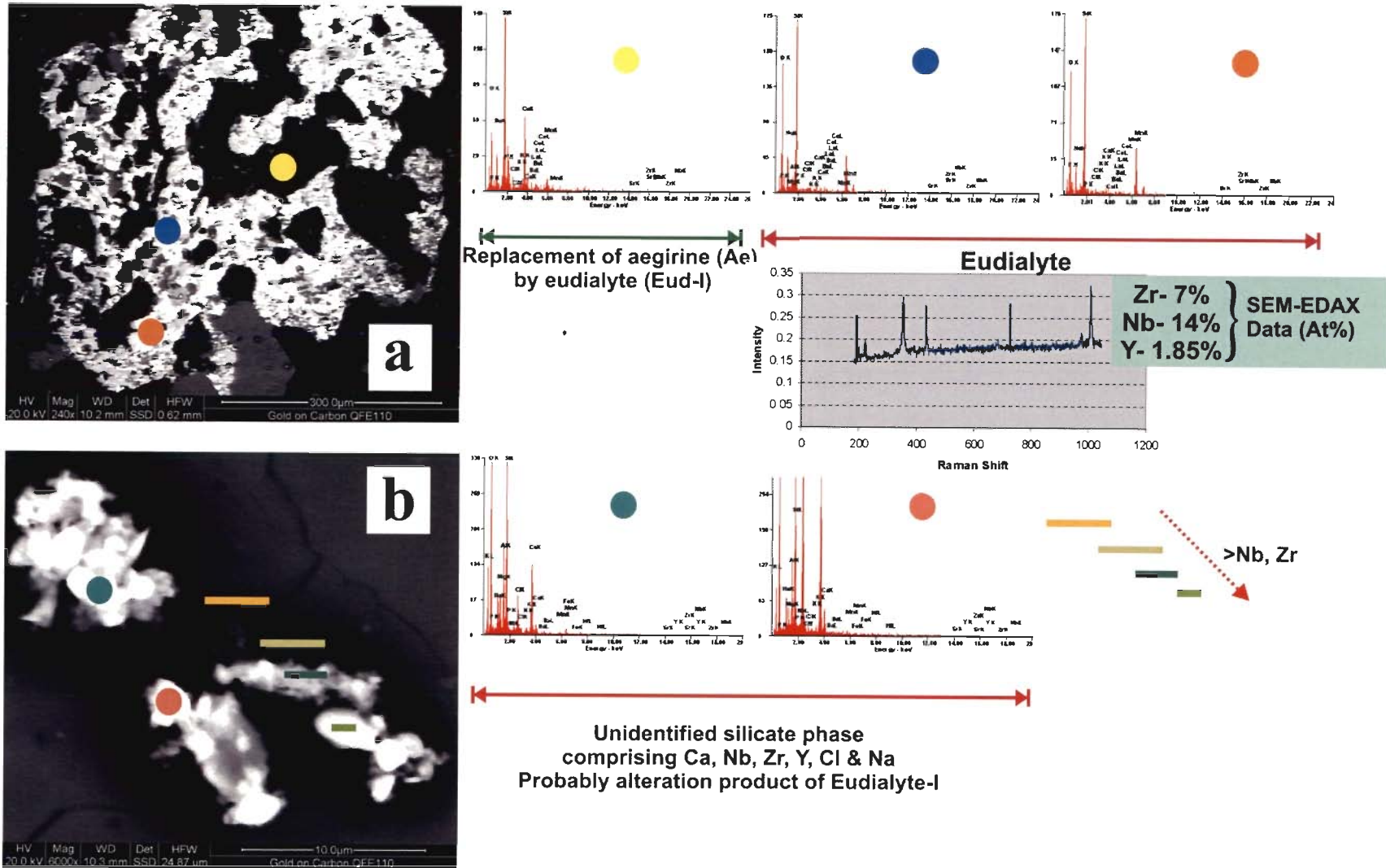


Fig. 3.21 (a) and (b) Compositions of eudialyte, NZS and some other unidentified phase analyzed by SEM-EDAX and Raman Spectroscopy respectively. For details see text (Post Magmatic Alterations of Strongly Banded Syenite Gneiss).

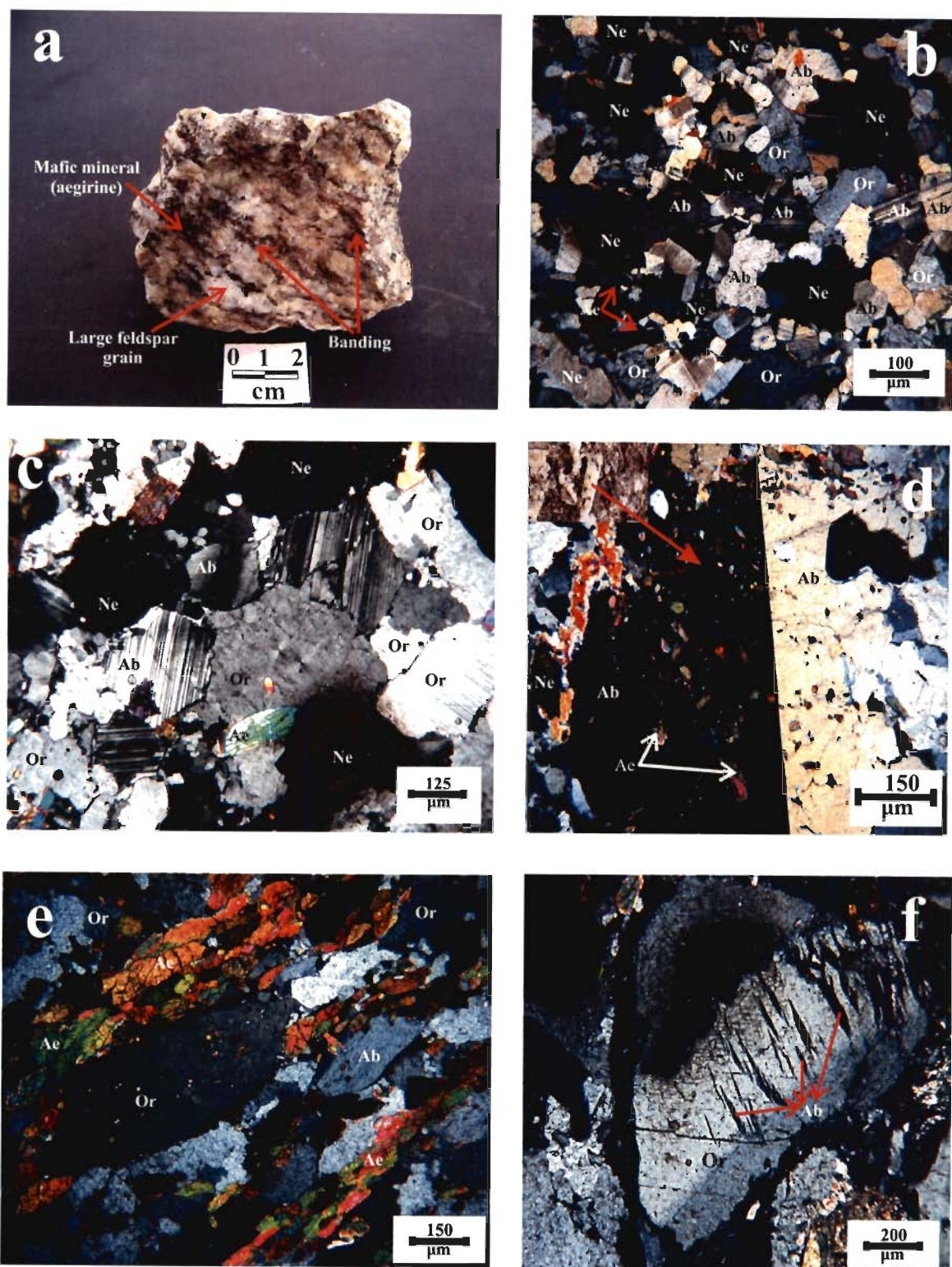


Figure 3.22 (a) Hand specimen of poorly banded syenite showing alternating banding of mafic and felsic minerals. Large plagioclase crystals are also visible. (b) and (c) Dominant mineral constituents of poorly banded syenite (for abbreviations see below) defining the porphyritic texture. (d) Large megacrysts of albite. (e) Alternating banding of mafic (aegirine) and felsic (feldspars and nepheline) minerals (f) Perthite texture in poorly banded syenite.

(Ab: Albite, Or: Orthoclase, Ne: nepheline, Ae: Aegirine)

3.13c) the composition is plotted at the orthoclase end indicating that compositionally they are pure orthoclase.

Albite: The next dominant mineral is albite. The albite grains are of comparatively smaller size and subhedral to anhedral in shape (Fig. 3.23b, c). They are colourless and showing prominent polysynthetic twinning of albite type in thin section. These plagioclase grains are showing first order grey interference colour. Analyses of the grains reveal that they are pure albite (Table 3.18). They consist of SiO₂ (>69.5%) and Al₂O₃ (>18.5%) and K₂O (>11%). The composition plot of the albite grains in the Ab-Or-An ternary diagram falls close to the albite end (Fig. 3.13c).

Nepheline: Nepheline content is about 5-10% by volume and the grains are subhedral to anhedral in shape (Fig. 3.22b, c). They are colourless under plane polarized light with first order grey interference color. At places these grains show patchy in appearances (Fig. 3.23a, Ne-II). Compositionally (Table 3.19), they are composed of SiO₂ (42.02-43.14%), Al₂O₃ (33.18-34.20%), Na₂O (15.39-17.29%) and K₂O (7.06-7.56%). The K/(Na+K) (atomic proportions) of nepheline varies from 22-24 with majority of 23 indicates that these nepheline grains are plutonic in origin (Trögger, 1969). The nepheline composition varies from Ne_{69.61}Ks_{219.02}Qtz_{9.36} to Ne_{77.35}Ks_{22.40}Qtz_{0.25} (Table 3.19) and falling within the Morozewicz-Buerger convergence field of plutonic nepheline (Fig. 3.14a), suggesting crystallization temperature was ~ 700°C. The most notable feature of the nepheline grains are decreasing content of silica in them and approaching towards the stoichiometric composition indicating significant cation exchange and re-equilibration with the late stage hydrothermal/deuteric fluid. As a result of such interaction of the late stage fluid and nepheline the nepheline grains are showing wide range of crystallization or equilibration temperature (Fig.3.14a). Composition of the nepheline when compared with the other

reported nepheline-syenite world-wide it has been noticed that they are remarkably similar to the Pilansberg alkaline complex of South Africa showing similar variation in nepheline composition (Fig. 31.14b). The close proximity of this nepheline towards ideal Morozewicz composition ($\text{Ne}_{75.0}\text{Ks}_{20.5}\text{Qtz}_{4.5}$) along with the presence of albite and microcline assemblage indicates that they are formed by either plutonic or metamorphic/metasomatic environment (Tilley, 1954, 1957). As the rock also containing microcline which is low temperature re-equilibration of monoclinic orthoclase to triclinic microcline (triclinicity) along with the textural evidences like granulose texture it is evident that the nepheline was formed under plutonic condition as indicated by the higher temperature range ($\sim 700^\circ\text{C}$) followed by the metamorphism and metasomatism and converging within the Morozewicz-Buerger field. The same is also evident when the nepheline composition plotted with nepheline compositions of other known nepheline syenites gneiss as that of the Haliburton-Bancroft area, York river, Blue Mountain (Tilley, 1954) and all are found to be plotted within the Morozewicz-Buerger field of convergence (Fig. 3.15).

Mica: Mica is present in very little amount (Fig. 3.22d, Fig. 3.23b) and represented by biotite (Fig. 3.24a). The grains are identified by its typical green colour with strong pleochroism from green to yellowish brown. The biotite grains are anhedral flake shaped and present as accessory mineral. They are typically showing evidences of absorption at feldspars grain boundaries (Fig. 3.23b). They are showing very high order green interference colour. Compositionally (Table 3.20) the biotites are characterized by very high amount of MnO (5.96-6.23%). Similar Mn rich biotite is reported from the miaskitic nepheline syenite of McGerrigle Plutonic Complex, Gaspé, Quebec, Canada (Wallace et al. 1990). The studied biotite grains when compared with that of the other nepheline syenite gneiss (Fig. 3.24b) they are found to be in close proximity of the biotite from Blue

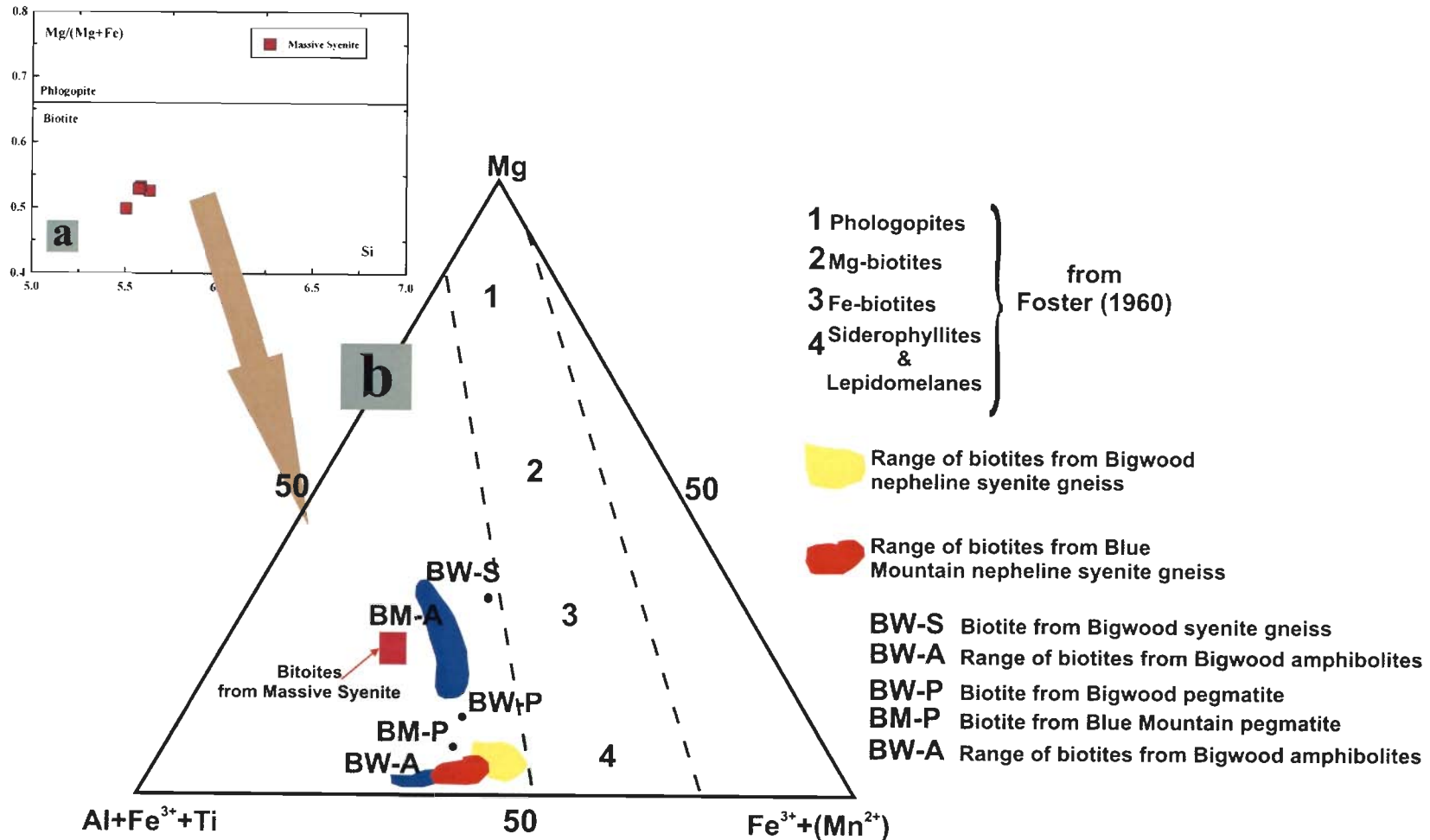


Fig. 3.24 (a) Composition of late stage biotites from massive syenite. (b) Comparison of the biotite on Mg - Al+Fe³⁺+Ti - Fe³⁺ (Mn²⁺) (after Foster, 1960) diagram from the studied massive syenite with the other well known nepheline syenite gneiss from Bigwood and Blue Mountain Complex of Ontario, Canada. The diagram shows the close proximity of the biotite with that of the Blue Mountain Amphibolites and Big Wood Syenites gneiss indicating formation of biotite during metamorphism.

Mountain amphibolites (Duke and Edgar, 1977). Moreover they are found to be falling within the range of Fe-biotite of Foster (1960). The other constituents are SiO₂ (34.66-36.15%), Al₂O₃ (18.72-19.30%), FeO (13.15-13.46%) and K₂O (9.03-10.23%). The relative enrichment of Fe²⁺ over Mg along with the very low Ti (Table 3.20) indicates that these biotites are formed at late stage.

Some random analyses of the opaque grains were carried out and it has been found that these are magnetite. At places magnetites are found to be replacing early formed eudialyte (Fig. 3.23c).

POST MAGMATIC ALTERATIONS

Similar to the nepheline syenite gneisses post magmatic metasomatic alteration by hydrothermal/deuteric fluid is also observed in this variety of syenite (Fig. 3.23c, d). At places patchy appearance of nepheline is observed (Fig. 3.23d). Moreover the fluid activity is very prominent throughout the rock and alterations particularly along the grain boundaries are visible (Fig. 3.23d). Late stage eudialyte formation and their presence within the fractures and partings (Fig. 3.23d) points towards late stage metasomatic alteration similar to the associated nepheline syenite gneisses. Many places complex mineral assemblage formed due to deuteric fluid interaction is also noticed (Fig. 3.23d).

The petrological and mineralogical character of this variety of syenite suggests that they have suffered extensive subsolidus metamorphic and metasomatic recrystallization similar to the nepheline syenite gneiss. But lack of primary/orthomagmatic mafic minerals like aegirine in nepheline syenite gneiss they are not showing any visible evidence of banding or layering. Presence of biotite along with the late stage magnetite indicates that biotites were buffered by MH (Fig. 3.25).

3.6 SUMMARY

Carbonatite and Pyroxenite association

The occurrence of carbonatite in association with alkali-pyroxenite in Beldih is somehow unusual in terms of the lack of usual association but not unique and reported from many other parts the world (Woolley and Kjarsgaard, 2008). In all the cases cited by Woolley and Kjarsgaard (2008) they have shown that such associations of alkali-pyroxenite (pyroxenite) and carbonatite are characteristic carbohydrothermal carbonatites as described by Mitchell (2005). Keeping aside the genesis of carbonatite for the time being (discussed later on Chapter 6) the studied carbonatite essentially containing calcite, apatite as principal mineral while amphibole, biotite, magnetite are making up the accessories. The amphibole grains of carbonatite are sodic-calcic in composition and represented by the richterite and magnesiokatophorite varieties. Both of them are low aluminum amphibole and characteristic of middle to late stage development of carbonatite (Hogarth, 1989). Thus it can be concluded that the carbonatite in Beldih area was formed at shallower depth and of hypabyssal origin. The most notable feature is the late stage hydrothermal/metasomatic fluid activity affected the rock similar to that of the nepheline syenites of Sushina described earlier. Fracture filling of the apatite by such late stage fluid (Fig. 3.26a, b) and interaction with the calcite grain is evident. The new mineral or phase which formed by such interaction is characteristically pink to violet in colour and shown by the marked circle in the Fig. 3.26 (a, b). Unfortunately due to lack of proper standards (EPMA) and unavailability of Raman Spectroscopy constrains characterization of these late formed phases.

The alkali-pyroxenite rock juxtaposed with the carbonatite is intruded by number of late stage calcite vein. This rock is giving signature of mixed mineralogy and dominated by the diopsidic pyroxene with significant acmite (aegirine) component. The two variety of amphibole has been noticed in this rock. The more crystalline variety is represented by the magnesiokatophorite. On

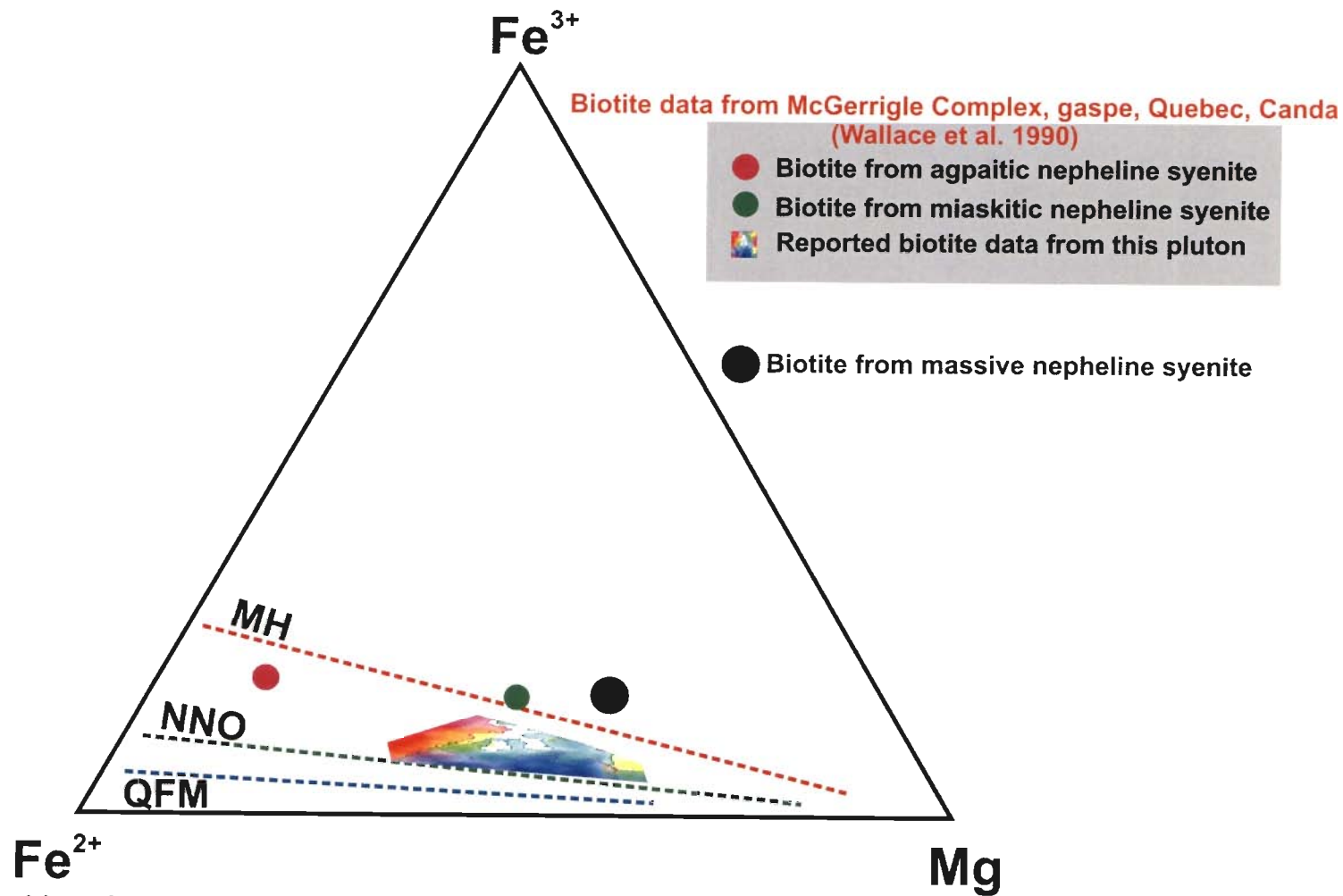


Fig. 3.25 The composition of biotite from massive syenite in terms of Fe^{3+} - Fe^{2+} - Mg. Lines representing oxygen fugacity buffers are from Wones and Eugster (1965). MH: magnetite-hematite, NNO: nickel-nickel oxide, QFM: quartz-fayalite-magnetite. The studied biotites are falling close to the MH buffer.

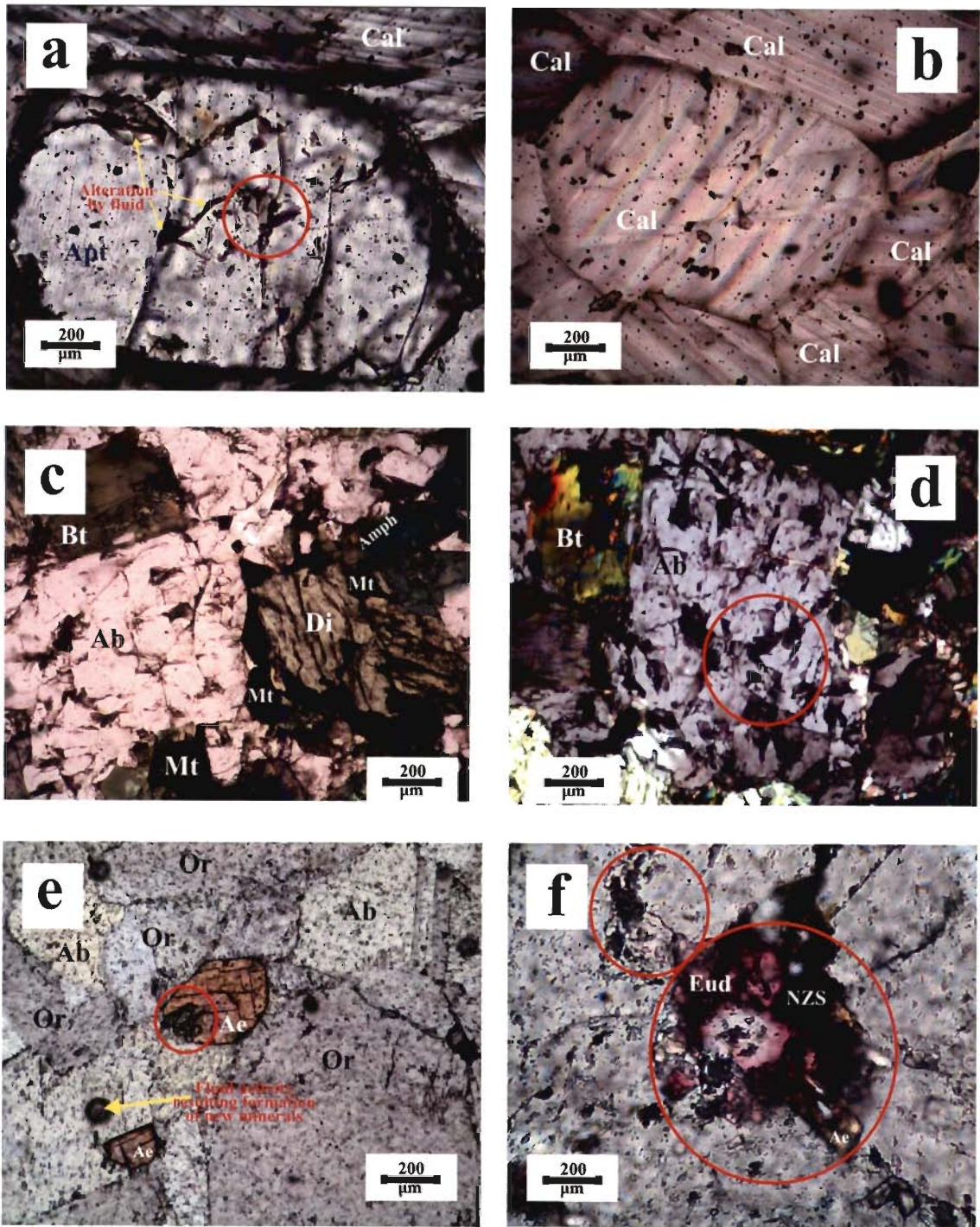


Fig. 3.26 Photomicrograph showing post magmatic alteration by hydrothermal/deuteric fluid. (a) Fracture filling by late stage mineral phase formed from the deuteric fluid (pink to violet colour) in apatite of carbonatite. (b) The same mineral is also present as small inclusion within the calcite grains (in carbonatite). (c) and (d) Prominent pink to violet colour mineral present in albite and biotite grains in alkali-pyroxenite. (e) Replacement of pyroxene (aegirine) by eudialyte the late stage deuteric fluid in poorly banded syenite gneiss. The other constituent grains (orthoclase-albite) are also carrying tiny grains of eudialyte. (d) Replace of aegirine by eudialyte and further formation of complex Na-Zr bearing silicates in poorly banded syenite gneiss. In all the photomicrograph the zone marked by the circle indicates pronounced effect of late stage alteration by deuteric fluid.

(Ae: Aegirine; Amph: Amphibole; Apt: Apatite; Ab: Albite; Bt: Biotite; Cal: Calcite; Di: Diopside; Eud: Eudialyte; Mt: Magnetite; NZS: Na-Zr Silicates)

the other hand pyroxene grains are often converted into amphibole and these varieties are represented by katophorite or taramite variety. Both of the variety is sodic-calcic in composition. The magnesiokatophorite is found to be the dominant amphibole in this rock. The rock is also containing apatite, albite, magnetite and ilmenite. The presence of albite, sodic-pyroxene along with the late stage calcite vein intrusion indicates that the rock has undergone intense alkali metasomatism. The presence of albite in the rock is an indication of fenitization which the rock has undergone probably during the carbonatite intrusion. The late stage vein filling assemblage by calcite-apatite-magnetite-ilmenite association is similar to the carbohydrothermal assemblage described by Mitchell (2005). However, similar to the carbonatite late stage metasomatic alteration (Fig. 3.26c, d) is also evident in this rock. This is mainly characterized by the presence late stage minerals (pink to violet coloured one in Fig. 3.26c, d) along fractures is indicative of the same.

A massive deposit of apatite-magnetite rock has been found in association with the carbonatite and pyroxenite. The rock is light colored (Fig. 3.10a) and dominantly composed of apatite (Fig. 3.10b). Pristine apatite grains are colorless and showing parallel extinction with imperfect basal cleavage which appears to be cross fractured (Fig. 3.10c). The igneous origin was proposed for this apatite-magnetite rock (Chakrabarty, 2002).

Nepheline Syenites

Depending on the silica saturation syenites are broadly classified into three categories namely: over-saturated, saturated and under-saturated. These three broad categories may be further subdivided in to three sub-categories depending on the kind of feldspar present i.e. potassic (orthoclase or microcline), sodicpotassic (perthites) or sodic (albite). All the syenitic rocks found at Sushina are under-saturated syenite. On the other hand based on their mineralogy, chemistry and alkalinity or agpaitic index nepheline syenites can also be broadly classified into two major categories: *agpaitic and miaskitic* variety (Sørensen, 1974). There exist two broad group of

nepheline syenite parageneses namely *hypersolvus* assemblages and *subsolvus* assemblages (Sørensen, 1974; Tilley, 1957; Hytönen, 1959; Wilkinson, 1965; Welman, 1970). The subsolvus assemblage is further subdivided into two major categories: primary igneous assemblages and recrystallized assemblages. The later variety i.e. recrystallized assemblage of nepheline syenite is commonly termed as *nepheline syenite gneiss* or *nepheline gneisses* and reported from the different part of the world e.g. Haliburton-Bancroft Belt (Blue Mountain Complex, Methuen Township) and Bigwood Complex (Sudbury) of Canada (Duke and Edgar, 1977). As described earlier different varieties of syenite are found about 40Km away from Beldih village at Sushina. There are two main varieties of syenite found in the Sushina area namely banded syenite and massive syenites. Based on the mesoscopic character the banded syenite can further be subdivided into two sub categories depending on the type of banding: poorly banded and strongly banded syenite gneiss. Both the poorly and strongly banded syenite gneiss is essentially composed of albite, orthoclase, nepheline and aegirine. The albite grains are large enough to call them as megacrysts and showing evidence of recrystallization and deformation. In general the area is dominated by the banded syenite. The other variety of nepheline syenite is characterized by the presence of orthoclase and nepheline as the principal mineral. The mafic mineral is very less and albite proportion also decreases substantially in this variety. Biotite is present and characterized by the significant amount of MnO. The end member composition of the feldspars, presence of microcline along with the nepheline composition falling within the Morozewicz-Buerger convergence field of plutonic nepheline indicate that the original rock (subsolvus nepheline syenitic assemblage) (Fig. 3.27) was formed by the igneous process and had undergone extensive metamorphism resulting the present day recrystallized assemblages similar to the *nepheline gneisses*. Subsolvus hydrothermal or deuteric alteration is also evident by the presence of eudialyte and some complex Na-Zr silicates (Fig. 3.26e, f). The most notable feature is the difference in mafic content in both the varieties of

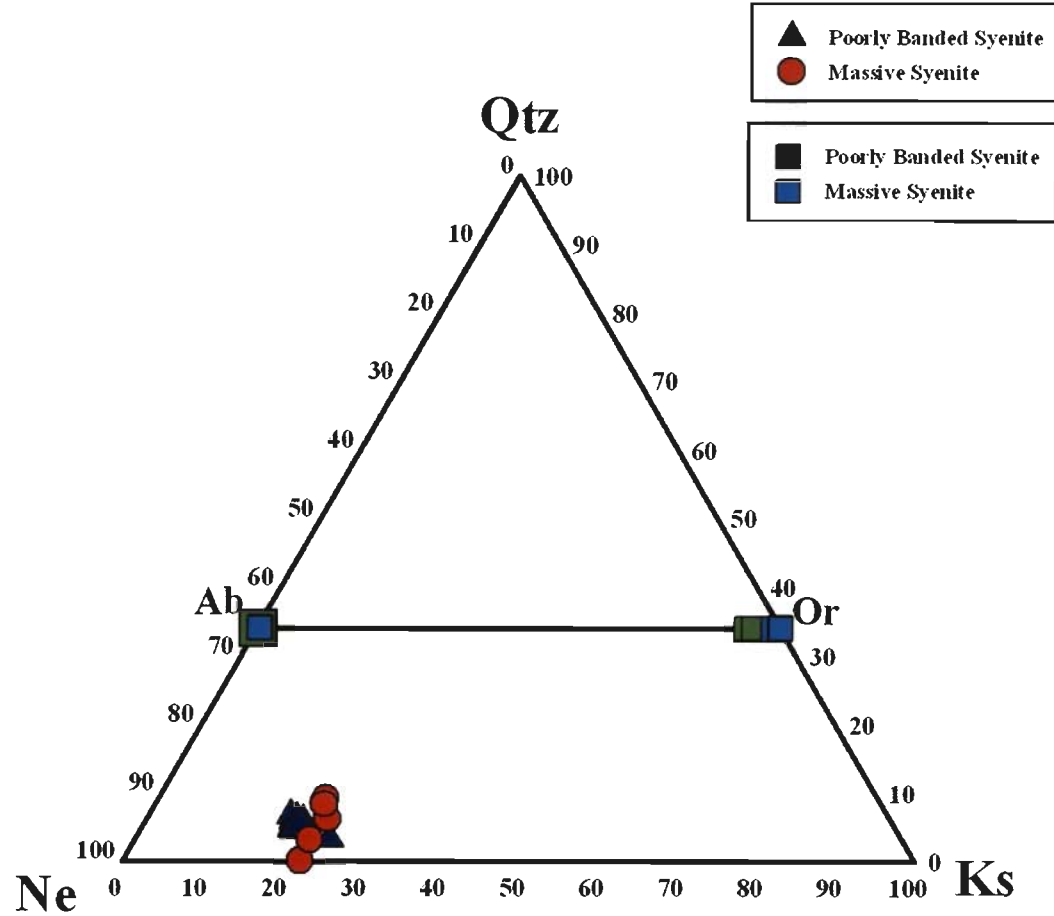


Fig. 3.27 Composition of nephelines and feldspars from nepheline syenite gneisses of the Sushina area plotted on the system $\text{NaAlSi}_3\text{O}_8$ (Ne)- KAlSi_3O_8 (Ks)- SiO_2 (Qtz). The studied nepheline syenite gneisses are similar to the nepheline syenite gneisses of the Bigwood and Blue Mountain Complex (cf. Duke and Edgar, 1977).

syenite. Extensive variation in nepheline composition particularly in the massive syenite suggests that the rock had undergone extensive subsolidus deuteric alteration. However, it is clear from the texture that three distinct textural features are present in the syenite. The primary igneous texture is represented by the porphyritic texture and phenocrysts of albite, orthoclase and nepheline (Fig. 3.12d, g). The metamorphic texture is evident from the prominent development of gneissic texture in banded syenites (Fig. 3.12e, 3.19d) and granulation of the constituting minerals in massive syenite (Fig. 3.22b, d). The metasomatic alterations are evident by the presence of eudialyte (Fig. 3.21, Fig. 3.20) and related minerals and at places the fluid movement is also evident which resulted crushing/granulation of the minerals (mostly felsic ones) (Fig. 3.20, 3.23). The textural and mineralogical features described earlier is indicative of miaskitic nature of the nepheline syenite during initial stages of formation and subsequently metamorphism and metasomatism of the primary mineralogical assemblage of miaskitic type (albite + orthoclase + nepheline + aegirine + apatite + zircon) push towards the agpaitic assemblage (miaskitic assemblage + eudialyte + Na-Zr-silicate + different varieties of apatite) and currently resembling agpaitic nepheline syenite gneiss. Irrespective of the origin of these rocks along the NSZ it is clear that an extensive regional metasomatism (probably by deuteric fluid) took place at later stage which is characterized by the presence of eudialyte in these rocks.

Table 3.1a: Composition of calcite in carbonatite

(Wt %)	1	2	3	4	5	6	7	8	9	10	11
Al₂O₃	-	-	-	-	-	-	-	-	0.22	-	-
FeO	1.32	1.14	1.21	1.28	0.37	0.40	0.33	0.31	0.35	0.31	0.34
MgO	1.13	1.10	0.94	0.99	0.39	0.44	0.31	0.42	0.43	0.28	0.28
MnO	0.44	0.38	0.40	0.43	0.15	0.16	0.15	0.22	0.18	0.14	0.16
CaO	53.21	51.76	52.76	52.14	53.14	52.74	53.33	54.27	52.06	52.55	53.97
Total	56.10	54.38	55.31	54.84	54.05	53.74	54.12	55.22	53.24	53.28	54.75

Table 3.1b: Composition of opaque in carbonatite

(Wt %)	Ilmenite					
	1	2	3	4	5	6
TiO₂	48.116	47.857	48.134	46.054	49.574	49.373
Al₂O₃	0.010	0.032	0.123	0.067	0.000	0.092
Cr₂O₃	0.011	0.023	0.021	0.013	0.028	0.000
Fe₂O₃	6.790	6.000	6.070	12.790	4.690	4.620
FeO	40.800	40.700	40.990	39.650	42.630	42.470
MnO	1.327	1.310	1.314	0.987	0.990	0.997
MgO	0.629	0.566	0.553	0.430	0.533	0.518
Total	97.683	97.088	97.205	99.991	98.445	98.070
Mol % of R₂O₃	6.820	6.680	6.280	12.910	4.720	4.760

Table 3.2: Composition of apatite from carbonatite

	1	2	3	4	5	6	7	8	9	10	11	12	13
SiO₂	0.14	0.09	0.12	0.10	0.09	0.07	0.13	0.04	0.07	0.03	0.05	0.04	0.07
Al₂O₃	0.02	0.00	0.01	0.01	0.00	0.00	0.04	0.00	0.01	0.00	0.00	0.00	0.00
FeO	0.00	0.04	0.00	0.05	0.00	0.00	0.00	0.00	0.04	0.02	0.00	0.00	0.00
MgO	0.06	0.02	0.01	0.01	0.01	0.00	0.02	0.01	0.01	0.00	0.00	0.00	0.01
CaO	53.16	54.40	54.57	55.15	55.03	54.95	54.99	52.11	52.48	53.64	53.88	53.22	53.86
MnO	0.03	0.05	0.04	0.07	0.00	0.00	0.01	0.02	0.07	0.05	0.00	0.04	0.00
P₂O₅	41.21	41.69	41.48	41.95	41.85	42.35	41.07	41.29	40.88	41.62	41.03	41.01	42.20
K₂O	0.00	0.00	0.00	0.00	0.00	0.00	0.00	0.00	0.00	0.00	0.00	0.02	0.00
Na₂O	0.29	0.30	0.24	0.22	0.25	0.25	0.24	0.30	0.28	0.27	0.30	0.21	0.24
Total	94.91	96.59	96.50	97.60	97.28	97.69	96.50	93.76	93.87	95.67	95.26	94.57	96.39
<i>Formula based on 25 O</i>													
Si	0.024	0.015	0.020	0.017	0.015	0.012	0.022	0.007	0.012	0.005	0.009	0.007	0.012
Al	0.004	0.000	0.002	0.002	0.000	0.000	0.008	0.000	0.002	0.000	0.000	0.000	0.000
Fe²⁺⁺	0.000	0.006	0.000	0.007	0.000	0.000	0.000	0.000	0.006	0.003	0.000	0.000	0.000
Mg	0.015	0.005	0.003	0.003	0.003	0.000	0.005	0.003	0.003	0.000	0.000	0.000	0.003
Ca	9.827	9.906	9.953	9.949	9.956	9.878	10.057	9.718	9.807	9.842	9.956	9.887	9.786
Mn	0.004	0.007	0.006	0.010	0.000	0.000	0.001	0.003	0.010	0.007	0.000	0.006	0.000
P	6.020	5.998	5.979	5.980	5.983	6.016	5.936	6.085	6.036	6.033	5.991	6.020	6.059
K	0.000	0.000	0.000	0.000	0.000	0.000	0.000	0.000	0.000	0.000	0.000	0.004	0.000
Na	0.097	0.099	0.079	0.072	0.082	0.081	0.079	0.101	0.095	0.090	0.100	0.071	0.079
Total	15.992	16.037	16.046	16.044	16.045	15.997	16.110	15.917	15.975	15.985	16.055	15.999	15.939

Table 3.2 (continued)

	14	15	16	17	18	19	20	21	22	23	24
SiO₂	0.09	0.12	0.09	0.06	0.08	0.06	0.05	0.08	0.09	0.11	0.07
Al₂O₃	0.00	0.00	0.00	0.01	0.01	0.00	0.02	0.03	0.01	0.00	0.00
FeO	0.12	0.00	0.02	0.12	0.00	0.00	0.05	0.00	0.00	0.00	0.00
MgO	0.00	0.02	0.01	0.02	0.00	0.01	0.01	0.04	0.03	0.00	0.00
CaO	53.50	53.80	53.76	53.66	53.65	53.30	52.44	51.66	53.40	53.07	53.63
MnO	0.01	0.00	0.00	0.00	0.08	0.04	0.00	0.04	0.00	0.03	0.00
P₂O₅	40.92	41.33	40.92	41.39	40.56	41.68	40.72	40.06	41.17	41.62	41.38
K₂O	0.00	0.00	0.00	0.02	0.01	0.00	0.00	0.00	0.00	0.00	0.01
Na₂O	0.24	0.23	0.27	0.17	0.26	0.19	0.23	0.30	0.22	0.20	0.23
Total	94.89	95.54	95.14	95.51	94.65	95.35	93.55	92.28	94.92	95.02	95.42
<i>Formula based on 25 O</i>											
Si	0.016	0.021	0.016	0.010	0.014	0.010	0.009	0.014	0.016	0.019	0.012
Al	0.000	0.000	0.000	0.002	0.002	0.000	0.004	0.006	0.002	0.000	0.000
Fe²⁺	0.017	0.000	0.003	0.017	0.000	0.000	0.007	0.000	0.000	0.000	0.000
Mg	0.000	0.005	0.003	0.005	0.000	0.003	0.003	0.011	0.008	0.000	0.000
Ca	9.919	9.892	9.945	9.871	9.991	9.795	9.833	9.827	9.876	9.777	9.870
Mn	0.001	0.000	0.000	0.000	0.012	0.006	0.000	0.006	0.000	0.004	0.000
P	5.995	6.005	5.982	6.016	5.968	6.052	6.034	6.021	6.018	6.059	6.018
K	0.000	0.000	0.000	0.004	0.002	0.000	0.000	0.000	0.000	0.000	0.002
Na	0.081	0.077	0.090	0.057	0.088	0.063	0.078	0.103	0.074	0.067	0.077
Total	16.031	16.006	16.049	15.991	16.077	15.938	15.973	15.998	15.993	15.926	15.992

Table 3.3: Composition of amphibole from carbonatite

(Wt%)	Magnesiokatophorite										Richterite			
	1	2	3	4	5	6	7	8	9	10	11	12	13	14
SiO ₂	50.47	49.47	50.34	50.06	51.98	49.76	49.95	50.82	50.73	50.49	50.22	55.19	55.67	55.45
Al ₂ O ₃	4.30	3.95	4.33	4.09	3.46	5.17	5.09	5.08	4.98	4.82	4.87	1.36	1.38	1.33
FeO*	13.12	13.14	13.32	12.77	13.10	14.85	14.72	15.06	13.95	13.70	13.78	11.99	11.87	11.84
MgO	15.01	14.93	15.02	14.94	15.84	14.03	14.01	13.84	14.58	14.80	14.76	17.26	17.03	17.23
MnO	0.05	0.04	0.08	0.12	0.08	0.06	0.05	0.08	0.06	0.11	0.08	0.06	0.06	0.13
CaO	5.47	5.23	5.36	5.10	5.00	4.51	4.63	4.57	5.38	5.62	5.66	4.30	4.25	4.08
K ₂ O	0.56	0.46	0.56	0.46	0.42	0.21	0.21	0.26	0.55	0.50	0.42	0.67	0.64	0.56
Na ₂ O	7.15	6.95	7.25	7.18	7.11	7.79	7.53	7.56	7.16	7.13	7.21	7.84	7.60	7.75
TiO ₂	0.74	0.66	0.73	0.74	0.74	0.70	0.67	0.45	0.53	0.73	0.75	0.27	0.30	0.30
Total	96.87	94.83	96.99	95.46	97.73	97.08	96.86	97.72	97.92	97.90	97.75	98.94	98.80	98.67
Si	7.341	7.337	7.312	7.372	7.457	7.223	7.267	7.336	7.309	7.280	7.251	7.786	7.829	7.814
Al ^{iv}	0.659	0.663	0.688	0.628	0.543	0.777	0.733	0.664	0.691	0.720	0.749	0.214	0.171	0.186
ΣT-site	8.000	8.000	8.000	8.000	8.000	8.000	8.000	8.000	8.000	8.000	8.000	8.000	8.000	8.000
Al ^{vi}	0.075	0.032	0.051	0.080	0.043	0.108	0.140	0.201	0.155	0.098	0.081	0.006	0.066	0.034
Ti	0.079	0.073	0.079	0.080	0.078	0.077	0.076	0.048	0.057	0.079	0.081	0.026	0.034	0.034
Fe ^{3+*}	0.577	0.660	0.646	0.584	0.569	0.821	0.730	0.673	0.598	0.602	0.634	0.441	0.406	0.440
Mg	3.251	3.298	3.255	3.283	3.388	3.035	3.038	2.977	3.130	3.180	3.177	3.626	3.574	3.623
Fe ^{2+*}	1.018	0.938	0.969	0.973	0.922	0.959	1.016	1.101	1.060	1.041	1.027	0.901	0.920	0.869
ΣC-site	5.000	5.000	5.000	5.000	5.000	5.000	5.000	5.000	5.000	5.000	5.000	5.000	5.000	5.000
Fe ₂ ^{2+*}	0.004	0.034	-	0.009	0.087	0.023	0.045	0.049	0.023	0.009	0.003	0.073	0.069	0.079
Mn ²⁺	0.006	0.009	0.009	0.018	0.009	0.007	0.006	0.010	0.007	0.013	0.010	0.008	0.008	0.017
Ca	0.856	0.829	0.838	0.805	0.767	0.702	0.722	0.707	0.831	0.867	0.876	0.652	0.642	0.618
Na	1.134	1.128	1.153	1.168	1.137	1.268	1.227	1.234	1.139	1.111	1.111	1.267	1.281	1.286
ΣB-site	2.000	2.000	2.000	2.000	2.000	2.000	2.000	2.000	2.000	2.000	2.000	2.000	2.000	2.000
Na	0.876	0.868	0.889	0.886	0.845	0.925	0.898	0.882	0.862	0.882	0.907	0.867	0.798	0.830
K	0.104	0.090	0.104	0.088	0.068	0.038	0.040	0.048	0.102	0.092	0.077	0.118	0.118	0.102
ΣA-site	0.980	0.958	0.993	0.974	0.913	0.964	0.938	0.930	0.964	0.974	0.984	0.985	0.916	0.932
Total	15.983	15.958	15.993	15.974	15.913	15.964	15.938	15.929	15.963	15.973	15.984	15.985	15.916	15.932

* Total Fe calculated as FeO ** Recalculated to Fe²⁺ and Fe³⁺

Table 3.3 (continued)

	Richterite										
(Wt%)	15	16	17	18	19	20	21	22	23	24	25
SiO ₂	53.50	53.59	54.16	52.79	53.50	54.77	54.47	54.29	54.33	54.91	54.05
Al ₂ O ₃	2.11	2.19	2.17	2.09	1.99	1.79	1.81	1.75	1.71	1.73	1.72
FeO [*]	12.69	12.71	13.02	12.12	12.36	12.13	12.01	13.15	13.51	12.75	12.80
MgO	16.40	16.25	15.87	15.79	16.22	16.54	16.64	16.27	16.07	16.23	16.20
MnO	0.09	0.11	0.07	0.14	0.10	0.07	0.12	0.05	0.08	0.10	0.14
CaO	4.31	4.41	4.23	4.75	4.25	4.49	4.52	3.84	3.41	4.41	4.44
K ₂ O	0.62	0.67	0.61	0.56	0.59	0.63	0.62	0.48	0.34	0.60	0.58
Na ₂ O	7.78	8.13	7.33	7.13	7.82	7.90	7.72	7.87	8.14	6.97	6.99
TiO ₂	0.47	0.46	0.50	0.40	0.39	0.42	0.39	0.13	0.09	0.43	0.43
Total	97.97	98.52	97.96	95.77	97.22	98.74	98.30	97.83	97.68	98.13	97.35
Si	7.641	7.619	7.741	7.761	7.678	7.749	7.721	7.741	7.753	7.815	7.771
Al ^{iv}	0.359	0.359	0.259	0.239	0.322	0.251	0.279	0.259	0.246	0.185	0.229
ΣT-site	8.000	7.978	8.000	8.000	8.000	8.000	8.000	8.000	8.000	8.000	8.000
Al ^{vi}	0.002	-	0.102	0.109	0.023	0.055	0.028	0.032	0.044	0.106	0.064
Ti	0.052	0.051	0.052	0.044	0.043	0.043	0.043	0.017	0.009	0.043	0.043
Fe ^{3+*}	0.515	0.598	0.429	0.383	0.569	0.442	0.477	0.599	0.652	0.393	0.380
Mg	3.494	3.442	3.385	3.409	3.469	3.484	3.516	3.459	3.422	3.446	3.471
Fe ^{2+*}	0.937	0.909	1.032	1.055	0.897	0.976	0.936	0.893	0.873	1.012	1.042
ΣC-site	5.000	5.000	5.000	5.000	5.000	5.000	5.000	5.000	5.000	5.000	5.000
Fe ^{2+*}	0.059	0.005	0.094	0.023	0.017	0.010	0.017	0.075	0.079	0.108	0.124
Mn ²⁺	0.009	0.017	0.009	0.017	0.009	0.008	0.017	0.009	0.009	0.009	0.017
Ca	0.661	0.675	0.644	0.739	0.656	0.680	0.689	0.582	0.523	0.675	0.682
Na	1.271	1.303	1.253	1.221	1.318	1.302	1.277	1.334	1.389	1.208	1.177
ΣB-site	2.000	2.000	2.000	2.000	2.000	2.000	2.000	2.000	2.000	2.000	2.000
Na	0.893	0.935	0.775	0.779	0.856	0.856	0.851	0.840	0.857	0.708	0.775
K	0.120	0.120	0.104	0.104	0.104	0.118	0.120	0.086	0.068	0.102	0.104
ΣA-site	1.013	1.055	0.879	0.883	0.960	0.974	0.971	0.926	0.925	0.810	0.879
Total	16.013	16.033	15.879	15.883	15.930	15.974	15.971	15.627	15.925	15.810	15.879

* Total Fe calculated as FeO ** Recalculated to Fe²⁺ and Fe³⁺

Table 3.3 (continued)

(wt%)	Richterite											
	26	27	28	29	30	31	32	33	34	35	36	37
SiO₂	55.33	55.73	54.98	55.36	55.32	54.75	54.78	54.42	54.04	54.42	54.04	53.74
Al₂O₃	1.15	1.13	1.57	1.65	1.59	0.70	0.82	0.78	1.49	1.30	1.28	1.32
FeO*	11.94	11.65	12.65	11.74	12.60	10.37	10.69	10.34	14.13	13.33	13.03	12.69
MgO	16.97	17.31	16.26	16.25	16.34	17.09	17.07	17.06	14.93	15.66	15.40	15.34
MnO	0.11	0.09	0.06	0.06	0.08	0.11	0.12	0.09	0.05	0.05	0.06	0.05
CaO	4.26	4.19	4.02	4.23	4.13	3.73	3.71	3.70	3.05	2.84	3.11	3.06
K₂O	0.64	0.68	0.43	0.53	0.50	0.70	0.71	0.71	0.60	0.78	0.73	0.76
Na₂O	7.25	7.73	7.32	7.02	7.14	7.63	7.68	7.58	7.90	8.46	8.26	8.16
TiO₂	0.30	0.31	0.18	0.39	0.30	0.35	0.34	0.36	0.37	0.57	0.65	0.62
Total	97.95	98.82	97.47	97.23	98.00	95.43	95.92	95.04	96.56	97.41	96.56	95.74
Si	7.866	7.853	7.855	7.904	7.856	7.942	7.906	7.919	7.841	7.800	7.828	7.844
Al^{iv}	0.134	0.147	0.145	0.096	0.144	0.058	0.094	0.081	0.159	0.200	0.172	0.156
ΣT-site	8.000	8.000	8.000	8.000	8.000	8.000	8.000	8.000	8.000	8.000	8.000	8.000
Al^{vi}	0.054	0.039	0.119	0.181	0.122	0.062	0.046	0.053	0.096	0.019	0.047	0.071
Ti	0.034	0.034	0.019	0.041	0.032	0.038	0.043	0.043	0.041	0.062	0.071	0.068
Fe^{3+*}	0.359	0.423	0.412	0.317	0.411	0.354	0.403	0.379	0.525	0.627	0.507	0.478
Mg	3.596	3.596	3.461	3.458	3.459	3.695	3.672	3.701	3.228	3.345	3.324	3.338
Fe^{2+*}	0.957	0.908	0.989	1.003	0.976	0.851	0.836	0.824	1.110	0.947	1.051	1.045
ΣC-site	5.000	5.000	5.000	5.000	5.000	5.000	5.000	5.000	5.000	5.000	5.000	5.000
Fe^{2+*}	0.102	0.048	0.111	0.082	0.109	0.052	0.052	0.058	0.079	0.024	0.021	0.026
Mn²⁺	0.017	0.008	0.008	0.008	0.010	0.013	0.015	0.011	0.007	0.006	0.007	0.007
Ca	0.649	0.635	0.616	0.647	0.628	0.580	0.574	0.577	0.474	0.436	0.482	0.478
Na	1.232	1.309	1.265	1.263	1.253	1.355	1.359	1.354	1.440	1.534	1.490	1.489
ΣB-site	2.000	2.000	2.000	2.000	2.000	2.000	2.000	2.000	2.000	2.000	2.000	2.000
Na	0.776	0.807	0.763	0.680	0.713	0.792	0.791	0.784	0.784	0.817	0.831	0.819
K	0.120	0.118	0.079	0.096	0.090	0.130	0.130	0.132	0.111	0.143	0.135	0.142
ΣA-site	0.886	0.925	0.842	0.776	0.803	0.922	0.921	0.916	0.895	0.960	0.966	0.961
Total	15.886	15.925	15.842	15.777	15.802	15.921	15.920	15.916	15.895	15.962	15.966	15.960

* Total Fe calculated as FeO ** Recalculated to Fe²⁺ and Fe³⁺

Table 3.4: Composition of clinopyroxene from alkali-pyroxenite

(Wt%)	1	2	3	4	5
SiO ₂	53.92	53.70	53.85	53.59	53.58
TiO ₂	0.740	0.760	0.710	0.800	0.680
Al ₂ O ₃	1.750	1.720	1.77	1.700	1.910
FeO*	12.24	13.42	12.55	12.25	12.01
MnO	0.160	0.280	0.170	0.160	0.180
MgO	7.820	7.640	7.790	8.080	7.940
CaO	16.73	16.22	16.72	17.27	17.08
K ₂ O	0.000	0.000	0.020	0.000	0.060
Na ₂ O	4.080	4.430	4.090	4.080	3.960
Cr ₂ O ₃	0.080	0.070	0.050	0.050	0.060
Total	97.52	98.24	97.72	97.98	97.46
<i>Formula based on 6 O</i>					
Si	2.072	2.062	2.070	2.056	2.060
Ti	0.021	0.022	0.020	0.023	0.020
Al	0.079	0.078	0.080	0.077	0.087
Fe ²⁺	0.393	0.431	0.403	0.393	0.386
Mn ²⁺	0.005	0.009	0.006	0.005	0.006
Mg	0.448	0.437	0.446	0.462	0.456
Ca	0.689	0.667	0.689	0.710	0.704
K	0.000	0.000	0.001	0.000	0.003
Na	0.304	0.330	0.305	0.303	0.296
Cr	0.003	0.002	0.001	0.002	0.002
Total	4.013	4.038	4.022	4.032	4.018
<i>Mol.% end members</i>					
CaTiAl ₂ O ₆	2.242	2.311	2.124	2.413	2.123
CaAl ₂ SiO ₆	2.002	1.786	2.124	1.626	2.495
NaFeSi ₂ O ₆	32.453	34.664	32.395	31.794	31.423
Ca ₂ Si ₂ O ₆	34.641	32.983	34.466	35.205	35.032
Fe ₂ Si ₂ O ₆	4.750	5.305	5.204	4.722	4.777
Mg ₂ Si ₂ O ₆	23.912	22.952	23.686	24.239	24.151
<i>Recalculated into acmite-hedenbergite-diopside</i>					
Ac	35.368	37.292	35.142	34.652	34.419
Hd	52.119	49.384	51.389	52.836	52.908
Di	12.513	13.324	13.469	12.512	12.673

* Total Fe calculated as FeO+Fe₂O₃ and FeO calculated by combining all Na₂O as acmite

Table 3.5: Composition of amphibole from alkali-pyroxenite

(Wt%)	MK										
	1	2	3	4	5	6	7	8	9	10	11
SiO ₂	47.35	47.51	47.54	46.77	48.30	47.30	48.67	47.81	47.73	47.50	48.43
Al ₂ O ₃	6.55	6.57	6.60	6.97	5.86	6.38	6.33	6.20	6.48	6.95	6.60
FeO*	16.13	15.91	15.66	15.75	15.42	15.55	14.91	15.49	15.75	15.67	15.23
MgO	9.57	9.55	9.79	9.70	10.27	9.95	11.32	9.73	9.63	9.51	9.95
MnO	0.10	0.28	0.19	0.20	0.23	0.25	0.14	0.29	0.15	0.16	0.08
CaO	6.33	6.88	6.15	6.29	6.32	6.25	6.38	6.31	6.37	6.21	6.09
K ₂ O	0.74	0.71	0.69	0.64	0.76	0.67	0.66	0.65	0.65	0.58	0.57
Na ₂ O	5.73	5.67	5.83	5.86	5.56	5.79	6.00	5.73	5.71	6.09	6.08
TiO ₂	2.36	2.40	1.88	1.83	1.33	1.88	1.56	1.66	1.64	1.76	1.62
Cr ₂ O ₃	0.02	0.00	0.04	0.01	0.02	0.03	0.05	0.06	0.06	0.00	0.11
Total	94.88	95.48	94.37	94.02	94.07	94.05	96.02	93.93	94.17	94.43	94.76
<i>Formula based on 23 O</i>											
Si	7.236	7.220	7.282	7.207	7.404	7.276	7.291	7.351	7.324	7.270	7.352
Al ^{iv}	0.764	0.780	0.718	0.793	0.596	0.724	0.709	0.659	0.676	0.730	0.648
ΣT-site	8.000	8.000	8.000	8.000	8.000	8.000	8.000	8.000	8.000	8.000	8.000
Al ^{vi}	0.416	0.397	0.474	0.473	0.463	0.433	0.409	0.475	0.496	0.524	0.533
Ti	0.271	0.274	0.217	0.212	0.153	0.217	0.176	0.192	0.189	0.203	0.185
Cr ³⁺	0.002	0.000	0.005	0.001	0.002	0.004	0.006	0.007	0.007	0.000	0.000
Fe ^{3+*}	0.000	0.000	0.000	0.000	0.000	0.000	0.000	0.000	0.000	0.000	0.013
Mg	2.180	2.163	2.235	2.228	2.346	2.281	2.527	2.230	2.202	2.169	2.251
Fe ^{2+**}	2.062	2.022	2.006	2.030	1.977	2.000	1.853	1.992	2.021	2.006	1.933
ΣC-site	4.931	4.856	4.937	4.944	4.941	4.935	4.971	4.896	4.915	4.902	4.915
Fe ^{2+**}	0.000	0.000	0.000	0.000	0.000	0.000	0.000	0.000	0.000	0.000	0.000
Mn ²⁺	0.013	0.036	0.025	0.026	0.030	0.033	0.018	0.038	0.019	0.021	0.010
Ca	1.037	1.120	1.009	1.039	1.038	1.030	1.024	1.040	1.047	1.018	0.991
Na	0.950	0.844	0.966	0.935	0.932	0.937	0.958	0.922	0.934	0.961	0.999
ΣB-site	2.000	2.000	2.000	2.000	2.000	2.000	2.000	2.000	2.000	2.000	2.000
Na	0.748	0.827	0.766	0.816	0.721	0.790	0.785	0.786	0.765	0.846	0.791
K	0.144	0.138	0.135	0.126	0.149	0.132	0.126	0.128	0.127	0.113	0.110
ΣA-site	0.892	0.965	0.901	0.942	0.870	0.922	0.911	0.914	0.892	0.959	0.901
Total	15.823	15.821	15.837	15.886	15.812	15.856	15.898	15.809	15.810	15.861	15.816

* Total Fe calculated as FeO ** Recalculated to Fe²⁺ and Fe³⁺

Table 3.5 (Continued)

(Wt%)	MK				K/T				
	12	13	14	15	16	17	18	19	20
SiO ₂	47.11	40.38	42.13	41.32	41.33	41.80	41.92	41.78	41.87
Al ₂ O ₃	6.73	12.03	10.84	10.78	14.81	10.58	10.67	10.64	10.63
FeO*	15.78	19.00	20.26	21.01	20.69	19.84	20.58	20.30	20.46
MgO	9.59	6.83	7.28	7.45	7.20	7.64	7.48	7.41	7.41
MnO	0.24	0.17	0.13	0.24	0.16	0.10	0.21	0.05	0.09
CaO	6.75	8.32	7.96	7.83	7.77	8.02	8.11	7.84	7.68
K ₂ O	0.75	0.71	0.63	0.62	0.62	0.69	0.64	0.62	0.70
Na ₂ O	5.69	4.60	5.28	5.4	5.47	5.20	5.31	5.48	5.44
TiO ₂	1.98	0.33	0.27	0.36	0.39	0.29	0.28	0.34	0.33
Cr ₂ O ₃	0.00	0.00	0.00	0.03	0.01	0.03	0.00	0.09	0.04
Total	94.62	92.37	94.78	95.04	94.53	94.20	95.20	94.55	94.65
<i>Formula based on 23 O</i>									
Si	7.223	6.477	6.584	6.442	6.481	6.563	6.527	6.543	6.548
Al ^{iv}	0.777	1.523	1.416	1.558	1.519	1.437	1.473	1.457	1.452
ΣT-site	8.000	8.000	8.000	8.000	8.000	8.000	8.000	8.000	8.000
Al ^{vi}	0.439	0.752	0.581	0.423	0.494	0.521	0.486	0.507	0.508
Ti	0.228	0.040	0.032	0.042	0.046	0.034	0.033	0.040	0.039
Cr ³⁺	0.000	0.000	0.000	0.004	0.001	0.004	0.000	0.011	0.005
Fe ^{3+*}	0.000	0.260	0.432	0.732	0.616	0.486	0.559	0.531	0.567
Mg	2.191	1.633	1.696	1.731	1.683	1.790	1.736	1.729	1.727
Fe ^{2+**}	2.023	2.289	2.216	2.008	2.097	2.119	2.121	2.127	2.109
ΣC-site	4.881	4.975	4.957	4.940	4.937	4.954	4.935	4.945	4.955
Fe ^{2+**}	0.000	0.000	0.000	0.000	0.000	0.000	0.000	0.000	0.000
Mn ²⁺	0.031	0.023	0.017	0.032	0.021	0.013	0.028	0.007	0.012
Ca	1.109	1.430	1.333	1.308	1.306	1.349	1.353	1.316	1.287
Na	0.860	0.547	0.650	0.660	0.673	0.638	0.619	0.677	0.701
ΣB-site	2.000	2.000	2.000	2.000	2.000	2.000	2.000	2.000	2.000
Na	0.831	0.884	0.950	0.972	0.990	0.945	0.984	0.987	0.949
K	0.147	0.145	0.126	0.123	0.124	0.138	0.127	0.124	0.140
ΣA-site	0.978	1.029	1.076	1.095	1.114	1.083	1.111	1.111	1.089
Total Cations	15.860	16.003	16.032	16.035	16.051	16.039	16.046	16.057	16.042

* Total Fe calculated as FeO ** Recalculated to Fe²⁺ and Fe³⁺

MK: Magnesiokatophorite, K/T: Katophorite/Taramite

Table 3.6: Composition of biotite from the alkali-pyroxenite

	1	2	3	4	5	6
SiO₂	38.68	39.33	38.42	36.87	38.33	36.78
TiO₂	1.12	1.06	1.4	0.81	1.17	2.28
Al₂O₃	12.78	13.26	13.59	12.41	12.53	12.33
Cr₂O₃	0	0.01	0.02	0	0	0
FeO	15.63	14.42	15.27	14.81	15.15	15.78
MnO	0.09	0.2	0.13	0.14	0.15	0.2
MgO	13.46	13.26	12.82	15.9	17.19	16.5
CaO	0.03	0	0.1	0.04	0.07	0.06
Na₂O	0.32	0.3	0.3	0.15	0.23	0.15
K₂O	8.7	8.57	8.28	12.45	12.42	12.3
Total	90.81	90.41	90.33	93.58	97.24	96.38
<i>Formula based on 22O</i>						
Si	6.046	6.117	6.009	5.743	5.728	5.588
^{IV}Al	1.954	1.883	1.991	2.257	2.207	2.208
^{VI}Al	0.400	0.547	0.514	0.021	0.000	0.000
Ti	0.132	0.124	0.165	0.095	0.132	0.261
Cr	0.000	0.001	0.002	0.000	0.000	0.000
Fe²⁺	2.043	1.875	1.997	1.929	1.893	2.005
Mn	0.012	0.026	0.017	0.018	0.019	0.026
Mg	3.137	3.074	2.989	3.692	3.830	3.737
Ca	0.005	0.000	0.017	0.007	0.011	0.010
Na	0.097	0.090	0.091	0.045	0.067	0.044
K	1.735	1.700	1.652	2.474	2.368	2.384
Total	15.561	15.437	15.444	16.281	16.255	16.263
Mg/(Mg+Fe)	0.606	0.621	0.599	0.657	0.669	0.651

Table 3.7: Composition of plagioclase feldspar in alkali-pyroxenite

	1	2	3	4	5	6	7	8	9	10	11	12
SiO₂	69.71	69.66	70.24	69.35	69.43	69.85	69.31	69.09	69.07	68.65	69.01	69.1
Al₂O₃	18.88	19.09	19.07	18.76	19.25	19.13	19.15	19.03	19.11	19.56	19.22	19.39
FeO	0.28	0.10	0.07	0.00	0.11	0.07	0.06	0.00	0.00	0.11	0.00	0.00
MgO	0.02	0.01	0.02	0.00	0.00	0.00	0.00	0.02	0.01	0.01	0.01	0.02
CaO	0.04	0.03	0.08	0.23	0.15	0.09	0.25	0.15	0.19	0.55	0.19	0.19
MnO	0.06	0.05	0.00	0.09	0.00	0.00	0.03	0.00	0.00	0.00	0.00	0.05
P₂O₅	0.00	0.02	0.02	0.03	0.02	0.00	0.00	0.01	0.00	0.02	0.09	0.01
K₂O	0.03	0.01	0.01	0.01	0.00	0.04	0.01	0.01	0.04	0.03	0.05	0.03
Na₂O	12.4	12.28	12.36	12.07	11.88	12.01	12.01	12.02	12.02	11.66	11.96	11.95
Total	101.46	101.31	101.91	100.62	100.91	101.19	100.83	100.33	100.48	100.59	100.62	100.82
<i>Formula based on 8 O</i>												
Si	3.011	3.008	3.014	3.014	3.005	3.015	3.005	3.009	3.005	2.986	2.998	2.996
Al	0.961	0.972	0.964	0.961	0.982	0.973	0.979	0.977	0.98	1.002	0.984	0.991
Fe²⁺	0.01	0.003	0.003	0.000	0.004	0.003	0.002	0.000	0.000	0.004	0.000	0.000
Mg	0.001	0.001	0.001	0.000	0.000	0.000	0.000	0.001	0.000	0.001	0.000	0.001
Ca	0.002	0.001	0.004	0.011	0.007	0.004	0.012	0.007	0.009	0.026	0.009	0.009
Mn	0.002	0.002	0.000	0.003	0.000	0.000	0.001	0.000	0.000	0.000	0.000	0.002
P	0.000	0.001	0.001	0.001	0.001	0.000	0.000	0.000	0.000	0.001	0.003	0.000
K	0.001	0.000	0.000	0.001	0.000	0.002	0.001	0.001	0.002	0.002	0.003	0.002
Na	1.038	1.028	1.028	1.017	0.997	1.005	1.01	1.015	1.014	0.983	1.007	1.005
Total	5.027	5.018	5.016	5.011	4.999	5.002	5.01	5.01	5.012	5.004	5.008	5.009
Ab	99.712	99.903	99.612	98.834	99.303	99.406	98.729	99.218	98.927	97.230	98.822	98.917
Or	0.096	0.000	0.000	0.097	0.000	0.198	0.098	0.098	0.195	0.198	0.294	0.197
An	0.192	0.097	0.338	1.069	0.697	0.396	1.173	0.684	0.878	2.572	0.884	0.886

Table 3.8: Composition of calcite from the alkali-pyroxenite

	1	2	3	4	5	6	7	8	9	10	11	12
SiO ₂	0.05	1.29	1.29	0.07	0.02	0.45	0.02	0.02	0.05	0.06	0.06	0.05
Al ₂ O ₃	0.02	1.29	1.29	0.01	0.01	0.66	0.04	0.03	0.04	0.00	0.08	0.07
FeO	0.07	0.41	0.41	0.00	0.06	0.29	0.29	0.16	0.13	0.09	0.10	0.02
MgO	0.05	0.28	0.28	0.07	0.03	0.19	0.07	0.06	0.07	0.05	0.08	0.07
CaO	53.26	50.78	50.78	53.14	55.20	53.15	52.94	53.45	53.13	52.81	53.45	52.11
MnO	0.11	0.07	0.07	0.15	0.08	0.11	0.17	0.08	0.08	0.08	0.17	0.18
P ₂ O ₅	0.00	0.12	0.12	0.04	0.03	0.05	0.08	0.03	0.00	0.01	0.03	0.02
K ₂ O	0.00	0.09	0.09	0.01	0.00	0.00	0.00	0.00	0.01	0.01	0.02	0.00
Na ₂ O	0.03	0.32	0.32	0.03	0.03	0.08	0.03	0.04	0.04	0.04	0.07	0.04
Total	53.59	54.65	54.65	53.52	55.46	54.98	53.64	53.87	53.55	53.15	54.06	52.56

Table 3.9: Composition of apatite, ilmenite and magnetite from the alkali-pyroxenite

	Apatite			Ilmenite				Mt	
SiO ₂	0.14	0.19	0.12	SiO ₂	0.03	0.02	0.16	0.08	1.96
Al ₂ O ₃	0.02	0.10	0.00	Al ₂ O ₃	0.02	0.00	0.08	0.00	0.59
FeO	0.20	0.07	0.00	FeO	44.08	44.31	43.88	43.52	89.82
MgO	0.03	0.03	0.00	MgO	0.12	0.12	0.23	0.18	0.35
CaO	52.95	51.97	53.80	CaO	0.13	0.11	0.12	0.21	0.30
MnO	0.01	0.00	0.10	MnO	3.29	3.52	3.39	3.70	0.00
P ₂ O ₅	38.47	39.10	38.68	P ₂ O ₅	0.01	0.00	0.02	0.00	0.00
TiO ₂	-	-	-	TiO ₂	49.70	50.08	51.80	51.85	0.44
Cr ₂ O ₃	-	-	-	Cr ₂ O ₃	0.00	0.07	0.00	0.00	0.03
K ₂ O	0.01	0.00	0.00	K ₂ O	0.00	0.00	0.00	0.00	0.18
Na ₂ O	0.37	0.11	0.26	Na ₂ O	0.04	0.04	0.03	0.01	0.24
Total	92.20	91.66	93.00	Total	97.42	98.27	99.71	99.55	93.91
<i>(O)</i>	<i>Formula based on 25 O</i>			<i>(O)</i>	<i>Formula based on 3 O</i>				<i>32</i>
Si	0.025	0.034	0.021	Si	0.001	0.000	0.004	0.002	0.766
Al	0.004	0.021	0.000	Al	0.001	0.000	0.002	0.000	0.272
Fe	0.030	0.011	0.000	Fe	0.963	0.960	0.929	0.924	29.324
Mg	0.008	0.008	0.000	Mg	0.005	0.004	0.009	0.007	0.202
Ca	10.199	9.990	10.282	Ca	0.004	0.003	0.003	0.006	0.127
Mn	0.002	0.000	0.015	Mn	0.073	0.077	0.073	0.080	0.000
P	5.855	5.939	5.842	P	0.000	0.000	0.000	0.000	0.000
Ti	-	-	-	Ti	0.976	0.976	0.986	0.990	0.129
Cr	-	-	-	Cr	0.000	0.001	0.000	0.000	0.008
K	0.002	0.000	0.000	K	0.000	0.000	0.000	0.000	0.089
Na	0.129	0.038	0.090	Na	0.002	0.002	0.002	0.001	0.181
Total	16.255	16.054	16.256	Total	2.025	2.023	2.008	2.010	31.098

Mt: Magnetite

Table 3.10: Composition of orthoclase from poorly banded syenite gneiss

	1	2	3	4	5	6	7	8	9	10	11	12
SiO₂	65.76	65.78	65.55	65.75	65.82	66.11	65.86	66.22	66.25	66.02	66.39	65.95
Al₂O₃	18.06	18.01	17.93	17.92	17.98	17.90	17.76	17.80	17.84	18.24	17.79	17.94
FeO	0.05	0.02	0.00	0.03	0.00	0.10	0.09	0.01	0.02	0.09	0.05	0.14
MgO	0.02	0.03	0.03	0.02	0.02	0.00	0.00	0.00	0.00	0.03	0.01	0.00
CaO	0.00	0.00	0.00	0.00	0.00	0.00	0.02	0.00	0.00	0.01	0.00	0.01
MnO	0.03	0.04	0.02	0.03	0.06	0.00	0.00	0.00	0.04	0.00	0.03	0.00
K₂O	14.10	14.28	14.20	14.28	14.88	14.29	14.48	14.46	14.57	14.17	14.63	14.38
Na₂O	0.54	0.65	0.59	0.50	0.41	0.47	0.46	0.61	0.49	0.62	0.50	0.50
Total	98.56	98.81	98.32	98.53	99.17	98.87	98.67	99.1	99.21	99.18	99.4	98.92
<i>Formula based on 8 O</i>												
Si	3.038	3.037	3.038	3.043	3.034	3.045	3.046	3.047	3.047	3.034	3.048	3.042
Al	0.983	0.980	0.979	0.978	0.977	0.972	0.968	0.965	0.967	0.988	0.962	0.975
Fe	0.002	0.001	0.000	0.001	0.000	0.004	0.004	0.000	0.001	0.003	0.002	0.005
Mg	0.001	0.002	0.002	0.001	0.001	0.000	0.000	0.000	0.000	0.002	0.001	0.000
Ca	0.000	0.000	0.000	0.000	0.000	0.000	0.001	0.000	0.000	0.001	0.000	0.001
Mn	0.001	0.002	0.001	0.001	0.002	0.000	0.000	0.000	0.001	0.000	0.001	0.000
K	0.831	0.841	0.840	0.843	0.875	0.840	0.854	0.849	0.855	0.831	0.857	0.846
Na	0.048	0.058	0.053	0.045	0.036	0.042	0.041	0.054	0.044	0.056	0.045	0.044
Total	4.906	4.922	4.916	4.912	4.929	4.906	4.917	4.918	4.917	4.915	4.918	4.914
Ab	<i>5.461</i>	<i>6.452</i>	<i>5.935</i>	<i>5.068</i>	<i>3.952</i>	<i>4.762</i>	<i>4.576</i>	<i>5.980</i>	<i>4.894</i>	<i>6.306</i>	<i>4.989</i>	<i>4.938</i>
Or	<i>94.539</i>	<i>93.548</i>	<i>94.065</i>	<i>94.932</i>	<i>96.048</i>	<i>95.238</i>	<i>95.313</i>	<i>94.020</i>	<i>95.106</i>	<i>93.581</i>	<i>95.011</i>	<i>94.949</i>
An	<i>0.000</i>	<i>0.000</i>	<i>0.000</i>	<i>0.000</i>	<i>0000</i>	<i>0.000</i>	<i>0.112</i>	<i>0.000</i>	<i>0.000</i>	<i>0.113</i>	<i>0.000</i>	<i>0.113</i>

Table 3.11: Composition of albite from poorly banded syenite gneiss

	1	2	3	4
SiO₂	69.65	70.23	69.22	69.08
Al₂O₃	19.41	19.58	19.22	19.11
FeO	0.02	0.13	0.10	0.08
MgO	0.00	0.00	0.00	0.00
CaO	0.01	0.01	0.00	0.00
MnO	0.00	0.00	0.00	0.00
K₂O	0.07	0.10	0.07	0.06
Na₂O	11.04	11.20	10.90	11.07
Ba₂O	0.00	0.03	0.02	0.02
Total	100.2	101.28	99.53	99.42
<i>Formula based on 8 O</i>				
Si	3.022	3.019	3.024	3.023
Al	0.993	0.992	0.990	0.986
Fe²⁺	0.001	0.005	0.004	0.003
Mg	0.000	0.000	0.000	0.000
Ca	0.001	0.000	0.000	0.000
Mn	0.000	0.000	0.000	0.000
Na	0.929	0.934	0.923	0.940
K	0.004	0.005	0.004	0.003
Ba	0.000	0.000	0.000	0.000
Total	4.95	4.955	4.945	4.955
Ab	99.465	99.468	99.569	99.682
Or	0.428	0.532	0.431	0.318
An	0.107	0.000	0.000	0.000

Table 3.12: Composition of nepheline from poorly banded syenite gneiss

	1	2	3	4	5	6	7	8	9	10	11	12
SiO₂	43.03	43.04	42.88	42.71	43.04	42.70	43.25	43.15	42.97	42.45	43.12	42.89
Al₂O₃	33.28	33.03	33.78	33.77	33.60	33.71	33.71	33.97	33.56	33.46	33.69	33.75
FeO	0.08	0.20	0.09	0.15	0.14	0.10	0.11	0.04	0.20	0.00	0.17	0.10
MgO	0.02	0.03	0.00	0.02	0.02	0.00	0.01	0.00	0.00	0.01	0.00	0.01
CaO	0.00	0.02	0.00	0.00	0.00	0.02	0.04	0.01	0.00	0.06	0.12	0.07
MnO	0.08	0.05	0.03	0.00	0.00	0.00	0.14	0.08	0.00	0.00	0.00	0.03
K₂O	6.38	6.56	6.30	6.51	6.53	6.45	6.09	6.44	6.44	6.39	6.69	6.67
Na₂O	16.58	16.75	16.65	16.68	16.90	16.56	16.78	16.89	16.57	16.65	16.48	16.49
Total	99.45	99.68	99.73	99.84	100.23	99.54	100.13	100.58	99.74	99.02	100.27	100.01
<i>Formula based on 32 O</i>												
Si	8.33	8.34	8.28	8.25	8.28	8.27	8.31	8.27	8.30	8.26	8.29	8.27
Al	7.59	7.54	7.68	7.69	7.62	7.69	7.63	7.67	7.64	7.67	7.64	7.67
Fe⁺⁺	0.01	0.03	0.01	0.02	0.02	0.02	0.02	0.01	0.03	0.00	0.03	0.02
Mg	0.01	0.01	0.00	0.01	0.01	0.00	0.00	0.00	0.00	0.00	0.00	0.00
Ca	0.00	0.00	0.00	0.00	0.00	0.00	0.01	0.00	0.00	0.01	0.03	0.02
Mn	0.01	0.01	0.00	0.00	0.00	0.00	0.02	0.01	0.00	0.00	0.00	0.00
K	1.58	1.62	1.55	1.60	1.60	1.59	1.49	1.57	1.59	1.59	1.64	1.64
Na	6.23	6.29	6.23	6.25	6.30	6.22	6.25	6.28	6.21	6.28	6.15	6.17
Total	23.76	23.84	23.76	23.82	23.84	23.78	23.74	23.81	23.77	23.81	23.77	23.79
Ne	74.73	75.43	75.28	75.73	76.10	75.20	75.23	75.91	74.78	76.06	74.11	74.54
Ks	18.91	19.43	18.73	19.43	19.35	19.27	17.96	19.03	19.10	19.21	19.80	19.84
Qtz	6.36	5.13	5.99	4.84	4.55	5.53	6.81	5.06	6.12	4.74	6.09	5.62

Ne: Nepheline, Ks: Kalsilite, Qtz: Silica

Table 3.13: Composition of pyroxene from poorly banded syenite gneiss

(Wt%)	1	2	3	4	5	6	7
SiO ₂	53.60	53.97	54.23	53.93	54.24	54.01	53.78
TiO ₂	0.03	0.05	0.09	0.13	0.01	0.13	0.11
Al ₂ O ₃	2.43	2.75	2.77	2.88	2.54	2.90	2.70
FeO*	25.48	24.32	24.36	23.13	24.46	24.15	24.14
MnO	0.02	0.32	0.14	0.52	0.06	0.06	0.24
MgO	0.11	0.27	0.23	0.39	0.06	0.21	0.22
CaO	0.04	0.63	0.62	0.95	0.03	0.34	0.54
K ₂ O	0.01	0.03	0.01	0.02	0.00	0.00	0.00
Na ₂ O	13.34	13.52	13.36	13.25	13.65	13.43	13.44
Cr ₂ O ₃	0.00	0.00	0.00	0.00	0.03	0.00	0.00
Total	95.06	95.86	95.81	95.20	95.08	95.23	95.17
<i>Formula based on 6</i>							
Si	2.064	2.052	2.066	2.064	2.079	2.068	2.061
Ti	0.001	0.001	0.003	0.004	0.000	0.004	0.003
Al (T)	0.000	0.000	0.000	0.000	0.000	0.000	0.000
Al (M1)	0.110	0.123	0.124	0.130	0.115	0.131	0.122
Fe ^{3+*} (T)	0.000	0.000	0.000	0.000	0.000	0.000	0.000
Fe ^{3+*} (M1)	0.757	0.766	0.725	0.718	0.740	0.723	0.749
Fe ^{2+*}	0.064	0.007	0.052	0.022	0.044	0.050	0.024
Mn ²⁺	0.001	0.010	0.005	0.017	0.002	0.002	0.008
Mg	0.006	0.015	0.013	0.022	0.003	0.012	0.013
Ca	0.002	0.026	0.025	0.039	0.001	0.014	0.022
K	0.000	0.001	0.000	0.001	0.000	0.000	0.000
Na	0.996	0.997	0.987	0.983	1.014	0.997	0.998
Cr	0.000	0.000	0.000	0.000	0.000	0.000	0.000
Total	4.000	4.000	4.000	4.000	4.000	4.000	4.000
Jadeite	12.28	13.53	14.01	14.70	13.11	14.76	13.59
Aegirine	84.25	84.10	81.63	81.23	84.56	81.58	83.53
Quad	3.48	2.37	4.36	4.07	2.33	3.66	2.87
Name	<i>Ae</i>	<i>Ae</i>	<i>Ae</i>	<i>Ae</i>	<i>Ae</i>	<i>Ae</i>	<i>Ae</i>

Ae: Aegirine

* Total Fe calculated as FeO, ** Recalculated to Fe²⁺ and Fe³⁺

Table 3.14: Compositions of nepheline and its' alteration to sodalite from the poorly banded syenite gneiss. Two examples of replacement of nepheline by analcime are also shown.

	Neph	Neph	Neph	Anl	Anl	Sod
SiO ₂	40.95	41.04	43.37	55.587	57.323	42.768
Al ₂ O ₃	35	34.8	35.65	29.025	30.179	32.870
FeO	0.06	0.07	0.08	0.069	0.001	0.002
MnO	0.04	0.03	0.02	0.000	0.000	0.408
MgO	0	0.01	0.03	0.000	0.000	0.000
CaO	0	0	0	0.000	0.000	4.732
Na ₂ O	15.82	15.28	14.19	8.291	8.993	17.992
K ₂ O	8.07	7.88	7.59	0.092	0.037	0.019
Total	99.94	99.11	100.95	93.064	96.533	98.798
	<i>Formula based on 32 O</i>			<i>6 O</i>		<i>19 O</i>
Si	7.974	8.031	8.236	1.955	1.946	5.393
Al	8.032	8.025	7.978	1.203	1.207	4.885
Fe	0.010	0.011	0.013	0.002	0.000	0.000
Mn	0.007	0.005	0.003	0.000	0.000	0.044
Mg	0.000	0.003	0.008	0.000	0.000	0.000
Ca	0.000	0.000	0.000	0.000	0.000	0.639
Na	5.972	5.797	5.224	0.565	0.592	4.399
K	2.004	1.967	1.838	0.004	0.002	0.003
Total	23.999	23.839	23.304	3.729	3.747	15.364
Ne	<i>74.90</i>	<i>72.18</i>	<i>63.43</i>	-	-	-
Ks	<i>25.14</i>	<i>24.49</i>	<i>22.32</i>	-	-	-
Qtz	<i>-0.03</i>	<i>3.33</i>	<i>14.25</i>	-	-	-

Ne/Nephe: Nepheline; Ks: Kalsilite; Qtz: Silica, Anl: Analcime; Sod: Sodalite

Table 3.15: Composition of albite from strongly banded syenite gneiss

	1	2	3	4	5	6	7	8	9	10	11
SiO₂	69.51	69.55	69.42	69.71	69.25	69.81	69.19	69.26	69.72	69.59	69.10
Al₂O₃	19.07	18.92	18.92	18.93	18.65	19.00	18.14	18.92	19.02	18.70	18.85
FeO	0.06	0.04	0.03	0.06	0.21	0.00	0.06	0.12	0.00	0.01	0.00
MgO	0.02	0.03	0.00	0.01	0.01	0.00	0.02	0.01	0.01	0.00	0.00
CaO	0.04	0.01	0.00	0.01	0.00	0.02	0.29	0.01	0.00	0.03	0.00
MnO	0.00	0.00	0.00	0.00	0.00	0.00	0.23	0.00	0.00	0.00	0.02
K₂O	0.08	0.14	0.08	0.05	0.06	0.05	0.07	0.06	0.04	0.03	0.11
Na₂O	12.07	12.02	12.41	12.08	11.95	12.17	11.99	12.21	12.10	12.08	12.13
Total	100.85	100.71	100.86	100.85	100.13	101.05	99.99	100.59	100.89	100.44	100.21
<i>Formula based on 8 O</i>											
Si	3.011	3.017	3.012	3.019	3.021	3.017	3.029	3.010	3.017	3.025	3.013
Al	0.974	0.967	0.967	0.966	0.959	0.968	0.936	0.969	0.970	0.958	0.969
Fe⁺⁺	0.002	0.001	0.001	0.002	0.008	0.000	0.002	0.005	0.000	0.000	0.000
Mg	0.001	0.002	0.000	0.001	0.000	0.000	0.001	0.001	0.001	0.000	0.000
Ca	0.002	0.000	0.000	0.001	0.000	0.001	0.014	0.000	0.000	0.001	0.000
Mn	0.000	0.000	0.000	0.000	0.000	0.000	0.008	0.000	0.000	0.000	0.001
K	0.004	0.008	0.004	0.003	0.003	0.003	0.004	0.003	0.002	0.002	0.006
Na	1.014	1.011	1.044	1.014	1.011	1.020	1.017	1.029	1.016	1.018	1.026
Total	5.008	5.006	5.028	5.006	5.002	5.009	5.011	5.017	5.006	5.004	5.015
Ab	<i>99.412</i>	<i>99.215</i>	<i>99.618</i>	<i>99.607</i>	<i>99.704</i>	<i>99.609</i>	<i>98.261</i>	<i>99.709</i>	<i>99.804</i>	<i>99.706</i>	<i>99.419</i>
Or	<i>0.392</i>	<i>0.785</i>	<i>0.382</i>	<i>0.295</i>	<i>0.296</i>	<i>0.293</i>	<i>0.386</i>	<i>0.291</i>	<i>0.196</i>	<i>0.196</i>	<i>0.581</i>
An	<i>0.196</i>	<i>0.000</i>	<i>0.000</i>	<i>0.098</i>	<i>0.000</i>	<i>0.098</i>	<i>1.353</i>	<i>0.000</i>	<i>0.000</i>	<i>0.098</i>	<i>0.000</i>

Table 3.16: Composition of pyroxene from strongly banded syenite gneiss

	1	2	3	4	5	6	7	8	9	10
SiO ₂	54.27	53.81	53.78	54.24	54.10	54.05	53.63	53.75	53.91	53.83
TiO ₂	0.24	0.34	0.34	0.33	0.24	0.30	0.24	0.26	0.29	0.31
Al ₂ O ₃	2.60	2.33	2.34	2.89	2.80	2.43	2.66	2.52	2.92	2.79
FeO*	23.49	23.76	23.74	22.66	22.18	23.82	23.99	22.83	24.62	24.34
MnO	0.56	0.63	0.88	0.45	0.50	0.31	0.30	0.55	0.18	0.20
MgO	1.54	1.67	1.68	1.60	2.17	1.62	1.44	1.85	0.98	1.25
CaO	2.58	3.03	3.00	2.47	3.34	2.34	2.04	2.90	1.24	1.73
K ₂ O	0.02	0.00	0.01	0.00	0.00	0.00	0.02	0.00	0.01	0.00
Na ₂ O	12.06	11.94	11.98	12.33	11.55	12.22	12.63	11.94	13.01	12.66
Cr ₂ O ₃	0.05	0.00	0.06	0.04	0.02	0.00	0.00	0.00	0.05	0.03
Total	97.41	97.51	97.81	97.01	96.90	97.09	96.95	96.60	97.21	97.14
<i>Formula based on 6 O</i>										
Si	2.045	2.029	2.022	2.043	2.046	2.041	2.022	2.038	2.027	2.028
Ti	0.007	0.010	0.010	0.009	0.007	0.009	0.007	0.007	0.008	0.009
Al (T)	0.000	0.000	0.000	0.000	0.000	0.000	0.000	0.000	0.000	0.000
Al (M1)	0.115	0.104	0.104	0.128	0.125	0.108	0.118	0.113	0.129	0.124
Fe ^{3+**} (T)	0.000	0.000	0.000	0.000	0.000	0.000	0.000	0.000	0.000	0.000
Fe ^{3+**} (M1)	0.661	0.693	0.705	0.666	0.616	0.688	0.749	0.674	0.747	0.726
Fe ^{2+**}	0.079	0.056	0.041	0.048	0.085	0.064	0.007	0.050	0.027	0.041
Mn ²⁺	0.018	0.020	0.028	0.014	0.016	0.010	0.010	0.018	0.006	0.006
Mg	0.087	0.094	0.094	0.090	0.122	0.091	0.081	0.105	0.055	0.070
Ca	0.104	0.122	0.121	0.100	0.135	0.095	0.082	0.118	0.050	0.070
K	0.001	0.000	0.000	0.000	0.000	0.000	0.001	0.000	0.000	0.000
Na	0.881	0.873	0.873	0.900	0.847	0.895	0.923	0.878	0.948	0.925
Cr	0.001	0.000	0.002	0.001	0.001	0.000	0.000	0.000	0.001	0.001
Total	4.000	4.000	4.000	4.000	4.000	4.000	4.000	4.000	4.000	4.000
Jadeite	12.89	11.25	11.18	14.27	14.01	11.92	12.48	12.39	13.80	13.28
Aegirine	73.83	75.25	76.04	74.10	69.15	75.81	79.06	74.18	79.71	77.81
Quad	13.28	13.51	12.78	11.63	16.84	12.27	08.47	13.42	6.49	8.91
Name	<i>Ae</i>	<i>Ae</i>	<i>Ae</i>	<i>Ae</i>	<i>Ae</i>	<i>Ae</i>	<i>Ae</i>	<i>Ae</i>	<i>Ae</i>	<i>Ae</i>

Ae: Aegirine

* Total Fe calculated as FeO, ** Recalculated to Fe²⁺ and Fe³⁺

Table 3.17 Composition of eudialyte and Na-Zr bearing silicates from strongly banded syenite gneiss

	Eud	Eud	Eud	Eud	NZS	NZS
SiO₂	44.16	43.66	46.39	44.76	31.35	44.36
Al₂O₃	1.53	0.68	0.70	0.33	0.32	0.17
FeO	0.35	5.38	0.21	0.28	0.41	0.33
MnO	7.17	5.47	7.48	7.22	0.22	0.22
MgO	0.27	0.99	0.16	0.16	0.18	0.03
CaO	13.10	10.16	13.48	13.48	1.08	0.36
Na₂O	7.92	8.36	7.40	7.55	5.99	4.49
K₂O	0.55	0.37	0.56	0.54	0.05	0.00
Cl	0.73	0.44	0.76	0.72	0.04	0.08
BaO	0.23	0.15	0.72	0.12	0.00	0.00
ZrO₂	11.94	9.53	11.77	11.58	35.16	35.84
	87.95	85.43	89.63	86.74	74.80	85.88
O_Cl	0.17	0.10	0.17	0.17	0.01	0.02
Total	87.78	85.33	89.46	86.57	74.79	85.86
	<i>Formula based on 78 O</i>				<i>7 O</i>	
Si	14.53	16.06	15.18	15.02	0.53	0.70
Al	0.59	0.29	0.27	0.13	0.01	0.00
Fe²⁺	0.10	1.65	0.06	0.08	0.01	0.00
Mn	2.00	1.70	2.07	2.05	0.00	0.00
Mg	0.13	0.54	0.08	0.08	0.00	0.00
Ca	4.62	4.00	4.72	4.85	0.02	0.01
Na	5.05	5.96	4.69	4.91	0.20	0.14
K	0.23	0.17	0.23	0.23	0.00	0.00
Cl	0.41	0.27	0.42	0.41	0.00	0.00
BaO	0.03	0.02	0.09	0.02	0.00	0.00
Zr	19.16	17.09	18.77	18.95	2.90	2.76
Total	46.85	47.84	46.59	46.74	3.67	3.61

Table 3.18: Composition of feldspars from massive syenite

	1	2	3	4	5	6	7		1	2	3
SiO₂	64.13	63.56	64.87	64.67	64.54	64.04	64.13	SiO₂	69.61	70.30	70.97
Al₂O₃	17.20	17.41	17.40	17.30	17.51	17.63	17.20	Al₂O₃	19.40	19.55	18.68
CaO	0.00	0.03	0.05	0.04	0.05	0.06	0.02	CaO	0.02	0.03	0.02
Na₂O	0.16	0.00	0.00	0.00	0.00	0.00	0.00	Na₂O	11.18	10.96	12.24
K₂O	17.45	17.01	17.39	17.21	17.69	17.76	17.45	K₂O	0.13	0.07	0.11
FeO	0.02	0.45	0.22	0.40	0.29	0.24	0.16	FeO	0.05	0.00	0.03
Ba₂O	0.00	0.00	0.00	0.00	0.00	0.00	0.00	Ba₂O	0.00	0.06	0.00
Total	98.97	98.46	99.92	99.62	100.08	99.73	98.97	Total	100.39	100.98	102.06
<i>Formula based on 8 O</i>											
Si	3.018	3.005	3.020	3.020	3.008	2.999	3.018	Si	3.018	3.025	3.037
Al	0.954	0.970	0.955	0.952	0.962	0.973	0.954	Al	0.991	0.992	0.942
Ca	0.000	0.001	0.002	0.002	0.002	0.003	0.001	Ca	0.001	0.002	0.001
Na	0.015	0.000	0.000	0.000	0.000	0.000	0.000	Na	0.940	0.915	1.016
K	1.048	1.026	1.033	1.025	1.052	1.061	1.048	K	0.007	0.004	0.006
Fe²⁺	0.001	0.041	0.020	0.037	0.026	0.021	0.015	Fe²⁺	0.002	0.000	0.001
Ba	0.000	0.000	0.000	0.000	0.000	0.000	0.000	Ba	0.000	0.001	0.000
Total	5.036	5.044	5.029	5.035	5.050	5.056	5.036	Total	4.9597	4.938	5.003
<i>Ab</i>	<i>1.411</i>	<i>0.000</i>	<i>0.000</i>	<i>0.000</i>	<i>0.000</i>	<i>0.000</i>	<i>0.000</i>	<i>Ab</i>	<i>99.156</i>	<i>99.349</i>	<i>99.316</i>
<i>Or</i>	<i>98.589</i>	<i>99.903</i>	<i>99.807</i>	<i>99.805</i>	<i>99.810</i>	<i>99.718</i>	<i>99.905</i>	<i>Or</i>	<i>0.738</i>	<i>0.434</i>	<i>0.587</i>
<i>An</i>	<i>0.000</i>	<i>0.097</i>	<i>0.193</i>	<i>0.195</i>	<i>0.190</i>	<i>0.282</i>	<i>0.095</i>	<i>An</i>	<i>0.105</i>	<i>0.217</i>	<i>0.098</i>

Table 3.19: Composition of nepheline from massive syenite

	1	2	3	4	5	6	7	8	9
SiO ₂	43.14	42.19	42.85	43.03	43.43	42.94	42.94	42.02	42.40
Al ₂ O ₃	34.20	34.03	33.70	33.18	33.27	33.23	34.15	32.97	32.83
CaO	0.01	0.01	0.00	0.00	0.00	0.00	0.00	0.00	0.00
Na ₂ O	15.61	15.44	15.39	17.17	16.72	17.40	15.57	17.02	17.29
K ₂ O	7.14	7.53	7.06	7.56	7.52	7.56	7.17	7.70	7.49
FeO	0.34	0.18	0.37	0.23	0.15	0.14	0.14	0.00	0.03
Total	100.44	99.38	99.37	101.17	101.10	101.26	99.97	99.70	100.03
<i>Formula based on 32 O</i>									
Si	8.281	8.209	8.310	8.277	8.331	8.256	8.276	8.213	8.253
Al	7.740	7.807	7.706	7.525	7.526	7.534	7.761	7.597	7.535
Ca	0.003	0.002	0.000	0.000	0.001	0.000	0.000	0.000	0.000
Na	5.807	5.825	5.785	6.402	6.219	6.487	5.817	6.447	6.525
K	1.748	1.870	1.747	1.854	1.840	1.855	1.763	1.919	1.859
Fe ⁺⁺	0.055	0.028	0.061	0.036	0.025	0.022	0.023	0.000	0.004
Total	23.633	23.741	23.609	24.094	23.941	24.153	23.640	24.177	24.177
Ne	70.12	70.96	69.61	77.35	74.65	78.57	70.29	78.50	79.06
Ks	21.11	22.78	21.02	22.40	22.09	22.47	21.30	23.37	22.53
Qtz	8.77	6.26	9.36	0.25	3.26	-1.04	8.41	-1.86	-1.59

Table 3.20: Composition of mica from massive syenite

	1	2	3	4
SiO ₂	36.15	34.66	35.51	35.11
Al ₂ O ₃	19.30	19.03	18.91	18.72
FeO	13.46	14.11	13.37	13.15
MgO	8.37	7.90	8.54	8.27
MnO	5.96	6.23	6.05	6.22
CaO	0.01	0.07	-	-
K ₂ O	9.03	9.97	9.81	10.23
Na ₂ O	0.20	0.17	0.12	0.14
TiO ₂	0.10	0.09	0.09	0.08
Total	92.58	92.23	92.39	91.91
<i>Formula based on 22 O</i>				
Si	5.628	5.504	5.580	5.570
^{IV} Al	2.372	2.496	2.42	2.43
^{VI} Al	1.169	1.066	1.083	1.07
Fe ²⁺	1.753	1.873	1.758	1.744
Mg	1.943	1.869	2.000	1.955
Mn	0.786	0.838	0.805	0.836
Ca	0.002	0.011	0.000	0.000
K	1.794	2.020	1.967	2.071
Na	0.059	0.054	0.038	0.042
Ti	0.012	0.011	0.010	0.010
Total	15.517	15.742	15.660	15.727
Mg/(Mg+Fe)	0.526	0.499	0.532	0.529

Geochemical work was carried out for both the bulk rock as well as for key minerals apatite and calcite. The bulk rock geochemistry was done by XRF followed by further analysis of the pellets by LA-ICPMS. In each case the LA-ICPMS data was standardized using the data obtained from XRF. The minerals are separated by heavy liquid separation followed by the identification of the minerals using Raman Spectroscopy and finally the analysis were carried out by LA-ICPMS. The zircon grains are separated from the syenite rock and they are used for isotopic studies by Thermal Ionization Mass Spectrometer (TIMS) and discussed in the next chapter. In the first part of the chapter the bulk rock chemical analysis will be discussed followed by the mineral chemistry.

4.1 ANALYTICAL TECHNIQUE

The detailed specifications of the instruments: XRF and LA-ICPMS, used for the bulk-rock analysis are given below. All the geochemical analysis was carried out at the Institute of Isotope Geology and Mineral Resources, ETH Zurich.

A) XRF: Routine analyses of major elements in whole rock were carried out on Li-tetraborate pellets at IMP (Institute for Mineralogy and Petrology), ETH Zurich following the procedure given by Nisbet et al. (1979) and Dietrich et al. (1984). The flowchart of the procedure is given in Fig. 4.1. WD-XRF of Axios by PANalytical was used. Though both major and trace element analysis was done by XRF, but only the major element (oxides) data (Table 4.1) have been used for describing bulk-rock geochemistry. The error limit of the data presented in this work is within the limit of 3%.

B) LA-ICP MS: The trace element geochemistry data produced by XRF has been compared with the similar data set generated by LA-ICPMS. For all practical purposes both data sets show very good match. However, the number of trace elements analyzed by LA-ICPMS was more. Individual mineral grains, separated from bulk-rock were also analyzed by LA-ICPMS. For better parity and control, the trace element data generated for both bulk-rock and minerals by LA-ICPMS have been used for further interpretation. The apatite and calcite grains were separated from the alkali-pyroxenite and the carbonatite using crushing, sieving, magnetic procedure and later the standard heavy liquid separation technique. The spot analyses were carried out by the same LA-ICPMS. The spot size diameter was 40 μ m or 20 μ m, depending on the grain-size. The standardizations were done on NIST glass standard SRM-610. LAM-TRACE data reduction software is used for finalization of the data. The raw data was recalculated using. All the analysis presented in this study presented is within error limit of $\pm 2\%$.

4.2 CARBONATITE

It has been mentioned in previous chapter that the Purulia carbonatite has undergone severe meteoritic water action. So it is hard to collect fresh samples from the outcrops. Based on the petrography and mineralogy of thin sections, four carbonatite samples (ANK 1, 3, 4 and 5, Table 4.1) are chosen for chemical analysis. Previously it has been mentioned that only one variety of carbonatite is found at Beldih and mineralogically they are found to be calico-carbonatite. All the analyzed samples are characterized by low SiO₂ (1-1.2%) except sample number ANK 3 where it reaches up to 5.3%, though falling well within the range of average calico-carbonatite (Woolley and Kempe, 1989). The other major oxides: Al₂O₃, MnO, TiO₂, Na₂O and K₂O are low in amount and no significant variations have been observed in between the samples (Fig. 4.2). The MgO

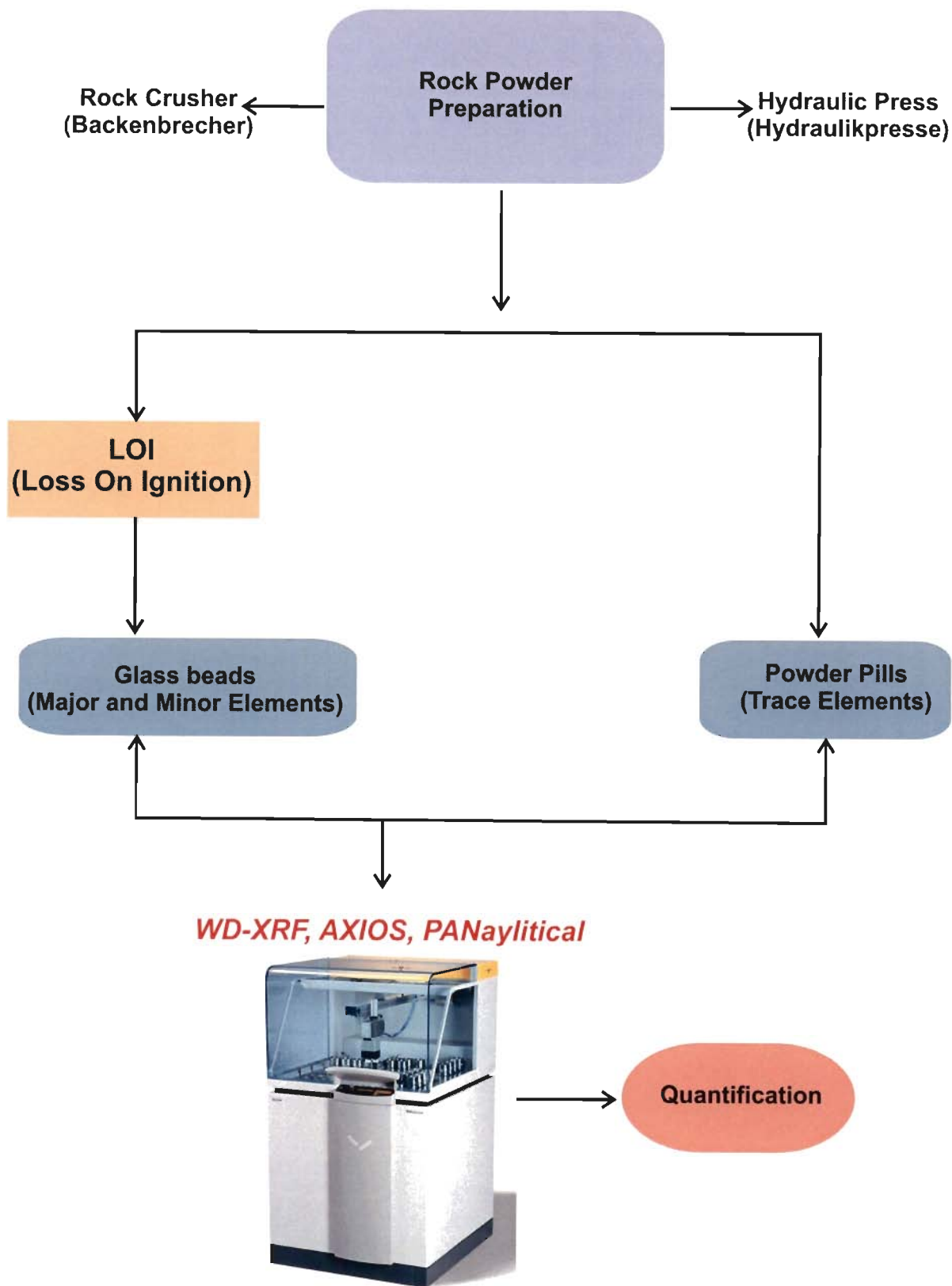


Fig. 4.1 Schematic diagram showing steps of bulk rock analysis by XRF

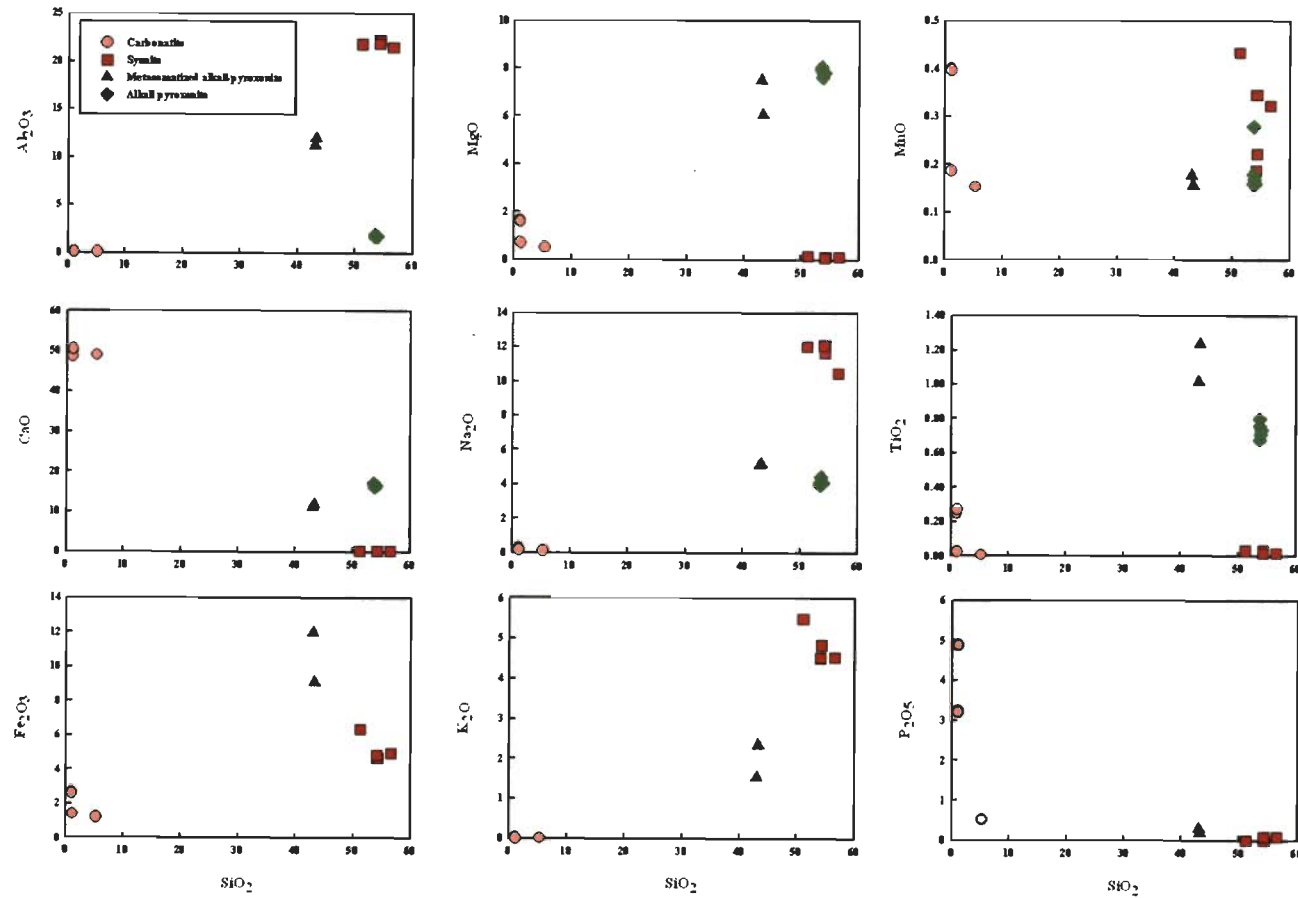


Fig. 4.2 Plots of range of oxides (Wt%) for carbonatite, metasomatized or altered alkali-pyroxenite, alkali-pyroxenite and nepheline syenite. (Harker variation diagrams). Considerable scatter is observed for CaO, Al₂O₃, Na₂O, K₂O, Fe₂O₃ and MgO (For detailed descriptions see text under the corresponding sections)

content is slightly variable and lies within the range of 1.6 to 0.6%. The Fe_2O_3 content, mainly contributed by the magnetite, varies between 1.2-2.7%, whereas the P_2O_5 content, contributed by the apatite, lies between 3.2-4.8%, except for ANK 3, where both of these oxides (Fe_2O_3 and P_2O_5) are low (Fig. 4.2). The sample number ANK 3 represents apatite and magnetite poor part of carbonatite. All the carbonatite samples are mostly constituted of CaO (Fig. 4.2, Table 4.1) which can be attributed to the presence of about 90% of modal calcite. The analyzed carbonatites when plotted in a CaO-(FeO+ Fe_2O_3 +MnO)-MgO ternary diagram of Le Bas and Streckeisen (1991) are expectedly found to be calico-carbonatite (Fig. 4.3) and all other major oxides are falling well within the range of average calico-carbonatite, given by Woolley and Kempe (1989).

The carbonatite samples were analyzed for 37 trace elements using LA-ICPMS. The results are shown in Table 4.1. The carbonatite is characteristically high in Sr (8500-11300 ppm), Ba (800-1800ppm) & ΣREE -content (1500-2100ppm). The primitive mantle (Sun and McDonough, 1989) normalized values of selected trace elements as plotted in spider diagram (Fig. 4.4a) fall in the range of 0.2 to 2500. The Purulia carbonatite is comparatively enriched in all incompatible elements with respect to the primitive mantle value (Sun and McDonough, 1989) (Fig. 4.4a). However, with respect to the primitive mantle, the concentration level of Rb, Hf and Zr for Purulia carbonatite is low. The normalized value for Rb is about 0.2 and indicates depletion of this element during fractionation though biotite and phlogopite are present in accessory amount. The variation of normalized value of Hf and Zr is close to unity. The compatible trace elements (Sc, V, Co, Cr and Ni) show very minor variation (Table 4.1) and the implications will be discussed in the Chapter 6. The Purulia carbonatite is comparatively enriched in large ion lithophile elements (LILE) compared to Primitive mantle (Sun and McDonough, 1989) particularly in Ba (250 times), Sr (up to 2500 times) and U (300 times). Relative enrichment of these elements are well within the range of average calico-carbonatite value of Woolley and Kempe (1989). Replacement of Ca by Sr

and Ba, in Ca bearing minerals like calcite and apatite resulted higher concentrations of these two trace elements. On the other hand, the Purulia carbonatite is also relatively enriched in Th (member of LILE group) and Nb (member of HFSE group) compared to primitive mantle but the level of enrichment goes only up to 10-100 times (Fig. 4.4a). These two elements are also falling within the range of average calico-carbonatite but towards the lower end (Woolley and Kepme, 1989). The Ta value of two samples is very close to the concentration to that of average calico-carbonatite but the concentration of Ta in remaining two samples is about 5 times lower. Out of four carbonatite samples, there is noticeable difference in Nb, Th and Ta content. Two samples (ANK 1 and ANK 4) show relatively higher concentration of these elements compared to other two (ANK 3 and ANK 5). The most noticeable feature of the studied carbonatite is much lower concentration of Nb compared to the world average (Woolley and Kempe, 1989; Fig. 4.4a), which is characteristics of carbohydrothermal origin (Mitchell, 2005).

The analyzed carbonatite samples are relatively enriched in LREE compared to that of the HREE and the Σ REE is mainly contributed by the LREE (La to Sm) (Fig. 4.4b) (Table 4.1). The concentration of the individual REE is towards the lower side of the average calico-carbonatite (Woolley and Kempe, 1989). The total REE abundance (Σ REE) of the Purulia carbonatite ranges from 1436.13 to 2114.24 ppm, with La/Yb ratio (La/Yb_n) varies from 47.66 to 89.64 (Table 4.1) and both the parameters are falling within the range of average calico-carbonatite (Σ REE= 654.5-8099ppm, $(La/Yb_n)= 60-133$). In two samples (ANK 1 and 4) the (La/Yb_n) ratios are found to be lower than the average calico-carbonatite value, this is mainly due the fact that they are enriched in HREE in comparison to other two samples. Chondrite-normalized (Sun and McDonough, 1989) REE pattern of the carbonatite shows that the REE values are ranging from 50 to 2000 with respect to the chondrite value (Fig. 4.4b). The LREE enrichment varies from 1500-2000 times and the same for HREE is only 20-40 times and thus LREE enrichment is 75-50 times higher than HREE,

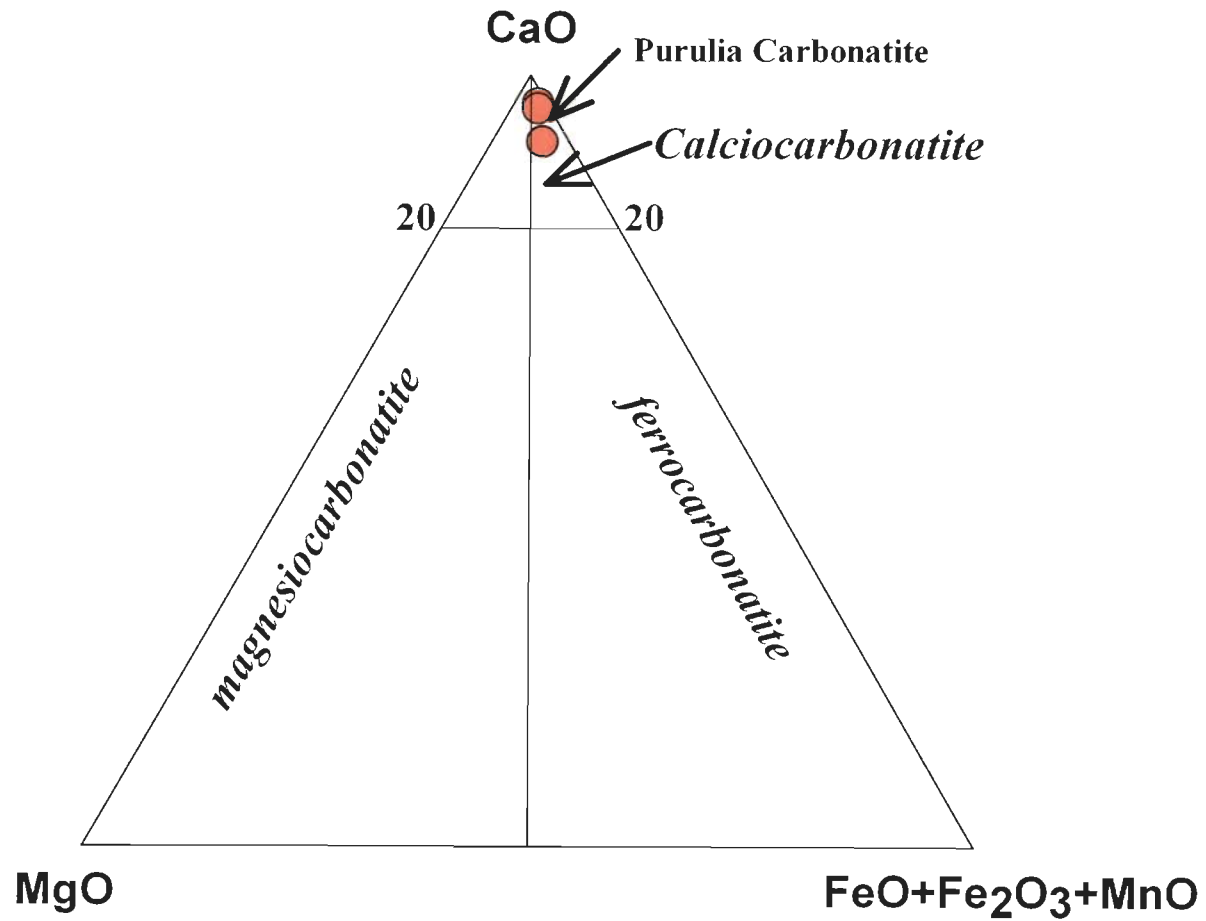


Fig. 4.1 Chemical classification of Purulia carbonatite in a CaO-(FeO+Fe₂O₃+MnO)-MgO ternary plot (Weight percent of oxides) (after Le Bas and Streckeisen, 1991)

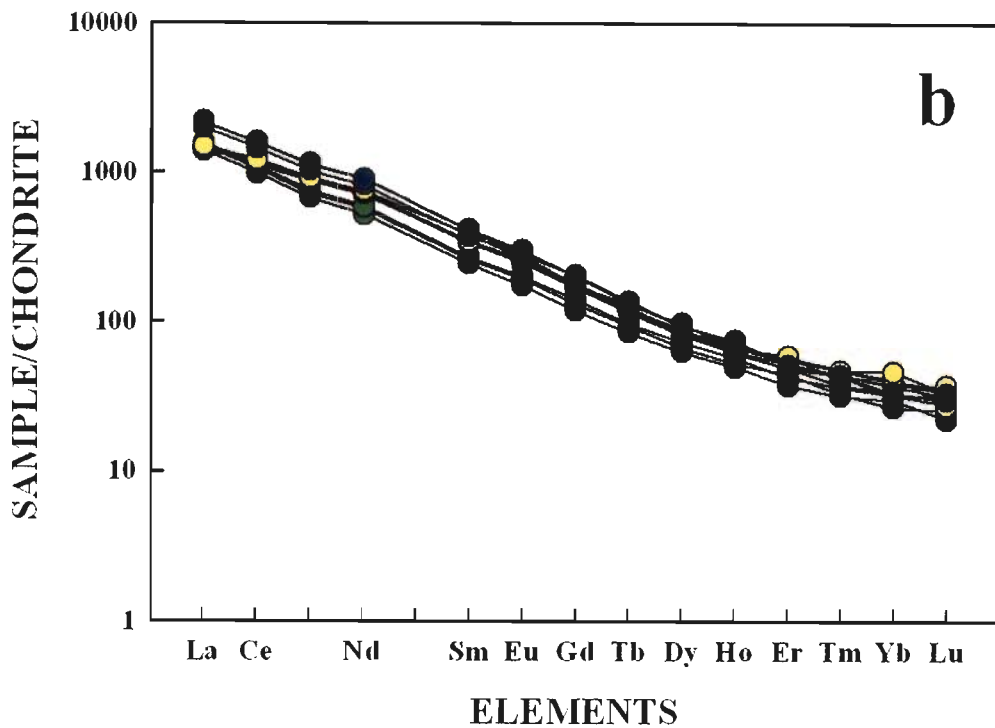
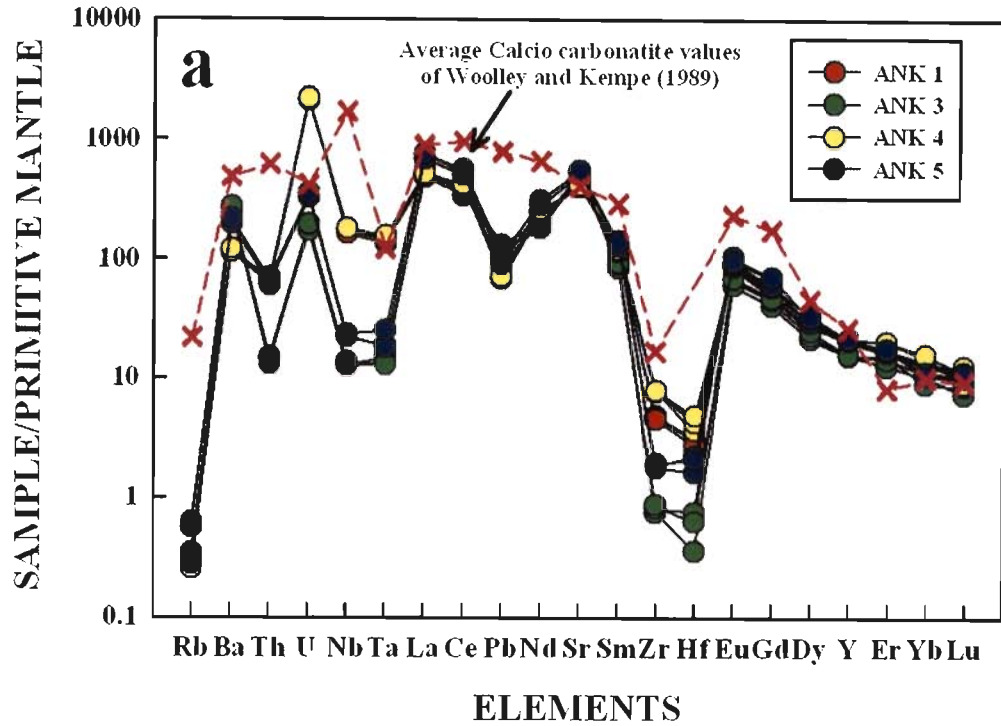


Fig. 4.4 (a) Primitive mantle normalized spider diagram for carbonatite. The Purulia carbonatites are compared with the average calico-carbonatite values given by Woolley and Kempe (1989). (b) Chondrite normalized REE plot of Purulia carbonatite. In this plot similar symbols are used as that of the spider diagram. Normalizing values are from Sun and McDonough (1989).

which is very much characteristic of any carbonatite. The overall REE trend i.e. LREE enrichment over the HREE is mainly controlled by the presence of calcite and apatite in carbonatite.

It has been noticed that out of the four samples, sample number ANK 1 and ANK 4 are very similar than that of the rest two samples i.e. ANK 3 and ANK 5. The first group (ANK 1 and ANK 4) is characterized by the relatively higher amount of TiO₂, Fe₂O₃, MnO, Sc, Co, V, Sr, Nb, U, Th, Y, Zr and Ta than the second group (ANK 3 and ANK 5). The second group is containing higher amount Ba. The higher relative abundances of elements like Nb, U, Th, Y, Zr and Ta can be attributed to the presence of pyrochlore (?) in the first group of samples though this mineral was not found during petrographic investigation under the microscope.

4.3 ALKALI-PYROXENITE

Petrographically this rock is dominantly composed of alkali-pyroxene and the original rock, *i.e.*, alkali-pyroxenite, has undergone alkali-metasomatism as described in the previous chapter. It shows sharp contact relationship with carbonatite. The bulk-chemical composition of this metasomatically altered rock shows that it is chiefly consisting of SiO₂, Al₂O₃, Fe₂O₃, MgO and CaO (Table 4.1). The major oxides are not showing any significant variations when plotted in the different Harker variation diagrams (Fig. 4.1). In a TAS (Total Alkali versus Silica) plot (Cox et al., 1979) for plutonic rocks, this rock is plotted very close to ijolite (Fig. 4.5). The CIPW Norm calculation of bulk-rock composition (Table 4.2) of this rock also supports its alkalic affinity.

It is obvious from petrography that the original mineral composition of the rock has been perturbed due to alkali-metasomatism. So, the bulk-chemistry is also not a true representation of the composition of this rock which must have gained or lost some major elements. To calculate this effect, based on petrography it may be safely assumed that the rock originally was monomineralic and considered to be alkali-pyroxenite. In that case, the chemical composition of the pyroxene

(Table 3.4) crystals should be the same as the bulk-composition of this rock. Considering the original composition of the alkali-pyroxenite as that of the pyroxene the effect of alkali-metasomatism can be clearly visible in all the Harker variation diagrams (Fig 4.2). The enrichment of SiO_2 , Al_2O_3 , TiO_2 and loss of CaO is clearly visible in this plot. The most noticeable feature is the introduction of Na and K due to alkali-metasomatism. The Na is mainly contributed by the pure albite and that of the K by the phlogopite, both them were formed during the process of alkali-metasomatism. Assuming the same hypothesis, the effect of alkali-metasomatism is calculated and presented in the Table 4.3. It has been found that the alkali-metasomatism caused substantial enrichment of Al_2O_3 , Na_2O , K_2O , and MgO with the removal of CaO to the originally unaltered alkali-pyroxenite (Fig. 4.6a, b). The SiO_2 , TiO_2 and P_2O_5 content increased slightly in the metasomatized rock (Fig. 4.6a, b). The total Fe, as Fe_2O_3 , remains same in both the original and altered rock. Thus it is evident that the rock has undergone intense alkali-metasomatism during fenitization caused by carbonatite intrusion. The initial peralkalinity indices (PI) or agpaitic index (AI) ($\text{PI/AI} = \text{mol. Na}_2\text{O} + \text{K}_2\text{O} / \text{Al}_2\text{O}_3$) calculated based on pyroxene composition is very high (3.85). Though the altered rock got further enriched in alkalis ($\text{Na}_2\text{O} + \text{K}_2\text{O}$) but the magnitude of Al_2O_3 enrichment is much higher thus lowering the peralkalinity indices or agpaitic index drastically to 0.9.

The alkali-pyroxenite shows minor variation in trace element concentration (Table 4.1). They are characterize by higher concentration of Ba (>1300ppm), Sr (1639ppm), and Nb (>80ppm) and comparatively lower Th (>3 ppm) content. The Rb concentrations are comparatively higher (>25 ppm) in comparison to the associated carbonatite. This is mainly due the presence of mica (biotite/phlogopite), which generally carries K in their structure and replaced by Rb. Among the HFSE, the rock is relatively enriched in Ta (>1.1 ppm) in comparison to the Zr, Hf. The primitive mantle (Sun and McDonough, 1989) normalized values of selected trace elements as plotted in

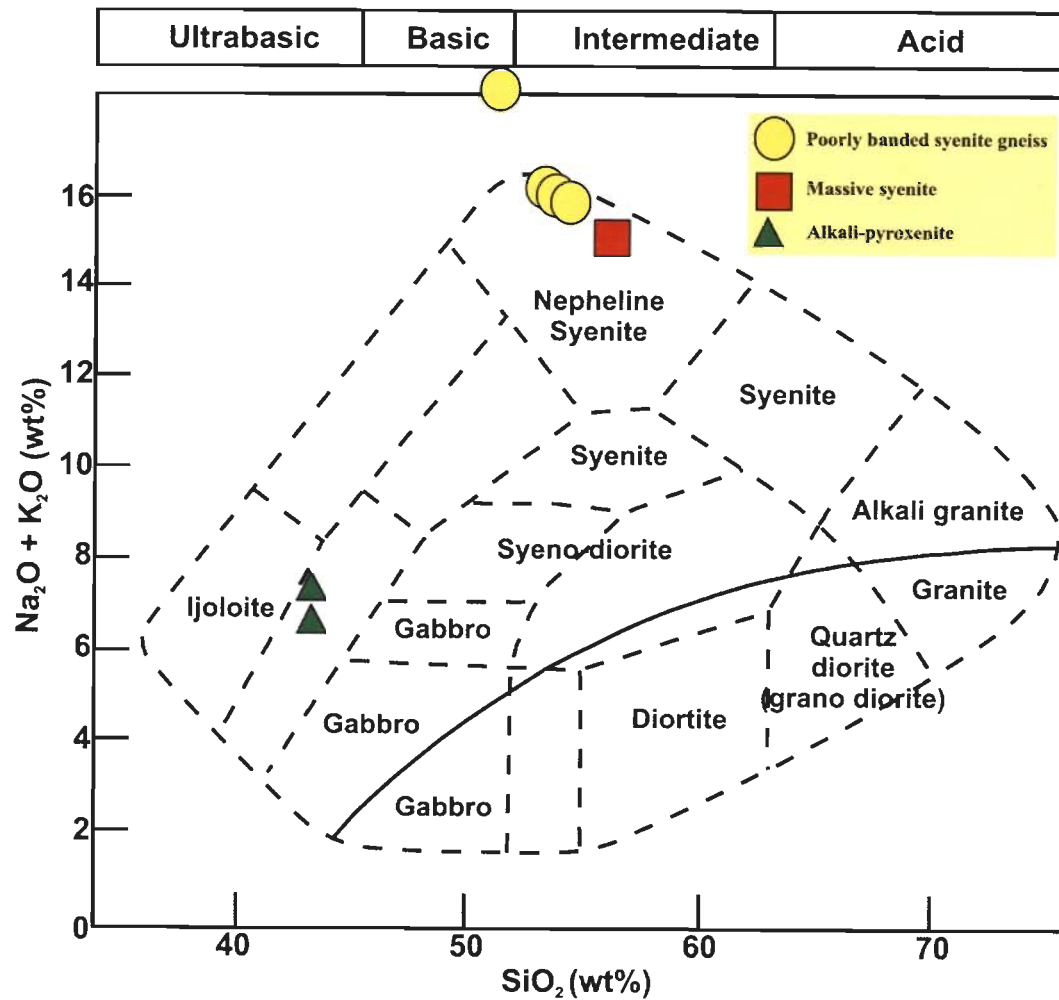


Fig. 4.5 Total Alkali versus Silica (TAS) plot of the silicate rocks viz. metasomatized alkali-pyroxenite (alkali-pyroxenite in the figure) and nepheline-syenites. One sample is showing higher amount of alkalis.

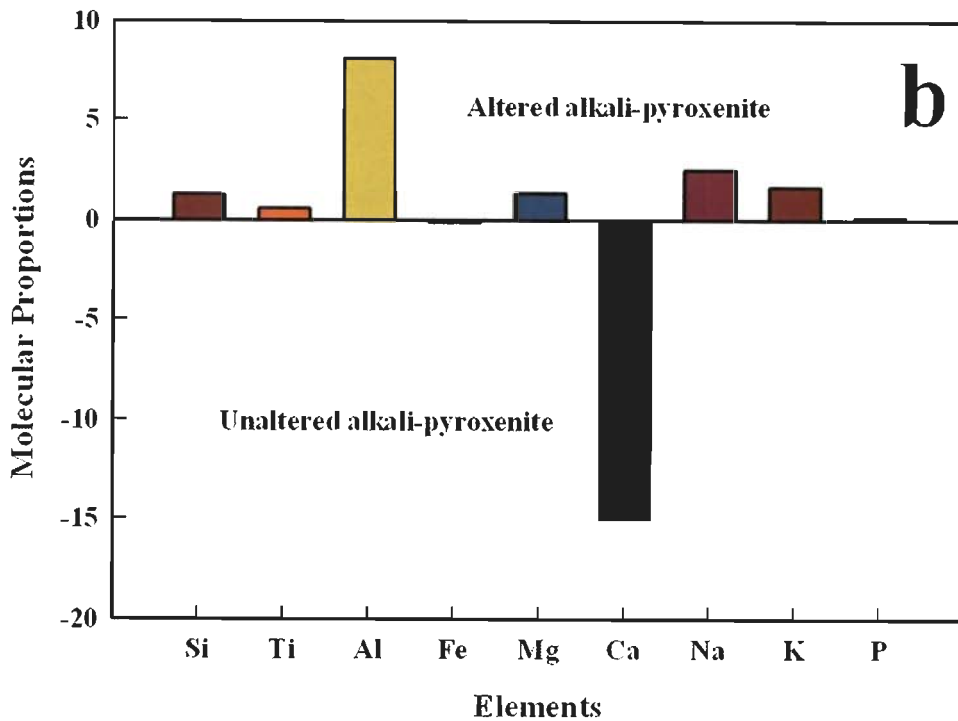
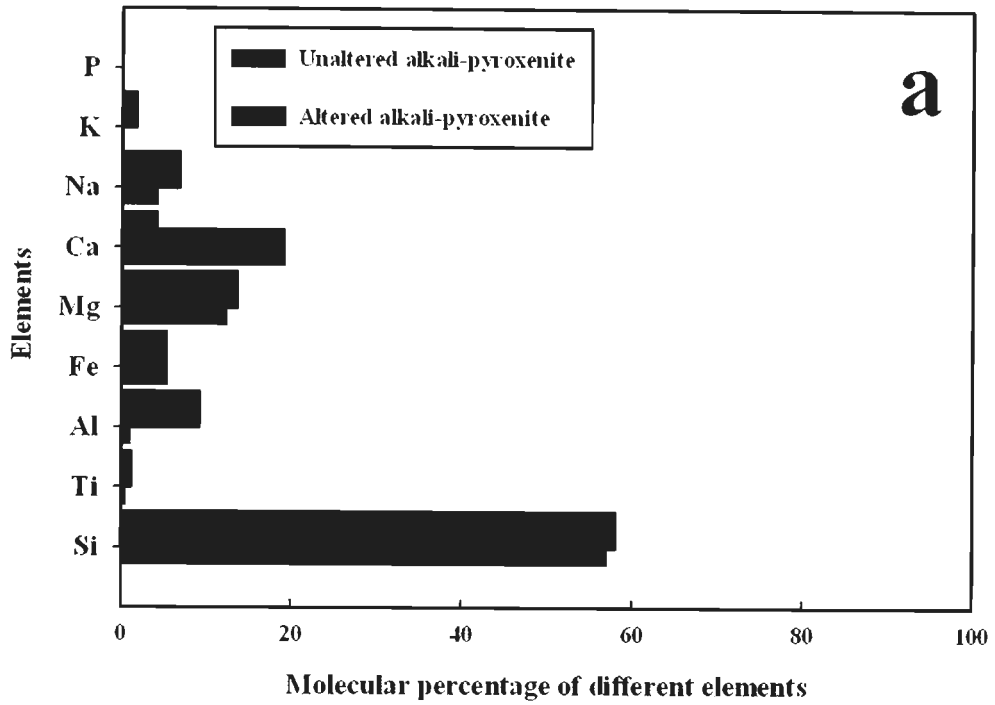


Fig. 4.6 (a) and (b) Graphical representation of the elementary loss and gain of elements between the alkali-pyroxenite (igneous) and altered alkali-pyroxenite (metasomatized alkali-pyroxenite) during alkali-metasomatism.

spider diagram (Fig. 4.7a) fall in the range of 10 to 400. The rock is comparatively enriched in all incompatible trace elements with respect to the primitive mantle value (Sun and McDonough, 1989). Though they are enriched in incompatible elements but lower level of enrichment for Th (10 times), Hf (8 times) and Zr (10 times) has been observed (Fig. 4.7a). On the other hand they are relatively enriched in Ba (400 times), Sr (90 times), Nb (150 times) and Ta (40 times) with respect to the other elements (Fig. 4.7a). The higher concentration of Sr and Ba can be attributed to the presence of numerous thin calcite veins in this rock.

Like carbonatite the total REE concentration of this rock is mainly contributed by the LREE. The total REE abundance (Σ REE) of the alkali-pyroxenite is much lower in comparison to that of the near by carbonatite and ranges between 246 to 322 and that of the La/Yb_n-ratio ranging from 30 to 46. Chondrite-normalized REE pattern of this rock shows that the REE values are varying from 300 to 6 with respect to the chondrite (Sun and McDonough, 1989) (Fig. 4.7b). The LREE enrichment varies about 200-350 times and the same for HREE is only 6-9 times and thus LREE enrichment is 33 to 38 times higher than HREE (Fig. 4.7b).

The higher concentration of compatible elements (Sc, V, Cu, Co, Zn) is expected in a rock rich in ferro-magnesian minerals like pyroxene, in this case original alkali-pyroxenite. These elements are also immobile in nature, so they are not removed during alteration process. However, the effect of fenitization in trace element concentration is very much pronounced by the enrichment in certain incompatible trace elements like Rb, Ba, Sr and Nb as observed in this rock. Phlogopite is the main carrier phase for Rb (K in phlogopite replace by Rb) and this mineral was formed during fenitization. The possible carriers of Ba and Sr are calcite and apatite, occurring as veins. The increase of Nb may be attributed to the formation of nioborutile during alkali-metasomatism (Fig. 4.8). Similar enrichment of these elements is also reported from the other fenitized rock from different part of the world e.g. those are found at Fen, Norway (Kresten, 1988).

4.4 NEPHELINE SYENITE

Based on field occurrence and petrographic study two varieties of nepheline syenite are present: banded syenite (further subdivided into poorly banded syenite gneiss and strongly banded syenite gneiss) and massive syenite. Both the variety of syenites as evidenced by their mineralogy and texture, to some extent retained part of the igneous character even if affected by later metamorphism. Post-magmatic alteration by deuteric fluid is also evident in these rocks. So the trace element geochemistry will not be a true representative of the pristine igneous rock but will reflect mixed igneous, metamorphic and metasomatic signatures. The strongly banded syenite gneiss is intensely metamorphosed as mentioned in the earlier chapter and maximum change in trace element and isotope geochemistry is expected in this variety. Moreover, during heavy liquid separation this rock also did not yield any zircon or apatite grain necessary for study of U-Pb systematics. Due to these reasons this variety of syenite has been excluded from major and trace element analysis too. On the other hand, poorly banded syenite gneiss is the most dominant rock type among all the syenites and the massive syenite has undergone least post-magmatic changes. Henceforth, only massive and poorly banded syenites are discussed.

Five representative nepheline syenite samples are chosen for chemical analysis out of which four are poorly banded syenite gneiss (ANK 2, 6, 7 and 8) and one is massive syenite (ANK 9). All the analyzed data are given in Table 4.1. The poorly banded syenite gneisses are comparatively enriched in total alkalis ($\text{Na}_2\text{O}+\text{K}_2\text{O}$) in comparison to the massive syenite. The Al_2O_3 content is almost similar in both the varieties (21.4 to 22.2%). The PI (peralkalinity indices) or agpaitic index is more than 1 (1.1 to 1.2) for poorly banded syenite gneiss where as the same for the massive syenite is close to 1 (1.03, Table 4.1). The agpaitic index of the massive syenite is well below 1.2 and can be termed as miaskitic syenites. Rocks with more than 1 PI are termed as 'Peralkaline'

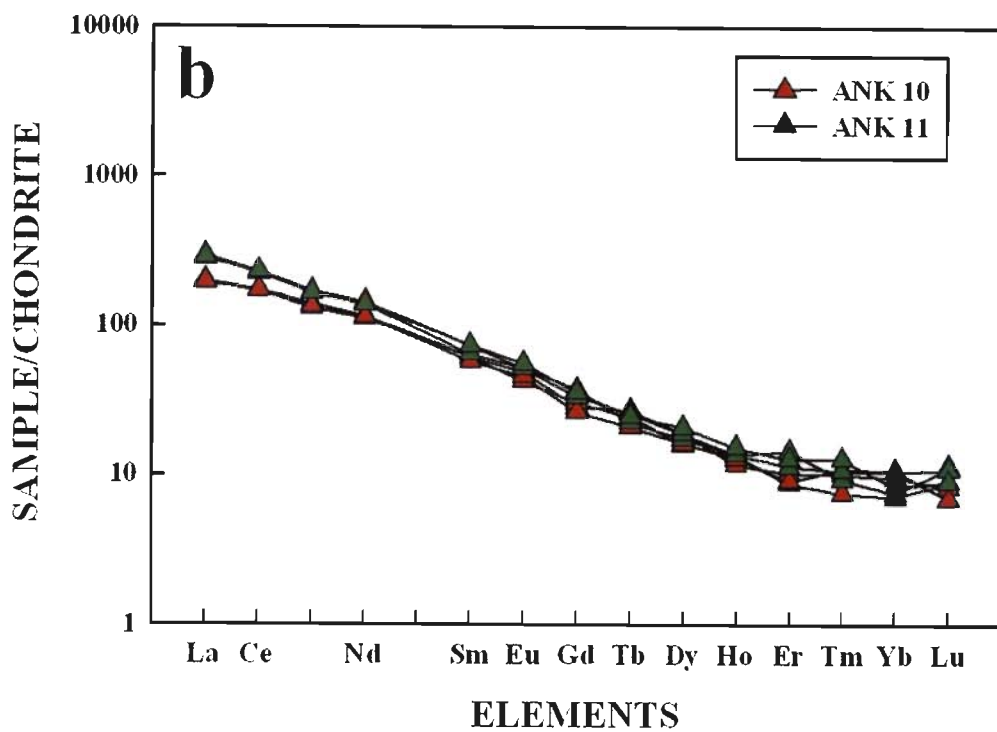
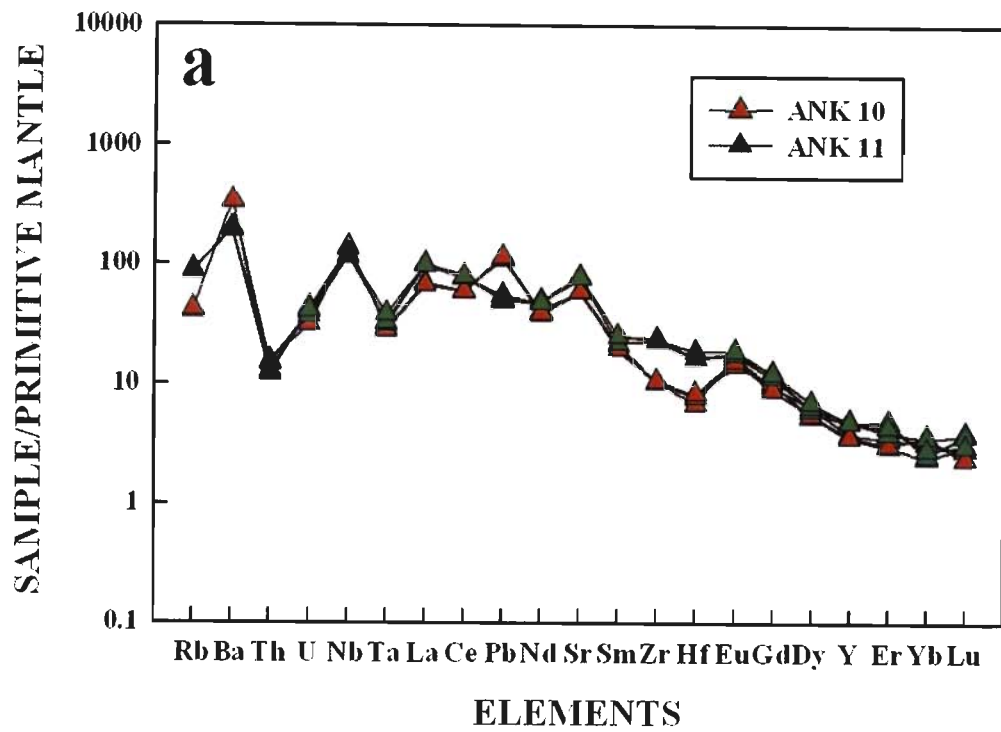


Fig. 4.7 (a) Primitive mantle normalized spider diagram for alkali-pyroxenite. (b) Chondrite normalized REE plot of fenitized alkali-pyroxenite (alkaline-ultramafic). Normalizing values are from Sun and McDonough (1989).

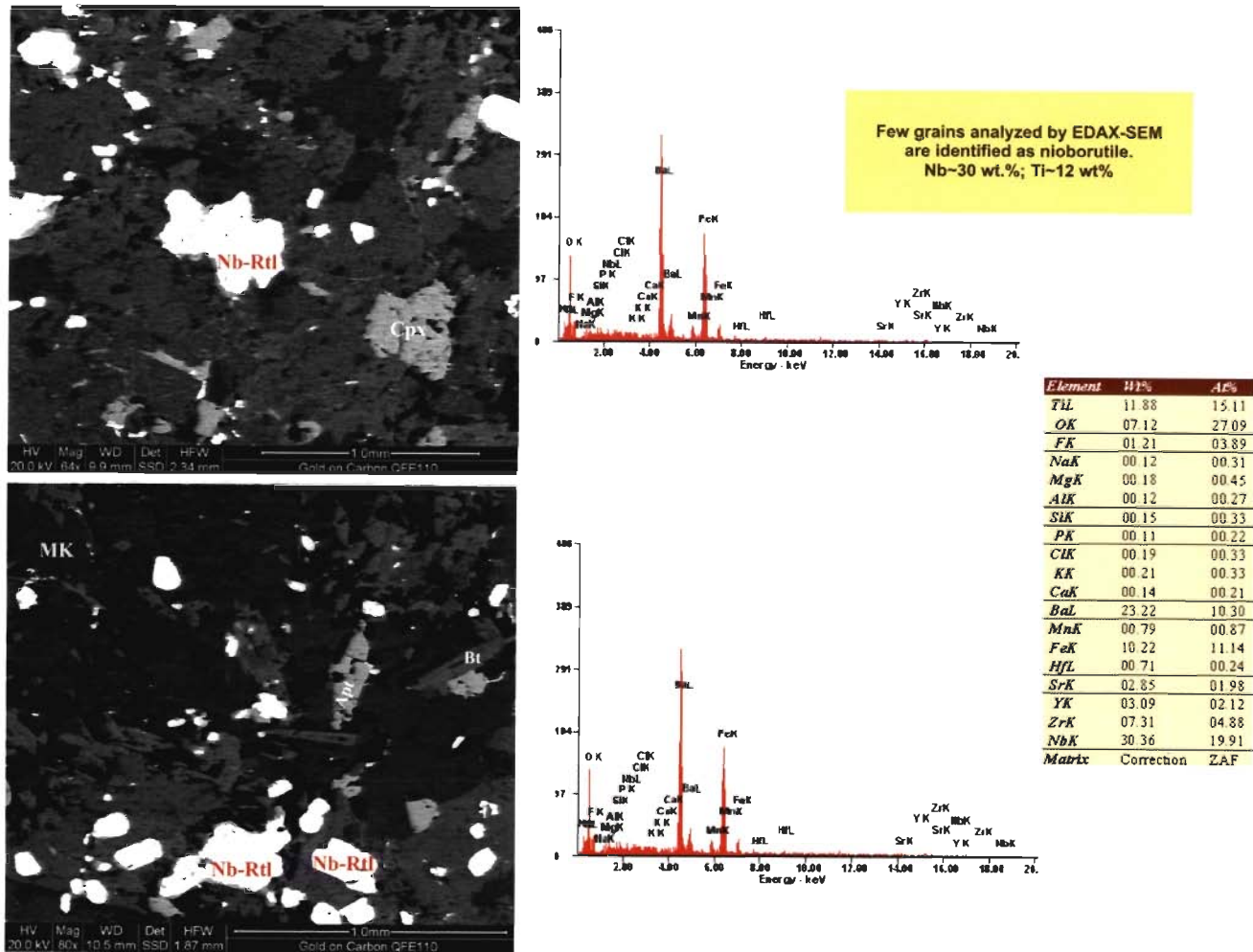


Fig. 4.8 BSE image showing presence of nioborutile in alkali-pyroxenite. These grains were analyzed by SEM-EDAX. (Nb-Rtl: Nioborutile; Cpx: Clinopyroxene; Apt: Apatite; Bt: Biotite, MK: Magnesiokataphorite)

rocks (Currie, 1989) or if the same is ≥ 1.2 they are termed as agpaitic nepheline syenites (Ussing, 1912; Fersman, 1929; Goldschmidt, 1930). In both the cases the poorly banded nepheline syenite gneisses are 'Peralkaline' or agpaitic in nature in its present form. This has been already mentioned in the previous chapter that the rocks were originally emplaced as miaskitic type ($PI < 1$ or agpaitic index ≤ 1.2) and later metasomatically alters to agpaitic type syenites. Other than alkalis both the varieties of syenites are enriched in SiO_2 and Al_2O_3 but the massive syenite is slightly more enriched in SiO_2 in comparison to the poorly banded syenite (Fig. 4.2). There is no significant variation is observed in CaO , TiO_2 , Fe_2O_3 , MgO and P_2O_5 between the two varieties of syenite when plotted in the Harker variation diagrams (Fig. 4.2). The MnO content is found to be variable among major oxides and it varies between 0.19 to 0.35% (Fig. 4.2). In a TAS plot (Cox et al., 1989) all the samples are expectedly plotted into nepheline syenite quadrant (Fig. 4.5). CIPW Norm is calculated and shown in Table 4.2. None of the syenites are found to be containing free quartz is in well accordance with the petrographic study. So, it is obvious that these rocks were originally formed from an undersaturated silica-poor alkaline magma. CIPW Norm also suggests that the massive syenite is containing much higher amount of plagioclase but lower nepheline in comparison to the poorly banded syenites (Table 4.2). The higher amount of SiO_2 can thus be attributed to the higher proportions of feldspar present in massive syenite. It has been mentioned earlier that the rock is containing only few biotite grains and aegirine is completely absent. The similar feature also found in normative calculations of this rock, the rock is found to be totally free from acmite (aegirine) (Table 4.2).

Both the varieties of syenite is characterized by the higher concentrations of Rb (111-141 ppm), Pb (6-60 ppm), Th (6-85 ppm), and U (2.4-15 ppm) but comparatively lower in Ba (65-105 ppm) and Sr (120-255 ppm). All the syenites are substantially enriched in HFSE: Zr (2267-2850 ppm), Hf (37-66 ppm), Nb (76-186 ppm) and Ta (9.6-42 ppm). The primitive mantle normalized (Sun and

McDonough, 1989) spider plot (Fig. 4.9a) shows that they are essentially enriched in all incompatible elements with respect to the primitive mantle and fall in the range of 10 to 1100 indicating that the enrichment and/or depletion of certain element(s) with respect to the primitive mantle in the order of 110 magnitudes. The spider variation diagram (Fig. 4.9a) reveals that all the syenites are essentially enriched in Rb (200 times), Th (60-1000 times), U (100-650 times) and Pb (80-800 times) while depleted in Ba (9-35 times) and Sr (5-11 times) with respect to the other incompatible trace elements. They are enriched in all HFSE analyzed i.e. Zr (180-360 times), Hf (108-270 times), Nb (100-650 times) and Ta (200-1000 times). Other trace elements which are plotted in the spider variation diagram is showing very similar pattern for both the varieties of syenite.

The syenites are characterized by the higher concentrations of LREE in comparison to the HREE. The total abundances of REE (Σ REE) vary between 193 to 485 ppm and that of the (La/Yb_n) is 12 to 16. The chondrite normalized (Sun and McDonough, 1989) REE pattern for both the varieties showing that the REE content varies from 150-400 (LREE) and 12-43 (HREE) times (Fig. 4.9b). All the syenites are characterized by the enrichment of the REE with respect to the chondrite value (Sun and McDonough, 1989). It should be mentioned here that both varieties of syenite being discussed are rich in either sodic (poorly banded) or potassic (massive) feldspars. So, the REE, especially the LREE should substitute Na⁺ in sodic feldspar i.e. albite. These rocks are characterized by relatively steeper LREE compared to flatter HREE pattern. The relative enrichment of LREE is mainly controlled by the feldspars (mostly albite) that present within these rocks, though the relatively flatter HREE pattern is not controlled by the feldspars. Such pattern is may be due the presence of zircon as an accessory mineral. Zircon (ZrSiO₄) generally having low LREE and high HREE content. Though the zircon is present as an accessory mineral but their presence resulted relative enrichment of HREE. Here the LREE is mainly fractionated into feldspar

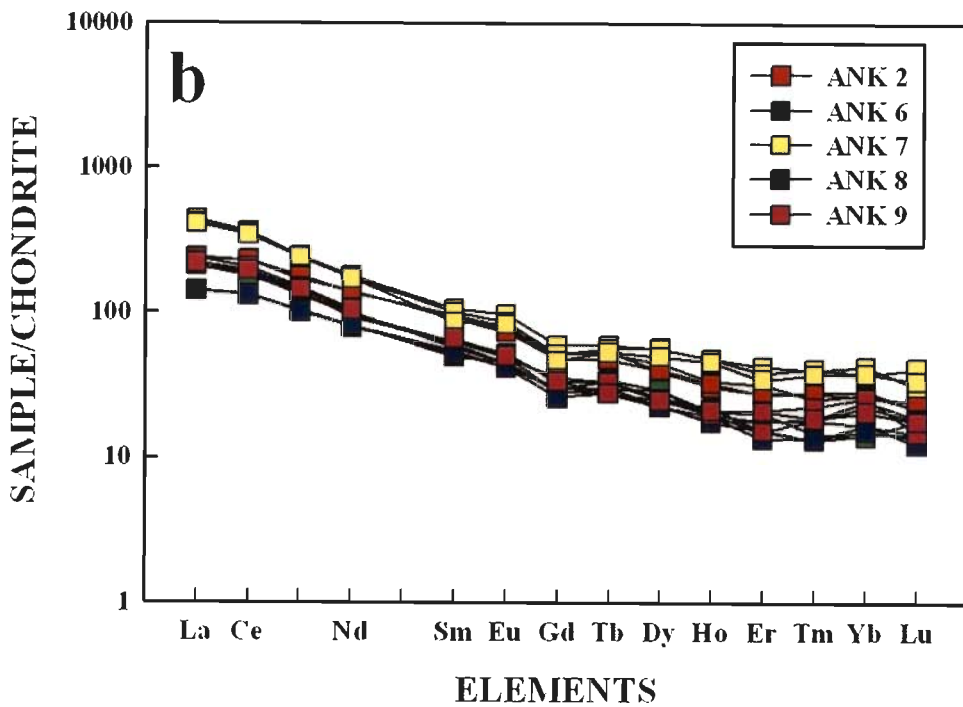
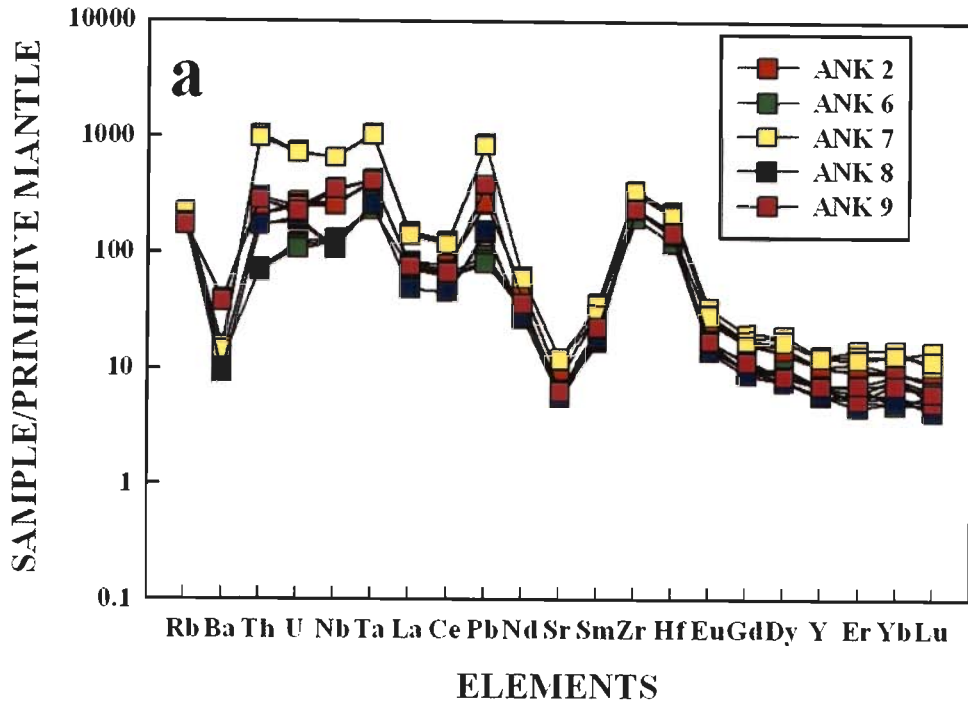


Fig. 4.9 (a) Primitive mantle normalized spider diagram of nepheline-syenites (ANK 2, 6, 7, 8 are poorly banded syenite gneiss and ANK 9 is massive syenite) from Sushina. (b) Chondrite normalized REE plot of nepheline-syenites. Normalizing values are from Sun and McDonough (1989).

along with zircon. The presence of minor amount of monazite or pyrochlore as accessory mineral phase like zircon can not be ruled out, as these minerals are characterized by the very similar trend observed in syenites. Relatively enriched concentration of Nb, Sr, Th and Pb in the sample number ANK 2, 7 and 9 may support this guess. These minerals are characterized by the lesser enrichment or depletion of LREE and MREE relative to HREE (Hanson, 1980). Moreover all the syenite is characteristically devoid of Eu anomaly which is common for feldspar bearing rocks. Eu anomaly mainly occurs due to the presence of Ca-plagioclase i.e. anorthite. Sushina syenites are devoid of Ca-plagioclase (whole rock as well as normative) (anorthite) but enriched in albite (Na-plagioclase) and orthoclase (K-feldspar) and thus showing no Eu anomaly in all these rocks.

4.5 SUMMARY OF BULK ROCK CHEMISTRY

Carbonatite and Pyroxenite association

The Purulia carbonatite is characterized by very low amount of most of the major oxides except CaO and P₂O₅ in comparison to the associated alkali-pyroxenite. The higher amount of these oxides can be attributed to the presence of calcite (90% by volume) and apatite (2-5% by volume) in the carbonatite respectively. The alkali-pyroxenite is containing much higher amount of SiO₂, Al₂O₃, Na₂O and K₂O in comparison to the carbonatite and the order is as alkali-pyroxenite>carbonatite. The high amount of alkalis (Na₂O+K₂O), along with TiO₂, Al₂O₃, MgO and P₂O₅ in alkali-pyroxenite (Fig. 4.6a, b), can be ascribed mainly due to alkali-metasomatism which took place due to near vicinity middle-late stage carbonatite intrusion.

The trace element compositions of these rocks are also variable. In general carbonatite is expectedly enriched in Sr (8500-11200 ppm), Ba (797-1784 ppm) and REE. Between carbonatite and alkali-pyroxenite, carbonatite is relatively enriched in Sr, Th, U and Nb, while the later is enriched in all compatible elements (Sc, V, Co, Ni, Cu and Cr), Ba and Rb. The higher

concentration of Ba and Rb in altered alkali-pyroxenite is due to alkali-metasomatism responsible for enrichment of these elements. The Ba is mainly concentrated into the calcite and apatite veins and that of the Rb in phlogopite, which formed due to biotitization. The primitive mantle normalized (Sun and McDonough, 1989) spider diagram (Fig. 4.10a) of these two rocks reveals that all the rocks are enriched relative to the primitive mantle (Sun and McDonough, 1989). The Purulia carbonatite is relatively poorer in Rb (0.30 times), Zr (0.40 times) and Hf (0.80 times) while enriched in Sr (500 times), La (600 times), Ce (500 times) and Sm (150 times) and Nb (13 times for two samples and about 100 times for other two) (Fig. 4.10a) in comparison to the alkali-pyroxenite with respect to the primitive mantle. The similar behaviour of Ta as Nb is observed in carbonatite. The alkali-pyroxenite is enriched in Rb (100 times), Zr (23 times) and Hf (20 times), relative to the carbonatite. The REE pattern of both carbonatite and alkali-pyroxenite in a chondrite normalized (Sun and McDonough, 1989) plot showing enrichment of REE relative to the chondritic value. However, the REE content of the Purulia carbonatite is much higher compared to the associated alkali-pyroxenite. The concentrations of LREE and MREE are higher relative to the HREE in these rocks (Fig. 4.10b).

Nepheline Syenite

Owing to the different mineralogical character of the different varieties of nepheline syenites their agpaitic index also varies from poorly banded nepheline syenite gneiss to massive syenite. The first group is characterized by the higher agpaitic index and thus in its present form resembles to *agpaitic nepheline syenite gneiss* and that of the massive syenite are *miaskitic* as their agpaitic index is close to unity. The agpaitic nature of the poorly banded syenite gneiss can be attributed by the two major mineralogical observations. The first one is the presence of abundant mafic minerals (mostly aegirine) and the second one is the late stage replacement of the aegirine by eudialyte

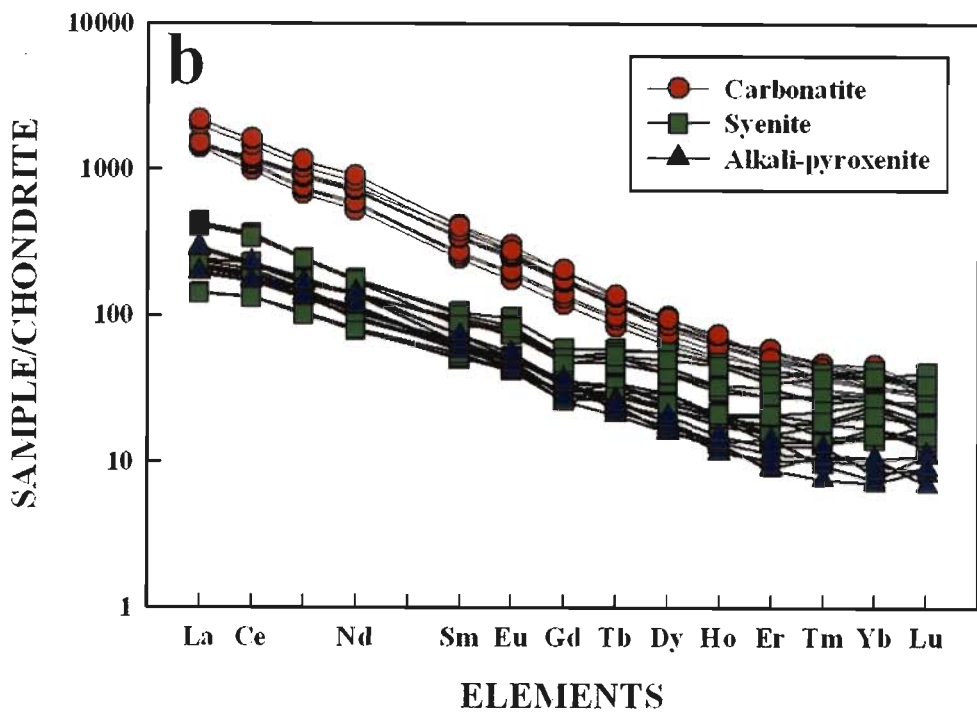
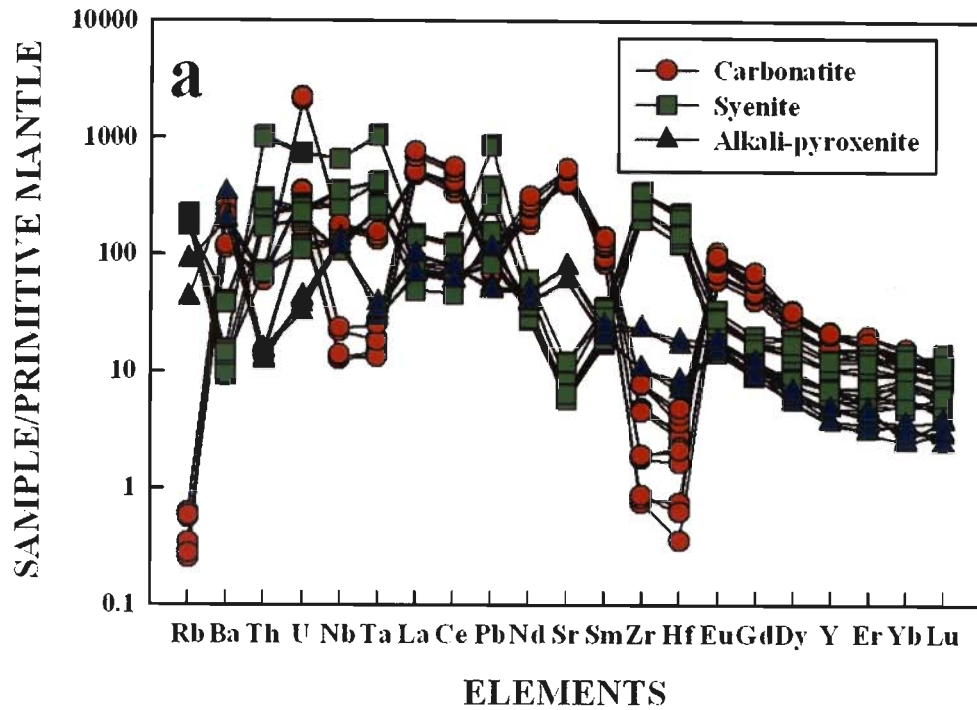


Fig. 4.10 (a) Primitive mantle normalized spider diagram of three different rocks viz. carbonatite, alkali-pyroxenite and all varieties of nepheline syenites. (b) Chondrite normalized REE plot of the above mentioned rocks. Normalizing values are from Sun and McDonough (1989).

and/or Na-Zr silicates by the deuteritic fluid. The nepheline-syenite is characterized by relatively higher concentration of Rb (200 times), Th (500-1000 times), U (100-700 times), Nb (100-700 times), Pb (80-800 times), Zr (300 times), Hf (200 times) and Ta (250-1000 times) while poor in Sr (10 times) and Ba (10 times) relative to the primitive mantle value (Fig. 4.10a). The REE concentrations of both the varieties of syenites are almost similar. Irrespective of their different mineralogy their REE trend is similar. The nonexistence of Eu anomaly in nepheline syenite is due to absence Ca in plagioclase which is purely sodic or albitic in composition.

4.6 MINERAL CHEMISTRY

Carbonatite and alkali-pyroxenite both are containing fluoroapatite which is already discussed in Chapter 3. In addition to this, some key minerals like zircon, monazite which is particularly useful for isotopic study were also looked for using heavy liquid separation. During heavy liquid separation apatite is found to be the common mineral present in these rocks along with zircon, which is only found in nepheline-syenite (poorly banded syenite gneisses and massive syenite). Both apatite and zircon were not yielded from the strongly banded syenite gneiss and excluded for bulk rock as well as mineral chemistry studies. The apatite grains, separated from all these rocks, were analyzed using LA-ICPMS. Each apatite grain was analyzed twice and the average of the two analyses is finally tabulated. The simulated analytical condition for LA-ICPMS analysis was same as that of the whole rock is discussed previously. It must be mentioned here that during the calculation of the LA-ICPMS data for apatites from nepheline syenites, the in-put value for calibration was done as per stoichiometric value of CaO (55.4 wt%) in apatites. This was done due to lack of EPMA data for these apatite grains. The calibration of the apatites from the carbonatite and alkali-pyroxenite was done twice at stoichiometric values of CaO (55.4 wt%) as well as using the CaO obtained from EPMA data. It has been noticed that the difference between two data sets

are negligible. Thus the data obtained for the present work is reliable and interpretation is practical and reasonable as well.

Heavy liquid separation method was used to separate the apatite grains followed by their identification using Ramon Spectroscopy and described below.

4.6.1 ANALYTICAL PROCEDURE

A) Heavy Liquid Separation: This procedure was carried out on sample size between 100-300 μ . The magnetic and non-magnetic fractions were separated using an MTS (Magnetic Trommel Scheider) under revolution speed: 75 r.p.m and voltage: 15 amp. Non-magnetic fraction is then used for heavy liquid separation. Initially the purpose of the heavy liquid separation was to investigate the presence of some key minerals like zircon, monazite etc. which are commonly used for mineral dating. Apatite being a common accessory mineral in all the rocks was also recovered. Two different liquids of different density were used to separate apatite and zircon. Firstly, methylene iodide (MI) (MI-GEE made by National Biochemical Laboratory, Illinois, USA) of density 3.325 (very close to specific gravity) (at room temperature) was used. The fraction heavier than MI was used for further separation using 'Clerici solution' having density (nearly equal to its specific gravity) of 4.2 (at room temperature). The apatite grains (fluroapatite) are generally having density in the range of 3.1 to 3.2 and thus separated in the fraction which is heavier than MI but lighter than Clerici. Zircon was found in poorly banded and massive syenites and expectedly found in the fractions heavier than Clreici.

B) Ramon Spectroscopy: The micro-Raman spectrometer is a DILOR Lab Ram instrument equipped with an Olympus microscope, an internal He-Ne laser and an external Ar laser. Three exciting wavelengths: 488 nm, 514.5 nm and 632 nm are available in this instrument. In the

present study the Raman Spectra were collected on a freshly broken surface with confocal Lab Ram system (Jobin-Yvon), using the 488 nm of an external argon laser with typically 200 mW of laser power at the sample surface. Typically, the spectra were collected with 4 acquisitions of 30 seconds each. Different fractions (heavier as well as lighter than MI and Cöerici) were studied under Ramon Spectroscopy and the different spectra curve for different mineral like calcite, aegirine, apatite and zircon were studied carefully to identify these grains. The spectral response curve for apatite and calcite grain is shown in Fig. 4.11.

4.6.2 APATITE AND CALCITE FROM THE CARBONATITE

Based on trace element geochemistry, two samples of carbonatite were chosen for study of apatite. In addition to apatite few calcite grains have also been analyzed from one of the carbonatite samples (ANK 1). The trace elemental composition of both apatite and calcite is presented in Table 4.4. Apatite grains of the two analyzed samples are characterized by very high REE content ranging from 4832-8860 ppm (Table 4.4) in comparison to the calcite (Σ REE= 378-500 ppm). The apatite grains are essentially enriched in LREE and thus having higher $(La/Yb)_n$ (62-132) in comparison to the calcite grains (7-8). The calcite grains are expectedly enriched in Sr (9585-10,800 ppm), comparison to the apatite (6225-8000ppm) due to substitution of Ca by Sr, in calcite. Rb, Th, U, Nb and Zr is almost absent in calcite (except U in Cal 9 & 10) but containing small amount of Pb (10-18 ppm) and Y (54-92 ppm). On the other hand the apatite grains are containing varying amount of Th (37-118 ppm), U (1-98 ppm), Pb (8-16 ppm) and Y (170-387 ppm).

The primitive mantle normalized (Sun and McDonough, 1989) plot (actually termed as “extended chondrite-normalized incompatible distribution diagram”) of the apatite and calcite is shown in Fig. 4.12. All the plotted elements in calcite are enriched with respect to the primitive mantle value except for Rb, Th, Nb and Zr. On the other hand primitive mantle normalized plot reveals that of

the apatite grains are relatively enriched in Th, U, La, Ce, Pb, Nd, Y and some of the HREE (Gd, Dy, Er, Yb, Lu) while poor in Rb, Zr and Nb. The primitive mantle normalized average calcite and apatite plot along with the whole rock reveals that the whole rock Sr and Pb concentration is falling very close to that of these two minerals. It may be concluded that the Sr and Pb concentration is mainly contributed and controlled by both calcite and apatite only. The average concentration plot of the calcite and apatite along with the whole rock (Fig. 4.13a) reveals that ANK 1 is more enriched in the bulk U and Nb. Similar bulk Nb enrichment is also noticed in the sample number ANK 3 but the bulk U in this sample is less than that of the apatite. The contribution of U and Nb in the carbonatite may be due to presence of some very minor phases like pyrochlore(?) but such presence is not confirmed by either petrographically or by heavy liquid separation.

The chondrite normalized (Sun and McDonough, 1989) REE plot (Fig. 4.12) of both the apatite and calcite are enriched in REE with respect to the chondritic value. The REE plot shows that the apatite is highly enriched in REE and particularly in LREE in comparison to the calcite. The whole rock REE plot falls exactly in between the apatite and calcite indicating that the bulk REE budget is controlled by these two minerals (Fig. 4.13b). Though the modal concentration of calcite is 90% and about 18-20 times higher than apatite, the \sum REE concentration in apatite is more than 20 times higher compared to calcite. Thus this can be concluded that the total REE content of the carbonatite is controlled by the apatite and calcite and the higher LREE in the whole rock can be attributed mainly due to the presence of apatite. The further detail of the apatite and its implications in petrogenesis will be discussed on Chapter 6.

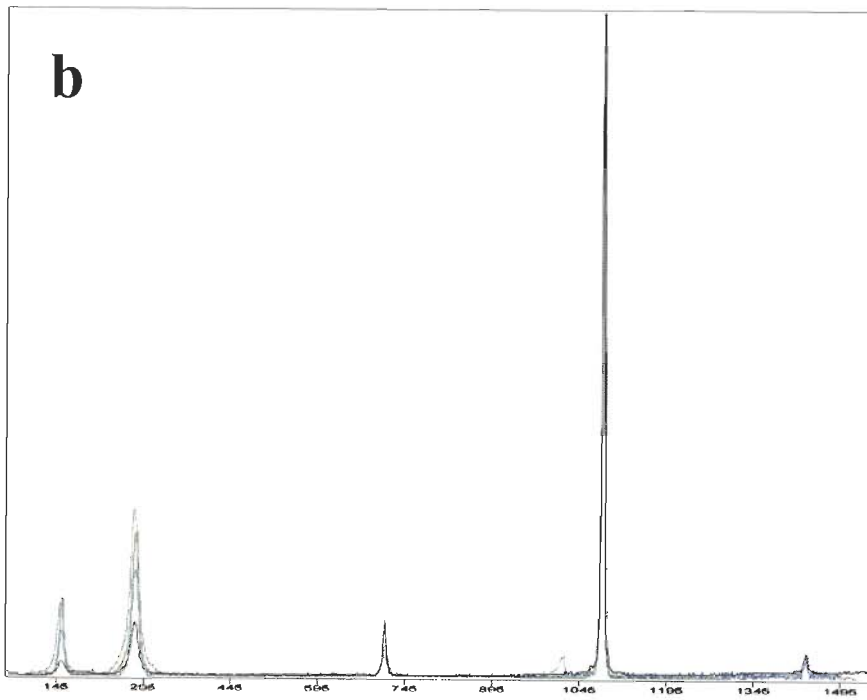
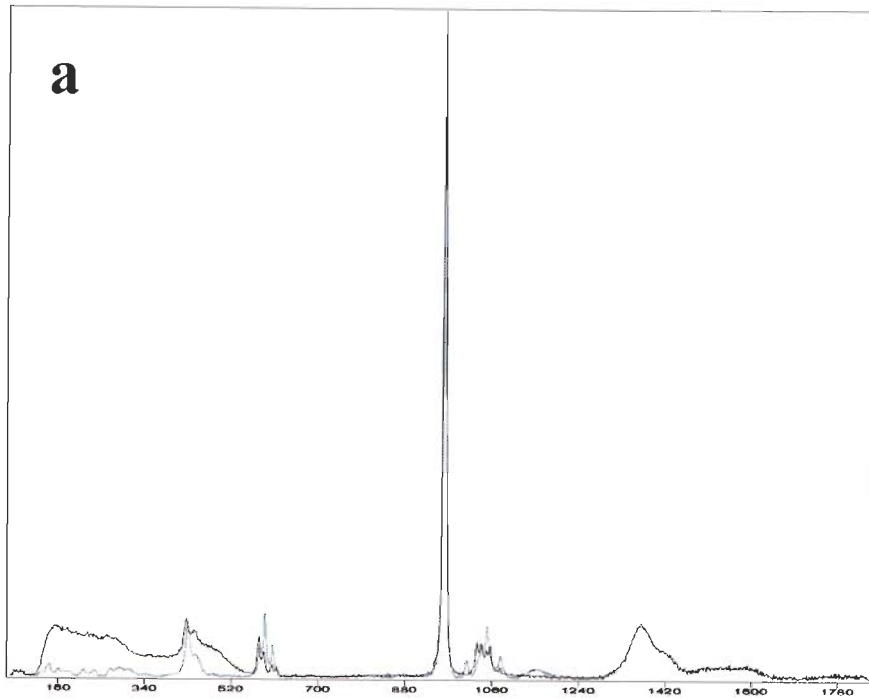


Fig. 4.11 (a) and (b) Raman spectral response curve of apatite and calcite from carbonatite. 97% match with the standard is noticed.

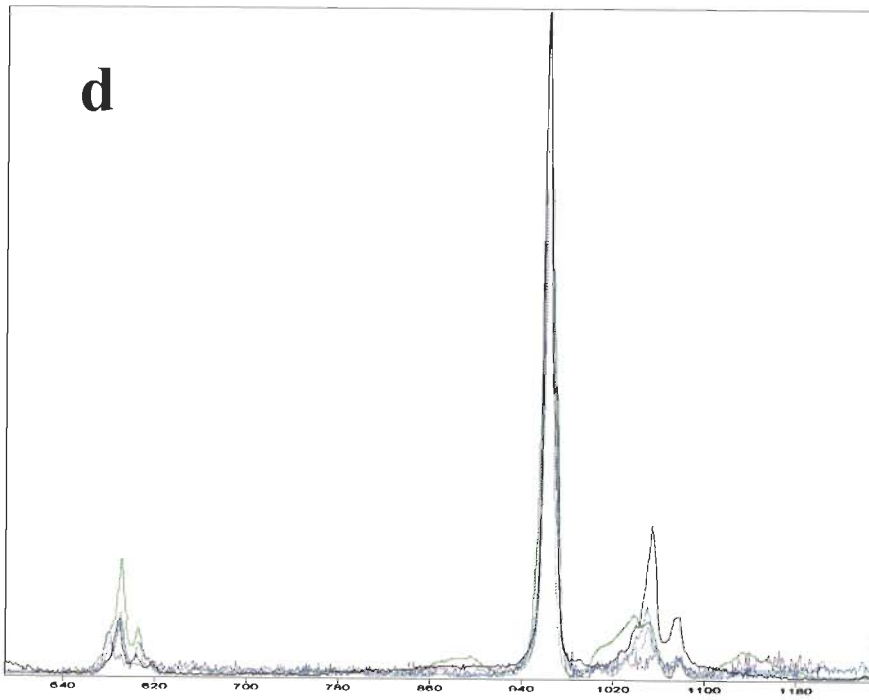
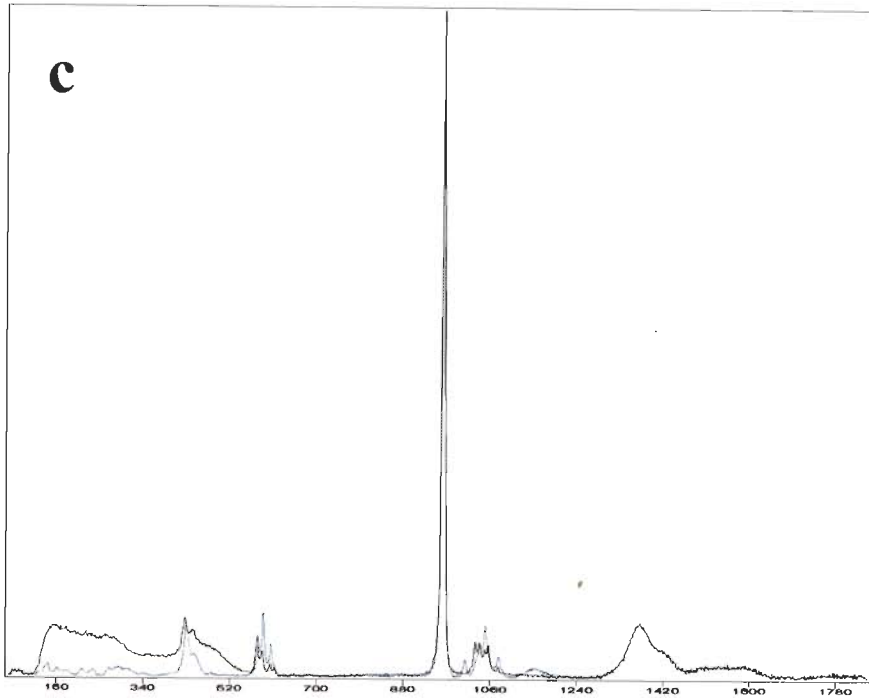


Fig. 4.11 (c) and (d) Raman spectral response curve of apatites separated from alkali-pyroxenite and nepheline syenites respectively.

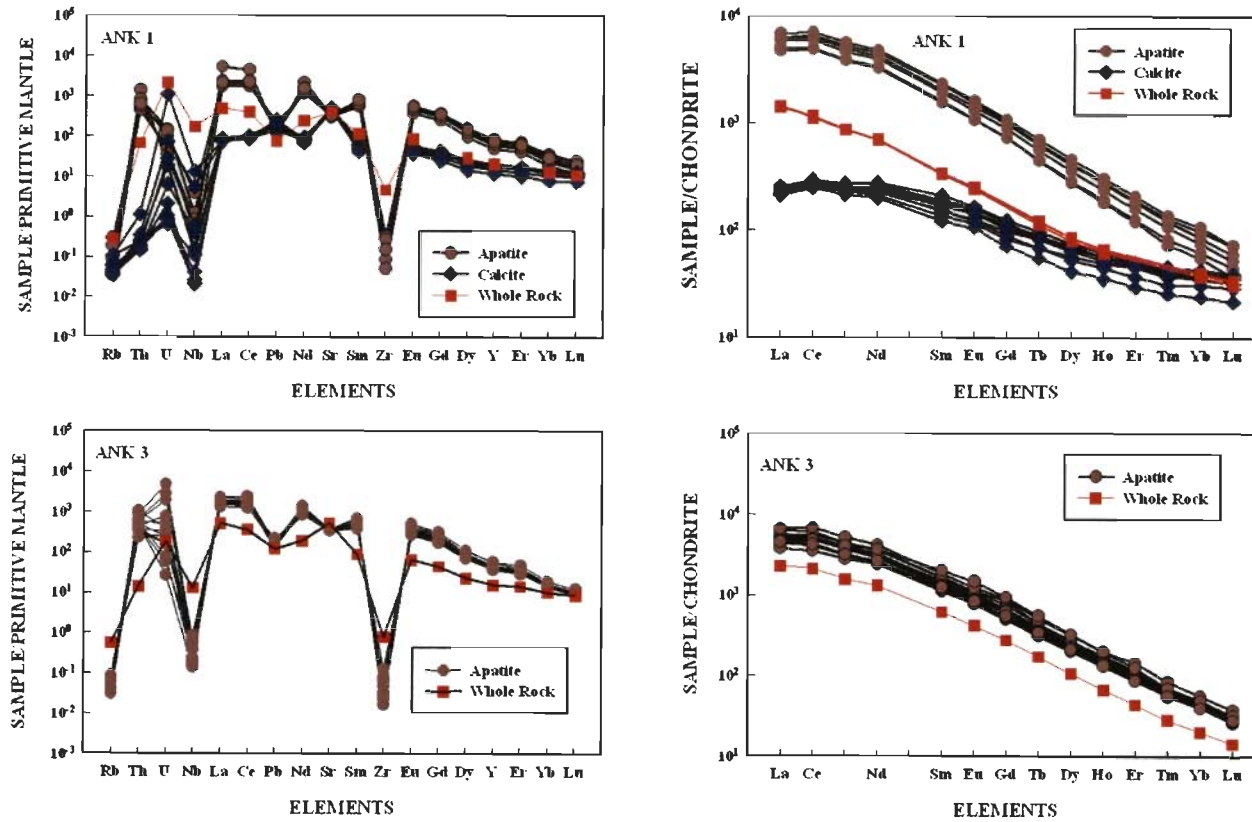


Fig. 4.12 Primitive mantle normalized spider diagram (column 1) and chondrite normalized REE plot (column 2) of the apatite and calcite separated from the Purulia carbonatite. Normalizing values are from Sun and McDonough (1989).

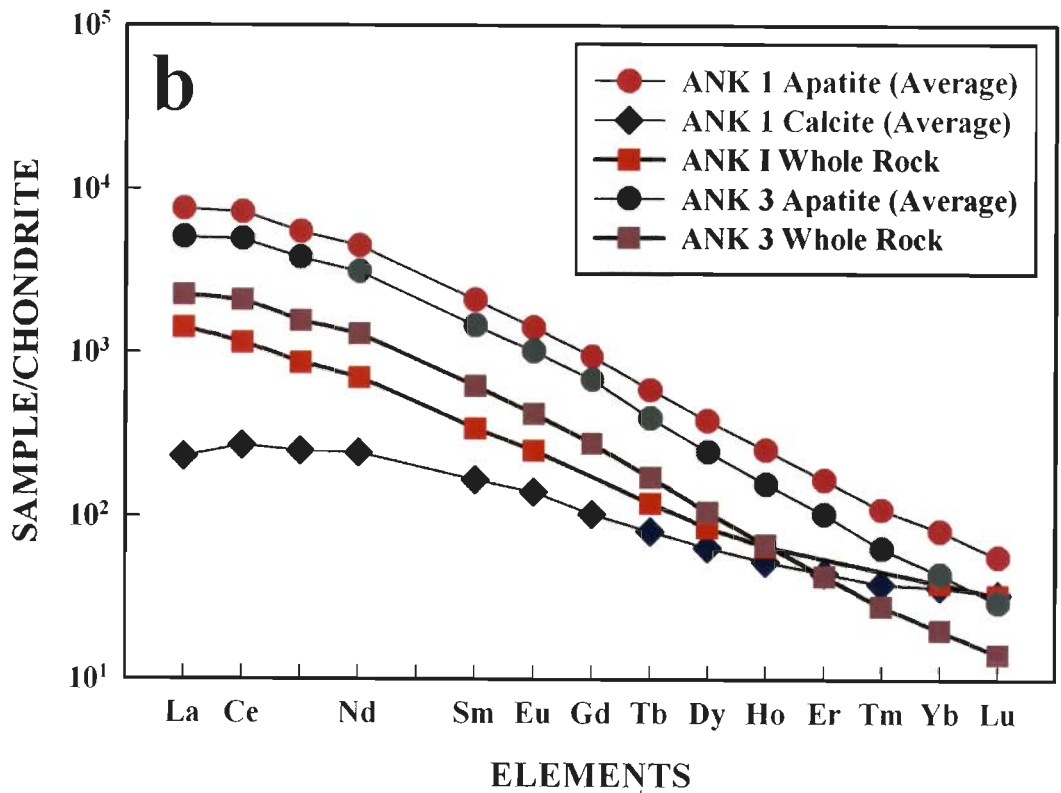
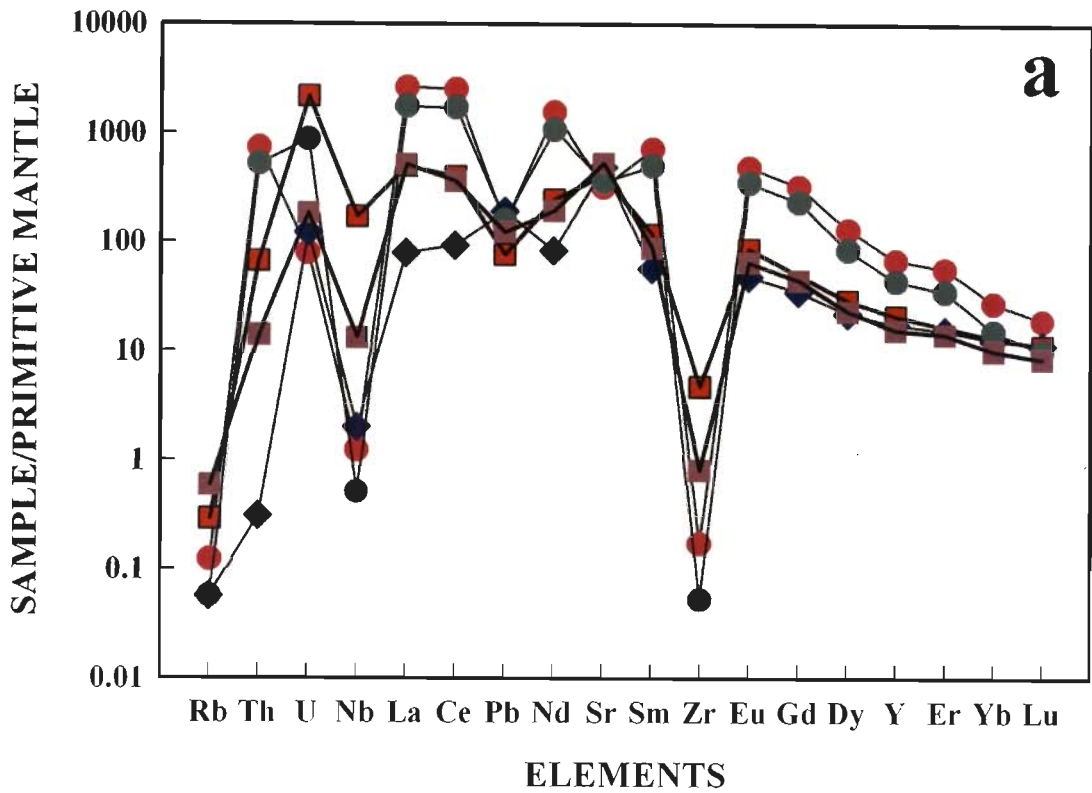


Fig. 4.13 (a) Primitive mantle normalized spider diagram of average calcite, apatite along with the whole rock from which these mineral grains were separated. (b) Chondrite normalized REE plot of average calcite, apatite along with the whole rock from which these mineral grains were separated. Normalizing values are from Sun and McDonough (1989).

4.6.3 APATITE FROM THE ALAKLI-PYROXENITE

Trace elements of apatite from two alkali-pyroxenites (ANK 10 and ANK 11) were analyzed and the data is presented in Table 4.5. It has been mentioned earlier that the apatite is introduced in this rock during the alkali-metasomatism by associated carbonatite intrusion. So, the apatite trace element chemistry will reflect the effect of alkali-metasomatism in this rock. In addition, comparison of apatite geochemistry from carbonatite and this rock will be a useful indicator of melt-fluid system active during carbonatite intrusion. In general, the apatite from alkali-pyroxenite is more enriched in REE compared to the carbonatite. The Σ REE and the $(La/Yb)_n$ vary from 7071 to 13231 ppm and from 54 to 73 respectively. Other than REE the apatite grains are enriched in Sr (5410-6560 ppm), U (6-13 ppm), Th (24-125 ppm) and Pb (8-70 ppm) while Rb, Nb and Zr are either not present or negligible. The Y concentration is variable and ranges from 380-599 ppm. It is much higher compared to the concentration in apatite of carbonatite decent.

Primitive mantle normalized plot (Sun and McDonough, 1989) shows that the apatite in this rock is relatively enriched in most of the incompatible elements except for Rb, Nb and Zr compared to the primitive mantle (Fig. 4.14). Relative enrichment of Th and U relative to primitive mantle is noticeable. Most of the REE like La, Ce, Nd and HREE are showing relatively higher concentrations in comparison to the other elements. Primitive mantle normalized spider plot also reveals that the bulk rock Pb concentration is very similar to that of the apatite and may be bulk Pb budget in the whole rock is mainly controlled by the apatite. The primitive mantle normalized average trace elemental composition of the apatite of both the rock is shown in the Fig. 4.15a. Most of the trace elements of the bulk rock except Pb, is falling well below the apatite trace elemental composition. In the primitive mantle normalized spider plot reveals the similar trends of apatite and bulk rock for majority of REE and other analyzed trace elements except Rb, Nb and Zr. The level of enrichment is certainly higher in apatite. Though apatite content in this rock seldom

exceeds 2% by volume, the role of apatite as a trace element contributor in bulk rock can not be ignored. However, the Rb, Nb and Zr of the bulk rock are dominated by the clinopyroxene and other silicate minerals. This can be very well established by the REE distribution pattern of the apatite and the bulk rock too and discussed in the next paragraph.

The chondrite normalized (Sun and McDonough, 1989) REE plot reveals that these apatite grains are enriched in REE with respect to the chondritic value (Fig. 4.14). They are more enriched in LREE than the HREE and the over all trend is very similar to that of the apatites from carbonatite. The Σ REE content is however higher for the apatites than alkali-pyroxenite. As mentioned earlier that the chondrite normalize plot of average apatite along with the bulk rock REE reveals that Σ REE of the apatite is having maximum control over the bulk rock Σ REE (Fig. 4.15b) reservoir. The rock is dominantly containing clinopyroxene which normally shows similar REE trend as that of the apatite (Hanson, 1980) but the Σ REE is much less in clinopyroxene. In conclusion, it can be inferred that though apatite is an accessory mineral in this but it is a major contributor of REE.

4.6.4 APATITE FROM THE NEPHELINE SYENITE

Trace elemental studies of apatite from two varieties of nepheline-syenites were carried out on two representative samples ANK 8 (poorly banded syenite gneiss) and ANK 9 (massive syenite). The apatite composition of these two syenites is significantly different and presented in Table 4.6. The apatite of the poorly banded syenite gneiss is characterized by higher concentrations of Sr (26367-31067) and Th (152-196 ppm) in comparison to the massive syenite. The massive syenite is having concentrations for these elements are 6295-25950 ppm and 80-233 ppm respectively. The apatite from the massive syenites is having higher concentration of Pb (49-307 ppm) and Y (660-19750) in comparison to the poorly banded syenite (Pb: 58-76 ppm, Y: 265-2190 ppm). The apatites of the

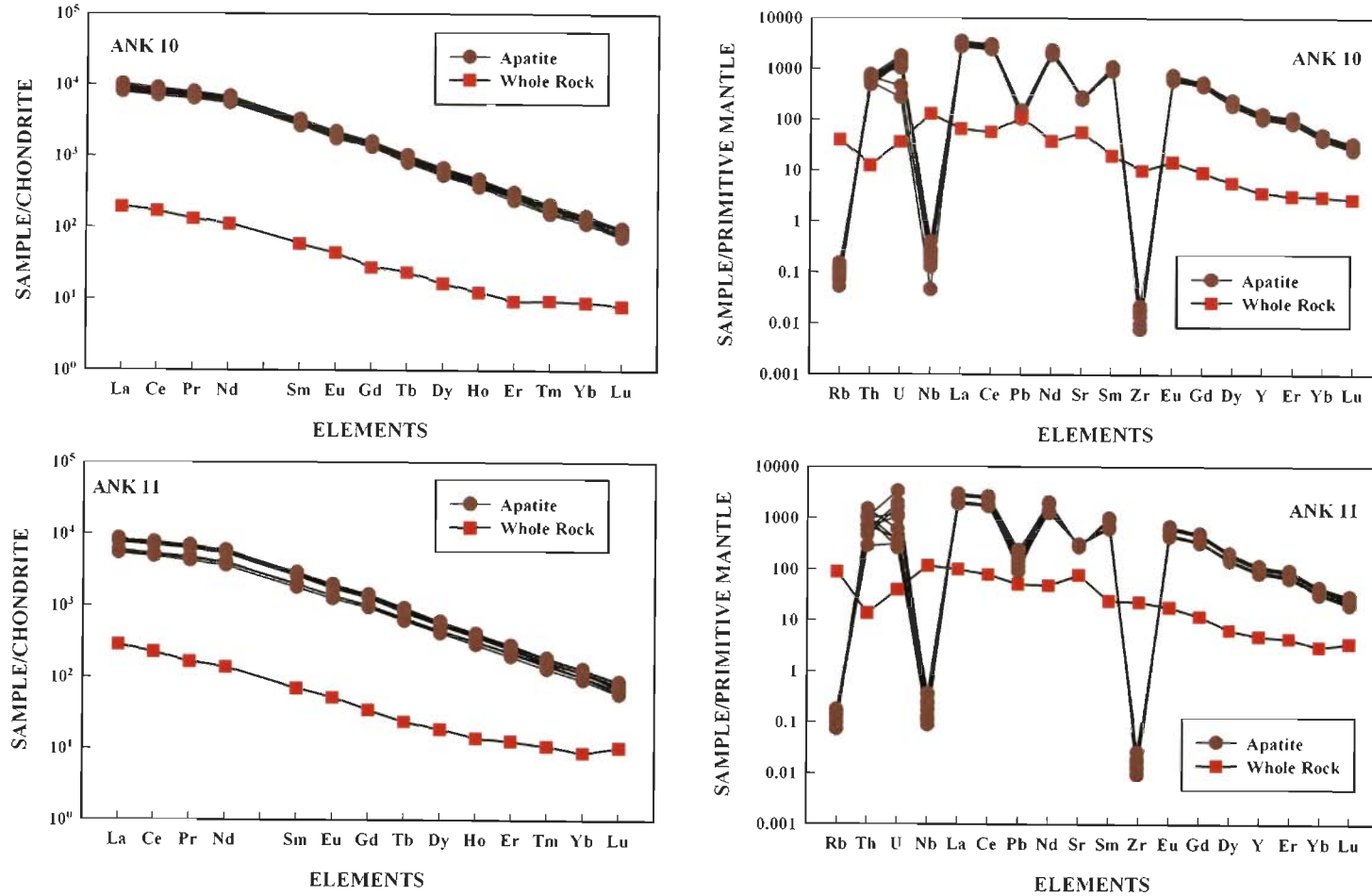


Fig. 4.14 Primitive mantle normalized spider diagram (column 2) and chondrite normalized REE plot (column 1) of the apatite separated from the alkali-pyroxenite. Normalizing values are from Sun and McDonough (1989).

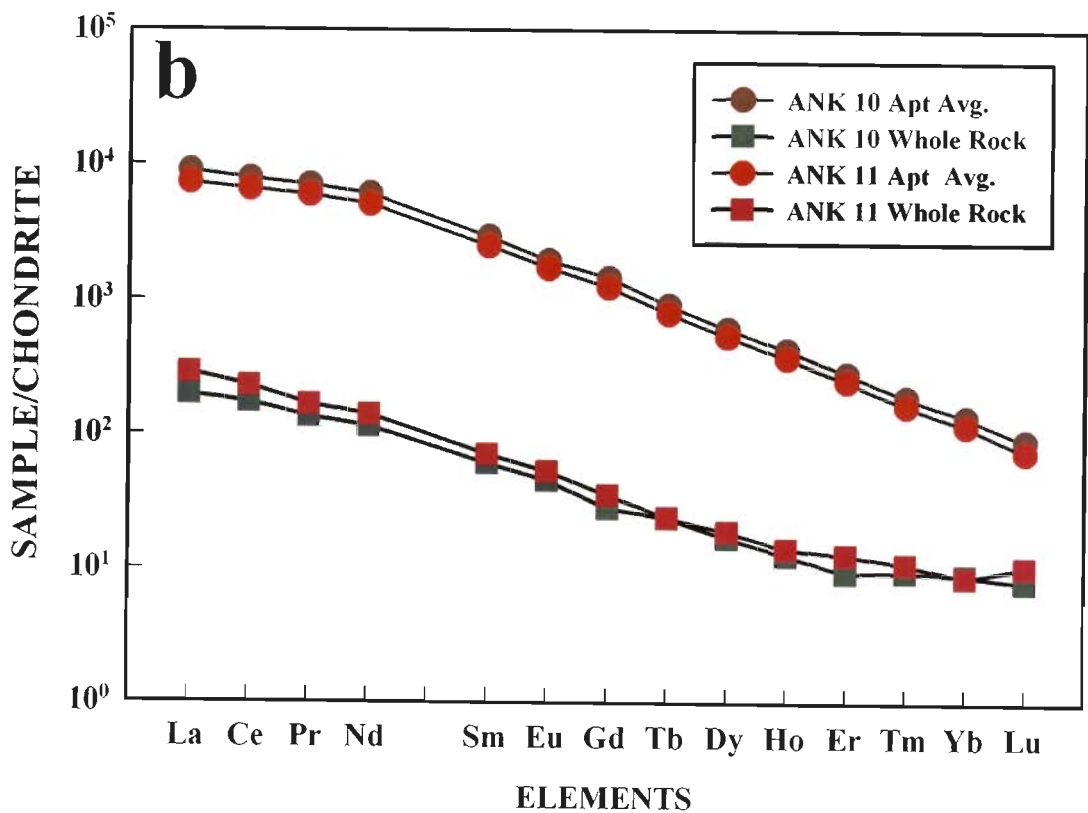
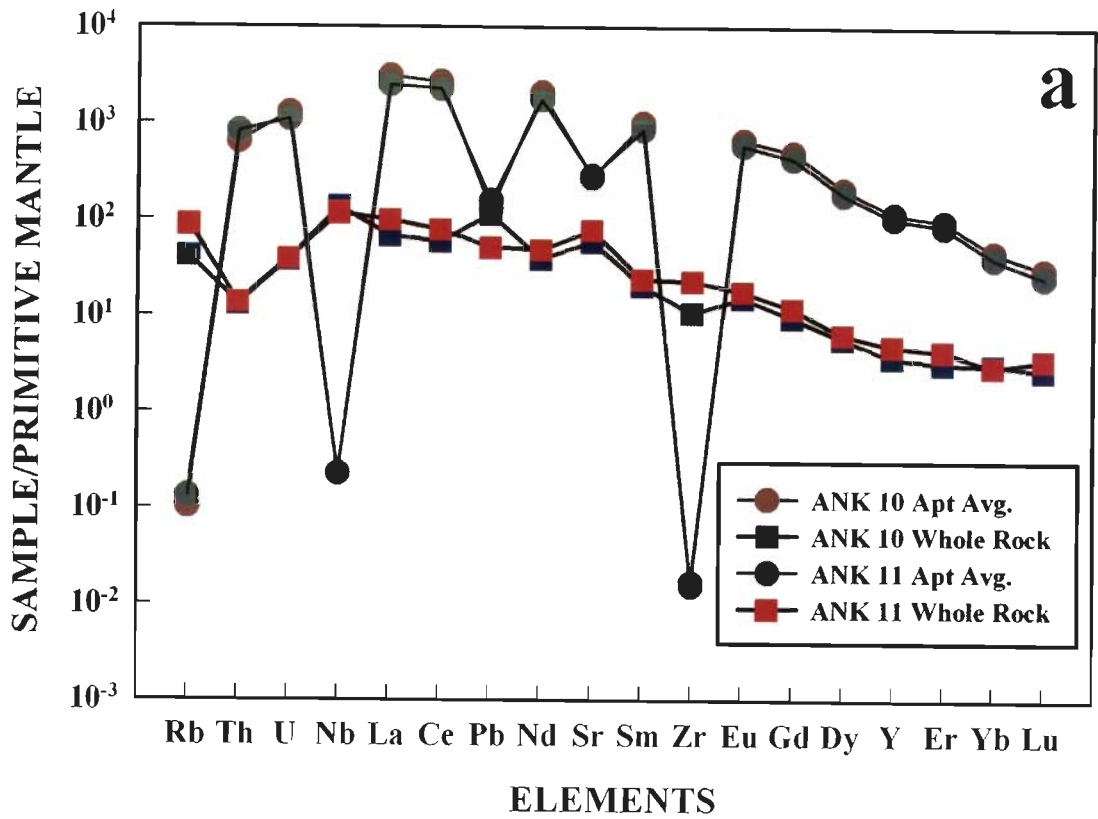


Fig. 4.15 (a) Primitive mantle normalized spider diagram of average apatite from the alkali-pyroxenite along with the whole rock. (b) Chondrite normalized REE plot of the same. Normalizing values are from Sun and McDonough (1989).

massive syenite are more enriched in Σ REE ranging from 25575-63201 ppm in comparison to the poorly banded syenite (27188-34565 ppm). Apatite from massive syenite is enriched in HREE thus having lower $(La/Yb)_n$ (2-279) value in comparison to the apatite from poorly banded syenite (148-771).

The primitive mantle normalized (Sun and McDonough, 1989) plot of the apatite from both the rocks reveals that they are enriched in the incompatible elements except for Zr and Nb with respect to the primitive mantle value while Rb falls close to unity value (Fig. 4.16). Only two apatite grains from the massive syenite (Apt 3 and 11) are showing higher concentrations of Zr which is uncharacteristic of apatite and may be due to presence of minute zircon(?) inclusion. The Zr concentration is found to be higher in these two apatite grains. The elevated MREE and HREE concentration is contributed by the zircon inclusion. The relatively low LREE is the combination of both zircon and apatite. In general Zr is enriched in MREE and HREE compared to the LREE. Thus, the REE trend shown by these apatite grains is the combinations of zircon and apatite and differs from the other apatite grains. The higher concentration of HREE is mainly due the presence of Zr inclusions. Apatites from both the rocks are relatively enriched in Th, Pb, Sr and most of REE. As mentioned previously, the HREE is relatively higher in massive syenite to that of the poorly banded syenite (Fig. 4.16). The primitive mantle normalized average plot (Fig. 4.17a) of the apatite trace element composition of the apatites shows the similar higher and lower values relative to the primitive mantle for these elements.

The chondrite normalized (Sun and McDonough, 1989) plot shows that apatite is essentially enriched in all the REE (Fig. 4.17). Some of the apatite from massive syenite (Apt 3, Apt 8 and Apt 11) is relatively more enriched in HREE and giving a typical apatite trend of REE i.e. enriched in LREE and HREE relative to the MREE. On the other hand, rest of the apatite analyses show very similar trend to that of the apatite from poorly banded syenite (ANK 8). Significant variation

in MREE and HREE is noticed from the apatites in poorly banded syenite. The chondrite normalize REE plot of average apatite from both type of syenite shows distinct difference in trend as well as concentration. The apatite of the massive syenite is relatively enriched in MREE and HREE in comparison to the poorly banded syenite (Fig. 4.17b). However, the bulk rock REE is unlikely to be influenced by the apatite as it is present as an accessory mineral phase. It is apparent that REE of the bulk rock is more controlled by the feldspars and also the pyroxene only for poorly banded variety. However, the significant point is the difference in the Σ REE, Sr and Y content between these two varieties of syenites.

4.6.5 SUMMARY OF THE APATITE MINERAL CHEMISTRY

Carbonatite and Pyroxenite association

Trace element geochemistry of the apatite, introduced during alkali-metasomatism, is a possible indicator of the alteration process. In addition, comparison between the apatite from the carbonatite and this rock will also be a useful marker of melt-fluid system active during carbonatite intrusion. In general, the apatite from altered alkali-pyroxenite is more enriched in REE compared to that of the carbonatite. The REE distribution pattern, particularly the enrichment of LREE over HREE is common for the apatite from both the alkali-pyroxenite (vein-filling assemblage) and associated carbonatite (Fig. 18a, b). Apatite grains from the carbonatite are characterized by high Σ REE, specially LREE with $(La/Yb)_n$ (62-132) with varying amount of Y (170-387 ppm), U (1-98 ppm), and Th (37-118 ppm). The calcite grains from the carbonatite are rich in Sr (9585-10,800 ppm) with appreciable Y (54-92 ppm). The Σ REE content of calcite is expectedly much lower compared to apatite 378-500 (Table 9).

The concentration of Y (380-599 ppm), U (6-13 ppm) and Th (24-125 ppm) is noticeable in alkali-pyroxenite. Increase in REE and the Y content in alkali-pyroxenite is possible indication of alkali-

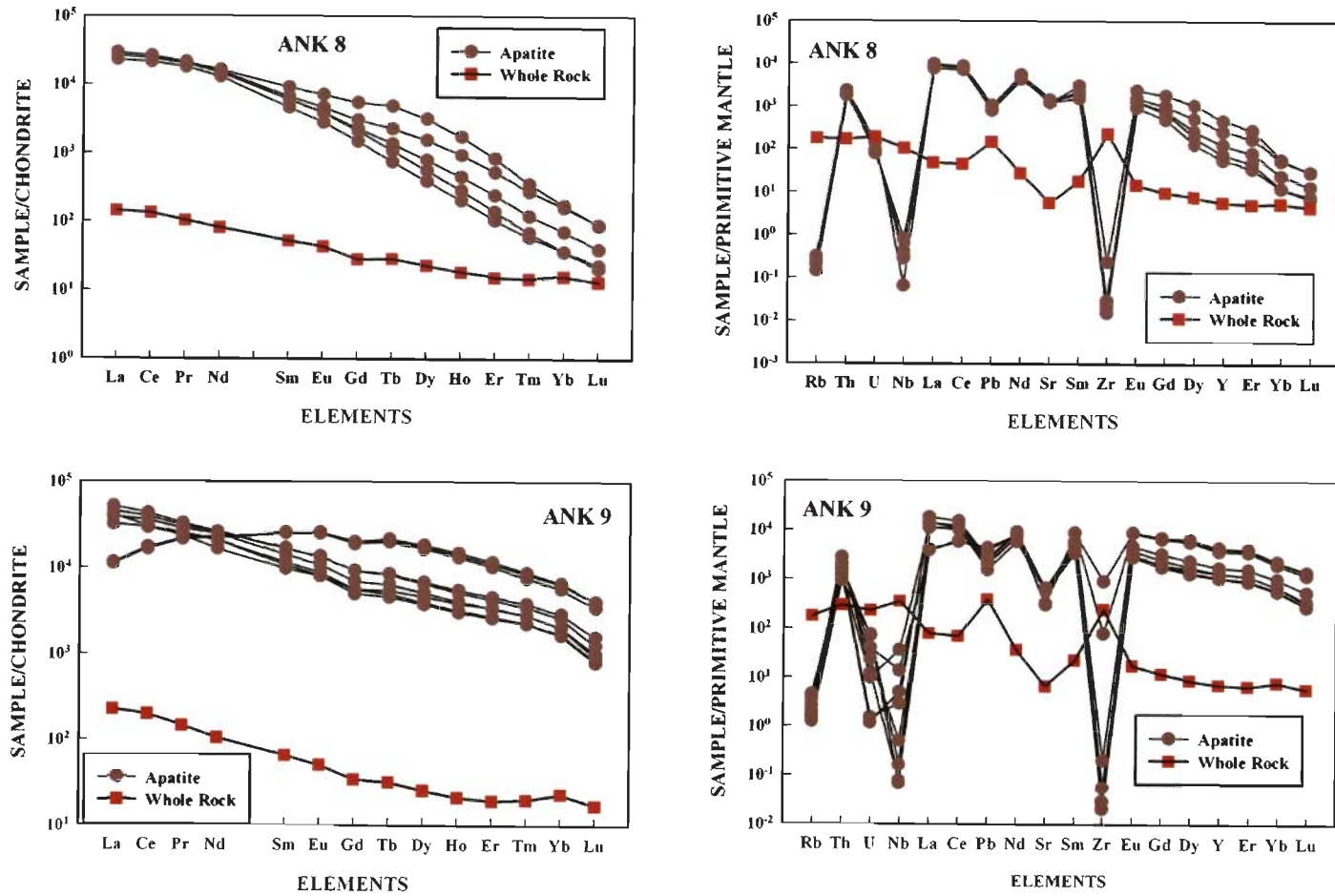


Fig. 4.16 Primitive mantle normalized spider diagram (column 2) and chondrite normalized REE plot (column 1) of the apatites separated from the nepheline-syenites (ANK 8: poorly banded syenite gneiss; ANK 9: Massive syenite). Normalizing values are from Sun and McDonough (1989).

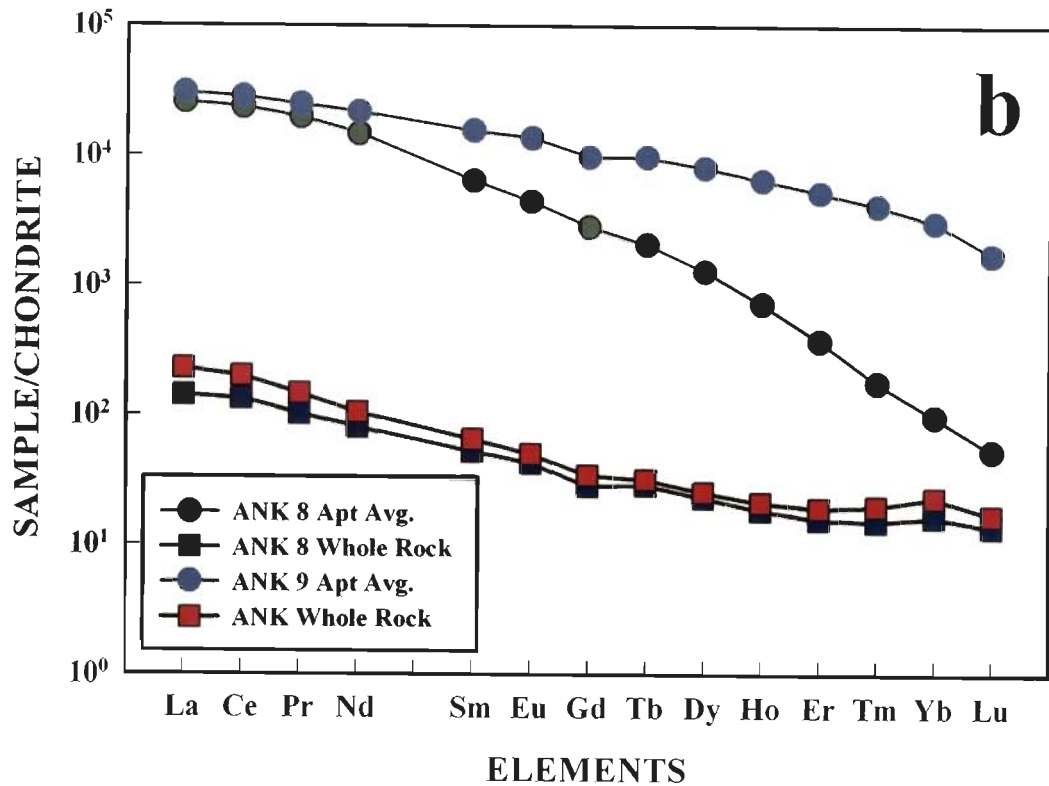
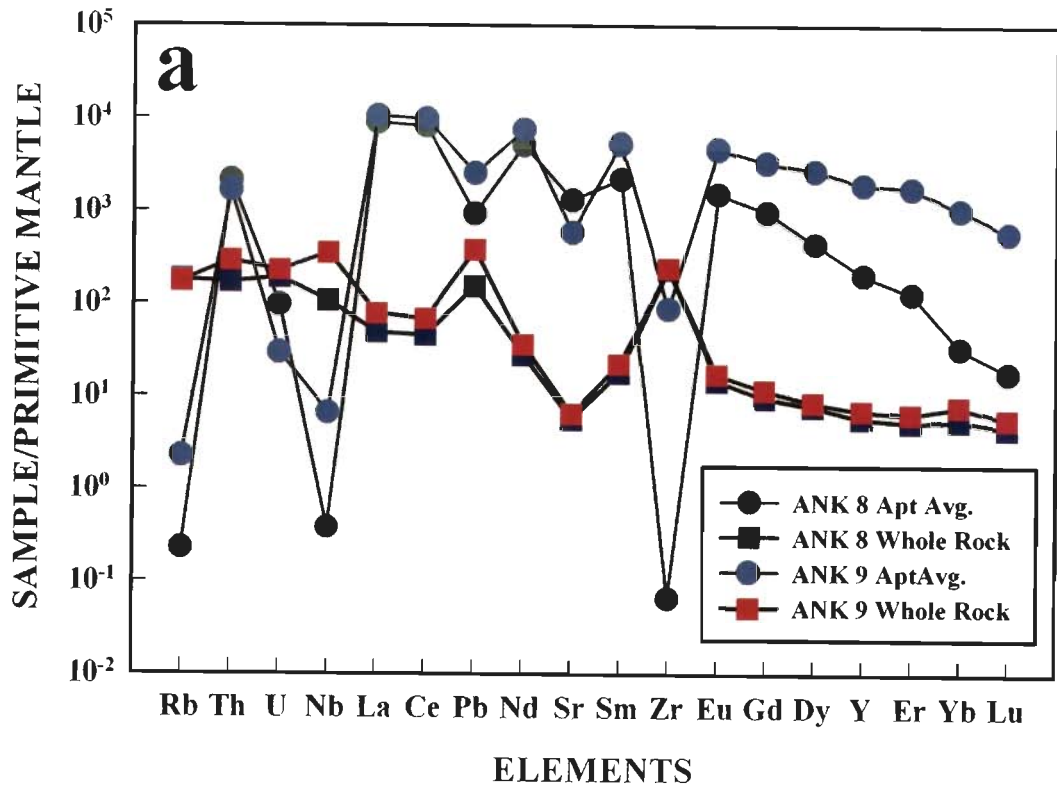


Fig. 4.17 (a) Primitive mantle normalized spider diagram of average apatite along with the whole rock from the nepheline-syenites. (b) Chondrite normalized REE plot of average apatite along with the whole rock from the nepheline-syenites (ANK8: poorly banded syenite gneiss, ANK9: Massive syenite). Normalizing values are from Sun and McDonough (1989).

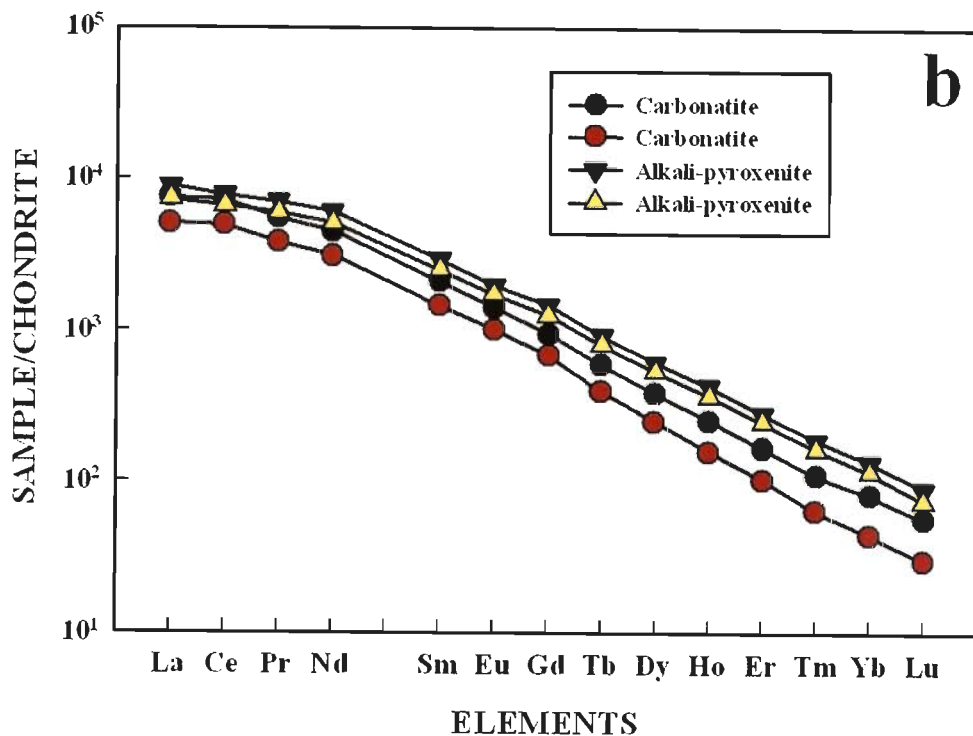
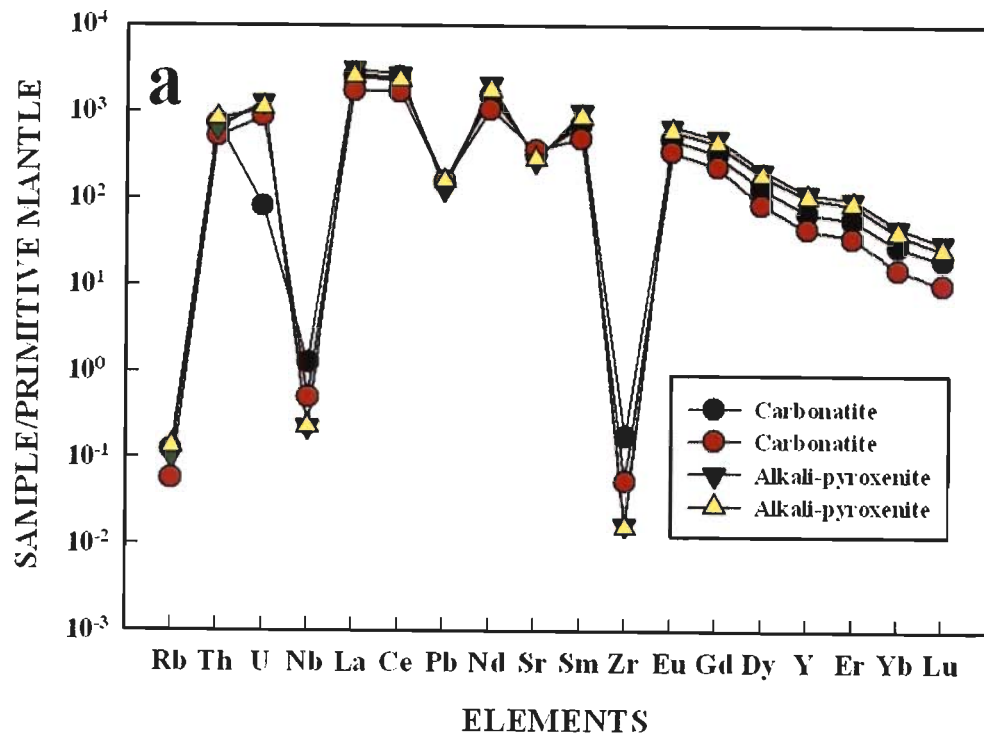


Fig. 4.18 (a) Primitive mantle normalized spider diagram of average apatite from the carbonatite and alkali-pyroxenite along with the respective whole rocks. (b) Chondrite normalized REE plot of average apatite of these rocks along with the respective whole rocks. Normalizing values are from Sun and McDonough (1989).

metasomatism which the former rock suffered by carbonatite intrusion. The Na₂O content of the apatite is almost similar though minor variation is observed within the individual rocks indicates that the alkalinity was near identical when the apatites were formed. This issue is discussed in details in Chapter 6. Though the modal apatite content in this rock seldom exceeds 1-2%, the overall incompatible element concentration of the altered rock and the REE distribution pattern is controlled mostly by the apatite (Fig. 13a). The accessory apatite introduced during alkali-metasomatism elevated the bulk REE budget which is supposed to be relatively much lower in the unaltered alkali-pyroxenite.

Nepheline Syenite

The apatite grains from the two syenites are highly enriched in Σ REE, the order is as follows: massive syenite > poorly banded syenite gneiss. The primitive mantle normalize (Sun and McDonough, 1989) plot of average apatite from all these two rocks reveals that they are almost having very similar pattern for incompatible elements and enriched with respect to the primitive mantle value except Rb, Nb and Zr other than massive syenite (Fig. 4.19a). The apatite from massive syenite is also characteristically enriched in HREE relative to the poorly banded syenite gneiss (Fig. 4.19a).

The chondrite normalized (Sun and McDonough, 1989) plot of these apatites shows that they are enriched in REE with respect to the chondritic value and the maximum enrichment is shown by the apatite of massive syenite (Fig. 4.19b). As discussed previously the REE pattern of apatite from two varieties of syenites is distinctly different. The REE of the apatites from the poorly banded syenite gneiss is relatively low (LREE in the order of 25000 times) compared to the massive syenite (LREE in the order of 35000 times). The noticeable feature is the relatively higher values of HREE in the massive syenite and that too for three apatites are extremely high (Fig. 4.19b). In general, the HREE is enriched in massive syenite (1600 times) in comparison to the poorly banded variety (56 times). The higher value of REE in the massive syenite is coupled with the high Na₂O and SrO content. Interestingly the SrO (or Sr in ppm. see table 4.6)

is almost double in the apatites of poorly banded syenite but the Na_2O content is relatively low. This has direct relevance with the 'pH' condition under which these apatites were formed and the detailed petrogenetic significance related to these observations is discussed in Chapter 6.

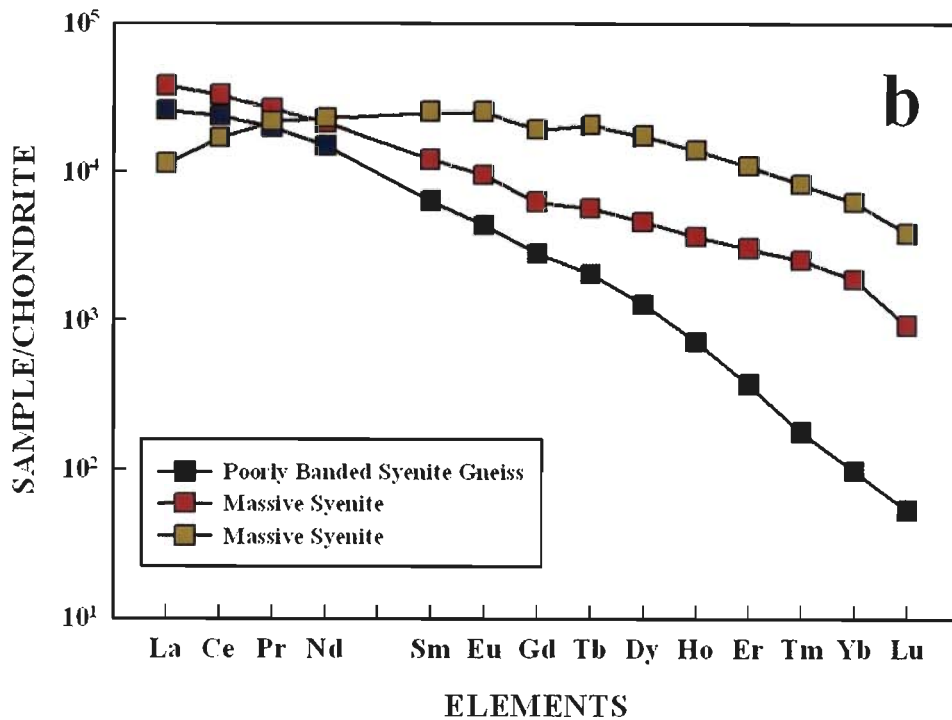
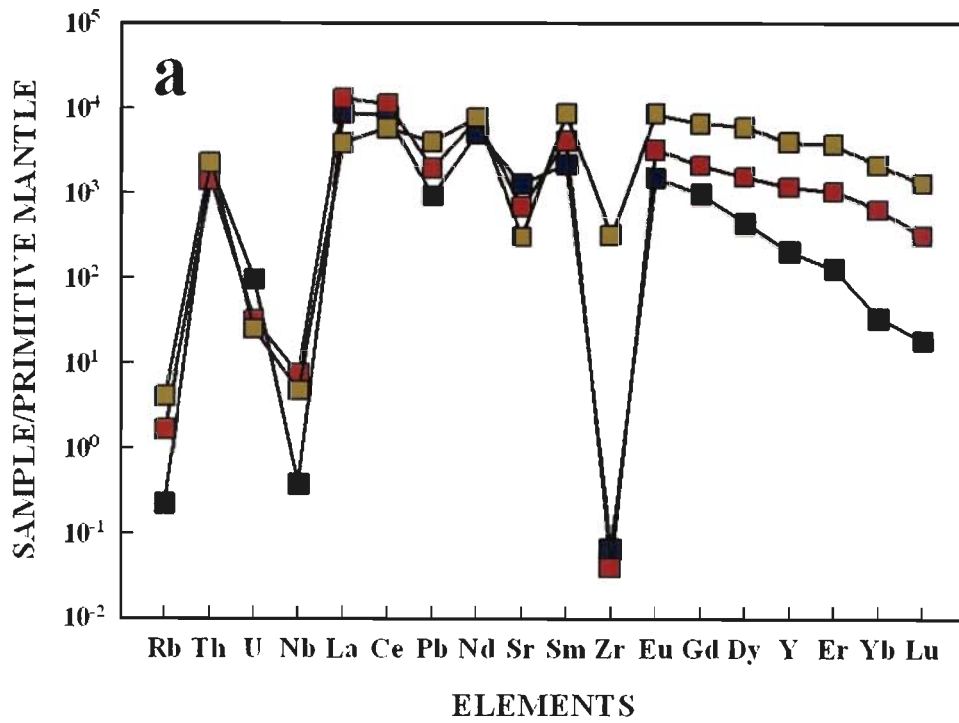


Fig. 4.19 (a) Primitive mantle normalized spider diagram of average apatite from the different varieties of nepheline syenites. (b) Chondrite normalized REE plot of average apatite of syenites. Normalizing values are from Sun and McDonough (1989).

Table 4.1: Whole rock analyses (major and trace elements) of representative carbonatites, syenites and alkali-pyroxenite

<i>Sample</i>	ANK 1	ANK 3	ANK 4	ANK 5	ANK 2	ANK 6	ANK 7	ANK 8	ANK 9	ANK 10	ANK 11
<i>Rock type</i>	C	C	C	C	SSY	SSY	SSY	SSY	SSY	AP	AP
<i>Major elements (wt.%)</i>											
SiO ₂	1.04	5.28	1.09	1.16	54.23	54.33	51.20	54.21	56.56	43.01	43.23
TiO ₂	0.25	0.01	0.27	0.03	0.02	0.04	0.03	0.02	0.02	1.02	1.24
Al ₂ O ₃	0.06	0.08	0.06	0.07	22.29	22.09	21.77	21.78	21.42	11.22	12.03
Fe ₂ O ₃	2.63	1.19	2.60	1.39	4.74	4.67	6.38	4.90	5.01	11.98	9.10
FeO	0.00	0.00	0.00	0.00	0.00	0.00	0.00	0.00	0.00	0.00	0.00
MnO	0.40	0.15	0.40	0.19	0.35	0.22	0.43	0.19	0.32	0.18	0.16
MgO	1.64	0.53	1.61	0.73	0.11	0.11	0.17	0.09	0.11	7.54	6.07
CaO	49.91	49.11	48.70	50.63	0.31	0.23	0.34	0.34	0.29	11.30	12.01
Na ₂ O	0.25	0.12	0.26	0.19	12.13	11.65	12.05	12.09	10.48	5.14	5.21
K ₂ O	0.01	0.01	0.02	0.01	4.51	4.84	5.50	4.54	4.53	1.54	2.35
P ₂ O ₅	3.23	0.53	3.21	4.88	0.03	0.01	0.01	0.10	0.10	0.31	0.20
Cr ₂ O ₃	0.00	0.00	0.00	0.00	0.00	0.00	0.00	0.00	0.00	0.02	0.02
NiO	0.01	0.00	0.01	0.00	0.00	0.00	0.00	0.00	0.00	0.01	0.01
H ₂ O	0.00	0.00	0.00	0.00	0.00	0.00	0.00	0.00	0.00	0.00	0.00
CO ₂	0.00	0.00	0.00	0.00	0.00	0.00	0.00	0.00	0.00	0.00	0.00
LOI	37.81	42.21	38.07	36.90	0.55	0.84	0.56	1.32	0.86	5.84	8.03
Total	97.23	99.23	96.30	96.17	99.28	99.03	98.44	99.57	99.71	99.10	99.65
<i>Trace elements (ppm)</i>											
Sc	6.25	1.13	6.16	3.22	2.80	1.74	3.95	2.69	1.80	38.47	18.33
V	31.77	12.31	37.93	25.86	8.45	8.86	10.70	8.45	9.75	289.29	189.93
Cr	12.10	bdl	21.55	8.75	16.54	18.42	17.44	12.80	11.97	154.75	115.71
Co	21.27	11.61	16.39	8.43	20.00	49.94	36.69	30.93	16.22	67.80	63.55
Ni	50.63	12.57	23.58	8.17	6.85	8.76	9.36	13.11	12.32	59.10	61.64
Cu	15.73	24.64	13.31	14.13	2.62	2.96	2.31	4.23	3.03	103.44	44.96

<i>Sample</i>	ANK 1	ANK 3	ANK 4	ANK 5	ANK 2	ANK 6	ANK 7	ANK 8	ANK 9	ANK 10	ANK 11
<i>Rock type</i>	C	C	C	C	SSY	SSY	SSY	SSY	SSY	AP	AP
Zn	18.30	8.49	7.53	5.25	53.02	33.70	121.58	46.19	343.40	72.25	64.40
Ga	9.89	53.04	23.42	35.95	44.18	43.75	45.48	42.75	41.98	83.90	51.15
As	2.74	1.53	2.81	2.59	1.24	bdl	1.64	1.46	1.16	3.82	1.37
Rb	0.18	0.37	0.16	0.19	112.85	122.23	141.59	114.63	111.37	26.33	55.71
Sr	8743.33	11112.24	8519.82	11294.52	173.71	129.09	255.71	120.62	139.38	1247.57	1639.94
Y	96.50	71.68	95.40	96.17	47.73	32.22	58.10	27.17	32.83	16.95	22.33
Zr	53.13	9.14	87.25	20.73	2618.74	2267.15	2850.00	2631.22	2692.34	119.10	260.50
Nb	121.00	9.44	126.83	16.02	186.12	89.55	463.58	76.34	251.23	96.23	83.01
Mo	bdl	0.23	bdl	0.55	1.21	1.00	0.77	0.99	1.01	0.80	0.61
Sn	3.86	6.98	8.06	5.13	13.97	16.22	18.57	14.81	14.57	8.42	8.28
Cs	0.02	0.03	bdl	bdl	0.79	2.62	1.08	4.09	4.15	1.75	2.57
Ba	808.67	1784.80	797.59	1442.09	86.57	83.48	105.27	65.09	275.20	2316.65	1351.15
Hf	0.91	0.18	1.32	0.62	45.27	37.78	66.89	44.73	46.11	2.40	5.32
Ta	5.71	0.57	6.15	0.85	16.78	9.66	42.19	10.77	17.02	1.19	1.41
W	8.33	4.93	5.80	3.41	24.71	23.31	34.15	24.62	27.09	11.78	18.96
Pb	5.41	8.69	4.92	7.16	18.87	6.26	60.25	10.76	27.28	8.00	3.66
Th	5.67	1.20	5.41	5.47	17.92	5.99	85.89	14.59	24.74	1.13	1.18
U	45.40	3.88	44.31	7.11	5.45	2.45	15.25	4.05	4.80	0.80	0.83
La	340.00	353.15	343.70	495.85	56.82	50.16	99.86	33.80	53.62	46.78	68.32
Ce	708.00	637.75	720.37	942.63	140.84	113.21	216.37	81.82	121.80	105.88	140.04
Pr	83.13	68.24	85.06	103.77	16.67	12.92	23.22	9.81	13.93	12.86	15.90
Nd	331.67	262.71	340.58	407.56	65.26	45.44	81.92	37.96	49.29	53.41	65.77
Sm	52.33	39.45	54.14	60.55	14.21	9.18	14.87	8.01	9.95	9.20	10.77
Eu	14.63	11.01	14.98	16.49	4.40	2.70	5.12	2.51	2.92	2.62	3.06
Gd	bdl	26.69	35.05	39.78	10.48	6.03	10.77	5.84	7.05	5.80	7.24
Tb	4.51	3.44	4.58	4.84	1.90	1.22	2.10	1.08	1.19	0.90	0.91
Dy	21.70	17.24	23.11	23.15	10.54	7.15	13.82	5.87	6.47	4.31	4.82

<i>Sample</i>	ANK 1	ANK 3	ANK 4	ANK 5	ANK 2	ANK 6	ANK 7	ANK 8	ANK 9	ANK 10	ANK 11
<i>Rock type</i>	C	C	C	C	SSY	SSY	SSY	SSY	SSY	AP	AP
Ho	3.73	3.02	3.76	3.95	1.84	1.15	2.67	1.05	1.20	0.72	0.80
Er	bdl	6.90	9.18	8.31	4.84	2.97	6.36	2.62	3.19	1.56	2.12
Tm	bdl	0.86	1.12	1.06	0.70	0.40	1.01	0.39	0.51	0.24	0.28
Yb	6.64	5.03	7.21	5.53	4.71	3.03	6.70	2.80	3.93	1.55	1.50
Lu	0.84	0.64	0.82	0.78	0.58	0.44	0.90	0.35	0.43	0.21	0.27
ΣREE	1567.19	1436.13	1643.68	2114.24	333.79	256.03	485.69	193.90	275.49	246.04	321.78
(La/Yb)_n	51.18	70.25	47.66	89.64	12.06	16.54	14.90	12.07	13.63	30.19	45.61
PI	-	-	-	-	1.11	1.10	1.18	1.14	1.03	0.90	0.92
Ba/Mn	0.20	1.19	0.20	0.76	0.02	0.04	0.02	0.03	0.09	1.29	0.84
Nb/Th	21.34	7.84	23.45	2.93	10.39	14.94	5.40	5.23	10.15	85.26	70.31
Ba/La	2.38	5.05	2.32	2.91	1.52	1.66	1.05	1.93	5.13	49.52	19.78
Nb/Pb	22.38	1.09	25.78	2.24	9.87	14.30	7.69	7.10	9.21	12.03	22.70
Rb/Sr	0.00	0.00	0.00	0.00	0.65	0.95	0.55	0.95	0.80	0.02	0.03
Y/Zr	1.82	7.84	1.09	4.64	0.02	0.01	0.02	0.01	0.01	0.14	0.09
Y/Ce	0.14	0.11	0.13	0.10	0.34	0.28	0.27	0.33	0.27	0.16	0.16
Nb/Th	21.34	7.84	23.45	2.93	10.39	14.94	5.40	5.23	10.15	85.26	70.31

C: Carbonatite, SSY: Nepheline Syenite, AP: Alkali-pyroxenite, ANK 9: Massive syenite, PI: Peralkalinity Indices

Table 4.2: Norm data for different varieties of syenite and alkali-pyroxenite

	ANK 2		ANK 6		ANK 7		ANK 8		ANK 9		ANK 10		ANK 11	
	Poorly Banded Syenite						Massive Syenite				Alkali-pyroxenite			
Normative Minerals	Weight %	Volume %	Weight %	Volume %	Weight %	Volume %	Weight %	Volume %	Weight %	Volume %	Weight %	Volume %	Weight %	Volume %
Quartz	0.00	0.00	0.00	0.00	0.00	0.00	0.00	0.00	0.00	0.00	0.00	0.00	0.00	0.00
Plagioclase	28.25	28.70	28.53	29.28	13.56	14.11	30.99	31.71	40.43	41.58	26.72	30.35	31.92	34.93
Orthoclase	26.93	28.00	28.64	30.08	32.54	34.65	26.87	28.13	26.88	28.29	10.04	11.73	14.43	16.22
Nepheline	33.57	34.91	31.48	33.06	36.71	39.09	30.19	31.60	21.42	22.54	10.45	12.21	7.79	8.76
Leucite	0.00	0.00	0.00	0.00	0.00	0.00	0.00	0.00	0.00	0.00	0.00	0.00	0.00	0.00
Kalsilite	0.00	0.00	0.00	0.00	0.00	0.00	0.00	0.00	0.00	0.00	0.00	0.00	0.00	0.00
Corundum	0.00	0.00	0.00	0.00	0.00	0.00	0.00	0.00	0.95	0.64	0.00	0.00	0.00	0.00
Diopside	0.00	0.00	0.00	0.00	0.00	0.00	0.00	0.00	0.00	0.00	12.37	11.01	4.76	4.09
Hypersthene	0.00	0.00	0.00	0.00	0.00	0.00	0.00	0.00	0.00	0.00	0.00	0.00	0.00	0.00
Wollastonite	0.00	0.00	0.00	0.00	0.00	0.00	0.00	0.00	0.00	0.00	0.00	0.00	0.00	0.00
Olivine	6.46	3.96	6.12	3.79	8.62	5.42	6.35	3.91	6.54	4.06	21.77	17.61	18.27	14.35
Larnite	0.00	0.00	0.00	0.00	0.00	0.00	0.00	0.00	0.00	0.00	0.00	0.00	0.00	0.00
Acmite	0.69	0.51	0.67	0.50	0.93	0.70	0.72	0.54	0.00	0.00	0.00	0.00	0.00	0.00
K ₂ SiO ₃	0.00	0.00	0.00	0.00	0.00	0.00	0.00	0.00	0.00	0.00	0.00	0.00	0.00	0.00
Na ₂ SiO ₃	1.96	2.18	0.77	0.86	3.75	4.26	0.24	0.27	0.00	0.00	0.00	0.00	0.00	0.00
Rutile	0.00	0.00	0.00	0.00	0.00	0.00	0.00	0.00	0.00	0.00	0.00	0.00	0.00	0.00
Ilmenite	0.04	0.02	0.08	0.04	0.06	0.03	0.04	0.02	0.04	0.02	1.94	1.22	2.36	1.43
Magnetite	0.00	0.00	0.00	0.00	0.00	0.00	0.00	0.00	0.36	0.19	0.87	0.50	0.65	0.36
Hematite	0.00	0.00	0.00	0.00	0.00	0.00	0.00	0.00	0.00	0.00	0.00	0.00	0.00	0.00
Apatite	0.09	0.08	0.02	0.02	0.02	0.02	0.23	0.19	0.23	0.20	0.72	0.67	0.46	0.42
Zircon	0.54	0.31	0.46	0.27	0.57	0.34	0.54	0.31	0.54	0.32	0.03	0.02	0.06	0.04
Perovskite	0.00	0.00	0.00	0.00	0.00	0.00	0.00	0.00	0.00	0.00	0.00	0.00	0.00	0.00
Chromite	0.00	0.00	0.00	0.00	0.00	0.00	0.00	0.00	0.00	0.00	0.03	0.02	0.03	0.02
Sphene	0.00	0.00	0.00	0.00	0.00	0.00	0.00	0.00	0.00	0.00	0.00	0.00	0.00	0.00
Pyrite	0.00	0.00	0.00	0.00	0.00	0.00	0.00	0.00	0.00	0.00	0.00	0.00	0.00	0.00
Halite	0.00	0.00	0.00	0.00	0.00	0.00	0.00	0.00	0.00	0.00	0.00	0.00	0.00	0.00
Fluorite	0.00	0.00	0.00	0.00	0.00	0.00	0.00	0.00	0.00	0.00	0.00	0.00	0.00	0.00
Anhydrite	0.00	0.00	0.00	0.00	0.00	0.00	0.00	0.00	0.00	0.00	0.00	0.00	0.00	0.00
Na ₂ SO ₄	0.00	0.00	0.00	0.00	0.00	0.00	0.00	0.00	0.00	0.00	0.00	0.00	0.00	0.00

Calcite	0.48	0.47	0.41	0.40	0.61	0.62	0.38	0.38	0.29	0.29	13.28	14.66	18.26	19.39
Na ₂ CO ₃	0.82	0.86	1.59	1.69	0.70	0.75	2.78	2.94	1.76	1.88	0.00	0.00	0.00	0.00
Total	99.83	100.00	98.77	99.99	98.07	99.99	99.33	100.00	99.44	100.01	98.22	100.00	98.99	100.01
Fe ³⁺ /(Total Fe) in rock	5.03	5.03	4.93	4.93	5.01	5.01	5.10	5.10	4.99	4.99	5.01	5.01	4.95	4.95
Mg/(Mg+Total Fe) in rock	4.37	4.37	4.46	4.46	5.01	5.01	3.51	3.51	4.17	4.17	55.49	55.49	56.93	56.93
Mg/(Mg+Fe ²⁺) in rock	4.59	4.59	4.68	4.68	5.26	5.26	3.69	3.69	4.38	4.38	56.76	56.76	58.17	58.17
Mg/(Mg+Fe ²⁺) in silicates	4.25	4.25	4.48	4.48	4.91	4.91	3.55	3.55	4.20	4.20	59.27	59.27	62.03	62.03
Ca/(Ca+Na) in rock	1.38	1.38	1.08	1.08	1.54	1.54	1.53	1.53	1.51	1.51	54.85	54.85	56.02	56.02
Plagioclase An content Differentiation Index	0.00	0.00	0.00	0.00	0.00	0.00	0.00	0.00	0.00	0.00	8.94	8.94	6.60	6.60
Calculated density, g/cc	88.75	91.61	88.65	92.42	82.81	87.85	88.05	91.44	88.73	92.41	47.21	54.29	54.14	59.91
Calculated liquid density, g/cc	2.66	2.66	2.66	2.66	2.67	2.67	2.66	2.66	2.68	2.68	2.94	2.94	2.85	2.85
Calculated viscosity, dry, Pas	2.43	2.43	2.43	2.43	2.45	2.45	2.43	2.43	2.44	2.44	2.69	2.69	2.64	2.64
Calculated viscosity, wet, Pas	0.32	0.32	0.33	0.33	0.26	0.26	0.32	0.32	0.38	0.38	0.11	0.11	0.12	0.12
Estimated liquidus temp., °C	0.30	0.30	0.31	0.31	0.24	0.24	0.30	0.30	0.35	0.35	0.11	0.11	0.12	0.12
Estimated H ₂ O content, wt. %	1128.08	1128.08	1123.26	1123.26	1174.88	1174.88	1131.34	1131.34	1089.30	1089.30	1328.81	1328.81	1330.96	1330.96
	0.85	0.85	0.89	0.89	0.59	0.59	0.88	0.88	1.13	1.13	0.21	0.21	0.25	0.25

Table 4.3: Mass balancing between the unaltered and the metasomatized alkali-pyroxenite

	Original alkali-pyroxenite				Metasomatized alkali-pyroxenite					
	(1)	(2)	(3)	(4)	(5)	(6)	(7)	(8)	(9)	(10)
SiO ₂	53.73	54.24	0.90	56.78	43.12	43.12	51.58	0.86	58.01	(+)
TiO ₂	0.74	0.75	0.01	0.59	1.13	1.13	1.35	0.02	1.14	(+)
Al ₂ O ₃	1.77	1.79	0.02	1.10	11.62	11.62	13.91	0.14	9.22	(+)
Fe ₂ O ₃	13.74	13.87	0.09	5.46	10.54	10.54	12.61	0.08	5.33	(~)
FeO	0.00	0.00	0.00	0.00	0.00	0.00	0.00	0.00	0.00	
MnO	0.19	0.19	0.00	0.00	0.17	0.17	0.20	0.00	0.00	
MgO	7.85	7.93	0.20	12.37	6.81	6.81	8.14	0.20	13.65	(+)
CaO	16.80	16.96	0.30	19.02	11.65	2.82	3.37	0.06	4.06	(-)
Na ₂ O	4.13	4.17	0.07	4.23	5.17	5.17	6.19	0.10	6.74	(+)
K ₂ O	0.02	0.02	0.00	0.01	1.94	1.94	2.32	0.02	1.67	(+)
P ₂ O ₅	0.03	0.03	0.00	0.02	0.26	0.26	0.31	0.00	0.15	(+)
NiO					0.01					
LOI					6.94					
Total	99.0	99.94	1.58	100.21	99.38	83.59	99.98	1.48	99.98	

- (1) Average composition of pyroxene in metasomatized alkali-pyroxenite (See Table 1), which is considered as bulk composition of the unaltered rock
- (2) This average values are recalculated to 100
- (3) Molecular proportions calculated by dividing respective molecular weight for each oxide i.e. column (2)/ (respective molecular weight)
- (4) Molecular proportion are recalculated to 100
- (5) Average compositions of the metasomatized alkali-pyroxenite.
- (6) Assumed that LOI is contributed by CO₂ released from calcite present as vein within alkali-pyroxenite. So, 6.94% CO₂ may combine with 8.83% of CaO to form calcite. This amount of CaO is deducted from the altered rock.
- (7) Column (6) recalculated to 100
- (8) Molecular proportions.
- (9) Molecular percentage recalculated to 100.
- (10) Elementary gain and loss during fenitization between original rock and the metasomatized rock.

Table 4.4: Trace element composition of apatite and calcite in the carbonatite

							<i>ANK 1</i>									
	<i>Apt 1</i>	<i>Apt 2</i>	<i>Apt 3</i>	<i>Apt 4</i>	<i>Apt 5</i>	<i>Apt 6</i>	<i>Cal 1</i>	<i>Cal 2</i>	<i>Cal 3</i>	<i>Cal 4</i>	<i>Cal 5</i>	<i>Cal 6</i>	<i>Cal 7</i>	<i>Cal 8</i>	<i>Cal 9</i>	<i>Cal 10</i>
La	1110	1610	1195	1450	1390	1460	53	58	61	50	55	56	51	61	52	50
Ce	2960	4287	3035	3820	3630	3960	163	164	166	151	177	175	167	181	159	150
Pr	363	533	366	468	439	494	24	22	22	23	26	25	25	26	23	20
Nd	1510	2213	1550	1960	1840	2100	117	106	99	110	130	125	126	125	106	93
Sm	237	358	244	314	292	346	27	24	21	26	32	29	29	26	23	19
Eu	63	94	63	84	76	90	9	7	7	8	10	9	10	9	7	6
Gd	152	223	151	202	182	213	24	20	17	22	26	22	25	22	19	15
Tb	17	26	17	23	21	24	3	3	3	3	4	3	3	3	3	2
Dy	73	118	71	105	92	108	18	17	15	18	20	17	19	17	14	11
Ho	11	18	10	16	14	16	3	3	3	3	4	3	3	3	3	2
Er	20	34	20	31	26	30	8	8	8	8	8	8	8	8	6	5
Tm	2	4	2	3	3	3	1	1	1	1	1	1	1	1	1	1
Yb	10	18	9	17	13	15	7	7	7	7	7	6	6	6	5	4
Lu	1	2	1	2	1	2	1	1	1	1	1	1	1	1	1	1
REE	6531	9538	6734	8495	8018	8860	457	443	430	431	500	480	474	487	421	378
(La/Yb)_n	74	63	91	62	77	72	5	5	6	5	5	6	6	7	7	8
Rb	0	0	0	0	0	0	0	0	0	0	0	0	0	0	0	0
Th	37	56	118	69	45	53	0	0	0	0	0	0	0	0	0	0
U	1	2	0	3	3	1	0	0	0	1	0	0	0	0	23	2
Nb	0	3	0	1	1	1	0	0	0	0	0	0	0	0	10	4
Pb	8	10	16	11	9	9	13	10	12	13	14	12	14	15	18	14
Sr	7150	6630	6680	6225	6950	6980	10450	9693	9980	10150	10800	10700	10700	10500	10395	9585
Zr	1	4	1	3	2	2	0	0	0	0	0	0	0	0	0	0
Y	276	387	225	354	298	345	89	89	79	85	92	85	88	81	69	54

	ANK 3													
	<i>Apt 1</i>	<i>Apt 2</i>	<i>Apt 3</i>	<i>Apt 4</i>	<i>Apt 5</i>	<i>Apt 6</i>	<i>Apt 7</i>	<i>Apt 8</i>	<i>Apt 9</i>	<i>Apt 10</i>	<i>Apt 11</i>	<i>Apt 12</i>	<i>Apt 13</i>	<i>Apt 14</i>
La	1295	1019	1270	1230	1470	1200	1255	1270	1120	1543	1095	892	1082	1066
Ce	3175	2485	3070	2900	3603	3083	3100	3415	2930	4103	2910	2128	2873	2564
Pr	375	289	362	349	415	367	373	416	344	487	344	265	375	299
Nd	1505	1125	1435	1370	1667	1467	1460	1700	1337	1913	1350	1115	1690	1220
Sm	220	170	215	204	246	229	213	257	200	283	198	182	307	190
Eu	59	45	57	54	65	62	58	66	51	72	50	47	86	49
Gd	138	103	132	124	154	139	135	174	131	186	129	109	193	114
Tb	14	12	14	14	16	15	15	17	14	19	13	12	21	13
Dy	60	51	61	57	68	63	63	69	61	82	57	51	83	54
Ho	9	8	9	8	10	9	9	9	9	11	8	7	11	8
Er	16	14	16	17	19	16	17	18	18	24	16	15	20	14
Tm	2	2	2	2	2	2	2	2	2	2	2	1	2	1
Yb	7	7	7	7	8	7	8	7	8	9	7	7	8	7
Lu	1	1	1	1	1	1	1	1	1	1	1	1	1	1
REE	6874	5329	6648	6338	7744	6661	6707	7420	6225	8737	6178	4832	6751	5599
(La/Yb)_n	132	104	126	118	124	119	109	124	102	116	114	92	93	113
Rb	0	0	0	0	0	0	0	0	0	0	0	0	0	0
Th	37	74	46	49	40	30	42	19	29	49	31	52	37	87
U	16	98	2	39	1	7	5	6	3	11	3	57	1	8
Nb	0	1	0	0	0	0	0	0	0	1	0	1	0	1
Pb	11	15	11	13	11	9	11	8	10	12	10	11	8	15
Sr	7465	7245	7355	7710	7470	7813	7330	7775	7627	8000	7535	7198	7895	7358
Zr	0	1	0	0	0	0	1	0	1	1	1	2	0	1
Y	190	169	192	194	220	207	201	209	202	266	183	170	249	181

Table 4.5: Trace elemental composition of apatite from alkali-pyroxenite

	ANK 10												
	Apt 1	Apt 2	Apt 3	Apt 4	Apt 5	Apt 6	Apt 7	Apt 8	Apt 9	Apt 10	Apt 11	Apt 12	Apt 13
La	2080	2150	2070	2020	2090	2280	1880	2190	1920	2030	2150	2220	2440
Ce	4570	4660	4520	4570	4760	5190	4280	4980	4490	4720	4940	5080	5510
Pr	627	640	621	642	673	734	606	694	634	661	687	714	764
Nd	2630	2680	2600	2760	2860	3140	2580	2920	2670	2790	2930	3020	3220
Sm	421	428	409	437	455	499	414	459	423	445	462	480	506
Eu	106	109	106	107	111	123	102	119	111	113	121	121	130
Gd	280	286	278	289	305	333	277	304	285	300	312	322	332
Tb	33	33	32	33	34	38	31	35	33	34	36	37	39
Dy	147	149	145	144	152	167	136	155	150	154	164	168	176
Ho	23	24	22	22	24	26	21	24	24	24	26	26	28
Er	45	46	44	44	46	50	40	47	45	47	49	51	53
Tm	5	5	5	4	5	5	4	5	5	5	5	5	5
Yb	23	24	24	21	21	24	19	23	23	22	24	25	25
Lu	2	2	2	2	2	2	2	2	2	2	2	3	3
REE	10993	11236	10879	11095	11536	12609	10392	11958	10814	11347	11908	12272	13231
(La/Yb)_n	64	65	61	67	73	69	69	68	61	65	64	63	69
Rb	0	0	0	0	0	0	0	0	0	0	0	0	0
Th	58	55	56	60	67	64	48	58	54	42	48	55	48
U	32	29	31	10	22	38	6	34	35	28	29	30	26
Nb	0	0	0	0	0	0	0	0	0	0	0	0	0
Pb	9	9	9	10	11	11	9	9	9	8	8	8	8
Sr	6040	6140	6150	5830	5790	5870	5650	5720	5410	5540	5660	5630	5890
Zr	0	0	0	0	0	0	0	0	0	0	0	0	0
Y	506	517	501	485	514	560	463	549	526	532	557	575	599

	ANK 11									
	Apt 1	Apt 2	Apt 3	Apt 4	Apt 5	Apt 6	Apt 7	Apt 8	Apt 9	Apt 10
La	1300	1270	1410	1800	1860	1950	2020	1810	1950	1950
Ce	3090	2960	3240	4200	4290	4550	4690	4220	4560	4500
Pr	433	401	454	595	604	647	660	591	645	631
Nd	1840	1700	1900	2500	2510	2710	2770	2480	2680	2620
Sm	302	275	307	409	409	437	447	396	425	417
Eu	80	73	81	107	105	116	116	101	113	108
Gd	204	194	209	277	269	295	298	265	284	275
Tb	24	23	25	32	32	34	35	30	33	32
Dy	111	106	116	140	137	155	155	136	149	146
Ho	18	16	18	21	21	23	24	21	23	22
Er	36	32	37	43	42	47	46	40	45	42
Tm	4	3	4	4	4	5	5	4	5	4
Yb	17	16	17	20	19	22	22	20	22	20
Lu	2	1	2	2	2	2	2	2	2	2
REE	7460	7071	7820	10150	10304	10993	11289	10116	10935	10769
(La/Yb)_n	54	58	58	63	69	62	65	65	63	69
Rb	0	0	0	0	0	0	0	0	0	0
Th	39	87	48	24	86	82	125	60	57	91
U	34	70	40	6	5	25	12	8	22	8
Nb	0	0	0	0	0	0	0	0	0	0
Pb	8	11	9	6	13	13	17	11	10	14
Sr	6360	6400	6560	5790	5850	5830	5850	5740	5860	5870
Zr	0	0	0	0	0	0	0	0	0	0
Y	403	380	418	471	471	524	540	469	525	490

Table 4.6: Trace element composition of apatite in nepheline-syenites

	ANK 8					ANK 9										
	Apt 1	Apt 2	Apt 3	Apt 4	Apt 5	Apt 1	Apt 2	Apt 3	Apt 4	Apt 5	Apt 6	Apt 7	Apt 8	Apt 9	Apt 10	Apt 11
La	6175	6143	6220	5345	6797	9230	12247	2640	7650	9725	10770	7560	2735	9180	5350	2720
Ce	14350	14733	14800	12850	15767	21800	26333	10110	17900	18650	24050	18250	10650	21350	11800	10310
Pr	1890	1977	1950	1685	2000	2710	3130	2050	2295	2235	2945	2415	2095	2590	1535	2055
Nd	6870	7560	7185	5985	7253	11667	12260	10450	9785	7760	12150	9755	10800	11100	5380	10600
Sm	902	1377	1006	695	905	2147	2580	3820	1635	1490	2540	1755	3825	1985	644	3885
Eu	224	407	266	162	221	631	775	1445	470	466	787	512	1440	594	160	1475
Gd	461	1109	617	302	428	1440	1913	3895	1036	1145	1905	1150	3860	1370	354	4090
Tb	51	181	85	28	40	241	320	764	172	204	312	186	741	232	47	797
Dy	201	801	391	99	143	1310	1747	4425	961	1180	1670	1012	4205	1270	212	4645
Ho	26	98	53	12	16	232	315	789	174	221	295	182	747	227	28	837
Er	41	138	88	18	24	554	758	1820	431	561	700	445	1685	555	47	1930
Tm	3	9	7	2	2	72	98	215	57	72	89	58	194	71	4	224
Yb	12	30	28	6	6	348	496	1090	283	346	444	291	974	348	14	1125
Lu	1	2	2	1	1	26	40	103	20	24	32	21	88	24	1	103
REE	31206	34565	32697	27188	33602	52406	63012	43615	42867	44079	58687	43590	44039	50896	25575	44795
(La/Yb)_n	357	148	160	606	771	19	17	1.74	19	20	17	18	2	18	279	1.73
Rb	0	0	0	0	0	1	2	3	1	1	2	1	2	1	0	3
Th	196	197	167	152	196	101	129	171	79	108	199	144	233	80	124	172
U	2	2	2	2	3	0	0	1	2	0	0	1	0	1	1	0
Nb	0	0	1	0	0	25	2	10	0	4	11	0	0	0	0	0
Pb	64	76	58	58	76	172	185	291	140	110	173	150	266	159	49	307
Sr	27350	26367	27750	26650	31067	13200	13000	6825	14050	12050	12200	13850	6295	13250	25950	6420
Zr	0	3	0	0	0	1	1	10030	0	0	1	0	2	0	0	880
Y	597	2190	1232	265	355	6000	7873	18450	4780	6040	7235	4970	16850	5830	660	19750

ISOTOPE GEOCHEMISTRY AND GEOCHRONOLOGY

Isotopic study of the rocks from Precambrian terrains like the Singhum-Chhotanagpur craton is a difficult proposition. The rocks of igneous affiliations intruded along the NSZ had also been subjected to metamorphic and metasomatic changes. As a result, the isotopic systematics had been disturbed several times. The isotopic study of nearby anorthosites (Bengal anorthosite) revealed several important events related to both igneous and then followed by several metamorphic events (Chatterjee et al., 2008, Maji et al., 2008). However, *with available facilities and time-frame*, an attempt has been made to find out the crystallization and/or metamorphic-metasomatic ages of the studied rocks viz. carbonatite, alkali-pyroxenite and nepheline-syenites/syenite-gneisses using different isotopic systematics with the help of bulk rock and the mineral separates. The bulk rock isotopic studies were carried out using Rb-Sr and Pb-Pb isotopic systematics. Conventional U-Pb zircon dating by ID-TIMS (Isotope Dilution-Thermal ionization Mass Spectrometer) technique was also attempted for nepheline-syenite.

5.1 ANALYTICAL TECHNIQUE

The heavy liquid separation method has already been discussed in the previous chapter Chapter 4, Section 4.5.1. This technique was used for zircon from the poorly banded syenite gneiss as well as massive syenite. The detailed methodology for the bulk rock samples as well as U-Pb zircon dating has been described in details.

A) Rb-Sr AND Pb-Pb WHOLE ROCK ISOTOPIC ANALYSIS

About 1 to 2 kg of fresh rock samples were cut down to small chips. After the conning and quartering these small chips for homogenization about 30-40 g of the chips was crushed into fine powder using a 'Ball Miller'. About 0.05-0.1 g of powder sample was taken into

small savillex beaker and 4 ml HF and 2 ml HNO₃ added to the sample and placed on the hot plate at 140°C for 2-3 days for acid digestion. The isotopic analyses were carried out at the Department of Isotope Geology and Mineral Resources, ETH Zurich using ID-TIMS techniques (Peytcheva et al., 2008). Sandwich column separation for Sr and Pb were carried out (EICHROM Sr resin and TRU Pb resin). NBS 987 and NBS 981 standards were used for observing machine drift. The mean of 7 runs during of the NBS 987 yielded an ⁸⁷Sr/⁸⁶Sr ratio of 0.710236±0.000023. All the isotopic analysis was carried out on a Finnigan MAT 262 system equipped with an ion counting system and presented in Table 5.1.

B) U-Pb IOTOPIC ANALYSIS OF ZIRCON

High precision ‘conventional’ U-Pb zircon isotopic analyses were carried out on single zircon grain obtained from the poorly banded and massive syenite. The analysis was carried out at the Institute of Isotope Geology and Mineral Resources, ETH Zurich on Finnigan MAT 262 Thermal Ionization Mass Spectrometer (TIMS). Few selected zircons were air abraded to remove the marginal outer zones with lead loss following the procedure given by Peytcheva et al. (2008). SRM 982 (equal Pb) was used as internal standard. The total blanks were less than 0.002 ng for both U and Pb following the detailed procedure described by Von Quadt et al. (2002). The PBDAT and ISOPLOT programme (Ludwig, 1988, 2003) was used for calculating the uncertainties and correlations of U/Pb ratios (Peytcheva, 2008). Stacey and Kramers (1975) correction values for common Pb were used for isotopic calculations. The entire ‘Concordia age’ plots were done using ISOPLOT software given by Ludwig (2003) and data is shown in Table 5.2.

5.2 CARBONATITE

The carbonatite dominantly consists of calcite as essential mineral and apatite as main accessory phase. The concentration of Sr in the bulk rock is about 1%, mostly contributed by these two minerals (Table 4.4). On the other hand amount of Rb in bulk rock is very low and <0.4 ppm. The reason for low Rb-content is near absence of any carrier phases. So, the study of Rb-Sr isotopic systematics is unlikely to contribute any significant idea about age of the Purulia carbonatite. The $^{87}\text{Sr}/^{86}\text{Sr}$ value should represent only the initial ratio, provided the system remained closed. However, it is very unlikely that the system was totally undisturbed in such a terrain of Precambrian age and suffered several episodes of tectono-thermal events (Maji et al. 2008).

Total four whole-rock samples of carbonatites, few grains of apatite and calcite were analyzed for study of Rb-Sr isotopic systematics. The samples, as expected, show extremely low $^{87}\text{Rb}/^{86}\text{Sr}$ ratios (0.00005 to 0.00009) and the values are scientifically meaningless. The textural study shows that the apatite crystals are early formed. Though the grains are slightly fractured but these fractures are restricted within apatite grains only. The $^{87}\text{Sr}/^{86}\text{Sr}$ ratio of apatite varies within a narrow range of 0.70340-0.70335. The whole-rock $^{87}\text{Sr}/^{86}\text{Sr}$ ratio also varies within the same limit (0.70340-0.70330). The ratio in calcite is more dispersed (0.70355-0.70340) compared to both the apatite and the whole rock. Such variation can be explained by the response of calcite during metamorphism and also indicates open system behaviour for Rb-Sr systematics. Texturally, it is supported by the well developed triple junction exhibited by calcite grain leading to mosaic texture (Fig. 3.2). However, on the other hand, the effect of such changes due to post-magmatic processes (metamorphism and metasomatism) in apatite is relatively less pronounced and supported by relatively narrow span of $^{87}\text{Sr}/^{86}\text{Sr}$ ratio. So, based on the available data it can be inferred that the initial $^{87}\text{Sr}/^{86}\text{Sr}$ ratio of the system was within 0.70330-0.70340 (Table 5.1). This ratio is

characteristics of mantle source (Faure and Hurley, 1963). Due to the very low $^{87}\text{Rb}/^{86}\text{Sr}$ value no well defined isochron is possible to infer (Fig. 5.1).

The Pb-Pb isotopic analyses (Table 5.1) of these carbonatite sample yielded very high $^{206}\text{Pb}/^{204}\text{Pb}$ ratio ranging from 21.53 to 83.94. Such high $^{206}\text{Pb}/^{204}\text{Pb}$ not uncommon and reported from the Newania and Sevattur, the two oldest carbonatite of the Indian subcontinent of 1551 Ma and 801 Ma respectively (Schleicher et al., 1997). The reported $^{206}\text{Pb}/^{204}\text{Pb}$ value for these two Precambrian carbonatite complexes is also very high and reaches maximum up to 268 ± 0.09 (Schleicher et al., 1997). Similar higher $^{206}\text{Pb}/^{204}\text{Pb}$ ratio (maximum up to 61.1 for the bulk rock and 89.5 for apatite) also reported from the Tikshezero carbonatite complex of Kola Alkaline Province, Russia (Tichomirowa et al., 2006). Such high values of the carbonatite may be related to its genesis from the HIMU mantle end member, which in general is having higher $^{206}\text{Pb}/^{204}\text{Pb}$ value and this value further increase with the increasing age (Hart, 1988). In spite of such higher $^{206}\text{Pb}/^{204}\text{Pb}$ ratio, the sample points are falling along a single line with regression coefficient of 0.99. The generated data set when plotted in a $^{206}\text{Pb}/^{204}\text{Pb}$ - $^{207}\text{Pb}/^{204}\text{Pb}$ isochron diagram using ISOPLOT yields a perfect four point isochron of 1370 ± 39 Ma age with MSWD value of 1.02 (Fig. 5.2). However, this isochron may not be true representative of crystallization age and may be a pseudo-isochron indicating a post-magmatic event. Thus the crystallization age should be older than 1.37 ± 0.4 Ga and intruded within the Chandil Formation supposedly 1.5 Ga old (Mazumder, 2005). The $^{206}\text{Pb}/^{204}\text{Pb}$ and $^{207}\text{Pb}/^{204}\text{Pb}$ values are significantly different and higher than the ratios assigned for the mantle end members (EM1, EM2, DMM and HIMU). The $^{208}\text{Pb}/^{204}\text{Pb}$ ratio falls within EM1 and DMM end members. So, source characterization may not be possible using the present data set.

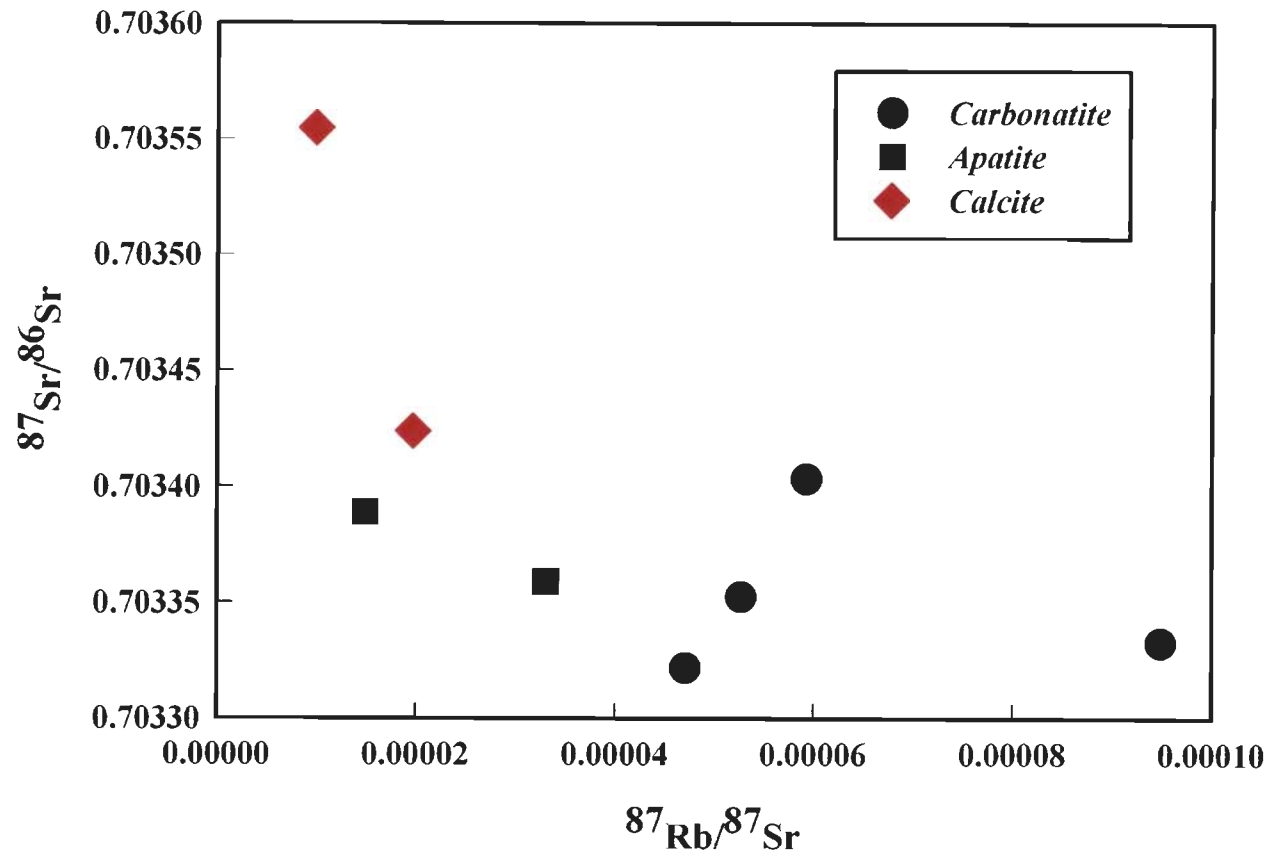


Fig. 5.1 $^{87}\text{Rb}/^{86}\text{Sr}$ vs. $^{87}\text{Sr}/^{86}\text{Sr}$ plot of carbonatites as well as mineral separates viz. calcite and apatite. No correlation has been noticed between the bulk rocks as well as for the minerals.

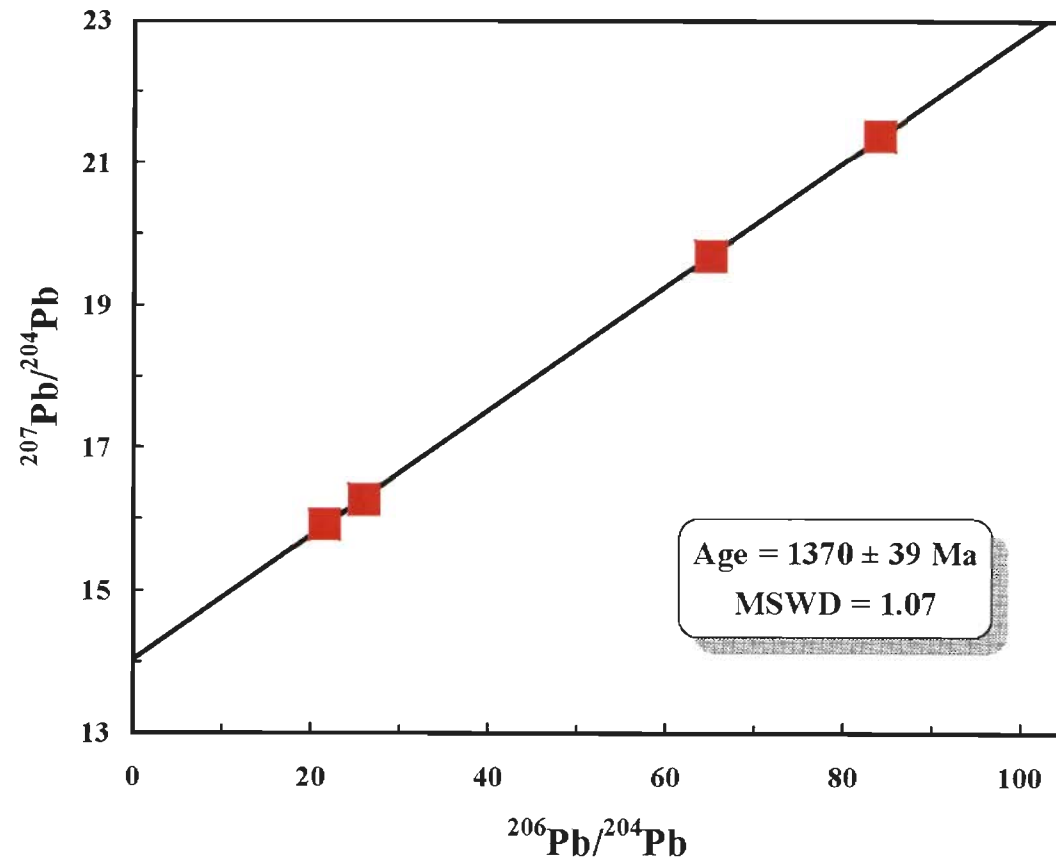


Fig. 5.2 $^{206}\text{Pb}/^{204}\text{Pb}$ - $^{207}\text{Pb}/^{204}\text{Pb}$ isochron (pseudo-isochron) for the carbonatites showing an age of about 1370 ± 39 Ma.

5.3 ALKALI-PYROXENITE

Rb-Sr and Pb-Pb isotopic analyses were carried out on the two samples (ANK 10 & 11) of alkali-pyroxenite. The age determination is not expected from this rock particularly that too from the bulk rock isotopic analysis as the rock had undergone alkali-metasomatism (finitization) due to carbonatite intrusion. However the Rb-Sr isotopic analysis of the two samples reveals that the measured $^{87}\text{Sr}/^{86}\text{Sr}$ is slightly higher (0.70505 to 0.70540) than that of the nearby carbonatite. The higher $^{87}\text{Sr}/^{86}\text{Sr}$ ratio may be attributed to the late stage calcite vein intrusion in the rock. Moreover the $^{87}\text{Rb}/^{86}\text{Sr}$ is also higher in this rock relative to the carbonatite which can be attributed due the presence of phlogopite in this rock. The $^{206}\text{Pb}/^{204}\text{Pb}$ ratio is relatively less in comparison to the carbonatite and lies in the range of 23.8 to 24.7 and that of the $^{208}\text{Pb}/^{204}\text{Pb}$ value is similar to that of the carbonatite (Table 5.1).

5.4 NEPHELINE SYENITE

The two varieties nepheline syenite/nepheline syenite gneiss has been used for the study of Rb-Sr systematic. The rock contains several Sr and Rb bearing phases. Whole rock Rb-Sr analysis were carried out on five samples of nepheline syenite out of which four are poorly banded syenite gneiss (ANK 2, 6, 7 & 8) and one is massive syenite (ANK 9). The whole rock Rb-Sr systematics reveals that all the syenites are having different $^{87}\text{Sr}/^{86}\text{Sr}_{(m)}$ (m = measured) isotopic composition varying from 0.7320 to 0.7559 and that of the $^{87}\text{Rb}/^{86}\text{Sr}$ is 1.5628 to 2.6825 (Table 5.1). The Rb-Sr whole rock isotopic compositions when plotted in the $^{87}\text{Rb}/^{86}\text{Sr}$ - $^{87}\text{Sr}/^{86}\text{Sr}$ diagram (Fig. 5.3) it is found that they are extremely scattered and isochron can not be generated from the generated whole rock data set. Opening up of the system due to deuteric alteration and metamorphism are two major responsible factors. The least value of $^{87}\text{Sr}/^{86}\text{Sr}_{(m)}$ is observed for massive syenite and that of the highest value for poorly banded nepheline syenite gneiss (ANK 6).

The Pb-Pb isotopic composition of the bulk rock reveals that the massive syenite is having the lowest value for both $^{206}\text{Pb}/^{204}\text{Pb}$ as well as $^{207}\text{Pb}/^{204}\text{Pb}$ (19.129 & 15.588 respectively). Poorly banded syenite gneisses are having variable Pb-Pb isotopic ratios (Table 5.1). The generated data when plotted in a $^{206}\text{Pb}/^{204}\text{Pb}$ and $^{207}\text{Pb}/^{204}\text{Pb}$ diagram, it has been found that there exists a good correlation between two varieties of syenite with regression value of about 0.89 (except for ANK 2) (Fig. 5.4). This gives an age of about 1278 ± 930 Ma with very high value of MSWD. Similar range of ages with similar MSWD (~ 40) also indicated by the poorly banded syenite gneiss and thus could correspond to the age of tectono-thermal event (metamorphism and/or metasomatism) affected these rocks.

5.4.1 ZIRCON DATING (U-Pb) OF NEPHELINE SYENITES

The heavy liquid separation technique was used to look for some key minerals like zircon and monazite. Few grains of zircon could be recovered from the ANK 2, ANK 7, ANK 8 and ANK 9. The recovered zircon crystals are having difference in size, color and form. The grains are anhedral to subhedral in shape. Most of the zircon grains were air abraded to remove the effect of inheritance and to reduce the Pb loss effect except for two zircon grains from sample from the poorly banded syenite (ANK 8).

All the zircons analyzed from the poorly banded nepheline syenite gneisses yielding a wide range of ages indicating that these ages are related to the post magmatic changes related to the metamorphic and/or metasomatic process.

The oldest age obtained from the poorly banded nepheline syenite gneiss (ANK 7) is giving an upper intercept age of about 1301 ± 9.6 Ma (Fig. 5.5). The Monte Carlo simulation which is considered to be the most reliable errors for Concordia-intercept is used to obtain the age from the zircon grains (Fig. 5.6) (Ludwig, 2003). The Pb loss is also observed here and the data points are

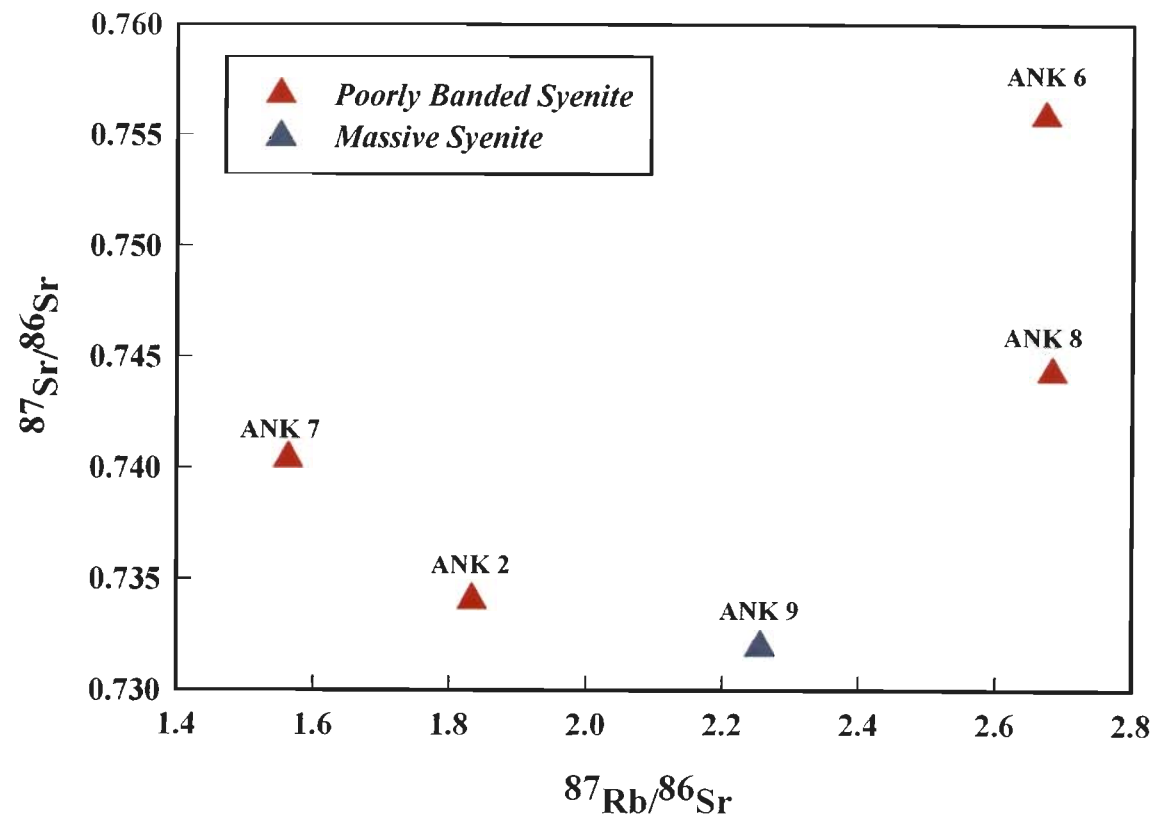


Fig. 5.3 $^{87}\text{Rb}/^{86}\text{Sr}$ vs. $^{87}\text{Sr}/^{86}\text{Sr}$ plot of whole rock nepheline-syenites. No correlation has been noticed between the bulk rock samples.

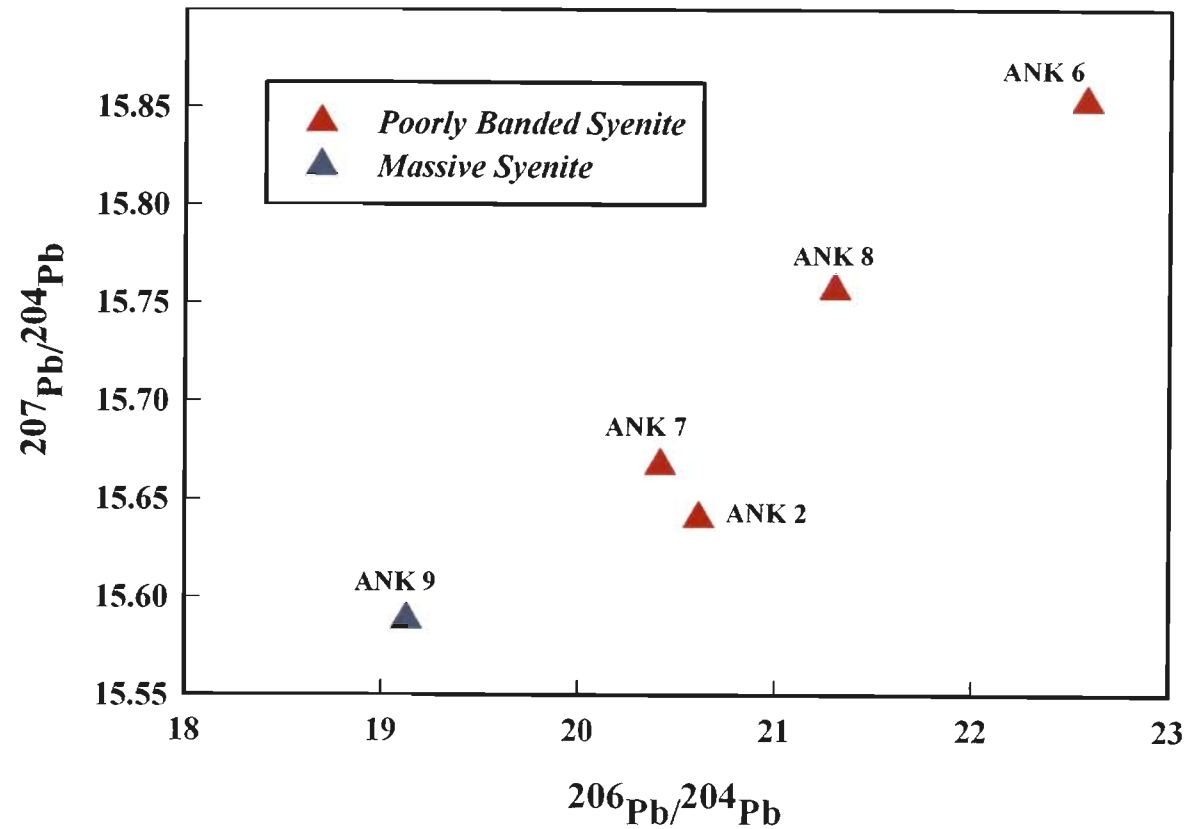


Fig. 5.4 $^{206}\text{Pb}/^{204}\text{Pb}$ vs. $^{207}\text{Pb}/^{204}\text{Pb}$ plot of whole rock nepheline-syenites. Linear correlation has been found between the bulk rock samples. ANK 2 showing evidences of Pb-mobility.

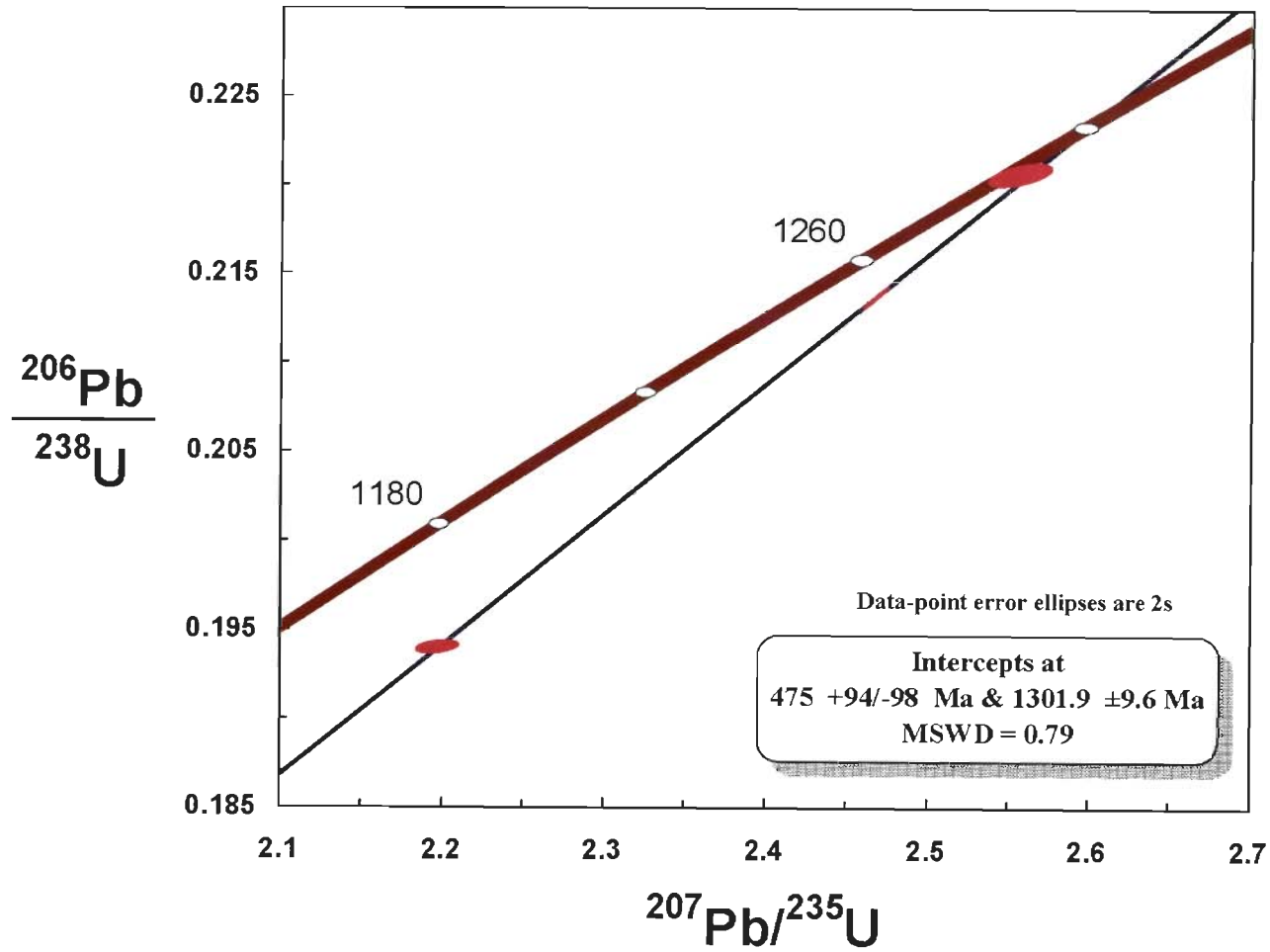
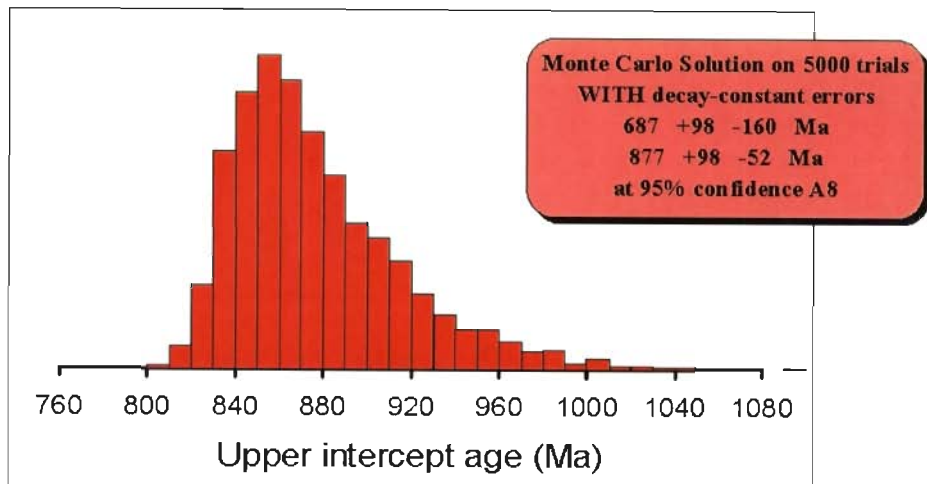
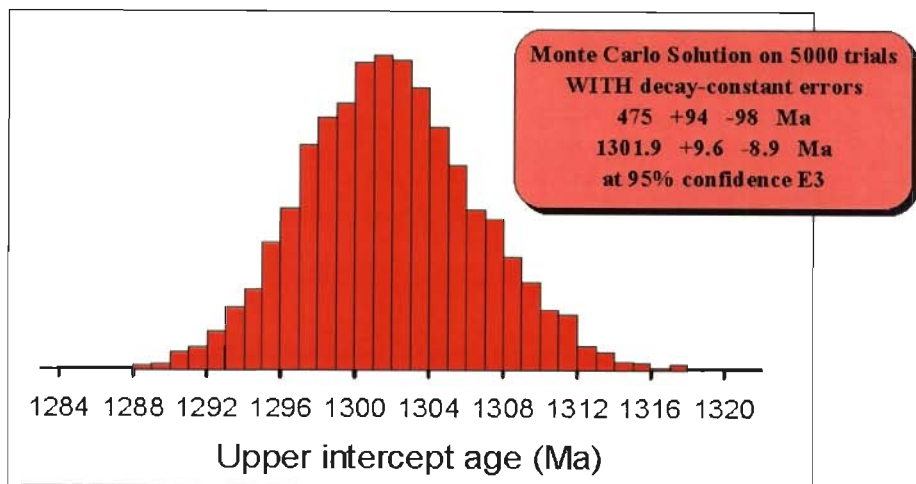


Fig. 5.5 U-Pb Concordia diagram of poorly banded syenite gneiss (ANK 7)



Model 1 Solution ($\pm 95\%$ -conf.) without [with] decay-const. errs on 3 points
 Lower intercept: 699 ± 140 Ma
 Upper intercept: 868 ± 63 [± 67] Ma
 MSWD = 0.15, Probability of fit = 0.70



Model 1 Solution ($\pm 95\%$ -conf.) without [with] decay-const. errs on 3 points
 Lower intercept: 475 ± 96 Ma
 Upper intercept: 1301.9 ± 5.5 [± 9.3] Ma
 MSWD = 0.79, Probability of fit = 0.37

Fig. 5.6 Monte Carlo Simulation histogram for two samples of poorly banded syenites: ANK 2 and ANK 7 respectively shown above.

discordant in nature. On the other hand four zircon analyses two of which are non-abraded and two are air-abraded were carried out from ANK 8. The non abraded zircons are giving an age of 817 ± 220 Ma and that of the abraded zircons giving an age of about 960 ± 32 Ma (Fig. 5.7). The 960 ± 32 Ma age is found to be more realistic as the error limit is found to be less.

Three analyses were carried out on the zircons from ANK 2 which gives an upper intercept age of about 877 Ma (Fig. 5.8). The effect of Pb-mobility is observed in the U-Pb Concordia plot and the data points are thus showing as a discordant plot. The youngest geological (tectono-thermal) event can thus be dated around 877 ± 52 Ma. Here also Monte Carlo simulation is used.

Three zircon grains from the massive syenite (ANK 9) were analyzed which are giving an upper intercept of 1513 Ma (Fig. 5.9). This is the oldest age obtained out of the all analyzed samples of nepheline syenite. Interestingly considering this age as the age of crystallization of this variety of syenite it has noticed that all the samples' initial $^{87}\text{Sr}/^{86}\text{Sr}$ ratio is coming below the BABI value ($t= 1500$ Ma.). This indicates that with respect to the 1500 Ma. event all the whole rock compositions are reset to the subsequent tectono-thermal events either related to metamorphic or metasomatic event or may be by the combination of both. Another interesting feature observed particularly for sample ANK 2 is that the whole rock as well as the analyzed zircon grains is showing evidences of Pb-mobility which could be related to the formation of these zircons under metasomatic condition similar to the one reported by Ashwal et al. (2007) from the nepheline syenite gneiss of Malawi.

5.5 SUMMARY

Carbonatite and Pyroxenite association

The Pb-Pb isotopic study reveals that the carbonatites are characterized by very high Pb-Pb (Carbonatite: $^{206}\text{Pb}/^{204}\text{Pb}$:21.5-83.9; $^{207}\text{Pb}/^{204}\text{Pb}$:15.9-21.3; $^{208}\text{Pb}/^{204}\text{Pb}$:36.8-38.1) ratio in

comparison to the alkali-pyroxenite (alkali-pyroxenite: $^{206}\text{Pb}/^{204}\text{Pb}$:23.8-24.7; $^{207}\text{Pb}/^{204}\text{Pb}$:16.3; $^{208}\text{Pb}/^{204}\text{Pb}$:37.8). Such high $^{206}\text{Pb}/^{204}\text{Pb}$ is also reported from the Newania and Sevattur carbonatite of Tamil Nadu by Schleicher et al. (1997) as well as from the other carbonatite complexes of the world viz. Tikshezzero carbonatite complex of Kola Alkaline Province, Russia (Tichomirowa et al., 2006) and Prairie Lake Complex (Known et al., 1989). The Pb-Pb gives an pseudo-isochron age of about 1.37 Ga for carbonatite. Considering the fact that the carbonatite is also affected by postmagmatic changes (metamorphic and/or metasomatic) the age of carbonatite can thus be considered as even older than the 1.37 Ga. This indicates that this carbonatite (Purulia carbonatite) could be the oldest carbonatite body which is being reported in the present work for the first time from the Singhbhum-Chotanagpur cratonic region.

The bulk rock Rb-Sr isotopic analysis reveals that the carbonatites are extremely low in $^{87}\text{Rb}/^{86}\text{Sr}$ ratio, which makes difficult to draw an isochron out of these data. Very low concentrations ^{87}Rb will certainly not contribute any significant amount of ^{87}Sr after crystallization of carbonatite and not affect the initial $^{87}\text{Sr}/^{86}\text{Sr}$ ratio. Thus the measured $^{87}\text{Sr}/^{86}\text{Sr}$ ratio can be considered as the initial $^{87}\text{Sr}/^{86}\text{Sr}$ ratio for the carbonatite which varies from 0.70332 to 0.70340. Moreover the initial $^{87}\text{Sr}/^{86}\text{Sr}$ is calculated considering a tectono-thermal event dated back to 1.37 Ga which affected the carbonatite is also found to be ranging from 0.70332 to 0.70339. The differences in the bulk rock as well as mineral (apatite and calcite) $^{87}\text{Sr}/^{86}\text{Sr}$ value of may be truly original or the higher value may reflect the effect of metamorphism or deuteritic alterations. Considering the petrography of the carbonatite the post magmatic changes by metamorphism or deuteritic alteration are found to be more realistic and the higher values can be attributed in response to the post magmatic changes. Considering the open system behaviour of the Rb-Sr systematics due to post magmatic tectono-thermal events the lowest value of $^{87}\text{Sr}/^{86}\text{Sr}$ ratio is somewhat representative of the least affected by later events. However, irrespective of the post magmatic changes the $^{87}\text{Sr}/^{86}\text{Sr}$ value is well

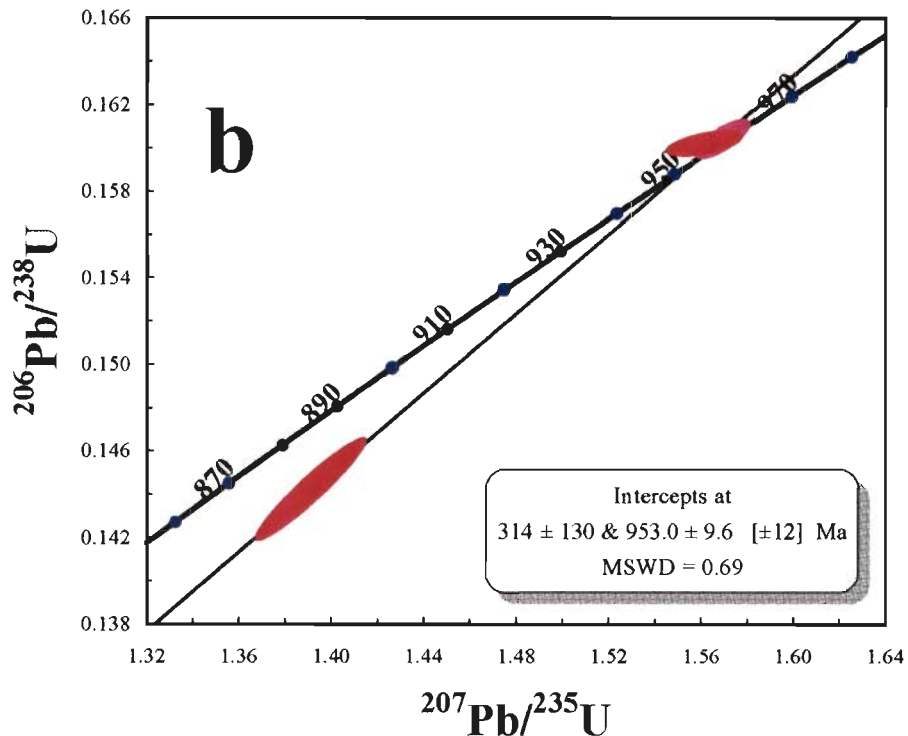
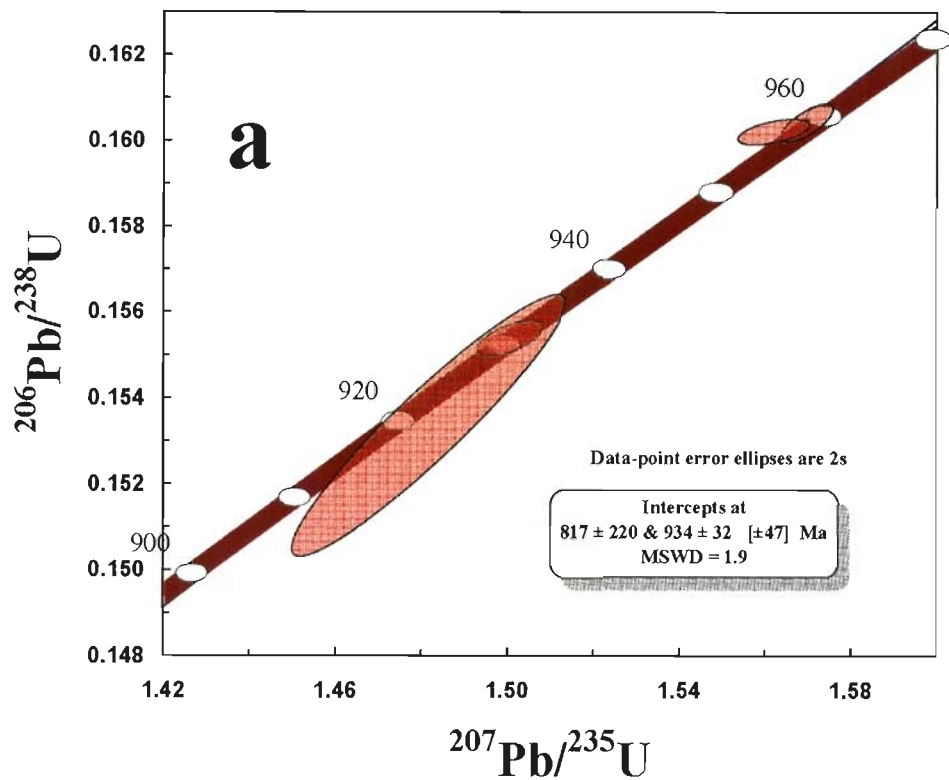


Fig. 5.7 U-Pb Concordia diagram of banded syenite sample ANK 8. (a) Both the air abraded and non abraded grains are together giving an age of about 934 Ma while a much more precise age is given by three point isochron with low MSWD and gives an age of ~960 Ma.

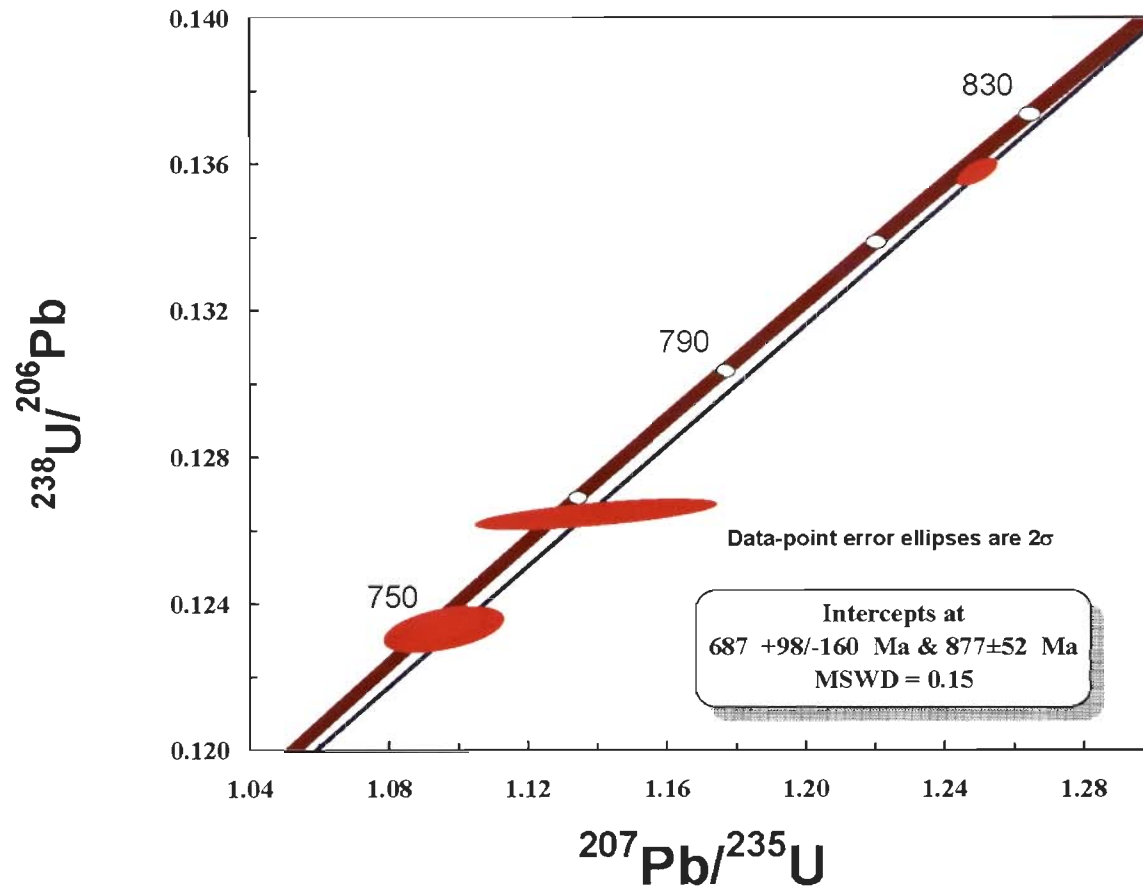


Fig. 5.8 U-Pb Concordia diagram of poorly banded syenite gneiss (ANK 2)

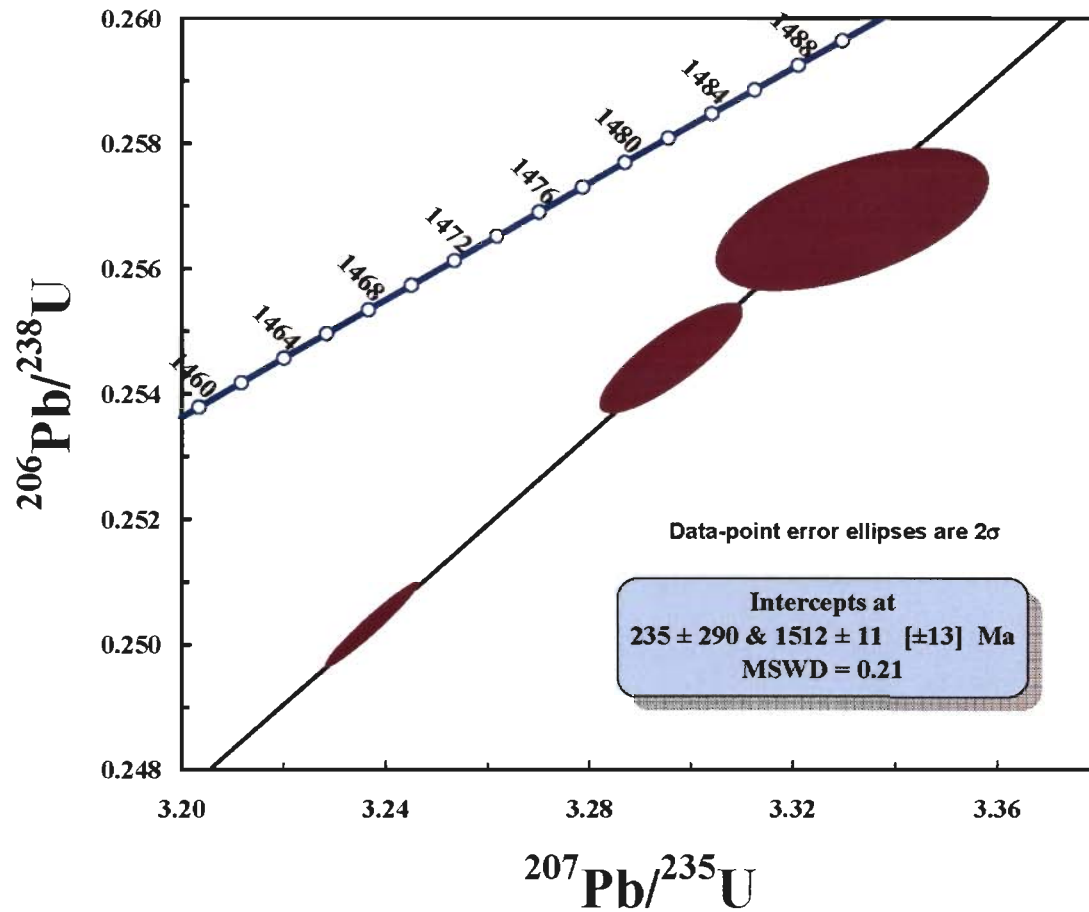


Fig. 5.9 U-Pb Concordia diagram of massive syenite sample ANK 9

within the range of magmatic carbonatite derived from the mantle source (<0.706 , Barker, 1989) and also 'normal-basalt' of Faure and Hurley (1963). In conclusion the above data suggests that the age of Purulia carbonatite is at least >1.4 Ga and their $^{87}\text{Sr}/^{86}\text{Sr}$ ratio is indicative of their mantle origin.

Nepheline syenites

The isotopic data obtained in the present work clearly showing that the studied isotopic systematics both the Rb-Sr and Pb-Pb; for nepheline-syenites were reset with respect to the age of their formation due to post magmatic disturbance by metamorphism and/or metasomatism. The zircon grains are yielding a wide range of ages also supporting the above mentioned fact. Though the $^{206}\text{Pb}/^{204}\text{Pb}$ vs. $^{207}\text{Pb}/^{204}\text{Pb}$ plot of the syenites are falling well within the range of EM1 and HIMU but it is difficult to establish that they were formed by the mixture of these two mantle end members as they suffered post magmatic tectono-thermal events by metamorphism and/or metasomatism. Hence considering the open system behaviour of both the studied systematics it is difficult to assess the origin of the nepheline syenites.

The bulk rock Rb-Sr isotopic studies of nepheline syenites reveal that they are having different $^{87}\text{Sr}/^{86}\text{Sr}$ (measured) ratios. The different $^{87}\text{Sr}/^{86}\text{Sr}$ certainly indicates post crystallization disturbance in the Rb-Sr systematics. The high $^{87}\text{Sr}/^{86}\text{Sr}$ value (0.73195-0.75586) indicates significant crustal component incorporation in the nepheline syenites during metamorphism and metasomatic activity which affected these rocks (Wasserburg et al. 1964). The least $^{87}\text{Sr}/^{86}\text{Sr}$ ratio is observed in the massive syenite and reaches maximum to the poorly banded syenite gneiss though both the rocks were suffered post magmatic tectono-thermal event.

Conventional U-Pb dating of zircon of poorly banded syenite gneiss reveals an oldest event at about 1.30 Ga followed by subsequent events at 953-960 Ma and 877 Ma respectively. All these

ages are representatives of subsequent metamorphic event and related to granulite to amphibolite facies of metamorphism reported from the nearby area and discussed in details in the Chapter 6. The oldest age obtained from the massive syenite is 1.51 Ga is similar to the intrusion age of Bengal anorthosite from the nearby Saltora area (Chatterjee et al. 2008, Maji et al. 2008). Considering this age as the age of crystallization for the nepheline syenites the $^{87}\text{Sr}/^{86}\text{Sr}$ ratio for all the studied samples are found to be falling below BABI. This indicates that with respect to this age (either crystallization/metamorphic age: 1512 Ma) all the studied samples were reset to new isotopic equilibrium thus giving value below BABI. The reported intrusion age of Bengal anorthosite is also from the gabbroic anorthosite which suffered metamorphism at ~950 Ma (Chatterjee et al. 2008). Maji et al (2008) reported poly-phase metamorphism from the western part of the present study area of Sushina between 1.4 Ga to 0.9 Ga. According to them the age of deformation that the anorthosite suffered may even be older than 1.4 Ga. considering the intrusion of anorthosites at 1.55 Ga. Present study also reveals that the massive syenite is least affected by metamorphism and metasomatism compared to the poorly banded syenite gneiss. Moreover the prismatic nature of the zircon from his variety of syenite is probably indicative of magmatic origin of these zircons (Pupin, 1980) and the age 1.51 Ga can be considered as age of crystallization of massive syenite (probably the poorly banded syenite gneisses also) followed by granulite to amphibolite facies of poly-phase metamorphism at 1.30 Ga and 0.9-1 Ga respectively. The youngest event obtained in the present study from the poorly banded nepheline syenite gneiss (ANK 2) showing the evidences of Pb-mobility (Fig. 5.4) and the all the analyzed zircons are plotted on or close to the concordia (Fig. 5.8) indicating that their formation at much later stage probably by recrystallization due to late stage metasomatic activity by deuteritic fluid which is in turn responsible for the formation of eudialyte and complex Na-Zr silicates in these rocks.

Table 5.1: Sr-Pb data from the carbonatite, nepheline-syenite and alkali-pyroxenite

	Rb (ppm)	Sr (ppm)	⁸⁷ Rb/ ⁸⁶ Sr	⁸⁷ Sr/ ⁸⁶ Sr	1σ	U (ppm)	Pb (ppm)	²⁰⁶ Pb/ ²⁰⁴ Pb	²⁰⁷ Pb/ ²⁰⁴ Pb	²⁰⁸ Pb/ ²⁰⁴ Pb
ANK 1	0.18	8743.33	0.00006	0.70340	0.000065	45.40	5.41	64.935	19.695	37.939
ANK 1 (Apt)	0.08	6769.17	0.00173	0.70336	0.00002	-	-	-	-	-
ANK 1 (Cal)	0.04	10295.33	0.00094	0.70356	0.00004	-	-	-	-	-
ANK 3	0.37	11112.24	0.00009	0.70333	0.00003	3.88	8.69	21.531	15.925	36.859
ANK 3 (Apt)	0.04	7555.39	0.00352	0.70339	0.00001	-	-	-	-	-
ANK 3 (Cal)	0.07	10000.00	0.00077	0.70342	0.00002	-	-	-	-	-
ANK 4	0.16	8519.82	0.00005	0.70335	0.00003	44.31	4.92	83.939	21.392	38.142
ANK 5	0.19	11294.52	0.00005	0.70332	0.00009	7.11	7.16	25.901	16.269	37.177
ANK 2	112.85	173.71	1.83361	0.73407	0.00007	5.45	18.87	20.420	15.667	39.656
ANK 6	122.23	129.09	2.67248	0.75586	0.00088	2.45	6.26	22.583	15.853	40.343
ANK 7	141.59	255.71	1.56282	0.74043	0.00031	15.25	60.25	20.614	15.640	42.184
ANK 8	114.63	120.62	2.68250	0.74436	0.00138	4.05	10.76	21.309	15.757	41.615
ANK 9	111.37	139.38	2.25528	0.73195	0.00008	4.80	27.28	19.129	15.588	38.634
ANK 10	26.33	1247.57	0.05957	0.70505	0.00007	0.80	8.00	23.807	16.342	37.874
ANK 11	55.71	1639.94	0.09588	0.70540	0.00010	0.83	3.66	24.769	16.292	37.884

Apt: Apatite
Cal: Calcite
ANK 1 & 3-5: Carbonatite
ANK 2 & 6-9: Nepheline-syenite
ANK 10 & 11: Alkaline-ultramafic rocks

Table 5.2: U-Pb isotope data for zircons from two varieties of nepheline syenites

N	Anal. N	Size fraction, μm	weight in mg	description	U ppm	Pb Ppm ®	Pb ppm ©	$^{207}\text{Pb}/^{235}\text{U}$	2 σ error %	$^{206}\text{Pb}/^{238}\text{U}$	2 σ error %	$^{207}\text{Pb}/^{206}\text{Pb}$	2 σ error %	Apparent ages			Rho
														$^{206}\text{Pb}/^{238}\text{U}$	$^{207}\text{Pb}/^{235}\text{U}$	$^{207}\text{Pb}/^{206}\text{Pb}$	
ANK 2																	
1	3310	100-300	12.2	Pinkish (an)	15.924	3.131	0.192	1.24987	0.374	0.13583	0.216	0.066738	0.292	821.04	823.35	829.62	0.626
2	3111	100-300	15.2	do	28.143	4.311	4.286	1.09599	1.285	0.12326	0.416	0.064490	1.151	749.29	751.41	757.72	0.469
3	3112	100-300	9.3	do	14.268	2.499	1.357	1.13993	2.473	0.12642	0.261	0.065396	2.302	767.43	772.48	787.10	2.7
ANK 7																	
4	3147	100-300	2.4	Transparent (an-sub)	30.708	21.835	1.996	2.55728	0.637	0.22076	0.237	0.084016	0.540	1285.87	1288.52	1292.92	0.563
5	3106	100-300	32.5	do	26.639	11.160	0.649	2.46789	0.249	0.21377	0.244	0.083730	0.046	1248.86	1262.67	1286.29	0.983
6	3108	100-300	18.3	do	18.039	12.334	0.961	2.19631	0.501	0.19394	0.165	0.082133	0.468	1142.71	1179.87	1248.71	0.357
ANK 8																	
7	3138A	100-300	12.5	Yellow (an-sub)	56.594	13.175	1.196	1.56967	0.316	0.16042	0.233	0.070967	0.212	959.10	958.30	956.49	0.741
8	3138B	100-300	12.5	do	56.594	13.147	1.197	1.56182	0.433	0.16021	0.154	0.070703	0.373	957.94	955.19	948.87	0.541
9	3136A	100-300	15.4	do	34.449	7.784	0.899	1.48144	1.753	0.15330	1.630	0.070087	0.597	919.44	922.82	930.90	0.940
10	3136B	100-300	15.5	do	33.890	7.767	0.940	1.50032	0.414	0.15534	0.220	0.070049	0.324	930.83	930.52	929.76	0.630
ANK 9																	
11	3141	100-300	15.9	Brown (l-prism)	33.495	20.181	0.596	3.29635	0.348	0.25456	0.285	0.093915	0.192	1461.97	1480.19	1506.41	0.834
12	3142	100-300	24.8	do	36.341	20.423	0.316	3.33193	0.659	0.25679	0.363	0.094107	0.550	1473.39	1488.57	1510.27	0.551
13	3144	100-300	18.9	do	77.560	34.646	0.703	3.23714	0.230	0.25027	0.222	0.093809	0.058	1439.89	1466.10	1504.25	0.967

CA – chemical abrasion; transp – transparent; prism- prismatic; Rho - correlation coefficient $^{206}\text{Pb}/^{238}\text{U} - ^{207}\text{Pb}/^{235}\text{U}$ ® Radiogenic Pb, © Common Pb

DISCUSSIONS

Petrogenesis of the Purulia carbonatite and associated rocks, exposed along Northern Shear Zone (NSZ), is a challenge due to: 1) very scanty and limited exposures, 2) the exposures are also scattered along tens of kilometers along NSZ and 3) intense meteoric water action. The present study aims to solve this knowledge-gap by systematic and detailed petrographic, geochemical and isotopic investigations using available limited number of samples representing these rocks. The geochemical and isotopic data are extensively used in characterizing the source of magma as well as geochronology of these rocks, which is important to build a realistic idea about the geodynamic evolution of this part of Eastern Indian Shield.

Bell (1994) summarized that the carbonatites are volumetrically insignificant but their widespread distribution on most of the continents along with the variation in age can provide the useful information on the nature of the sub-continental upper mantle (SCUM) over a long period of time (2.8 Ga to recent). This is because: (1) the carbonatites are characterized by the highest concentrations of REE ($\Sigma\text{REE}=72\text{-}15,515$ ppm, Henderson, 1984) along with Sr (average 7000 ppm) and in some cases Pb (118 ppm), (2) carbonatite melts are thought to rise rapidly to the surface because of its low viscosity and hence get very less time for reactions with the continental crust and thus the effects of crustal contamination of the mantle signatures should be minimized (Bell, 1994). Considering the above mentioned points carbonatites are suitable for deciphering the nature of the SCUM over a longer period of time and hence is of much greater importance in spite of its limited occurrences. The present chapter is divided into two parts based on the occurrence of the studied rocks i.e. *carbonatite and pyroxenite association* at Beldih and *nepheline syenite* at Sushina.

6.1 CARBONATITE AND PYROXENITE ASSOCIATION

6.1.1 *Field and Petrographic signatures*

In a Precambrian terrain like the present case, the rocks are mostly affected by extensive post magmatic deformation. At places such deformation may also be accompanied by metamorphism and/or metasomatism. The Purulia carbonatite is intruded within the country rock which suffered amphibolite to greenschist facies of metamorphism. So, it is difficult to retain the primary magmatic signatures in terms of texturally, mineralogically and geochemically. The most difficulties arises in determining the age of such rocks (metacarbonatite) as the isotopic systematics are disturbed in response to post magmatic deformational process. At times the metacarbonatites are indistinguishable with that of the marble owing to the similar response of metacarbonate and carbonatite under metamorphic conditions at amphibolite or even higher grade unless the identification of the metacarbonatite by the presence of particular diagnostic minerals such as pyrochlore. But such distinction also fails because not all the carbonatites contain pyrochlore (Le Bas, 2002). In this context the Purulia carbonatite is characterized by mosaic texture and dominantly consists of calcite (90% by volume) and apatite (2-5%), along with accessories like amphibole, biotite and magnetite. Such mineralogical assemblage even under highest grade of metamorphism does not greatly change the mineralogical assemblages of carbonatite as exemplified by the carbonatites from East India, Bull's Run carbonatite in Natal, some Ontario examples and those of the Canadian Cordillera gneissic rocks (Natarajan et al., 1994; Viladkar and Subramaian, 1995; Scogings and Forster, 1989; Moecher et al., 1997; Pell and Höy, 1989). So, the presence of polygonal calcite crystals with triple junction can be attributed to the rheological changes/readjustment particularly in response to post crystallization deformational activities. Presence of apatite, magnetite and accessory silicates are in well agreement with the

genesis the Purulia carbonatite by magmatic process. The most convincing evidence that the examined carbonatite is of magmatic origin is the effect of alkali-metasomatism in the associated alkali-pyroxenite.

The alkali-pyroxenite, present in association with the carbonatite, is dominantly consists of diopsidic pyroxene along with accessory amphibole of primary magmatic origin (Amph-I; Fig. 3.4c). Introduction of albite, biotite, phlogopite and numerous calcite veins are the result of alkali metasomatism during carbonatite intrusion. Alteration of alkali-pyroxene to alkali-amphibole is also caused by this process. This supports the intrusive (as a dyke) nature of the carbonatite and a later stage of formation relative to the alkali-pyroxenite.

6.1.2 Amphibole as a petrogenetic indicator in carbonatite and associated rocks

The Purulia carbonatite is characterized by the presence of two varieties of co-existing sodic-calcic amphibole of primary magmatic origin (Hogarth, 1989), magnesiokatophorite and richterite, is characteristics of the carbonatite. Distinctive optical character and chemistry of the amphiboles lead to investigate their petrogenetic significance. Chemical composition of the amphibole is controlled by the nature of the parent magma and the physico-chemical conditions, such as temperature, pressure, etc., prevailing during the crystallization. The substitution of Si^{4+} by Al^{3+} in T-site depends on total pressure, prevailing during the crystallization (Hammarstrom and Zen, 1986; Hollister et al., 1987). The similar analogy is also used by Hammarstrom and Zen (1986) and Hollister et al. (1987) for geobarometric calculations using hornblende from the calc-alkaline plutons. If other physico-chemical parameters remain unchanged, the Al-content in amphibole increases with increasing pressure. Hence, the variation in chemical composition of amphibole points towards a possible change in crystallizing condition.

The mineralogical, petrological and compositional data of amphibole from the Purulia carbonatite reveal that the presence of two similar, but mineralogically distinct varieties of sodic-calcic amphibole: magnesiokatophorite and richterite. Compared to richterite, the magnesiokatophorite, here, is Al-rich in T-site, the proportion of Al in this site is about 0.65 and 3-4 times more than that of richterite. The higher proportion of Al in T-site of magnesiokatophorite is attributed to the formation of this amphibole species at relatively higher pressure. The high Al-content in T-site is expected to influence cation occupancy in C-site and it should contain more amount of tetra- or trivalent cations, like Al^{3+} , Ti^{4+} and Fe^{3+} . The divalent cations, like Mg^{2+} , should be relatively low in C-site and this fact corroborated by the chemical composition of magnesiokatophorite (Table 3.3). Clear-cut positive correlation can be observed between Al^{3+} & Ti^{4+} and Al^{3+} & Fe^{3+} plots, which indicate Ti- and Fe^{3+} -enrichment with increasing Al-content (Fig.6.1a,b). On the other hand, expected negative correlation is also found between Al^{3+} - Mg^{2+} (Fig.6.1c). However, the higher content of CaO in magnesiokatophorite can be explained by coupled substitution between $\text{Si}^{4+}+\text{Na}_B$ and $\text{Al}^{3+}+\text{Ca}_B$ i.e. substitution of Si^{4+} by Al^{3+} in the lattice structure (Fig. 6.2a). Similar feature is also observed between Ca_B and Na_B (Fig. 6.2b). In both the cases strong negative correlation is very much clear. Thus the presence of the sodic-calcic amphibole with two distinct compositional modes in the Purulia carbonatite can possibly be attributed to the sudden change in pressure within the magma chamber. Relatively Al^{3+} and Ca^{2+} rich magnesiokatophorite started crystallizing along with calcite and apatite at a greater depth. Then, due to formation/reactivation of the NSZ, the carbonatite melt, along with the already-formed magnesiokatophorite crystals intruded into the shallower zone of the crust. Sudden intrusion of the magma to new site would drop the total pressure of the intruding magma, and further cooling of this magma seems to have caused crystallization of the richterite, which is characterized by the low Al-content. This small change in physico-chemical condition could be recorded in the amphibole mineral as they are very

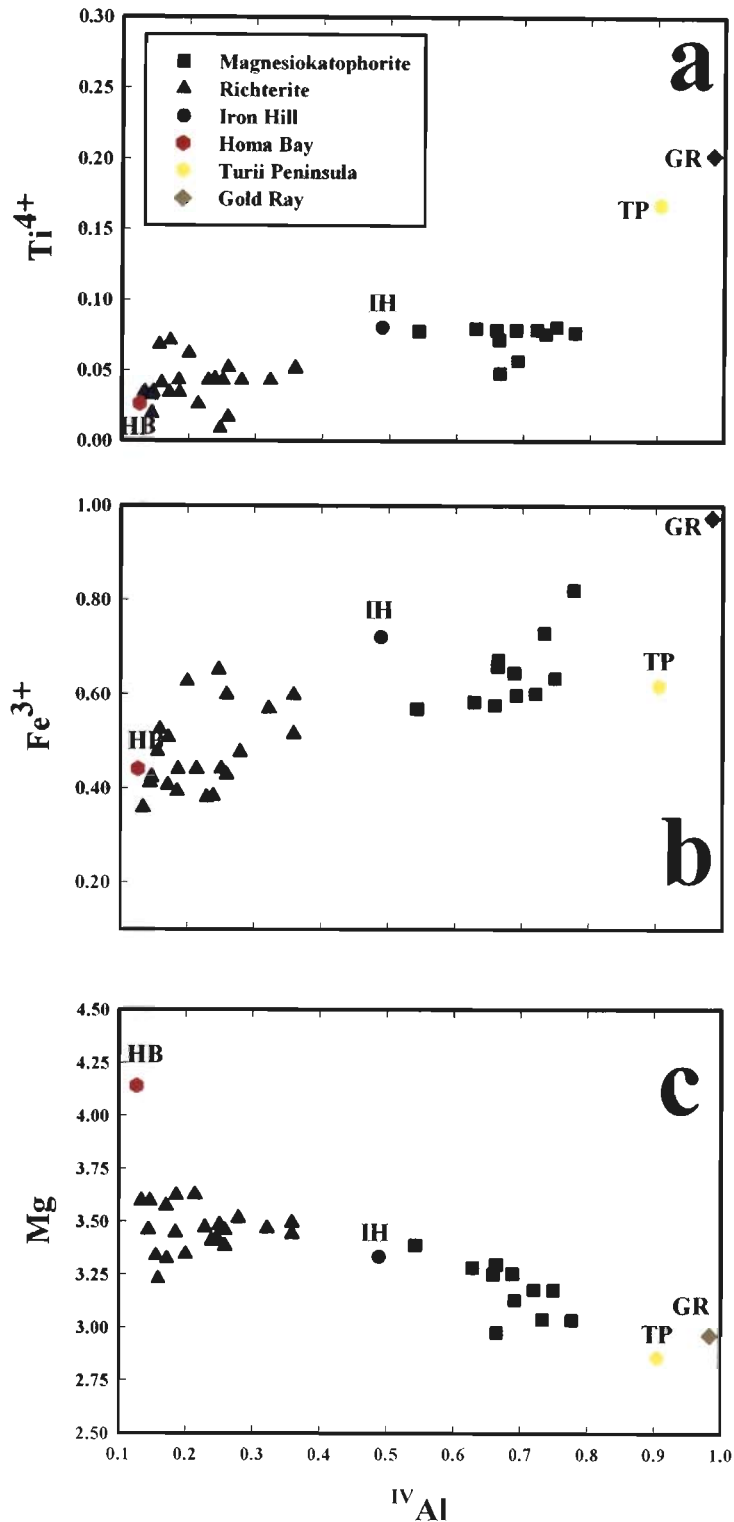


Figure 6.1 (a) $IVAl-Ti^{4+}$. (b) $IVAl-Fe^{3+}$ and (c) $IVAl-Mg$ plots of the amphibole from the Purulia carbonatite. $IVAl$ shows positive correlation with Ti^{4+} (a) and Fe^{3+} (b) and negative correlation with Mg (c) in richterite and magnesiokatophorite species. For comparisons the amphibole composition (Hogarth, 1989) from Iron Hill, Colorado; Homa Bay, Kenya; Turii Peninsula, Russia and Goldray, Ontario.

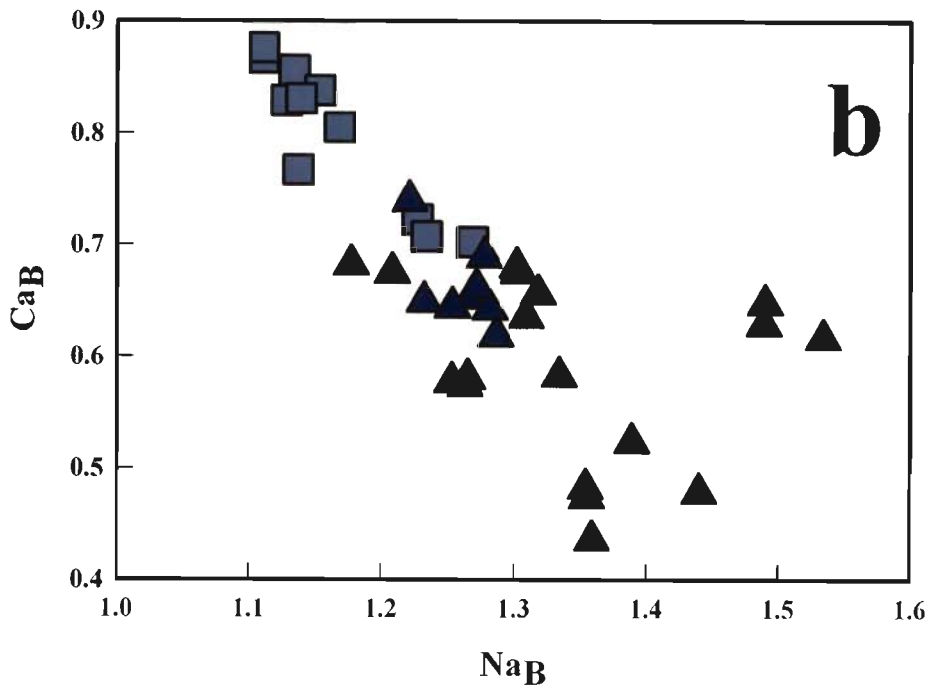
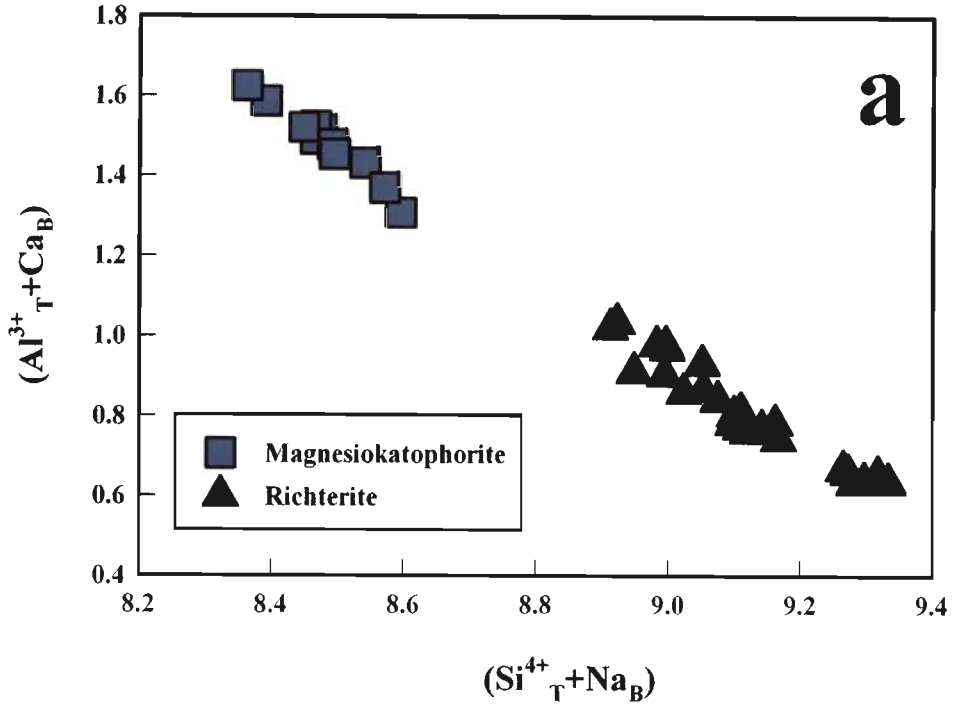


Figure 6.2 (a) $(\text{Si}^{4+} + \text{Na}_B) - (\text{Al}^{3+} + \text{Ca}_B)$ plot for the two varieties of amphibole – richterite and magnesiokatophorite. There are two distinct fields of these two types of amphibole with correlation coefficient of -0.9652 and -0.9805 for richterite and magnesiokatophorite, respectively. b. $\text{Na}_B - \text{Ca}_B$ plot of richterite and magnesiokatophorite, showing strong negative correlation between them in B – site.

sensitive to pressure variations. It is, therefore, assumed that the difference of the Al-content of the two varieties of the amphibole was due to only sudden change in the total pressure. In contrast, the effect of the temperature changes on the crystallization process was more gradual (Chakrabarty, et al., 2009).

Richterite is essentially a low-pressure, high-temperature variety of amphibole (Charles, 1975). The pressure varies approximately in the range of ~1 Kb or even less which in accordance to the model and genesis of richterite described above. Moreover, at temperature between 930° to 970°C and pressure 50 to 150 bars, this variety of amphibole decomposes to assemblage: rodderite+forsterite+diopside+melt+vapour (Charles, 1975). No such assemblage is observed in the studied carbonatite.

The total FeO content is more or less similar for both varieties of amphibole with slight variation in $Fe^{3+}/(Fe^{3+}+Fe^{2+})$ content. This ratio is 0.39 ± 0.05 for magnesiokatophorite and 0.31 ± 0.04 for richterite. The reliability of this data can be questioned as the oxidation state of Fe is calculated rather than experimentally determined. However overall variation is narrow and reflects more or less similar fO_2 prevailed during the ascent of the carbonatitic magma. Unfortunately no experimental data is available related to the buffering condition, fO_2 and temperature of formation for magnesiokatophorite.

The above phenomenon, however, can also be explained by the sudden changes in the magma composition by wall rock assimilation. However, no evidence has been found to support the changes in the magma composition by such wall-rock assimilation. Assimilation of the country rocks should, normally, introduce both Al and Si, in the magma without any major change in its composition. Therefore, assimilation is not considered to alter the amphibole composition, i.e., Al:Si ratio as this is mainly controlled by the total pressure. Another possibility may be the factor, such as silicate-carbonate immiscibility in the parent magma; if we assume the original magma

(alkaline in composition) with innumerable droplets of immiscible carbonate melt. With progressive differentiation, immiscible carbonate droplets are likely to start segregating and eventually may generate a number of small pools of segregated carbonate magma at different levels within the magmatic chamber. Composition of the amphibole crystals developed within individual pools of carbonate magma will, nevertheless, depend upon P-T-conditions prevailing within individual carbonate magma pools. The P-T condition would largely depend on the depth. Once these small carbonate magma pools are generated to a large carbonate magma body, the already-formed amphibole crystals of different composition will get mixed up but this process also cannot satisfactorily explain the co-existence of the two varieties of amphibole. Instead, it is expected that amphibole crystals thus formed should have a range of compositional variation. This implies that the total pressure has been higher during the formation of magnesiokatophorite than that of richterite. The co-existence of magnesiokatophorite and richterite, within the same carbonatite body indicates sudden change in the total pressure condition, and thus could be related to the intrusive nature of the carbonatite melt emplaced in the NSZ. Moreover the presence of such amphibole supports the primary magmatic signature of the Purulia carbonatite.

The alkali-pyroxenite too contains two different types of amphibole viz. magnesiokatophorite and katophorite and/or taramite, the former dominates over the other. The magnesiokatophorite is of magmatic origin same as that in carbonatite. Presence of magnesiokatophorite of primary origin indicates its formation at depth as described in case of carbonatite. The katophorite/taramite variety is basically an alteration of pyroxene due to intensive alkali-metasomatism (finitization) undergone during carbonatite intrusion. Differences in the CaO, MgO and total FeO content between these two varieties of amphibole (Table 3.5) along with the increase in Fe and Ca contents at the expense of Mg and alkalis can be attributed to the reducing conditions of formation and late-stage metasomatic overprint (Hogarth, et al., 1989; Currie et al., 1992). Similar feature is also

observed in crystals of magnesio-arfvedsonite-richterite from the Rainville mine in Quebec (Hogarth et al., 1987) and magnesio-riebeckite-winchite from the Mud Tank complex in Australia (Currie et al., 1992). High Al_2O_3 content of katophorite/taramite as noticed here is very unusual and only found in amphibole associated with schist like gedrite, alumino-tschermakite (Deer et al., 1992). Thus such a high Al_2O_3 content in katophorite/taramite is possible due to alkali-metasomatism only. The effect of alkali-metasomatism on alkali-pyroxenite due to carbonatite intrusion is discussed below.

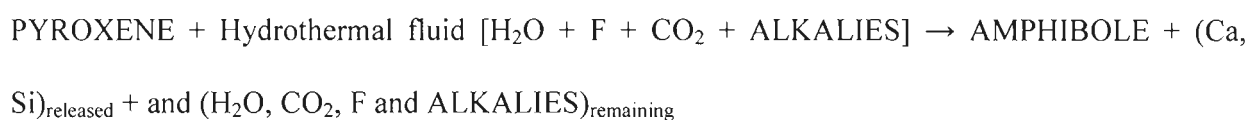
6.1.3 Effect of alkali-metasomatism in alkali-pyroxenite

The alteration of alkali-pyroxenite associated with the Purulia carbonatite is marked by two major changes: 1) alteration of pyroxene to amphibole and biotite and 2) vein-filling by calcite-albite-apatite-magnetite-ilmenite assemblage. In general, metasomatic alteration and 'finitization' related to alkaline magmatism is used as synonymous terms. The terminology 'finitization' is applied to the alteration of the country rock and Heinrich (1966, 1985) identified three principal types: sodic, potassic and sodic-potassic finitization. The sodic fenites are characterized by the abundance of sodic amphiboles, pyroxenes accompanied by Na-feldspar (albite) whereas in the potassic fenites K-feldspars (orthoclase) or microcline, low-Al phlogopite or biotite are the dominant minerals formed during finitization (Le Bas, 2008). The sodic-potassic fenites are characterized by the presence of above mentioned minerals in varying proportions. In general, earlier findings show that the fluid responsible for sodic finitization is dominated by F and Na_2CO_3 (Gittins et al. 1990; Jago and Gittins, 1991) rather than only H_2O (Treiman and Essene, 1992). The mineralogical and geochemical changes take place during finitization process, depends on number of parameters like T-P- $f\text{O}_2$ -pH etc. of the finitizing fluid. The present study is an attempt to estimate the role of fluid

- *composition, evolution, physico-chemical parameters, etc.*, and its effects in the alteration of alkali-pyroxenite, in a relatively smaller scale.

Composition of the fluid

The alteration of alkali-pyroxene to amphibole and biotite is the direct evidence of presence of H₂O and fluorine (F) in the fluid. The comparison of major element composition of pyroxene and Amph-II (Table 1 and 2) is used for ascertaining the cationic exchanges that took place by the reaction:



The above alteration of is mostly dominated by introduction of alkalis (mainly Na), H₂O and F. On the other hand, sporadic development of biotite, especially along the vein walls, at a later stage is indicative of K-metasomatism. The Mg removed during pyroxene alteration to Amph-II was used for the formation of biotite (Fig. 6.3). It is clear from the above reaction that with the advancement of alteration, the residual hydrothermal fluid would continuously be enriched in CO₂ over H₂O. During the subsequent vein filling, Na played dominant role which is well supported by the presence of albite. The formation of vein-filling calcite took place when XCO₂>XH₂O and the F played a major role during the formation of apatite. The relative enrichment of Y and HREE in vein-filling apatite compared to the apatite in carbonatite decent can be attributed to the dominance of fluoride complexing in the metasomatic fluid (Bühn, 2008). The above mentioned petrologic-geochemical evidences favour that the hydrothermal fluid was enriched in alkalis, CO₂ and F. The fluid composition changed continuously due to cooling and reaction with the parent alkali-pyroxenite. The comparison of whole rock geochemistry of the altered alkali-pyroxenite and the parent rock (assumed to be monomineralic) also supports the above view (Table 4.3).

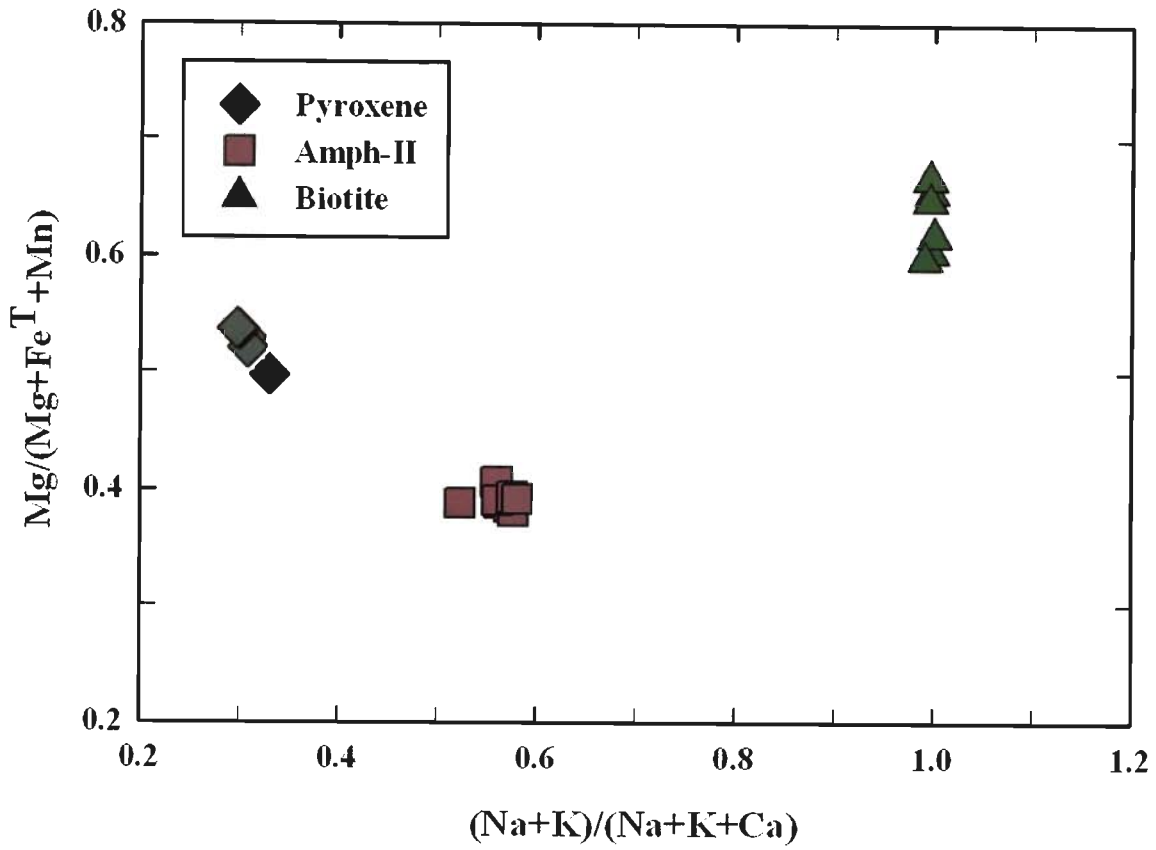


Fig. 6.3 $(Na+K)/(Na+K+Ca)$ vs. $Mg/(Mg+Fe^T+Mn)$ plot of pyroxene, Amph-II and biotite shows that the Mg released during the pyroxene alteration to the amphibole (Amph-II) was later introduced into the biotite. Also note the substantial increase in alkalinity $(Na+K)/(Na+K+Ca)$ during biotite formation.

The calculations here have been made after removing the effect of calcite introduced as vein-filled component. This table represents the alteration effects excluding vein-filling calcite.

The carbonatite derived hydrothermal fluid was poor in silica content compared to alkalis. The silica was leached during formation of Amph-II, was later used for the formation of alkali-feldspar during vein-filling stage.

Trace element geochemistry

The introduction of incompatible trace elements (Ba, Nb, Sr, Ta, Th, Zr and Hf) during metasomatism is well reflected in the whole-rock trace element geochemistry (Fig. 4.4a). Calcite, apatite, albite, biotite and ilmenite are the main carrier phases and discussed earlier. The REE budget of the altered alkali-pyroxenite is mainly contributed by the calcite and apatite formed by the hydrothermal fluid, thus resulting similar REE distribution pattern of the carbonatite and the altered alkali-pyroxenite. The Σ REE of the original alkali-pyroxenite can only be estimated if the contribution of apatite and calcite can be removed from the analyzed Σ REE of the altered rock. The contribution of the apatite and calcite to the bulk rock REE budget has been deducted in order to obtain the REE content of the original alkali-pyroxenite by a simple formula:

$[AAP_{REE} - \{(apatite_{REE} \times modal\% \text{ of apatite}) + (calcite_{REE} \text{ in AAP} \times modal\% \text{ of calcite in AAP} \times 1.31)\}]$. AAP: Altered Alkali-Pyroxenite. The Σ REE-content of apatite from altered rock is about 31% more compared to the apatite from carbonatite. Using this argument, it is assumed that the Σ REE is also 31% higher in the calcite from altered rock. The Σ REE content is found to be much lower in the original alkali-pyroxenite when compared with the altered rock (Fig. 6.4) and hydrothermal alteration caused enrichment of the REE. Moreover the higher Y and Σ REE of the apatite in the altered alkali-pyroxenite indicates that the mobilization of these elements took place by the hydrothermal fluid. It is already established that the fluid phase associated with the

carbonatite carry bulk of the Y and HREE relative to the magma (Bühn et al. 2001; Bühn, 2008). Now separation of this volatile phase would certainly give rise to carbo(hydro)thermal carbonatite (Mitchell, 2005) of secondary origin which will be enriched in HREE and Y. On the other hand, Sr behaves as compatible element during carbonatite formation and tends to remain in the crystal-melt phase rather than the fluid phase. So, the vein-filling apatite is enriched in Y and HREE and depleted in Sr compared to the apatite in the associated carbonatite (Fig. 6.5a). Similar relation has also been observed between the Y-(Nd/Ho)_{cn} (Fig. 6.5b) and Y-(Nd/Yb)_{cn} (Fig. 6.5c) suggesting that the MREE and HREE are fractionated more into the volatile phase rather than the magma.

Temperature, pressure and oxidation state

The sodic fenitization usually takes place at total pressure ranging 2-3 kbar (McKie, 1966; Vartiainen and Woolley, 1976; Le Bas, 1977). Using similar analogy it may be inferred that the sodic alteration of the alkali-pyroxenite also took place at similar pressure. Chakrabarty et al. (2009), based on the amphibole composition, has already been established hypabyssal origin of the Purulia carbonatite. The amphibole (Amph-I) composition of the alkali-pyroxenite is magnesiokatophorite (Table 2) and it contains more amount of Al in the T-site compared to the similar amphibole from carbonatite (Chakrabarty, et al., 2009). The absence of richterite which is essentially a low pressure and high temperature amphibole (Charles, 1975) also indicates that the alkali-pyroxenite was formed at greater depth relative to the associated carbonatite.

There is considerable variation observed in $[\text{Fe}^{3+}/\text{Fe}^{2+}+\text{Fe}^{3+}]$ -ratio among pyroxene, amphibole (Amph-II) and biotite (Fig. 6.6). This ratio is about 0.8 in the unaltered alkali-pyroxene and goes down to 0.2 when pyroxene alters to amphibole. The lowering of this ratio indicates less dominant role of $f\text{O}_2$ during alteration from pyroxene to amphibole or the environment was reducing (Fig. 6.6). The $[\text{Fe}^{3+}/\text{Fe}^{2+}+\text{Fe}^{3+}]$ -ratio of the biotite is very high around 1.0. The further late stage alteration of Amph-II to biotite or pyroxene to biotite took place at higher oxidation state. Increase

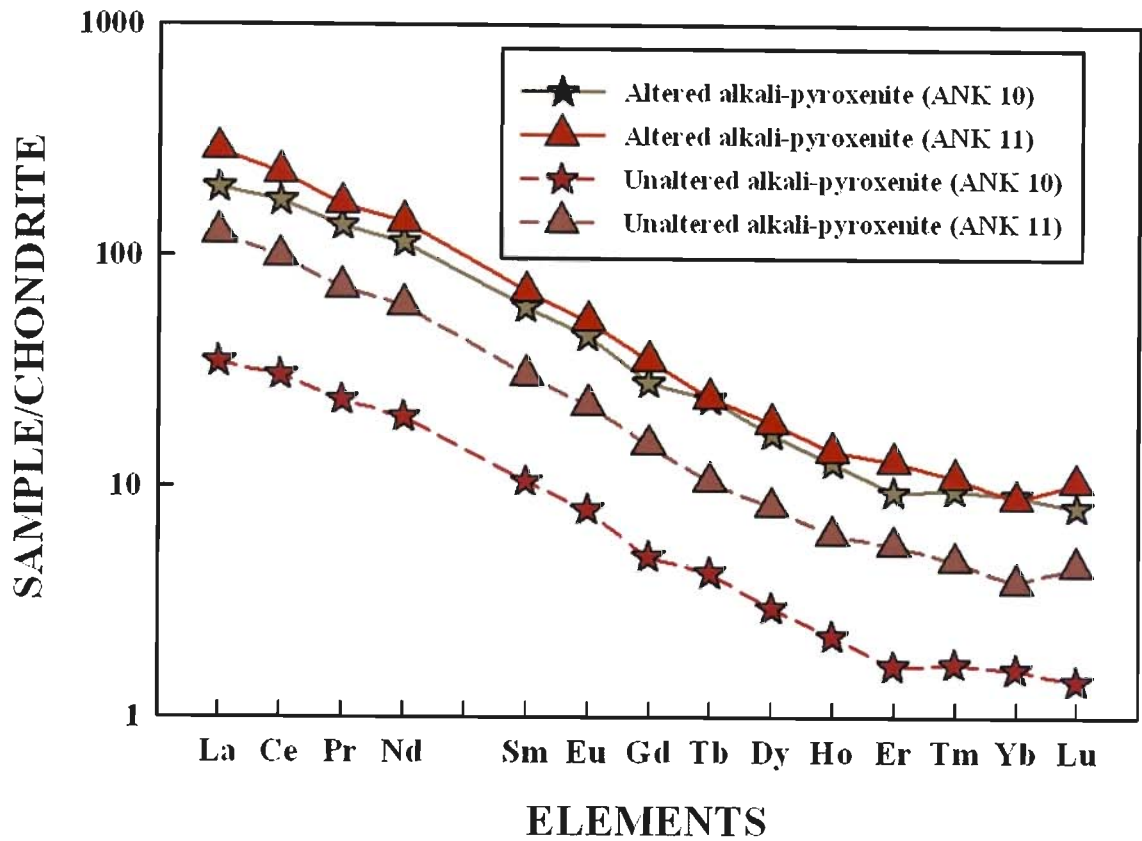


Fig. 6.4 REE plots of the metasomatized and unaltered alkali-pyroxenite. Please note the lower level of REE enrichment in the unaltered alkali-pyroxenite compared to the altered equivalent, suggesting introduction of REE during metasomatism. Normalizing values are from Sun and McDonough (1989).

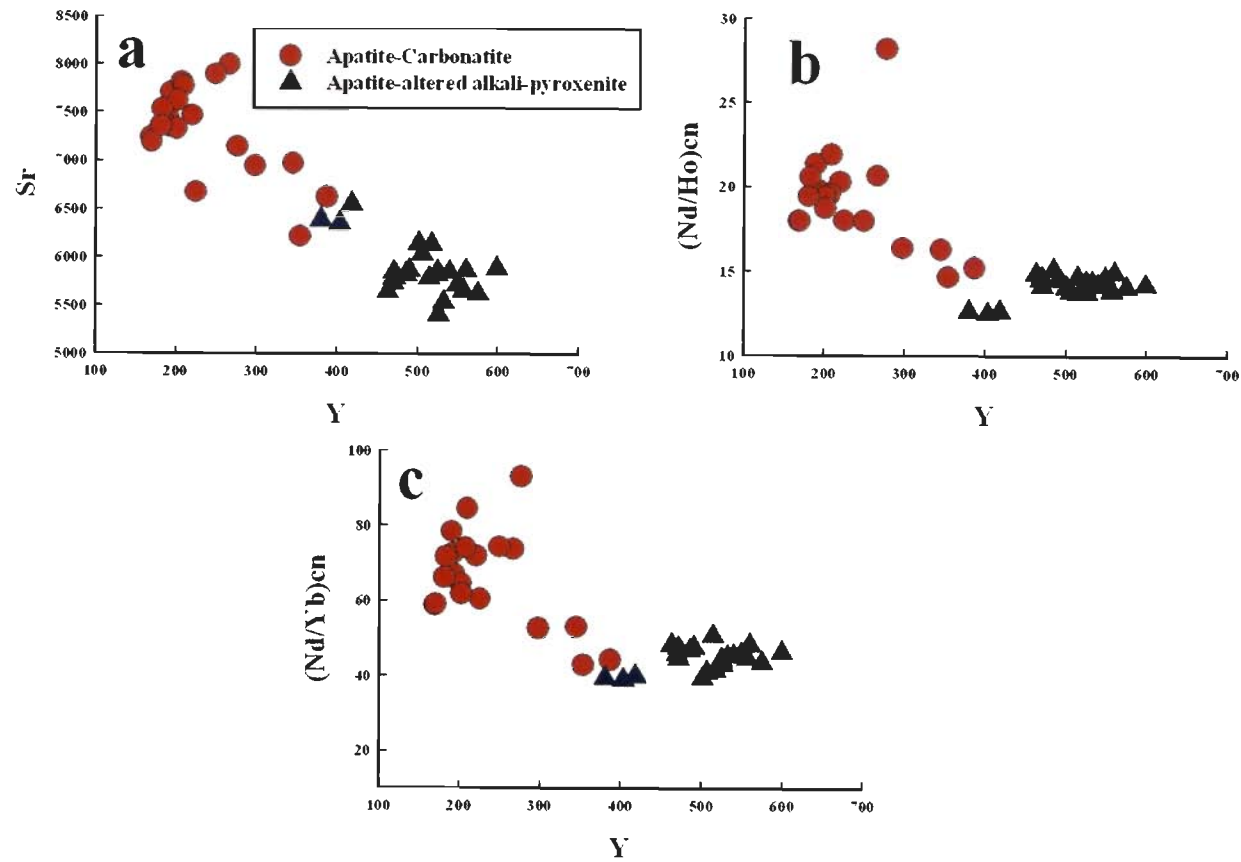


Fig. 6.5 Y-Sr (a), Y-(Nd/Ho)_{cn} (b) and Y-(Nd/Yb)_{cn} (c) plots of apatite from the metasomatized alkali-pyroxenite and carbonatite. See text for detail explanations.

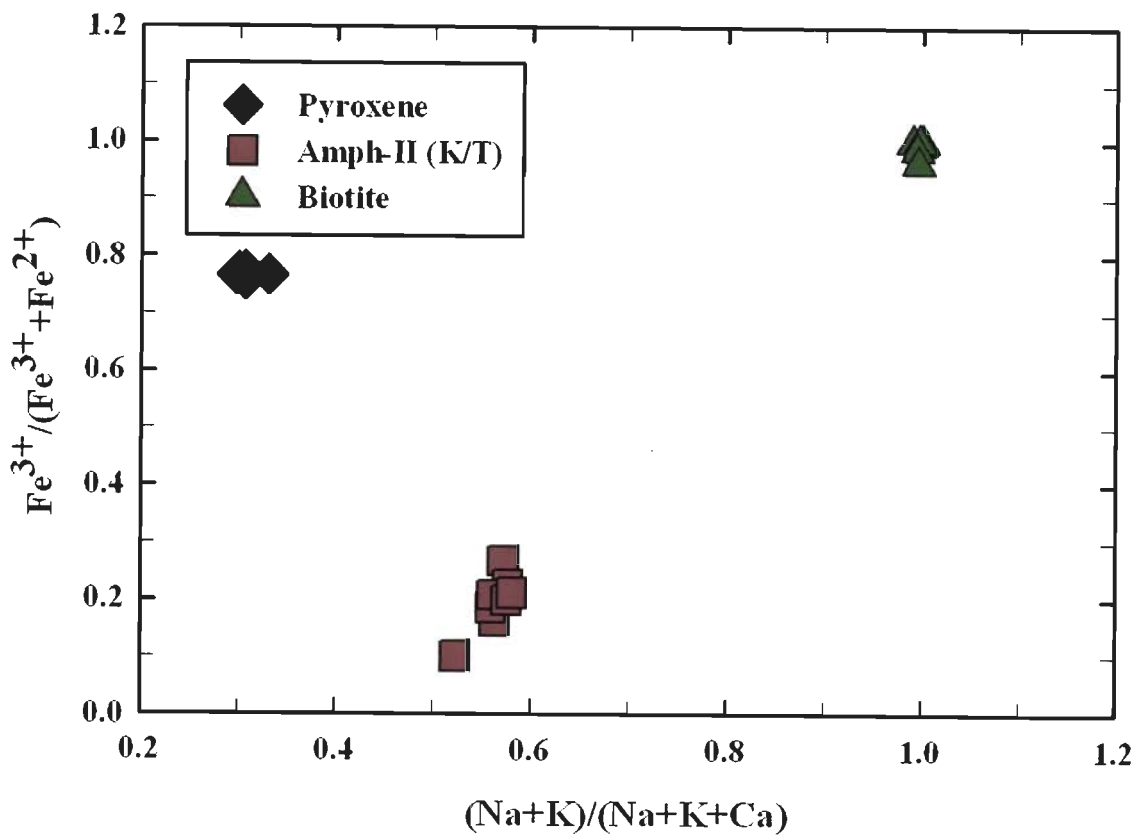


Fig. 6.6 $\text{Fe}^{3+}/(\text{Fe}^{3+}+\text{Fe}^{2+})$ (oxidation ratio) vs. $(\text{Na}+\text{K})/(\text{Na}+\text{K}+\text{Ca})$ (alkalinity) plot of pyroxene, Amph-II and biotite from the alkali-pyroxenite. The oxidation ratio is lower during alteration of pyroxene to Amph-II. The ratio was highest during formation of the biotite.

in oxidation ratio during the formation of late biotite is related to the development of calcite. The crystallization of calcite took place when X_{CO_2} was much more dominant than fO_2 . But after the calcite formation, the fO_2 condition of the hydrothermal fluid changed and increased substantially. Formation of oxide at this stage is also indicative of high $[Fe^{3+}/Fe^{2+}+Fe^{3+}]$ -ratio or fO_2 condition. The magnetite crystallized from hydrothermal fluid is characteristically low in Ti-content and the ilmenite is very low Mg but Mn rich. This is indicative of low temperature formation. The rough temperature range using magnetite-ilmenite composition is about 400-450°C and $\log fO_2$ is around -30 to -31 atm (Charmichael, 1967; Spencer & Lindsley, 1981; Andersen & Lindsley, 1985).

During the pyroxene alteration, increase in $[Na+K/Na+K+Ca]$ -ratio with lowering of $[Fe^{3+}/Fe^{2+}+Fe^{3+}]$ -ratio (Fig. 6.6) is noticeable. The 'F' must have played very major role in controlling this physico-chemical conditions. Thus the alteration process has affected both composition of the fluid and the oxidation state. The overall evolution of the alteration process in the study area is shown in a schematic diagram (Fig. 6.7).

6.1.4 Geochemical signatures

Trace elemental data provides the useful information to decipher the parental magma and evolutionary process of carbonatite and associated silicate rocks. In general carbonatite is enriched in Sr (8500-11200 ppm), Ba (797-1784 ppm) and REE. In the primitive mantle normalized plot (Fig. 4.4a) the Purulia carbonatite is characterized by poorer Rb, Zr and Hf while enriched in Sr, La, Ce and Sm (Fig. 4.4a) compared to the associated alkali-pyroxenite. The pattern of the carbonatite spider diagram is very similar to that of the world-average of the calico-carbonatite (Woolley and Kempe, 1989) other than Nb which is showing prominent negative anomaly. Between carbonatite and alkali-pyroxenite, carbonatite is relatively enriched in Sr, Th, U and Nb, while the later is relatively enriched in all compatible elements (Sc, V, Co, Ni, Cu and Cr), Ba and Rb. The relative enrichment of compatible elements supports the early crystallization of pyroxenite

compared to the carbonatite. On the other hand, introduction of incompatible elements in this rock is certainly caused by the metasomatic process. The metasomatized rock is enriched in Rb, Zr and Hf relative to the carbonatite.

This has been already established that the higher abundances of Ba and Sr and $Sr/Ba > 1$ are characteristics of carbonatites (Keller and Spettel, 1995). In case of Purulia carbonatite the Sr/Ba ranges from 6.23 to 10.81 and thus characterizing the carbonatite of primary magmatic origin as in Newania (Pandit et al., 2002) and is in well agreement with other reported carbonatite complexes of the India (Krishnamurthy, 1988). This ratio (Sr/Ba) ratio is also found to be falling distinctly within the range of calico-carbonatite (Woolley and Kempe, 1989). Enrichment of Ba in carbonatite and alkali-pyroxenite (Fig. 6.8a) in Ba-Sr plot is mainly due to the presence of calcite in these rocks. In general, calcite contains much higher concentration of Ba and Sr compared to the apatite (Kjarsagarrd, 1998). So, the calico-carbonatites (as in case of present study) containing almost 90% calcite, by volume, are enriched in Ba and Sr. Moreover, the apatite in middle to late stage carbonatite is generally enriched in Sr compared to the early stage carbonatites, which are generally enriched by F (Hogarth, 1989).

The Zr/Hf ratio for carbonatite is ranging from 33.57-66.35 which is very close to the averages of all carbonatites i.e. 59.6 (Chakhmouradian, 2006) but well below the carbonatites associated with alkali-ultramafic rocks (168.4) (Samoylov, 1984). But the enrichment of Zr over Hf can be attributed to the carbonate metasomatism in the mantle source (Rudnick et al., 1993).

Nb and Ta behave as a conjugate geochemical pair in most of the silicate igneous rocks and Nb preferentially fractionated into the silicate melts relative to the Ta (Veksler et al., 1998). The carbonatite showing variable concentrations of Nb (Fig. 6.8b, c) and the higher concentration of Nb along with U in two samples can be attributed to the possible presence of pyrochlore in small quantity. Moreover the Nb/Ta of carbonatite ranging from 18-21 which is very close to the

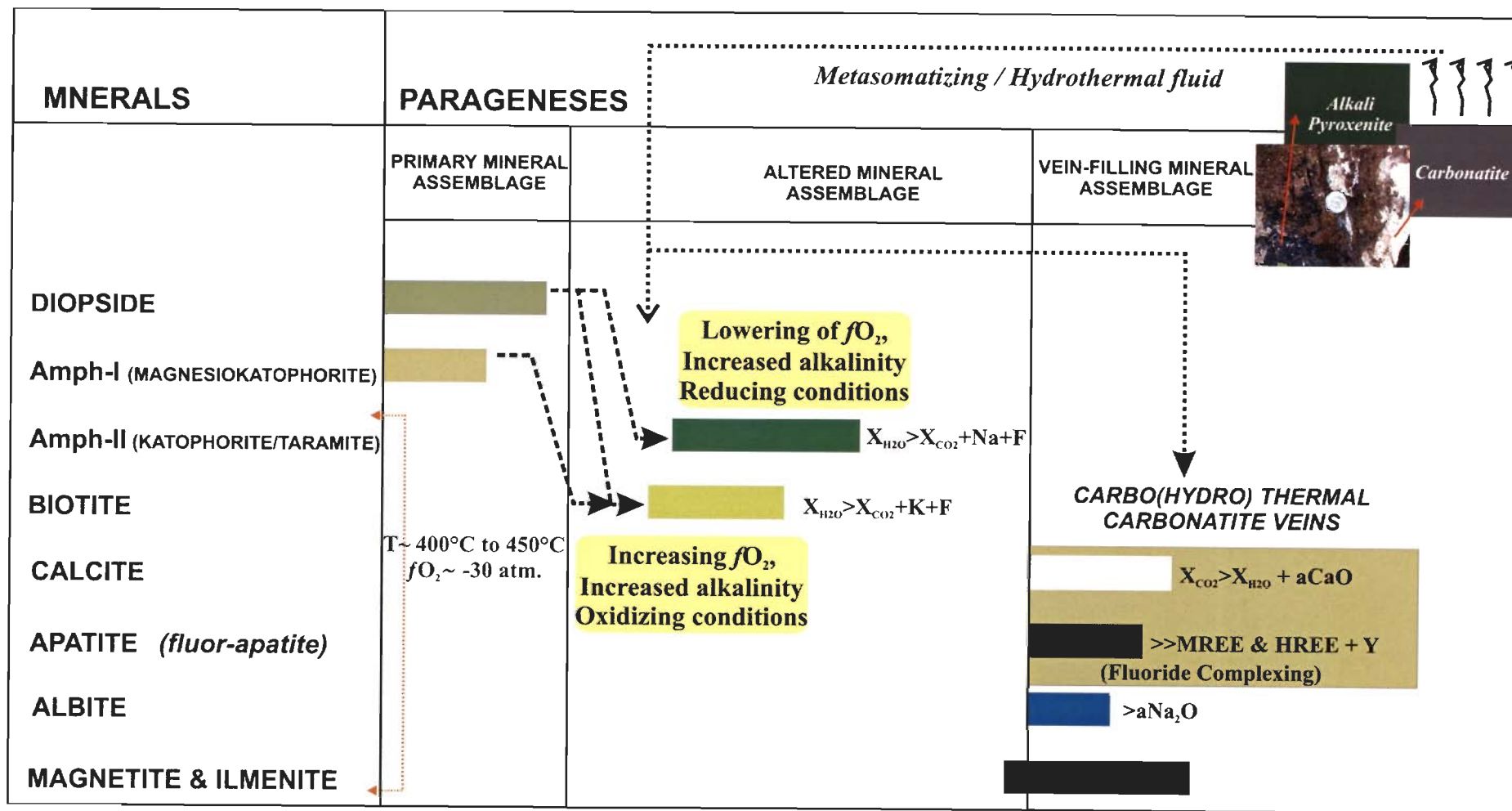


Fig. 6.7 Generalized sequence of formation of different mineral assemblages in the alkali-pyroxenite during metasomatic alteration.

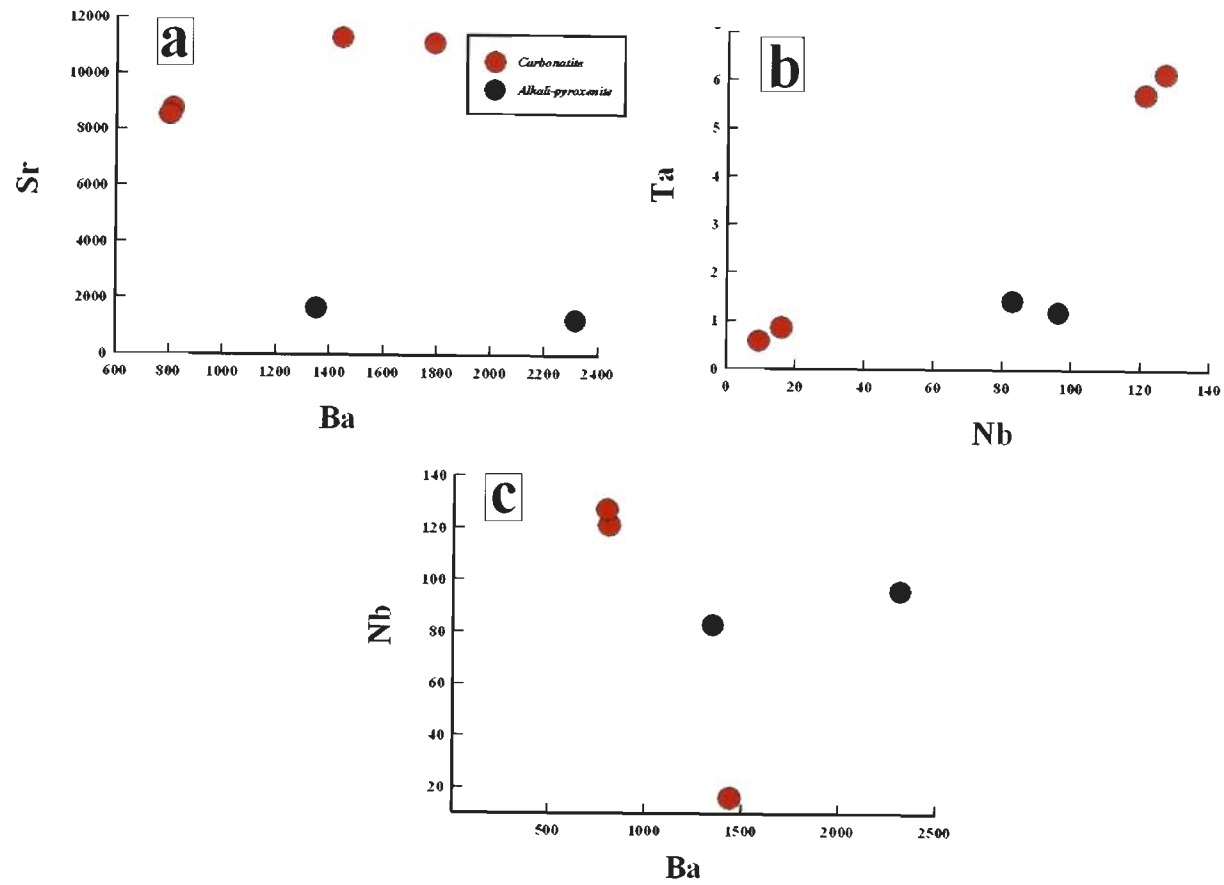


Fig. 6.8 Bivariant plot (whole rock samples) of different trace elements (a) Ba-Sr, (b) Nb-Ta and (c) Ba-Nb. (For detail description see section 6.1.4)

carbonatites (22.3) associated with alkali-ultramafic rocks (Samoylov, 1984). The Nb-Ta bivariate plot (Fig. 6.8b) between the carbonatite and alkali-pyroxenite reveals the opposite trend mentioned by the Veksler et al. (1998) relative enrichment of Nb in carbonatite and thus can not justify the formation of this carbonatite by the process of liquid immiscibility. It may be noted that alkali-pyroxenite have very low Nb-Ta content. This rock which crystallized at an early stage of fractionation was expectedly Nb-poor. A small amount of Nb has possibly been added to Nb-poor alkali-pyroxenite during late stage metasomatism. The most notable feature of the studied carbonatite is the depletion of HFSE and enrichment in LILE (except Th and U) compared to average carbonatite. Depletion in HFSE (extensive for Nb, Zr) invokes the possibility of formation of the Purulia carbonatite by fractional crystallization from a carbothermal fluid (Mitchell, 2005). Though, such depletion can not be taken as a thumb rule for carbothermal origin as many carbonatites of magmatic origin is also reported where they are essentially depleted in HFSE e.g. Eden Lake carbonatite, Manitoba, Canada (Chakhmouradian et al., 2008); Turij massif, Kola Peninsula, Russia (Dunworth and Bell, 2001); Bayan Obo, Mongolia, China (Le Bas et al, 1992). Again, the lack of usual silicate association of ijolitic-pyroxenite further strengthens the possibility of carbothermal derivative for the Purulia carbonatite (Woolley and Kjarsgaard, 2008). The present survey and world data base of Woolley and Kjarsgaard (2008) suggest that the association of only pyroxenite and carbonatite is commonly related to the carbothermal carbonatite. Hence, the available data set can not satisfactorily point out the exact process involved in the genesis of this carbonatite.

The REE enrichment follows the sequence: carbonatite>metasomatized alkali-pyroxenite. The REE have been introduced in alkali-pyroxenite by metasomatic process. The main carrier phases are calcite and apatite present as vein-filling in this rock. The REE trend along with the compositional gap points towards early formation of the alkali-pyroxenite relative to the

carbonatite resulted low Σ REE concentration in this rock. The overall similar trend of the chondrite normalized REE distribution pattern (Fig. 4.10b) is indicative of cogenetic nature of these two rocks.

6.1.5 Apatite and Calcite as petrogenetic indicators

Apatite (fluor-apatite) can be used as a good petrogenetic indicator in carbonatite system. The REE trend of apatite can give useful information regarding the process involved in the formation of carbonatite by liquid immiscibility or fractional crystallization (Bühn et al., 2001; Dawson and Hinton, 2003, Brassinnes et al., 2005). In the present case apatite is analyzed from carbonatite and metasomatized alkali-pyroxenite along with calcite analysis from the one carbonatite sample (Chapter 4, Section 4.5.2). The partition coefficients between apatite and calcite and vice-versa which are separated from the carbonatite are presented in Table 6.1. The partition coefficients reveal that the U, Sr, Pb is partitioned almost double in the calcite and similarly Rb and Y in the apatite. The apatite is characterized by the much higher partition coefficients in all the REE. Thus the major contributor and carrier of REE in carbonatite is apatite than the calcite and such inferences are very common and in well accord with the other known carbonatite complex of the world viz. Phalaborwa, South Africa (Dawson and Hinton, 2003); Vuoriyarvi, Kola Peninsula, Russia (Brassinnes et al., 2005). The similar feature is also summarized by Kjarsagarrd (1998) from the apatite and calcite from different carbonatites around the world.

The Y/Ho ratios in the apatites from three rocks are very similar (~ 23) and below the chondritic value of 27.7 (Sun and McDonough, 1989). The highest Y/Ho ratio being observed for calcite in carbonatite (27.16) very close to chondritic value. There is no general consistent behavior of Y/Ho fractionation observed in the carbonatite system.

It is widely recognized that carbonatites in general contain highest REE concentration, with relatively large amount of LREE. The present study also corroborates the similar feature where apatites are containing bulk of the REE with enriched LREE. The study on different carbonatites from different part of the world (Kjarsagarrd, 1998; Bühn et al., 2001) shows a steady decrease from La to Tm. Apatites of carbonatite when plotted in a $(La/Yb)_{cn}$ vs. $(La/Nd)_{cn}$, $La (cn)$ vs. $(La/Yb)_{cn}$ and Sr vs. Y plot (Fig. 6.9a, b, c) respectively shows a prominent positive correlation which is in accord with the apatite from the Kalkfeld and Ondrakorume (Namibia), Homa Mountain (Kenya) and Otjisazu (Namibia) (Bühn et al., 2001). Such similarity with the apatites from the above mentioned carbonatite complexes are in accord with the primary magmatic origin. Moreover, the negative correlation has been noticed between Y and Sr (Fig. 6.9d) is also well accord with the data set of Bühn et al (2001). The enrichment of MREE and HREE over LREE coupled with Y in the apatites of alkali-pyroxenite points the role of fluoride complexing responsible for the generation of these apatites and already discussed earlier (Section 6.1.3). The formation of these apatites were essentially related to the volatile enriched fluid phase expelled from the associated carbonatite and resulting the vein filling assemblage (calcite+apatite) in alkali-pyroxenite is somewhat similar to the carbothermal carbonatitic assemblage (Mitchell, 2005).

The REE composition of carbonatite fluorapatites can represent different stages of carbonatite differentiation (Bühn et al., 2001). It has been found that the early fluorapatites are characterized by the low ΣREE content, regardless of the REE content of the whole rock. Moreover they have low $(La/Yb)_{cn}$ generally below 100 and that of the $(La/Nd)_{cn}$ close to or below unity (Bühn et al., 2001). The similar feature is observed for the apatites in carbonatite and these ratios are found to increasing from carbonatite to metasomatized alkali-pyroxenite. This indicates that the apatite from the alkali-pyroxenite is certainly of late stage origin compared to the apatite of associated

carbonatite. The steady decrease in $(La/Yb)_{cn}$ in apatite from carbonatite i.e. humped or steeper REE trend does not support their crystallization by fractionation (Dawson and Hinton, 2003).

6.1.6 Isotopic Studies

Most of the younger carbonatite (≤ 200 Ma) of the globe are found to be generated by the mixing of EM I and HIMU mantle end members (Bell and Tilton, 2001, Bell and Blenkinsop, 1989). As most of the carbonatites are found in continental settings, the common assumption is that the metasomatized continental lithosphere plays an important role in the generation of the carbonatitic magma. On the basis of the Sr isotopes Bell et al. (1982) suggested that the Canadian carbonatites formed from magmas generated by melting of Archaean depleted sub-continental lithosphere and a long-lived heterogeneity in the upper mantle was present between 2800-1000 Ma.

In the present study an attempt has been made to estimate the source for the carbonatite on the basis of Sr and Pb isotope data. Limited data set along with the unavailability of the Nd isotopic data constrains the source characterization for these rocks. Moreover the very high $^{206}Pb/^{204}Pb$ (21.53 - 83.94) ratio of carbonatite made the source characterization extremely difficult. The repeat analysis of the two samples (ANK 1 and ANK 3) yielded very high $^{206}Pb/^{204}Pb$ ratio and it has been observed that the U ratio is also very high in these two samples. In spite of the high U concentration in these two samples the Pb concentration is found to be very similar with the other analyzed samples. The similar feature has also been reported from the Newania and Sevattur, the two oldest carbonatite of the Indian subcontinent of 1551 ± 46 Ma and 801 ± 10 Ma respectively (Schleicher et al., 1997). The reported $^{206}Pb/^{204}Pb$ value for these two Precambrian carbonatite complexes is also very high and reaches maximum up to 268 ± 0.09 (Schleicher et al., 1997). Similar higher $^{206}Pb/^{204}Pb$ ratio (maximum up to 61.1 for the bulk rock and 89.5 for apatite) also reported from the Tikshezero carbonatite complex of Kola Alkaline Province, Russia

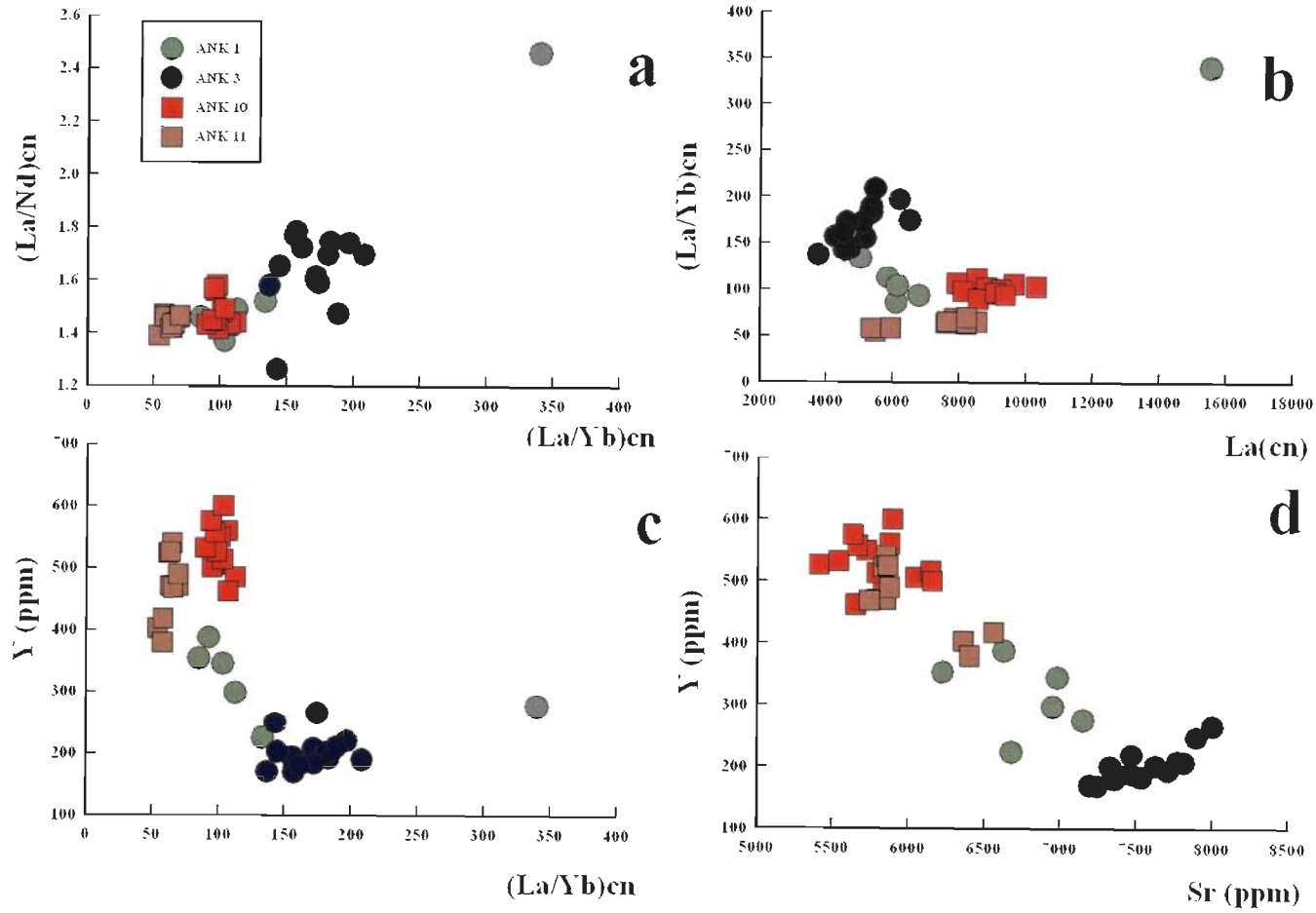


Fig. 6.9 Different bivariate plot of the apatite grains separated from the carbonatite and metasomatized alkali-pyroxenite. (For details see section 6.1.5)

(Tichomirowa et al., 2006). In case of the Newania it was postulated that the high Pb isotopic ratios can be attributed to the crystallization of U-rich mineral phases and Pb must have been resided in an intermediate reservoir, either enriched mantle or crust, prior to the carbonatite formation (Schleicher et al., 1997). Thus the contribution of the Pb from the crustal source is more likelihood and contributed to the bulk rock Pb budget. It has already been mentioned that the Pb concentration in all the analyzed carbonatite does not show significant variations in spite of the high U concentration in the two samples. There may be more than one explanation for such observation. One possibility is the presence of an intermediate reservoir with enrichment of Pb which is responsible for such high Pb isotopic ratio in carbonatite. The other mechanism that must allow such Pb enrichment is the mobilization of Pb in a metasomatic fluid and its subsequent removal from some mantle segment (Zindler and Hart, 1986). The $^{206}\text{Pb}/^{204}\text{Pb}$ ratio of carbonatites is well beyond the limits of the mantle end members: DMM, EM1 and HIMU and thus source characterization is not possible with the available data set generated in the present work. The only similarity is that the initial $^{87}\text{Sr}/^{86}\text{Sr}$ of the Purulia carbonatite is similar to that of the HIMU. Moreover the $^{87}\text{Sr}/^{86}\text{Sr}$ ratio when plotted against the model age (1.37 Ga) (Fig. 6.10) is found to be falling in the hatched area along the growth line for the Bulk Earth (DePaolo and Wasserburg, 1976; Nions et al., 1977; Allegre et al., 1979, Bell et al., 1982) indicating the depleted mantle source for the carbonatite. The above observation also indicates existence of mantle heterogeneity at ≥ 1.4 Ga and is in accordance with the long-lived mantle heterogeneity between 2800 to 1000 Ma (Bell et al., 1982). The similar mantle heterogeneity is also reported by Pandit et al. (2002) from the South India carbonatites (Hogenakal, Samalpatti, Sevattur, Pakkanadu). Thus the existence of long-lived mantle heterogeneity during Palaeo-Neoproterozoic can be invoked for the sub-continental mantle lithosphere under the Indian subcontinent.

6.1.7 *Petrogenetic model*

Two possibilities have been emerged regarding the genesis of the Purulia carbonatite: crystallization from a i) primary mantle derived carbonate magma or ii) late stage carbothermal fluid of unknown descent. Several arguments can be put forward in favour or against both the possibilities. For example, depletion in HFSE (strong Nb depletion with respect to the world average of calico-carbonatite given by Woolley and Kempe, 1989) coupled with association of alkali-pyroxenite favour the origin from carbothermal fluid (Mitchell, 2005; Woolley and Kjarsgaard, 2008). However, there are many examples carbonatites where the Nb concentration is low (similar to the studied carbonatite; e.g. Eden Lake carbonatite where Nb in calico-carbonatite is below detection limit and silicate rich carbonatite ~4 ppm.; Chakhmouradian et al., 2008) or even below the detection limit or absent of primary magmatic origin. The most convincing evidence in favour of the genesis of the Purulia carbonatite from primary carbonatitic magma of mantle origin lies within the $^{87}\text{Sr}/^{86}\text{Sr}$ ratio of the apatite (0.70340-0.70335) and whole rock (0.70340-0.70330) respectively. In spite of the post magmatic changes, the lowest $^{87}\text{Sr}/^{86}\text{Sr}$ ratio should reflect the least affected sample by post magmatic changes and the same is 0.70330 and in agreement with the mantle value for normal basalt and carbonatite (Faure and Hurley, 1963; Barker; 1989). It is already discussed that the carbonatite had undergone post magmatic deformational and tectono-thermal events related to metamorphism and metasomatism, to a lesser extent, but the $^{87}\text{Sr}/^{86}\text{Sr}$ is falling well within the range of mantle values in spite of the post magmatic changes. Primary magmatic/carbothermal origin debate cannot be resolved, at present, due to lack of further supporting evidences from Sm-Nd and stable isotope data.

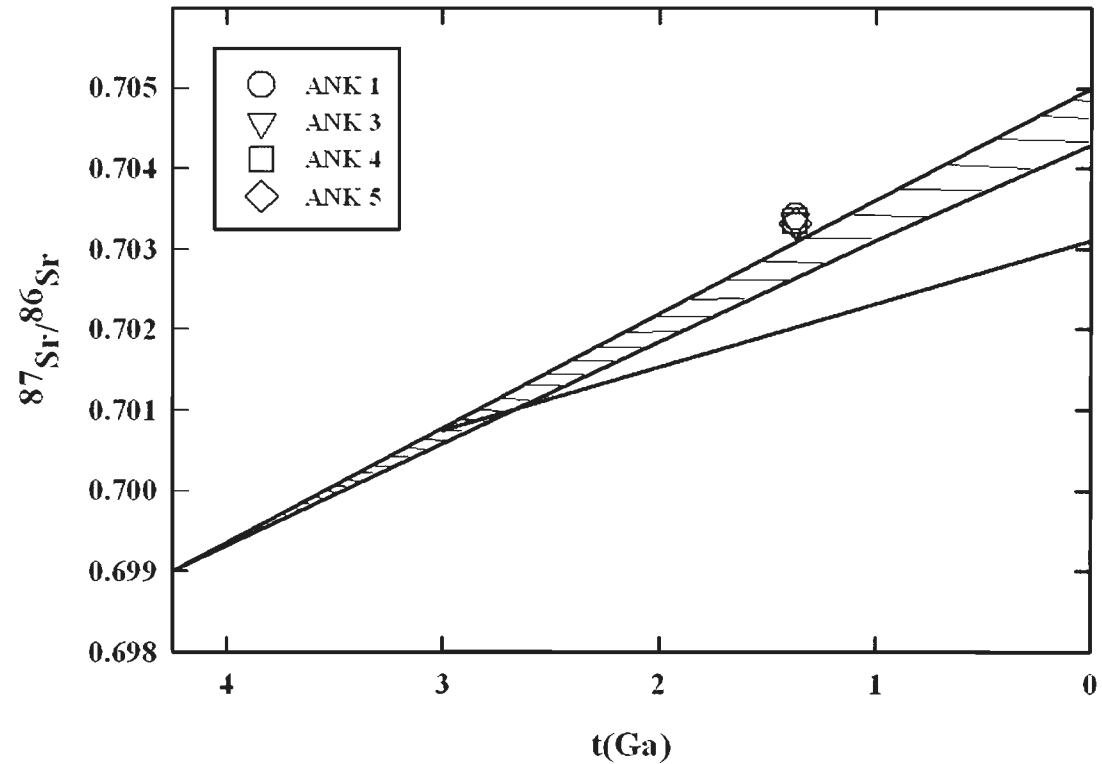


Fig. 6.10 $^{87}\text{Sr}/^{86}\text{Sr}$ growth lines for bulk Earth are contained within hatched envelope, the line shown is the best estimate for the depleted mantle source (Bell et al., 1982). The data of the Purulia carbonatite falls close to the hatched envelope. The age of the carbonatite (1.37 Ga) indicates the existence of long-lived mantle heterogeneity during this period of time.

6.2 NEPHELINE SYENITES

6.2.1 *Field and Petrographic signatures*

Floor (1974) gave a detailed account on the textural and chemical characteristics of alkaline rocks which were formed by the igneous or the metamorphic-metasomatic processes. The studied nepheline syenites are present within the host rock which in turn suffered metamorphism under greenschist to amphibolite facies condition. This makes difficult to distinguish the studied rocks of igneous or metamorphic-metasomatic origin. The distinction between the igneous and metamorphic-metamorphic process involved can be best attributed by the detailed systematic textural and mineralogical studies of these rocks as shown by Duke and Edgar (1977) from the famous alkaline complex of Canada e.g. Haliburton and Bancroft area. The present nepheline syenites are also remarkably similar to that of the nepheline syenite gneiss of Haliburton-Bancroft area. The field relations among the two varieties of studied nepheline syenites namely banded syenite and massive syenite is scanty and no contact or any other relations observed between them. They are exposed as individual litho-units covering an area of approximately 200x20 square meters. All the litho-units represent a dike like structure. The banded variety can further be subdivided into two sub-categories depending on the intensity of banding: poorly banded and strongly banded syenite gneiss. Both the poorly and strongly banded syenite gneiss is essentially composed of albite, orthoclase, nepheline and aegirine but the albite is the dominant felsic component in the later variety. On the other hand the massive syenite is characterized by the complete absence of mafic constituents except few late stage Mn-rich biotites. In both the variety post magmatic deformational activities related to metamorphism and metasomatism is prominent. Now, it is important to distinguish the effect and extent of post magmatic effect in the studied nepheline syenite and to estimate the same mineralogical assemblages were studied in details and

an attempt has been made to distinguish the metamorphic and igneous assemblage with the available limited data generated in this study.

6.2.1.1 *Feldspar and nepheline paragenesis*

In both the varieties of syenites the dominant felsic constituents are feldspars and nepheline. The banded syenites both the strongly and poorly banded syenites are characterized by the large albite, orthoclase (microcline) and nepheline. The grain size is relatively fine in the massive variety of syenite. The feldspars and nephelines of the studied nepheline syenites of both the variety are showing a narrow range of compositions (*Banded Syenite*: Or_{~95}Ab_{~5}An₀, Ab_{~99.5}Or_{~0.5}An₀, Ne_{74.5-76.1}Ks_{19.5-19.8}Qtz_{5.7-4.4}; *Massive Syenite*: Or_{~98.5}Ab_{~1.5}An₀, Ab_{~99.1}Or_{~0.8}An_{~0.1}, Ne_{69.61-77.35}Ks_{19.02-22.04}Qtz_{9.36-0.25}) (Fig. 3.27) indicating that they were recrystallized at low temperatures by metamorphic-metasomatic process. It has already been established that the whole rock compositional range of coexisting alkali feldspar and nepheline assemblages corresponds to equilibrium temperatures of 400-600°C (Perchuk and Ryabchikov, 1968). Assemblages formed below 500°C have a narrow range of composition and approaches towards the Morozewicz-Buerger convergence field indicating the adjustment of the composition of the minerals takes place during cooling and most probably during post magmatic recrystallization. The end member composition of the feldspars, presence of microcline along with the nepheline composition falling within the Morozewicz-Buerger convergence field of plutonic nepheline indicate that the original rock (subsolvus nepheline syenitic assemblage) (Fig. 3.27) was formed by the igneous process and had undergone extensive metamorphism resulting the present day recrystallized assemblages similar to the *nepheline gneisses*. Pure end member composition of the feldspars constrains accurate temperature estimates for the feldspar paragenesis. The temperature obtained using feldspar thermometry is quite different for the two varieties of syenite. The feldspars from banded variety (strongly banded syenite gneiss) yields a temperature of 500°C (Fig. 6.11) which is

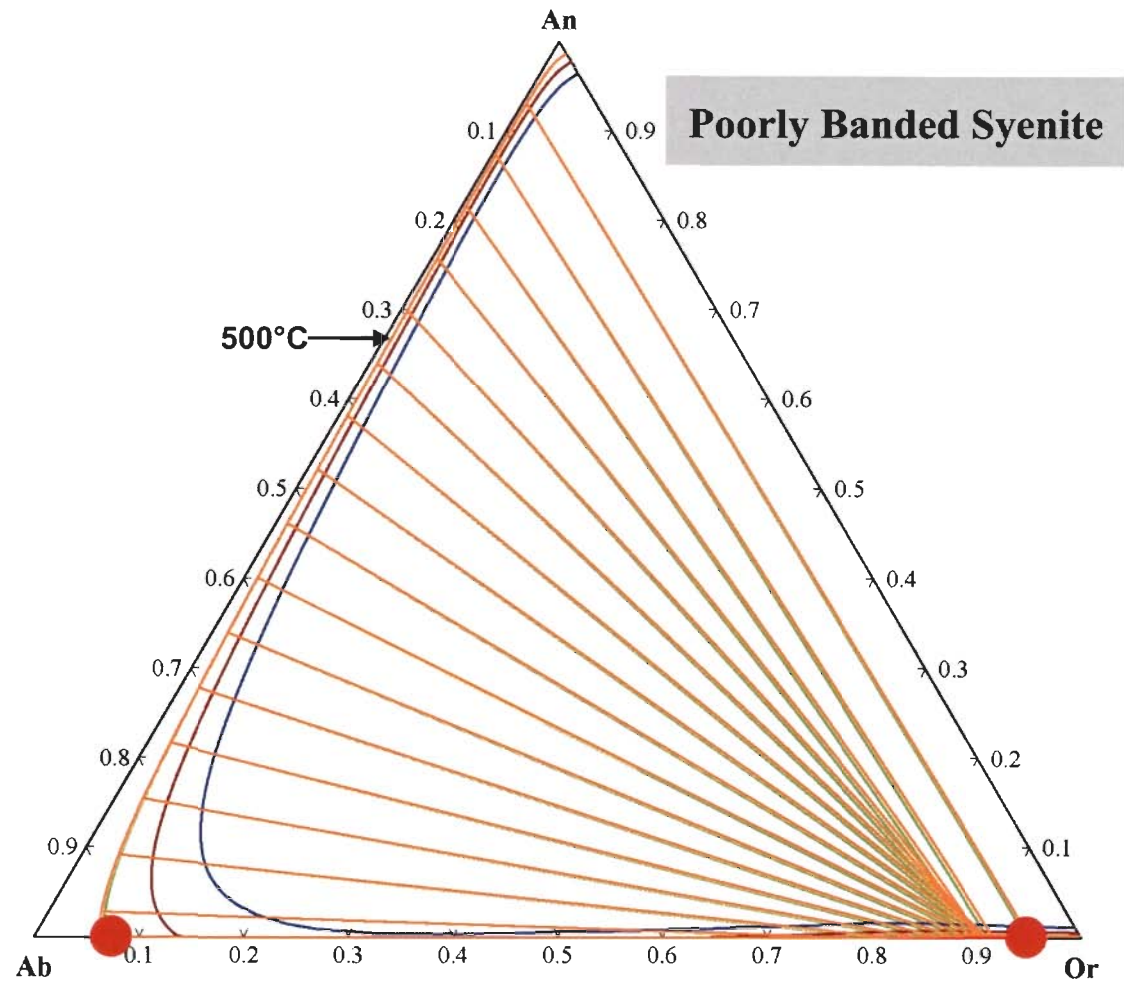


Fig. 6.11 Feldspar thermometry (of Fuhrman and Lindsley, 1988) used for banded syenite (poorly banded syenite gneiss) showing equilibration temperature of 500°C for albite and orthoclase.

consistent with co-existing nepheline falling within the Morozewicz-Buerger field of plutonic nepheline of 500-600°C temperature. On the other hand the coexisting nepheline and feldspars from the massive syenite yields contrasting temperature. The nepheline of this variety gives a temperature range of about ~700°C and that of the feldspar is 200°C (Fig.6.12). The consistent compositions of the nephelines on the Morozewicz-Buerger field convergence field indicate that the crystallizations have taken place close to the solidus temperature (Tilley, 1954). The plot of the nepheline parallel to the NaAlSiO₄- KAlSiO₄ join in the NaAlSiO₄- KAlSiO₄-SiO₂ system indicates that an exchange of material (K and Na) at subsolidus temperatures with constant Al/Si ratio (Hamilton, 1961). Alkaline rocks with decreasing temperature are susceptible to low temperature syngenetic metasomatic process which include microclinization (replacement of K by Na) and albitization (replacement of Na by K) (Perchuk and Ryabchikov, 1968). If this occurs below 500°C the nephelines will approach towards the Morozewicz compositions and the feldspars will be of pure end member compositions. On the other hand the low temperature of equilibration shown by the feldspars of massive syenite is also in agreement with the re-equilibration temperature of the nepheline syenites at McGerrigle alkaline complex (Wallace et al., 1990). Thus it is clear from the nepheline-feldspar paragenesis that the studied nepheline syenites were essentially formed under plutonic conditions and later subjected to post magmatic metamorphism and metasomatism which recrystallized the plutonic nepheline syenites to nepheline syenite gneiss. The equilibration crystallization temperature is estimated approximately close to the solidus as shown by the nepheline-feldspar paragenesis of the poorly banded syenite gneiss. The re-equilibration temperature goes down up to 200°C indicating subsolidus recrystallization for massive syenite. The subsolidus recrystallization was probably the result of deuteric alteration which the rock experienced after their formation. Microclinization, albite rimming (albitization), eudialyte formation and replacement of nepheline by analcime and sodalite are the direct

consequence of such low temperature metasomatic effect. Similar metasomatism is also reported from the several part of the world e.g. Motzfeldt Intrusion, South Greenland (Schönenberger and Markl, 2008); Pilansberg alkaline complex, South Africa (Liferovich and Mitchell, 2006) and termed such metasomatism as autometasomatism and the fluid (deuteric fluid rich in Na and Cl) is part of the magmatic system itself and not derived from an exogenous sources. Similar autometasomatism is also evident within the studied nepheline syenite and as a result of such subsolidus deuteric alteration of the original miaskitic nepheline syenite got enriched in alkalis, particularly in Na and changed towards agpaitic nepheline syenite.

6.2.1.2 Behaviour of pyroxene in response to metamorphism

Pyroxene is found to be the dominant mafic constituents of banded syenite and essentially acmitic (aegirine) in composition (Table 3.13, 3.16; Fig. 3.16). Al is characteristically partitioned to M1-site as ^{VI}Al (a.p.f.u.) and totally absent in ^{IV}Al (a.p.f.u.) or T-site. Such ^{VI}Al -site preference may be due to post-crystallization metamorphism suffered by these rocks (Woolley et al. 1996). Their work on the agpaitic and miaskitic nepheline syenite of the North Nyasa Alkaline Province (NNAP) of central and northern Malawi, eastern central Africa clearly distinguishes the metamorphic and igneous suites of pyroxene. In the present study, the pyroxene of the banded syenites is compared with that of the NNAP. The pyroxenes of banded variety of syenites are similar to that of the igneous group of Ilomba complex, Chikangawa and Chilwa province (Fig. 6.13a, b) of Woolley et al. (1996). These are characteristically enriched in ^{VI}Al (a.p.f.u) but the extent of enrichment is less compared to the Kasungu & Chipala complex and Ilomba complex (Fig. 6.13). On the other hand on a $^{VI}Al-(Na-Fe^{3+})$ plot, the pyroxene clearly falls within the metamorphic group similar to that of the ^{VI}Al rich type of Kasungu and Chipala complex (Fig. 6.14a). The same plot (Fig. 6.14b), when compared with the pyroxene of the Ilomba complex, falls

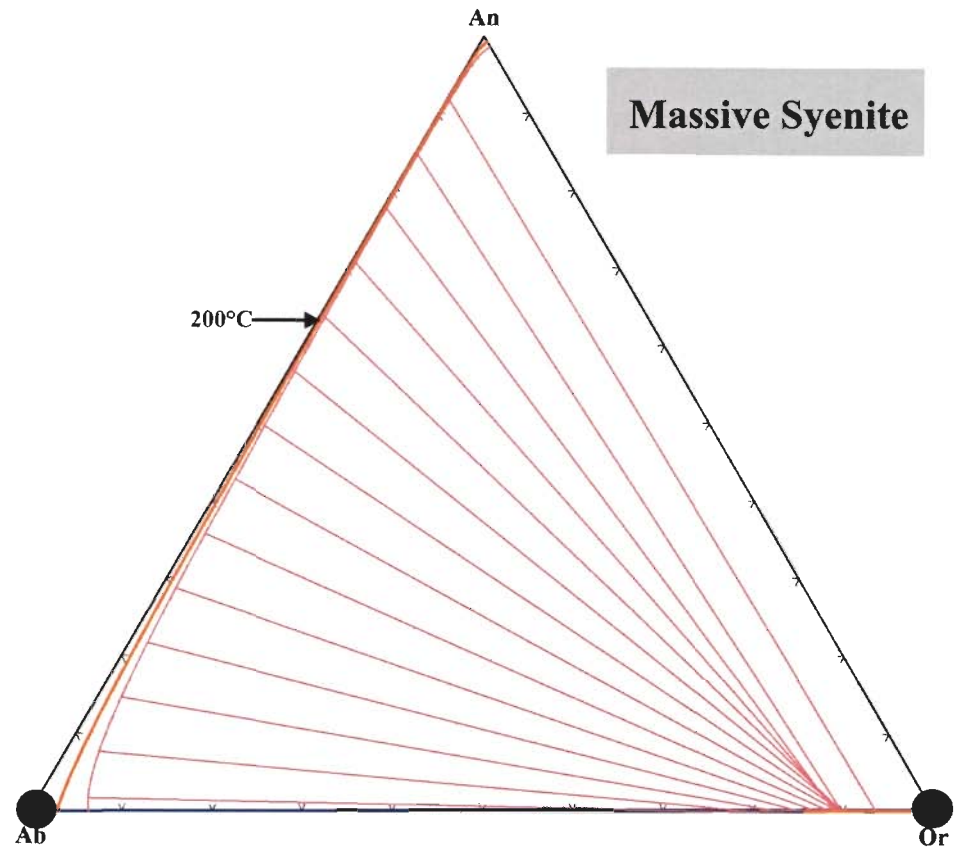


Fig. 6.12 Feldspar thermometry (of Fuhrman and Lindsley, 1988) used for massive syenite showing equilibration temperature of 200°C for albite and orthoclase.

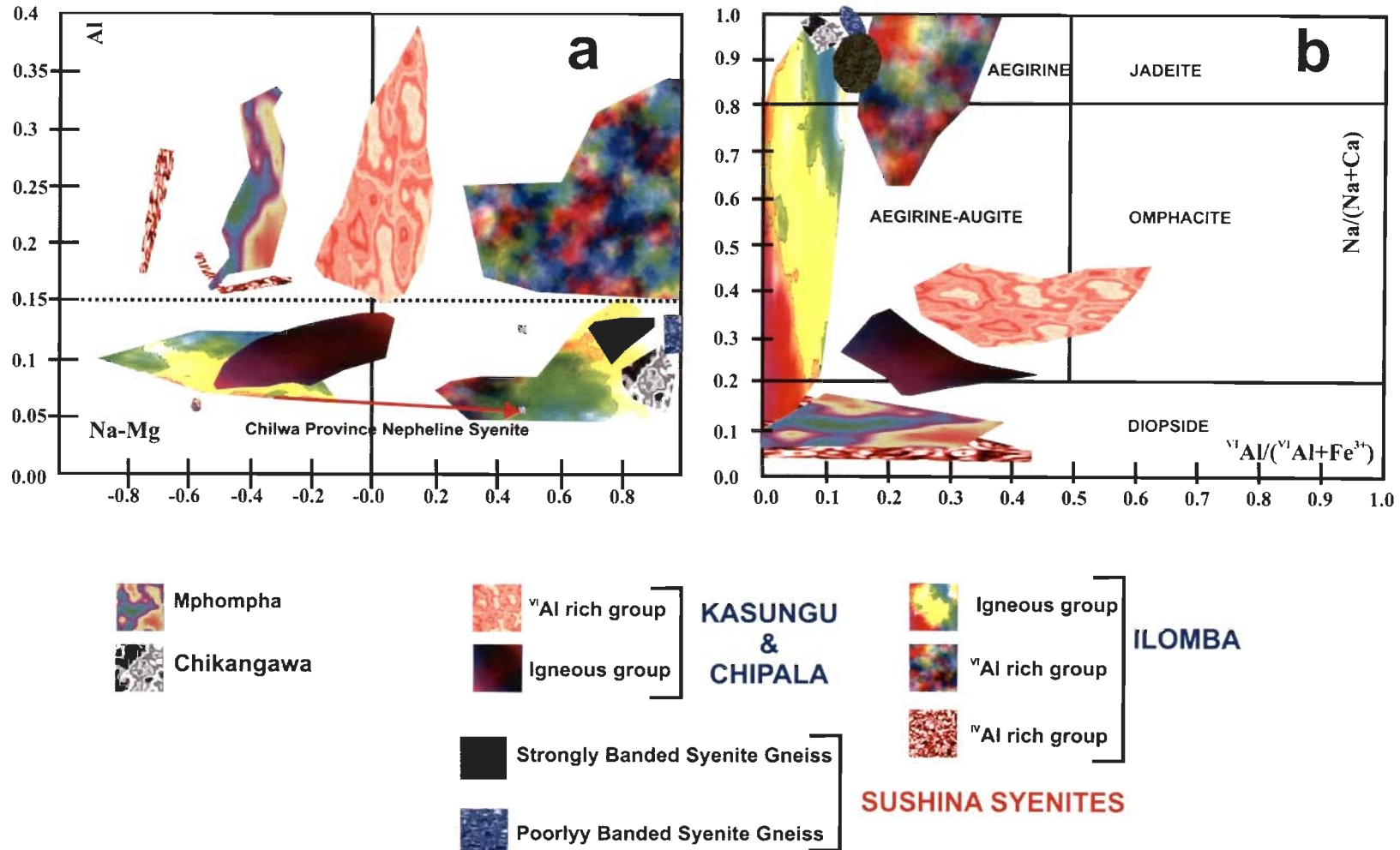


Fig. 6.13 Pyroxene from the banded syenite on (Na-Mg) vs. Al (a) and $[^{VI}Al/(^{VI}Al+Fe^{3+})]$ vs. $[Na/(Na+Ca)]$ (b) plots respectively showing their response in relation to the metamorphism. The pyroxene from this variety of syenite is compared with the NNAP pyroxenes of Woolley et al. (1996). (See section 6.2.1.2)

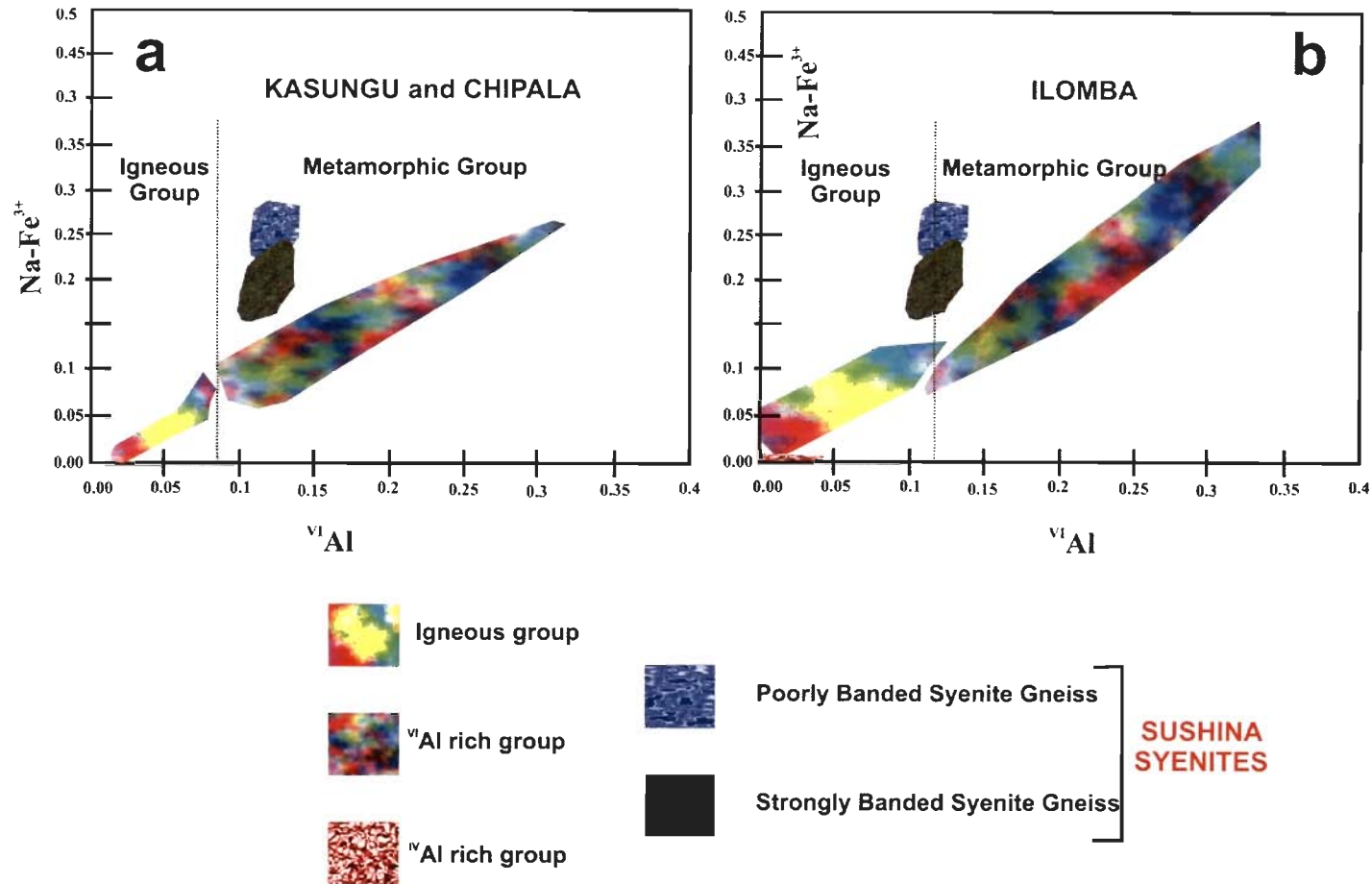


Fig. 6.14 Pyroxene from the banded syenite on a ^{VI}Al vs. $(Na-Fe^{3+})$ plot showing their response in relation to the metamorphism. The pyroxene from this variety of syenite is compared with the NNAP pyroxenes of Woolley et al. (1996). Analyzed pyroxenes are showing enrichment of ^{VI}Al and plotted in the field of metamorphic pyroxenes along with the Kasungu and Chipala pyroxenes (a). They are showing a transition between igneous and metamorphic pyroxenes when compare with the Ilomba pyroxenes. (See section 6.2.1.2)

on the boundary between the igneous and metamorphic groups. Occurrence of the aluminous pyroxene from the metamorphosed alkaline rocks has been reported from number of other localities (Fig. 6.15), which include Nkonglong nepheline syenite gneiss, Cameroon (Kornprobst et al. 1976), schistose nepheline syenite at Norra Kärr, Sweden (Adamson, 1944), undersaturated syenite in Japan (Iwasaki, 1960), nepheline gneiss in Ghana (Holm, 1971) and regionally metamorphosed nepheline syenite in the Grenville Province of Ontario (Lumbers, 1976). In the metamorphosed Red Wine alkaline complex, Labrador, of agpaitic descent, the pyroxene composition shows wide variation (Fig. 6.15) (Curtis and Gittins 1979). The similarity of ^{VI}Al-site preference of the Ilomba pyroxene with that of the Red Wine complex had shown by Woolley et al. (1996) and concluded that “the metamorphism of agpaitic rocks will give rise to aluminian aegirine and a jadeitic pyroxene, where as miaskitic alkaline rocks lead to aluminian aegirine-augite and an omphacitic pyroxene”. The pyroxene of the present study is Al₂O₃-enriched aluminian aegirine with significant jadeitic component (Table 3.13 and 3.16) and supports the above findings of Woolley et al. (1996). It is now clear that the banded syenite of the Sushina area was formed under plutonic condition and was miaskitic in nature. Then due to autometasomatism the rock was changed towards agpaitic composition and further metamorphism of this agpaitic assemblage resulted formation of the pyroxene of aluminian aegirine and jadeitic composition.

6.2.1.3 Biotite and other mineral paragenesis

Biotite is found in the massive variety of syenite which is characterized by high MnO content (Table 3.20). Similar biotite is also reported from the miaskitic nepheline syenite of McGerrigle complex of Quebec, Canada by Wallace et al. (1990). The massive variety of syenite in its present form retains its miaskitic character as evident from their agpaitic index (1.03) relative to the banded variety. The mineralogy of this variety of syenite is also in agreement with the same and

the relatively low agpaitic index can be attributed due to absence of aegirine in this variety. The fO_2 can be qualitatively estimated from the average composition of biotite plotted in a Fe^{3+} , Fe^{2+} and Mg diagram (Fig. 3.25, Wones and Eugster, 1965; Speer, 1984). The biotite in massive syenite indicates conditions above the magnetite-hematite buffer (Fig. 3.25), however, the presence of magnetite implies that that the estimate is higher than the actual value and this is possibly because of subsolidus oxidation due to interaction with the deuteritic fluid (Barriere and Cotton, 1979). On the other hand the lack of aegirine certainly indicates that the massive variety is formed at relatively low fO_2 compared to the banded variety.

Presence of eudialyte and complex Na-Zr silicate indicates post-magmatic autometasomatism causing microclinization as well as albitization. In general, the textural and mineralogical feature is indicative of miaskitic nature of the nepheline syenites formed by the igneous process. Subsequent metasomatism and metamorphism of the primary mineralogical assemblage of miaskitic type (albite + orthoclase + nepheline + aegirine + apatite + zircon) was pushed towards the agpaitic assemblage (miaskitic assemblage + eudialyte + Na-Zr-silicate + different varieties of apatite). The change from the miaskitic to agpaitic mineral assemblages along with the aegirine dominated mafic mineral in very late stage magmatic rocks may be related several partly mutually related factors, as follows.

- (1) A dominance of Fe^{3+} over Fe^{2+} in the melt would effectively inhibit crystallization of amphibole which commonly has a rather low Fe^{3+} content (Schönenberger and Markl, 2008). Similar feature is observed in the studied nepheline syenite. Both the varieties of nepheline syenites are characteristically devoid of amphibole and enriched in aegirine. Generally, the alkaline gneisses are characterized by the presence of amphibole (Floor, 1974). So, the change of oxidation state is evident between the banded and massive variety

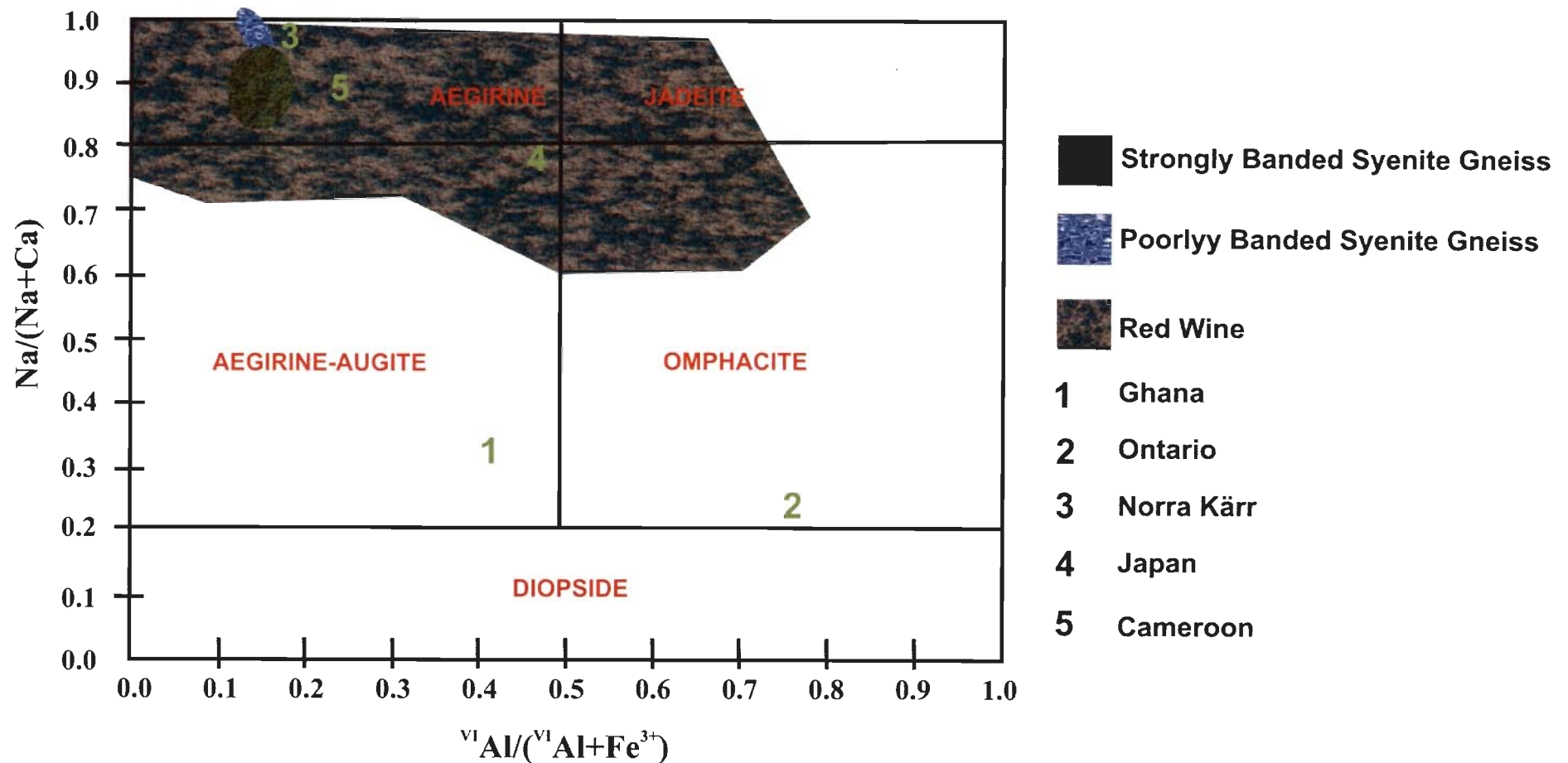


Fig. 6.15 Plot of $[{}^{\text{VI}}\text{Al}/({}^{\text{VI}}\text{Al}+\text{Fe}^{3+})]$ vs. $[\text{Na}/(\text{Na}+\text{Ca})]$ (after Woolley et al. 1996) for pyroxenes from metamorphosed alkaline rocks including Red Wine, Labrador (Curtis and Gittins, 1979), Ghana (Holm, 1971), Nkonglong, Cameroon (Kornprobst et al., 1976), Norra Kärr, Sweden (Adamson, 1944), Japan (Iwasaki, 1960) and Ontario (Lumbers, 1976). The pyroxenes from the banded variety of syenite falls with thin the metamorphosed alkaline rock of Red Wine complex. (See section 6.2.1.2)

of syenite. The former was probably formed under more oxidizing condition relative to the later one.

- (2) The formation of eudialyte may be mainly related to increase solubility of zircon (and possibly other HFSE; Schönenberger and Markl, 2008) in peralkaline melts because of high alkali/Al ratio restricts crystallization of zircon (Nicholls and Carmichael, 1969; Hoskin and Schaltegger, 2003). This may be the reason of total absence of zircon and the eudialyte grains are predominant in strongly banded syenite gneiss.

Thus it is evident from the above discussion that the syenites exposed along the NSZ was originally formed by the igneous process and later subjected to extensive metasomatism (by deuteritic fluid) and consanguineous metamorphism during post crystallization regional tectono-thermal events.

6.2.2 Geochemical signatures

The nepheline-syenites are essentially enriched in alkalis ($\text{Na}_2\text{O}+\text{K}_2\text{O}$). These nepheline-syenites are found to be peralkaline in nature and the peralkalinity index (PI) is lying in between 1 to 1.2. The maximum agpaitic index reaches up to 1.2 for banded variety while that of the massive one the same is 1. This is also reflected in the total alkali content between these two varieties of syenites. The banded variety is slightly enriched in total alkalis compared to the massive one. The origin of peralkalinity, commonly believed, is due to: (1) addition of alkali-rich material to normal compositions, (2) melting of peralkaline or other favorable protoliths and (3) subtraction of alkali poor material from normal compositions (Currie, 1989). Similarly, the peralkalinity developed in the banded variety of syenite is mainly due to the addition of alkalis by late-stage metasomatic process, reflected by the metasomatic mineral assemblages such as replacement of aegirine by eudialyte, nepheline by sodalite, analcime etc.

The nepheline-syenite is characterized by relatively higher concentration of Rb, Th, U, Nb, Pb, Zr, Hf and Ta while poor in Sr and Ba (Fig. 4.10a). The Nb/Ta ratio of the banded syenites is relatively low and reaches maximum to the massive syenite. Green (1995) found that Nb/Ta ratio vary widely for the alkaline rocks. He showed two distinct groups with higher and lower Nb/Ta ratio. The studied nepheline syenites falls in to the first group and similar values of Nb/Ta is also reported from the Kasungu-Chipala complex of NNAP (Eby et al., 1998). Experimental studies already established a possible F, Cl and CO₂ complexing of U in the aqueous phase under hydrothermal to magmatic condition (Romberger, 1984; Keppler and Wyllie, 1991; Peiffert et al. 1996). The Th/U ratio of the Sushina nepheline syenite varies from 2.44-5.63 and does not show any correlation with U-concentration (2.4-15.25). Based on this data it is not possible to decipher the role of hydrothermal fluid in introduction of U during metasomatic process.

In spite of the mineralogical differences between two varieties of studied syenite, they are indistinguishable in their REE trend. Similar REE trends of syenites may be related to i) their genesis from a common parental magma, ii) in response to post-magmatic deformational activity which they had undergone or iii) both. The role of second possibility in the Sushina syenite cannot be ruled out considering the mineralogical and textural features observed in the studied rock.

6.2.3 Apatite and other accessory composition and their paragenesis-a possible pH indicator?

Apatite in association with nepheline syenites was successfully used for the determination of alkalinity changes in many alkaline complexes e.g. Pilansberg alkaline complex South Africa (Liferovich and Mitchell, 2006), Illimaussaq complex, South Africa (Markl and Baumgartner, 2002; Markl, 2001), Gordon Butte, Crazy Mountain, Montana, USA (Chakhmouradian and Mitchell, 1999 and 2002), Lovozero complex, Kola Peninsula, Russia (Chakhmouradian et al. 2002). The extensive variations in the apatite group of minerals is reported from the Pilansberg

complex of South Africa (Liferovich and Mitchell, 2006) and owing to the similarity in the apatite paragenesis, this complex is chosen as the type area for the present study. It must be noted that the apatite group of minerals and their variation in terms of their chemical composition as described by Liferovich and Mitchell (2006) in the Pilansberg complex is from the lujavrite and the rock type in the present study is different from the above one. However, the textural and mineralogical investigation of the nepheline syenites, as described earlier (Chapter 3), clearly shows that they are severely affected by the post-magmatic alterations which resulted recrystallization, alteration and replacement of certain early formed minerals (e.g. aegirine, nepheline etc.). Limited field investigation does not support the presence of any extraneous fluid derivation in the form of late stage hydrothermal veins, intrusions of dykes etc. in association with the studied nepheline syenites. The only mineralized vein found along the NSZ is quartz veins which probably not related to such under saturated fluid bearing nepheline syenites. This implies that the origin of a consanguineous fluid related to magma from which these nepheline syenites were formed thus implying autometasomatic character of the post-magmatic alterations as reported from the Pilansberg complex (Liferovich and Mitchell, 2006). Such, autometasomatism caused replacement of nepheline by eudialyte, sodalite; alkali feldspars has been converted to ordered triclinic microcline and nepheline has recrystallized to the Morozewicz-Buerger convergence field. All of these evidences points towards a low temperature re-equilibration of the constituting minerals of igneous descent. Such consanguineous fluid according to Khomyakov (1990, 1995) usually reflects changes in alkalinity during the entire course of evolution of the different variety of mineral assemblage (agpaitic and miaskitic) following the '*alkalinity wave principal*'. A recent study by Markl and Baumgartner (2002) suggests pH of a 'deuteric fluid-nepheline syenite' system is mainly controlled by the activity of Na and Cl [$a(\text{Na})/a(\text{Cl}^-)$]. Breakdown or deposition of sodic and chloride rich mineral further influence this ratio. In the studied nepheline syenites the

formation of aegirine and breakdown of the same could have influenced this ratio. All the eudialyte formation in the banded variety of syenite is associated with the aegirine, in accordance with the proposed model of Markl and Baumgartner (2002). Textural and mineralogical studies suggest at least two stages of extensive alteration: the first stage associated with replacement of aegirine by eudialyte (Eud-I) and Na-Zr bearing silicate in the banded variety (Fig. 3.17, 3.18, 3.20) and the second stage by the formation of eudialyte (Eud-II) (Fig. 3.17). Interestingly, the massive variety of syenite which is devoid of aegirine also showing formation of tiny eudialyte grains (Fig. 3.23) and may be indicative of second generation of eudialyte formation. The eudialyte formation can be attributed to the maximum alkalinity stage as described earlier (section 6.21.3). The maximum alkalinity observed in the strongly banded syenite gneiss with the prominent development of eudialyte grains replacing aegirine (Fig. 3.20, 3.21).

Apatite is present both in the poorly banded syenite gneiss as well as in the massive syenite. The modal concentration of apatite in syenite very low compared to other two rock types. The only few grains of apatite from nepheline syenite could be obtained by heavy liquid separation and identified by Raman Spectroscopy. Raman Spectroscopy however not sophisticated enough to discriminate between the different compositional variants of apatite group. In order to examine the compositional variations between the apatites of two syenites, apatite grains were analyzed by LA-ICPMS. However, the present data set is not that much extensive as reported from the Pilansberg complex by Liferovich and Mitchell (2006) and hence only limited inferences can be drawn out of the generated data set. The Σ REE concentrations of the apatite from the two varieties of syenite are found to be reverse as that of the whole rock and follow the order: massive syenite > banded syenite (Fig. 4.17b). The apatite of the massive syenite is characterized by the extreme enrichment of the Y and Sr (Fig. 4.17a), high Σ REE coupled with the higher Na₂O (1.1-1.7 wt%, as determined by LA-ICPMS) and low SrO (0.6 to 2.5 wt.%) content compared to the apatite of poorly banded

syenite gneiss. Interestingly the SrO (or Sr in ppm. see Table 4.6) is almost double in the apatites of poorly banded syenite gneiss but the Na₂O content is relatively low (0.6-0.9 wt.%). The apatite of both these varieties of syenites in terms of Na₂O-REE₂O₃-SrO composition showing two distinct populations (Fig. 6.16) and this has direct relevance with the 'pH'. The apatites of the banded syenite is some how analogous to the Sr-Apatite/Sr-LREE-Apatite of Pilansberg complex as reported by Liferovich and Mitchell (their Sr-Ap and Sr-LREE-Ap respectively) (2006). However, the SrO content is much lower comparison to the above mentioned varieties of apatites of from the Pilansberg complex. On the other hand the higher Na₂O coupled with relatively higher LREE and low SrO content makes the apatites of massive syenite analogous to Sr-Na-LREE-Apatite of Liferovich and Mitchell (2006). The Sr-Apatite/ Sr-LREE-Apatites are formed at the maximum alkalinity stage and that of the Sr-Na-LREE-Apatite, at decreasing or low alkalinity stage (Liferovich and Mitchell, 2006). This is in accordance with the studied nepheline syenite where maximum alkalinity was observed in the banded variety of syenites (formation of Eud-I and Na-Zr silicates) followed by the low alkalinity at the massive syenite (formation of Eud-II). However, a logical explanation may be the presence of primary magmatic eudialyte grains and breakdown of such eudialyte released Cl⁻ and Na was released by the aegirine. But no primary eudialyte or sodalite is observed in the studied nepheline syenites and the cause of increasing Cl⁻ concentration in the deuteritic fluid is not clear at present. The increasing alkali content is also accompanied by the extensive alterations of alkali feldspar and nepheline and subsequently increased the pH resulting formation of eudialyte and Na-Zr silicates along with the replacement of nepheline by sodalite and analcime. As a result the original miaskitic assemblage converted to agpaite assemblage by changes of pH in the deuteritic fluid by the process of autometasomatism. However, complete absence of aegirine in the massive syenite can not be explained at present.

6.2.4 Geochronological status of the nepheline syenite and regional geology

The bulk rock isotopic studies related to different isotope systematics viz. Rb-Sr and Pb-Pb may not give factual information related to the genesis and source characterization owing to the open system behaviour of the nepheline syenites in response to post magmatic metasomatic and metamorphic overprints. However, the zircon ages obtained in the present study may be useful in envisaging the post magmatic effect on these rocks. The interpretation of the zircon ages too is not straight forward as the studied area had experienced amphibolite to greenschist facies of metamorphism affecting the Sushina nepheline syenite. A generalized map of the region showing different reported ages of different rock types is shown Fig. 6.17 along with the data generated in the present study. Chatterjee et al. (2008) reported the intrusive age of 1.55 Ga for the Bengal anorthosite (gabbroic anorthosite) from the Saltora area lying northeast of the present study area (Fig. 6.17). The lower intercept of 947 ± 27 Ma of gabbroic anorthosite according to them is related to the age of Grenvillian high-grade metamorphism. A similar estimate of polyphase metamorphism in the same area is also reported by Maji et al. (2008) (Fig. 6.17). Their geochronological data, based on monazite dating (CHIME), corresponds to, at least, four phases of metamorphism (M_1 - M_4) accompanied by related deformations (D_1 - D_4) in a wide span of time starting from >1.4 Ga to 0.9 Ga. The M_1 metamorphism and related D_1 deformation under granulite facies of metamorphism of >1.4 Ga may be even older considering the 1.55 Ga crystallization age of the Bengal anorthosite (Maji et al. 2008). The 0.96 Ga (960 ± 32 Ma, ANK 8, Fig. 5.7) and the 1.3 Ga (1301 ± 9.6 Ma, ANK 7, Fig. 5.5) ages obtained from the zircon of poorly banded syenite gneiss of Sushina correspond to the similar complex polyphase metamorphic episodes related to Grenvillian events. This observation is in accordance with the upper and lower intercepts of 1.3 Ga (1343 ± 160 Ma) and 0.9 Ga (877 ± 160) respectively (Fig. 6.18) obtained from the poorly banded syenite gneiss (ANK 7 & ANK 8). However, Maji et al. (2008) fail to explain

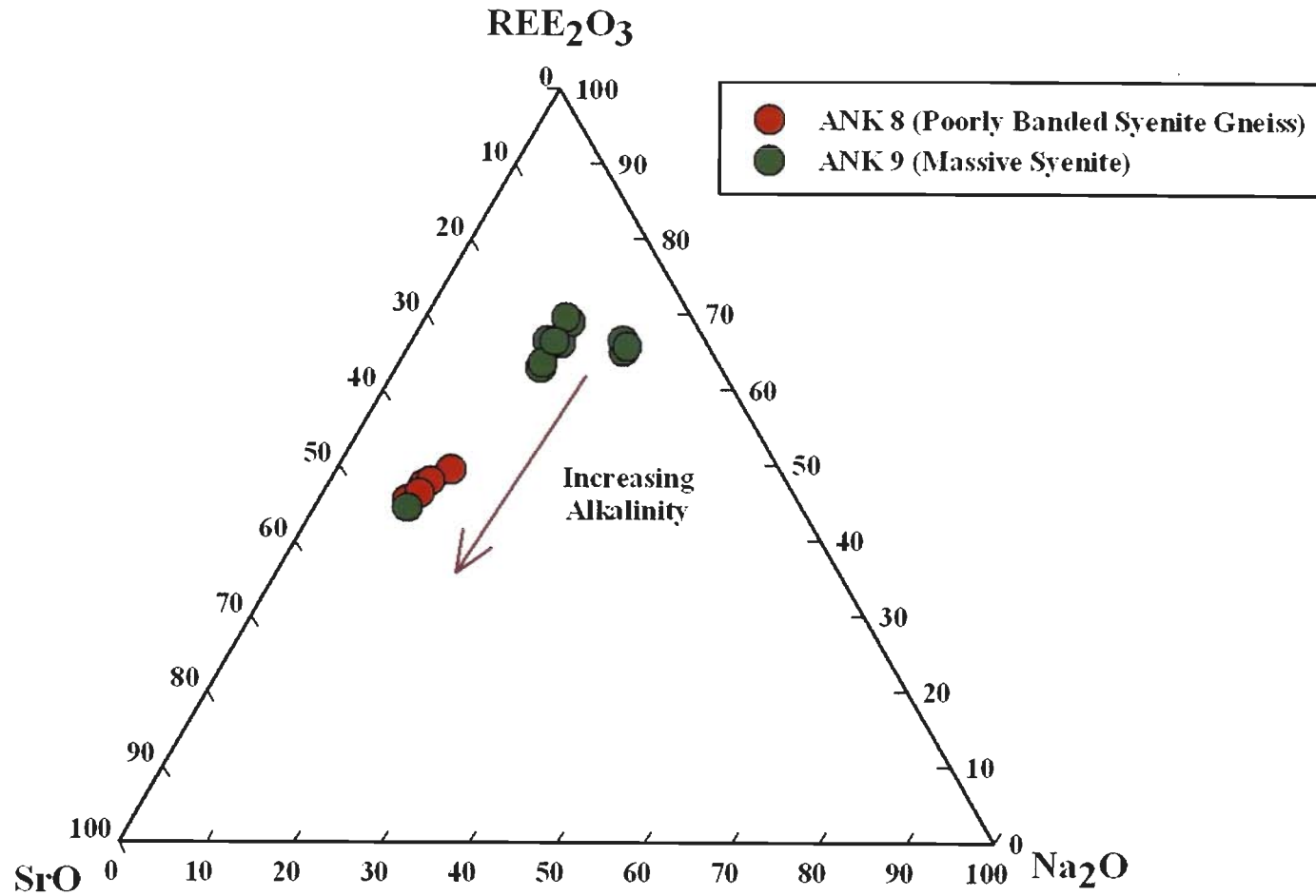


Fig. 6.16 Apatite from banded syenites (poorly banded syenite gneiss) in terms of Na_2O - REE_2O_3 - SrO ternary diagram. The apatites from the banded syenite were formed under maximum alkalinity and that of apatites of massive syenite at relatively low alkalinity. (See section 6.2.3)

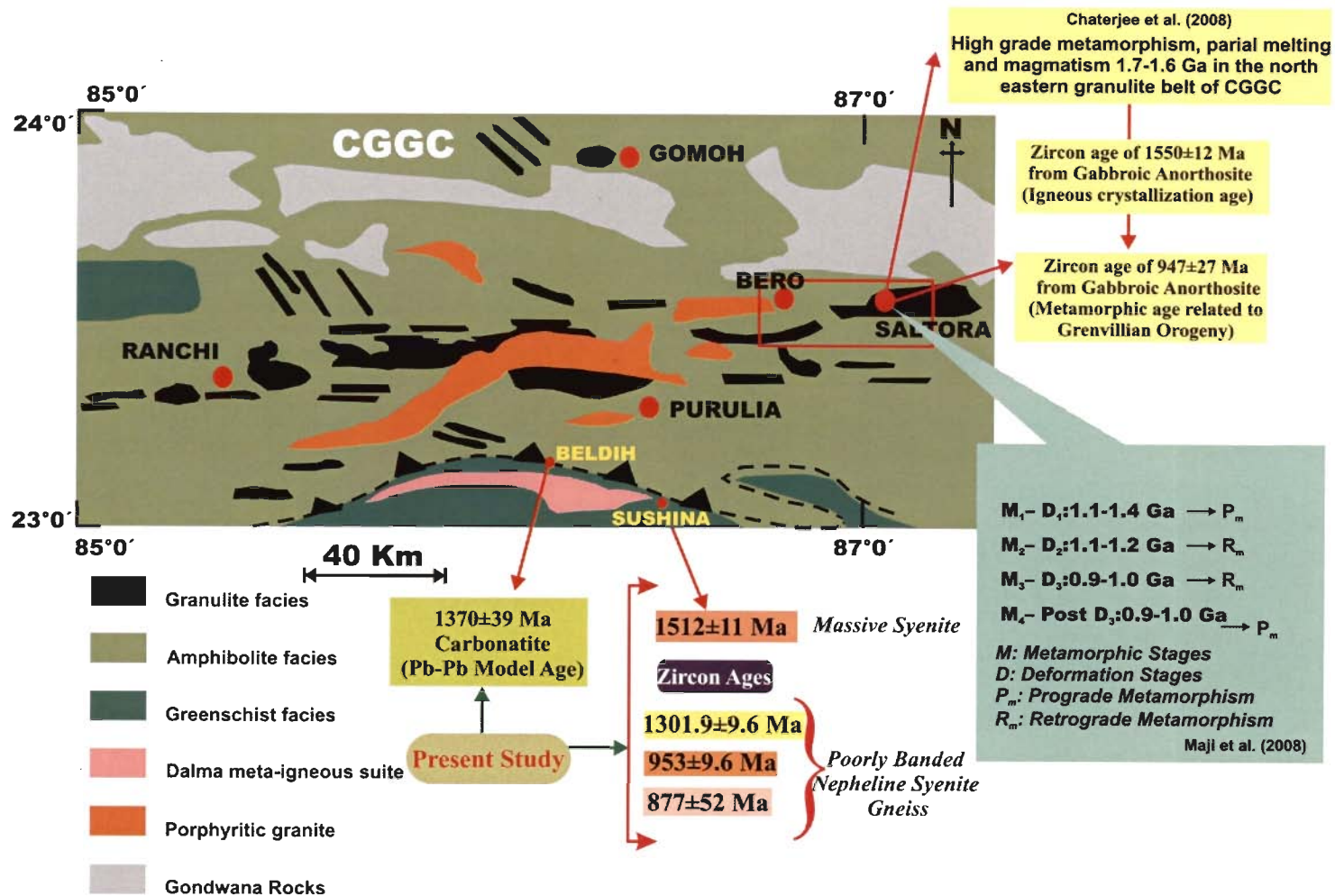


Fig. 6.17 Generalized schematic chronostratigraphic map of the study area along with the data set obtained in the present study. Geochronological data obtained from the near by Saltora area by Maji et al. (2008) and Chatterjee et al. (2008) is also included for ready reference. (See section 6.2.4)

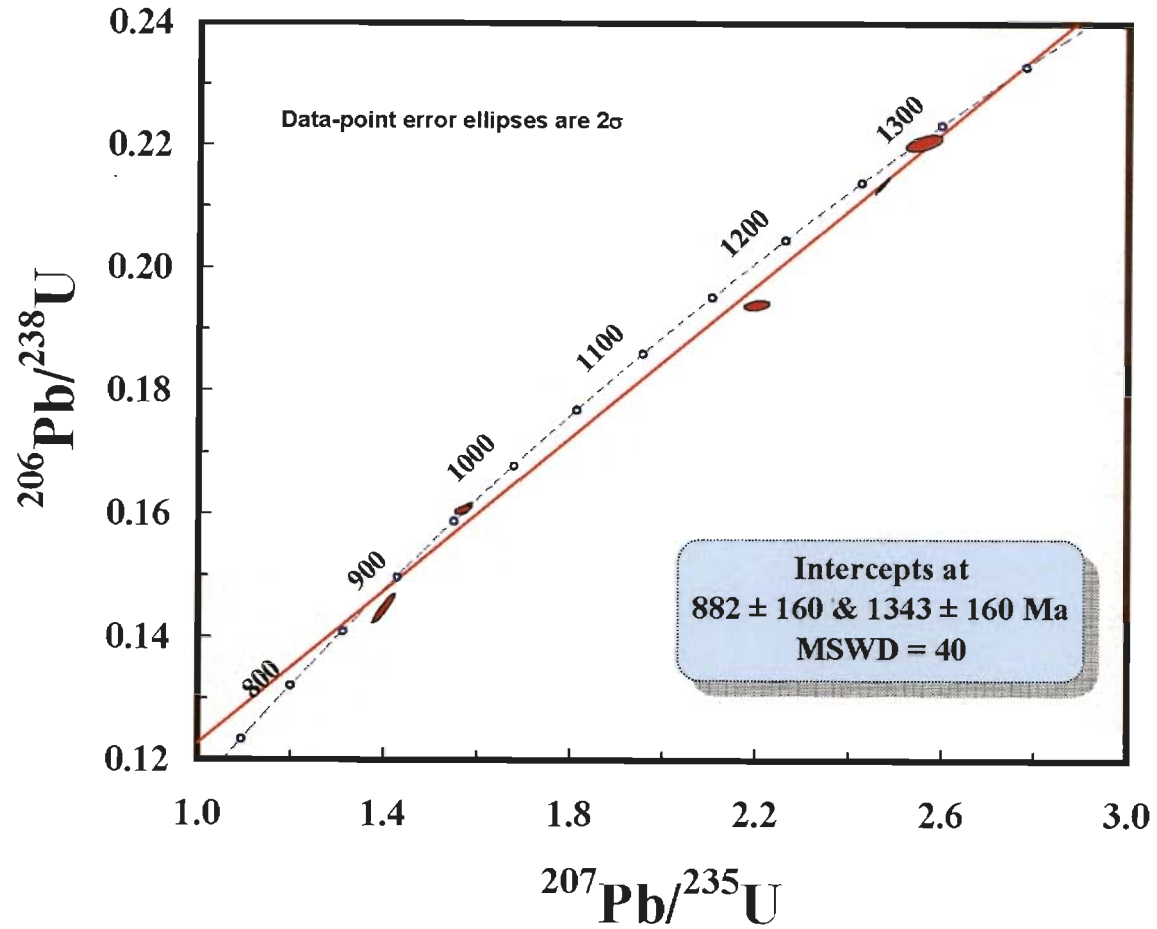


Fig. 6.18 Range of metamorphic ages obtained from the poorly banded syenite gneiss reflecting Grenvillian metamorphism affected the pre existing nepheline syenites. (See section 6.2.5)

their youngest monazite chemical age data of 830 Ma, from the margin of the monazite grains. A similar age of 877 ± 52 Ma (ANK 2, Fig. 5.8) showing evidences of Pb mobility and could be related to the metasomatic activity experienced by the banded variety of syenite. The maximum alkalinity is also evident in the banded variety of syenite from the apatite chemistry and the formation of Eud-I in accordance with the recrystallization and subsequent re-precipitation of the zircon grains in this variety of syenite. The maximum alkalinity certainly inhibit crystallization of minerals like zircon, baddeleyite from a melt and with decreasing alkalinity new zircon would precipitate showing the evidences of Pb mobility as seen in the present case. A similar feature of zircon formation by metasomatic process is described by Ashwal et al. (2007) from the nepheline syenite gneiss, Tambani, Mozambique, Malawi.

This has already been mentioned that the zircon oldest age data is obtained from the massive syenite (ANK 9) is 1.51 Ga similar to that of the Bengal anorthosite. Considering this age as the age of crystallization it is found that the initial $^{87}\text{Sr}/^{86}\text{Sr}$ is coming below the BABI value. The initial $^{87}\text{Sr}/^{86}\text{Sr}$ giving only a meaningful value if the age is at least 999 Ma which is in accordance with in the age obtained from the other samples. This indicates that the with respect to the 1.51 Ga event the bulk rock is reset to the younger metamorphic and metasomatic event of 0.9 to 1 Ga event. The concentration of common Pb is also found to be least in the zircons of the massive syenite (Table 5.2). In case of the banded syenite the common Pb concentration reaches up to 4.2 ppm. (Table 5.2). Moreover the decreasing alkalinity, as evidenced by the apatite chemistry, seems to be logical explanation favoring the presence of older magmatic zircon in this variety of syenite. However, from the ongoing discussion this can be concluded that the age of studied nepheline syenite complex could be dated back to ≥ 1.51 Ga.

6.3 GENETIC LINEAGE (?) BETWEEN THE STUDIED ROCKS

A recent study by Woolley and Kjarsgaard (2008) summarized different association of carbonatite and silicate rocks. The syenitic rocks are in general not common associates of carbonatite compared to the pyroxenite-ijolitic association. The main aim of the present study was to investigate the possible (?) genetic linkage between the carbonatite and associated silicate rocks. The association of pyroxenite is common and reported as many as 16 such association across the world (Woolley and Kjarsgaard, 2008). Woolley and Kjarsgaard (2008) in their survey also reported 23 occurrences around the globe where carbonatite is associated with pyroxenite and syenite. So, it is important to re-investigate the fact that whether these rocks are consanguineous or formed from the discrete batches of magma.

The two localities, Beldih and Sushina, of the present study area are spatially separated by 40 Km. Due to this spatial separation, it is not possible to envisage any genetic lineage between the carbonatite-pyroxenite associations at Beldih with the nepheline syenites at Sushina. The mineralogical and petro-chemical composition of the studied rocks do not show any common evolutionary trend between the carbonatite-pyroxenite associations with that of the nepheline syenites. Interestingly all studied rocks showing a similar REE trend with variation in \sum REE content. The similarity in such trends may be a mere coincidence or the similar geochemical composition of the source magma responsible for crystallization of these rocks. Other explanation for similar trend may be due to post magmatic metamorphic and metasomatic activities affecting these rocks. Interestingly the Y/H_o ratio of all the studied rocks is similar and can be attributed to the pervasive metasomatism during metamorphism resulted similarity in this ratio.

However the genesis of Sr-Ba enriched and HFSE depleted carbonatite as in Eden Lake, Manitoba, Canada (Chakhmouradian et al. 2008) in association with the syenite is a matter of considerable

debate among the petrologists. Some workers described these rocks as bona fide members of the carbonatites and derived from the mantle generated magma (e.g. Cooper and Reid, 2000; Xu et al. 2003) while few workers believed that their formation by metasomatic reworking of wall rocks or direct crystallization from Ca-Sr-Ba rich carbothermal fluids (Borisov, 1985; Mitchell, 2005). Mitchell (2005) suggested that these rocks were 'derived by extensive fractional crystallization of magmas of diverse genetic lineage at low temperature and pressure' and thus can be best termed as carbothermal residua rather than carbonatites. The amphibole composition of the Purulia carbonatite supports hypabyssal origin and thus related to their formation under a low pressure regime. However the temperature of crystallization of this carbonatite is not known. A prominent Nb negative anomaly (relative to world average of calico carbonatite of Woolley and Kempe, 1989) again characteristics of carbothermal origin for this carbonatite.

In general the co-genetic linkage between carbonatite and syenites invoke liquid immiscibility to link the two magma types (Viladkar and Subramanian, 1995; Xu et al. 2003). To test the possibility of immiscibility between the carbonatite and syenite, the trace elements with contrasting partitioning behaviors were chosen for best distribution in conjugate rocks (Harmer, 1999). On an average, the Ba is more compatible than Mn and La (~3.5 times and two times respectively) in a carbonate liquid relative to its conjugate silicate fraction whereas Nb and Th are more compatible in the silicate fraction whereas Pb and Nb is not mutually fractionated. Thus the published experimental data indicate that an immiscibly separated carbonate should have higher Ba/Mn, Ba/La and Nb/Th ratio and a comparable Nb/Pb ratio relative to its conjugate silicate counterpart (Chakhmouradian et al. 2008). Fig. 6.19 shows a mixed signature related to the above mentioned partitioning behaviour of the trace element pairs between the carbonatite and its conjugate (?) silicate counterpart i.e. nepheline syenite. The carbonatite is characterized by the higher Ba/Mn (0.20-1.19), Ba/La (2.32-5.08) ratio compared to their conjugate (?) silicate fraction (Ba/Mn: 0.02-0.09;

Ba/La: 1.05-5.03) (Fig. 6.19a, b). But in both the cases the magnitude of enrichment is much lower compared to the experimental results. Moreover, the Ba/Mn and Ba/La ratio is found to be higher for two samples where as the other two samples are showing very little or no variation in these ratios compared to the nepheline syenites. Similar feature is also observed for the Nb/Th (*Carbonatite*: 2.93-23.45; *Nepheline syenite*: 5.23-14.94) and Nb/Pb (*Carbonatite*: 1.09-25.78; *Nepheline syenite*: 7.1-14.30). All these ratios are overlapping for both the varieties of rocks and do not support the possibility of immiscibility between carbonatite and nepheline syenite.

To investigate the possibility of formation of the Purulia carbonatite from a carbothermal fluid fractionated from a syenitic magma the similar trace element pair is used in the present study as used by Chakhmouradian et al. (2008) for EL carbonatites and associated silicate rocks (syenites, melasyenites and quartz syenites). According to them a carbothermal fluid and their derivatives should be enriched in Rb/Sr, Y/Ce and Nb/Th ratio relative to their silicate counterpart at a comparable Y/Zr values (Table 4.1). Expectedly the Rb/Sr and Y/Zr ratios are low and high respectively in the Purulia carbonatite. The higher Y and Sr concentration in the carbonatite coupled with low Rb and Zr concentration due to lack of suitable carrier phases like phlogopite (Rb), Zircon (Zr) resulted substantial low values for Rb/Sr and higher value for Y/Zr compared to the nepheline syenites. On the other hand the higher concentration of Rb and Zr relative to the carbonatite resulting the higher Rb/Sr and lower Y/Zr values in the syenites (Table 4.1). In case of carbothermal origin the carbonatites should have a higher Y/Ce and Nb/Th ratios relative to their silicate conjugate (nepheline syenite in the present case). A complete opposite trend is observed for the Y/Ce and Nb/Th ratios (Fig. 6.19c) between the carbonatite and the nepheline syenite. These observations rule out the possibility that the genesis of the Purulia carbonatite by a carbothermal fluid, derived from the syenite magma. Furthermore, empirical and experimental evidences (Keppler and Wyllie, 1991; Bau, 1996; Buhn et al. 2003) suggest that a carbothermal fluid should

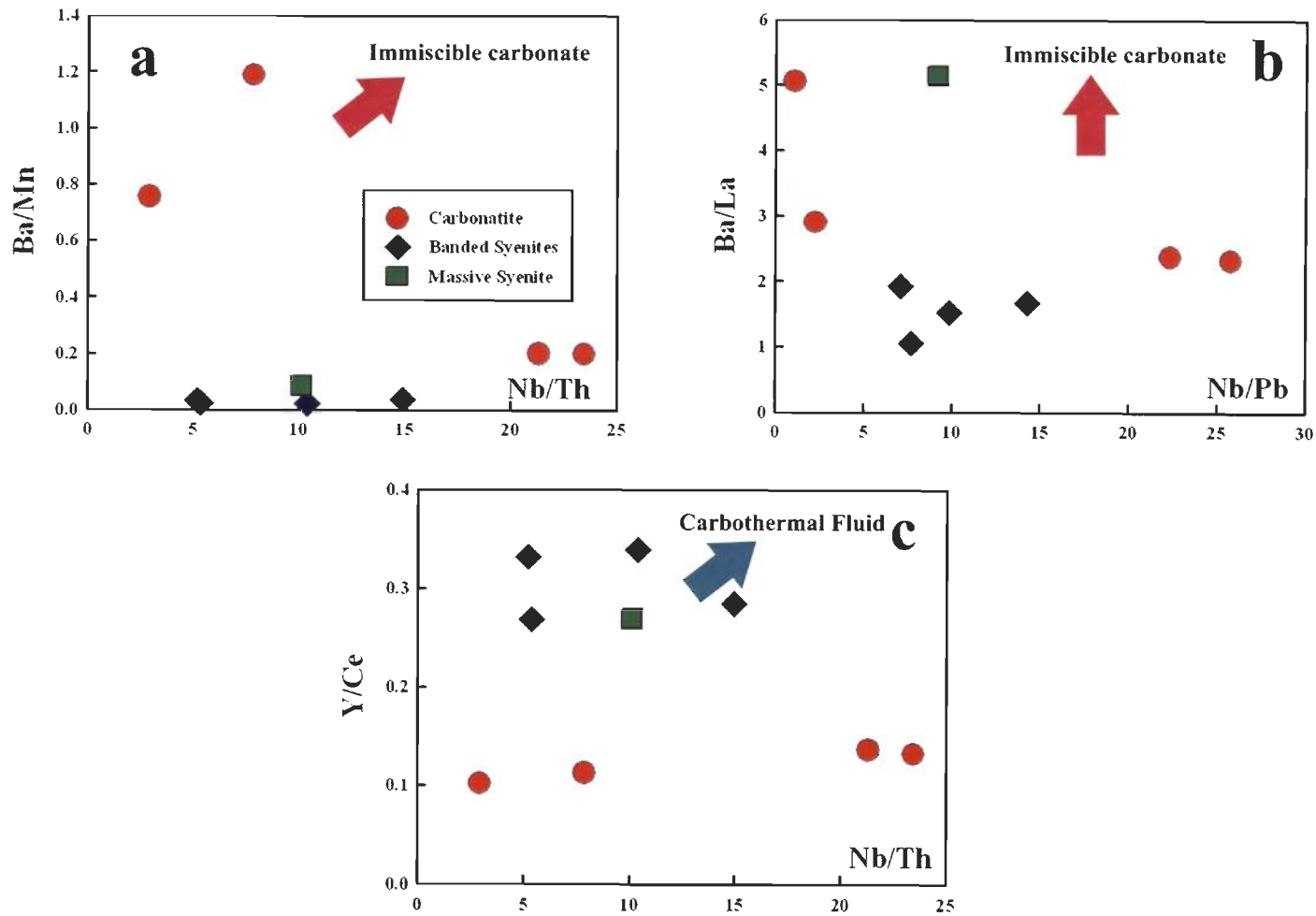


Fig. 6.19 Selected paired trace element ratios for carbonatite and nepheline syenites to find out the genetic link between these rocks. No common trend is observed. The bloc arrow indicates where the hypothetical immiscible carbonate magmas (a, b) and carbothermal fluids (c). (See section 6.3 for further details)

be enriched in Ho and U relative to their parent melt of igneous descent, ultimately producing sub-chondritic value of Y/Ho and Th/U values in the carbonatite. The Purulia carbonatites have Y/Ho ratio similar to that of the pyroxenite and syenites while the Th/U ratio is much lower compared to these two rocks and much below the chondritic or primitive mantle value. Thus it is clear from the above mentioned evidences that the *carbonatite-pyroxenite* at Beldih and *nepheline syenites* at Sushina is not consanguineous. The carbonatite probably formed from a discrete parent carbonatitic magma which is also evident from the measured $^{87}\text{Sr}/^{86}\text{Sr}$ ratio of the least altered sample and the apatite, both gives an $^{87}\text{Sr}/^{86}\text{Sr}$ (0.70340 and 0.70335 respectively) value of mantle signature.

Table 6.1: Element averages (from Table 4.4) and partitioning coefficients between apatite & calcite (vice versa) of carbonatite

Elements	Calcite	Apatite	Apt/Cal(k)	Cal/Apt(k)
Rb	0.04	0.08	2.18	0.46
Th	0.03	62.70	2386.33	0.00
U	2.57	1.67	0.65	1.54
Nb	1.45	0.90	0.62	1.61
Pb	13.59	10.52	0.77	1.29
Sr	10295.33	6769.17	0.66	1.52
Zr	0.00	1.98	nd	0.00
Y	80.95	314.14	3.88	0.26
La	54.62	1797.50	32.91	0.03
Ce	165.12	4435.28	26.86	0.04
Pr	23.69	521.08	22.00	0.05
Nd	113.65	2101.39	18.49	0.05
Sm	25.53	319.06	12.50	0.08
Eu	8.16	81.99	10.05	0.10
Gd	21.13	194.22	9.19	0.11
Tb	3.03	22.14	7.30	0.14
Dy	16.44	96.86	5.89	0.17
Ho	3.01	14.33	4.76	0.21
Er	7.51	27.52	3.66	0.27
Tm	0.99	2.80	2.83	0.35
Yb	6.33	13.86	2.19	0.46
Lu	0.85	1.43	1.69	0.59
REE	450.05	9629.46	21.40	0.05

CONCLUSIONS

Carbonatite is essentially composed of calcite with apatite along with magnetite, ilmenite, amphibole and biotite as accessories. The Purulia carbonatite is characterized by low HFSE content and comparable with the other reported carbonatite complexes e.g. Borra Carbonatite, Andhra Pradesh, India (Le Bas et al., 2002); Eden Lake carbonatite, Manitoba, Canada, (Chakhmouradian, et al., 2008); Turij massif, Kola Peninsula, Russia (Dunworth and Bell, 2001) etc. The detailed study on the amphiboles of the carbonatite point towards rapid upliftment of the carbonatite magma in to shallow level and thus the pressure variation within the magma chamber is recorded by the amphibole. On the other hand, the alkali-pyroxenite associated with the carbonatite had undergone extensive alkali-metasomatism during carbonatite intrusion resulting the alteration of the primary mineral assemblage with the formation of phlogopite and albite. The hydrothermal fluid expelled from the Purulia carbonatite was enriched in CO₂ and F in addition to H₂O. The H₂O and F were active during initial stages of metasomatism and altered pyroxene into amphibole and then biotite. During this process Na (dominant) and K was introduced and Ca was removed from the pre-existing alkali-pyroxene. The formation of biotite is the evidence for K-metasomatism.

The next stage of alteration process is characterized by vein-filling assemblage dominated by the calcite and apatite, analogous to the carbo(hydro)thermal carbonatites of Mitchell (2005). The Na remaining in the hydrothermal fluid was used for the precipitation of albite. Due to continuous loss of H₂O and F during amphibole and biotite formation, the remaining fluid was gradually got enriched in CO₂. The formation of calcite and apatite as vein-filling was controlled by XCO₂. The source of Ca may be both original fluid as well as the Ca removed during pyroxene to amphibole alteration. The alteration process was accompanied by the introduction of incompatible element,

including REE, in the system. The 'F' present in the hydrothermal fluid played most important role as the carrier above elements. The overall pressure is estimated to be around 2-3 kbar or less with temperature ranging around 400-450°C. The fO_2 -condition was low and suppressed by presence of CO_2 and alkalis. REE pattern of both the carbonatite and alkali-pyroxenite is similar indicating the genesis of these rocks from a common parental magma (?). Apatite and calcite are the dominant REE bearing phase in both the rocks. In spite of the post-magmatic changes of the carbonatite by Grenvillian metamorphic event, the bulk rock Rb-Sr isotopic study shows that the measured $^{87}Sr/^{86}Sr$ ratio is in well within the range of mantle values and supports genesis from primary magmatic carbonatite magma. However, the possibility of carbothermal fluid derivation is also can not be ruled out. Moreover the $^{87}Sr/^{86}Sr$ ratio suggests that the existence of long-lived heterogeneity in the mantle during the time of formation of these rocks which is well in accord with the world-wide mantle heterogeneity during 2800 to 1000 Ma period (Bell et al., 1982). Pb-Pb model age suggests that the Purulia carbonatite is at least ≥ 1.37 Ga old.

Nepheline syenite at Sushina area is petrographically composed of nepheline, albite and orthoclase. Aegirine is the dominant mafic constituents of the banded variety of syenite while the same is conspicuously absent in the massive variety. Pure end member compositions of the feldspars along with nepheline compositions converging towards the Morozewicz-Buerger field of plutonic/metamorphic-metasomatic assemblage suggest that the banded variety of syenite represent a recrystallized mineral assemblage of the original magmatic nepheline syenite and thus can be best termed as nepheline gneiss. Textural and mineralogical study reveals that these rocks were originally emplaced at plutonic condition and miaskitic in nature. Pervasive subsolidus or deuteritic alteration related to autometasomatism changed the original miaskitic composition towards the agpaitic type. Metamorphism consanguineous to metasomatism is also evident by the preferential partitioning of Al in the octahedral coordination rather than the tetrahedral one. The

effect of metasomatism and subsequent change in the alkalinity (pH) is best exemplified by the apatite group of minerals. The maximum alkalinity stage is represented by the Sr-LREE enriched apatite of the banded syenite and that of the Sr-Na-LREE apatite of the massive syenite indicate a lower or decreasing alkalinity stage. The formation of eudialyte and complex Na-Zr bearing silicate, partial replacement of nepheline by sodalite, analcime is the direct consequence of such increasing alkalinity in the banded variety of syenite. However the effect of deuteritic alteration in the massive syenite is somewhat less which can be attributed due to decreasing alkalinity of the deuteritic fluid. The maximum alkalinity stage caused dissolution of zircon as evident by the total absence of the same in the strongly banded syenite gneiss. However, Pb mobility is observed in one of the sample of banded syenite reflecting dissolution and re-precipitation of the zircon during the increasing and decreasing alkalinity stage respectively. This zircon grain yields an age of 877 ± 52 Ma. A complex poly-phase metamorphic activity is reported from the nearby area and the zircon ages of the poorly banded syenite gneiss corroborates the same. Zircons from the poorly banded syenite gneiss give an age range of 1.3-0.96 Ga indicating Grenvillian metamorphic event under amphibolite to greenschist facies condition. However the zircons of the massive syenite give an age of 1.51 Ga is somewhat similar to the intrusive age of the near by Bengal anorthosite.

The present work summarizes the following findings:

1. *Carbonatite-alkali-pyroxenite association at Beldih and the nepheline-syenites at Sushina are not consanguineous and derivative of the same alkaline magma.*
2. *The Purulia carbonatite is at least ≥ 1.37 Ga old.*
3. *The existence of long-lived mantle heterogeneity in the Eastern Indian Shield ≥ 1370 Ma, matches well with the reported world-wide mantle inhomogeneity over the similar time span i.e. 2800 to 1000 Ma (Bell et al., 1982).*

4. *Nepheline syenites of Sushina are now metamorphic-metasomatic rocks and represents nepheline gneisses or nepheline syenite gneiss.*
5. *Nepheline syenites suffered post magmatic subsolidus/deuteric alteration contemporaneous to Grenvillian metamorphic event dated back to 0.9-1.31 Ga.*
6. *Available data suggest the Sushina syenite is at least ≥ 1.51 Ga old.*
7. *Occurrence of rocks of alkaline and carbonatite affiliations of similar age along NSZ points towards direct role of the shear zone itself in magma generation.*
8. *Magma of varied composition probably was generated from mantle due to episodic reactivation of the NSZ.*
9. *Though the magma characteristics are different but all the intrusives may be genetically linked to same mantle.*

REFERENCES

- Abbott M. J. (1969).** Petrology of the Nandewar volcano, N.S.W., Australia. *Contribution to Mineralogy and Petrology*, 20, pp. 115-134.
- Acharyya, S. K. (1993).** Greenstones from Singhbhum craton, their Archaean character, oceanic crustal affinity and tectonics. *Proceedings of National Academy of Science, India, Section A*, 63, pp. 211-222.
- Acharyya, S. K. (2003a).** The nature of Mesoproterozoic Central Indian Tectonic Zone with exhumed and reworked older granulites. *Gondwana Research*, 6, pp. 197-214.
- Acharyya, S. K. (2003b).** A plate tectonic model for Proterozoic Crustal evolution of Central Indian Tectonic Zone. *Gondwana Geological Magazine*, 7, pp. 9-31.
- Adamson, O. J. (1944).** The petrology of the Norra Kärr district. An occurrence of alkaline rocks in southern Sweden. *Geol. För. Stockh. Förh.*, 66, pp. 113-255.
- Allégre, C. J., Ben Othman, D., Polve, M. and Richard, P. (1979).** The Nd-Sr isotopic correlation in mantle materials and geodynamic consequences. *Physics of the Earth and Planetary Interiors*, 19, pp. 293-306.
- Anderson, A. T. and Lindsley, D. H. (1985).** Model for the Ti magnetite or ilmenite geothermometers and oxygen barometers (Abstract), *Trans. Geophys. Union* 66, pp. 416.
- Appleyarde, C. (1974).** Syn-orogenic igneous alkaline rocks of eastern Ontario and northern Norway. *Lithos*, 7, pp. 147-169.
- Ashwal, L. D., Armstrong, R. A., Roberts, R. J., Schmitz, M. D., Corfu, F., Hetherington, C. J., Burke, K. and Gerber, M. (2007).** Geochronology of zircon megacrysts from nepheline-bearing gneisses as constraints on tectonic setting: implications for resetting of the U-Pb and Lu-Hf isotopic systems. *Contribution to Mineralogy and Petrology*, 153, pp. 389-403.
- Baksi, A. K. (1995).** Petrogenesis and timing of volcanism in the Rajmahal flood basalt province, northeastern India. *Chemical Geology*, 121, pp. 73-90.
- Banerjee, A. K. (1974).** On the stratigraphy and tectonic history of the Iron ore bearing and associated rocks of Singhbhum and adjoining areas of Bihar and Orissa. *Journal of geological Society of India*, 15(2), pp. 150-157.
- Barker, D. S. (1989).** Field relations of carbonatites. *In Carbonatites: Genesis and Evolution* (K. Bell, ed.). Chapman & Hall, London, U.K. pp. 38-69.
- Barriere, M. and Cotten, J (1979).** Biotites and associated minerals as markers of magmatic fractionation and deuteritic equilibration in granites. *Contribution to Mineralogy and Petrology*, 70, pp. 183-198.

- Basu, A. R., Renne, P. R., Dasgupta, D. K., Teichman, F. and Poreda, R. J. (1993).** Early and late alkali igneous pulses and a high ^3He plume origin for the Deccan flood basalts. *Science*, 261, pp. 902-906.
- Basu, S. K. (1988).** Investigation of Apatite and Other Associated Minerals in the Southern Shear Zone, Purulia District, West Bengal. *Unpublished Report Geological Survey of India*.
- Basu, S. K. (1989).** Investigation of Apatite and Other Associated Minerals in the Southern Shear Zone, Purulia District, West Bengal. *Extended Abstracts, Record Geological Survey of India*, 122, Point. 2, pp. 42.
- Basu, S. K. (1990).** Alkaline Carbonatite Complex in Precambrian of South Purulia Shear Zone: Its Characteristics and Mineral Potential. In: *Abstract Volume*, Seminar on Evolution of Precambrian Crust, pp. 52.
- Basu, S. K. (1993).** Alkaline-Carbonatite Complex in Precambrian of South Purulia Shear Zone, Eastern India: Its characteristics and mineral potentialities, *Indian Minerals*, 47, pp. 179-194.
- Basu, S. K. (2005).** Petrogenetic model for evolution of Alkaline-Carbonatite Complex along Tamar-Porapahar Shear Zone in North Singhbhum Proterozoic Mobile Belt, Eastern India and its metallogenic aspects, *Journal of Geological Society of India*, 62, pp. 250-252.
- Bau, M. (1996).** Controls on the fractionation of isovalent trace elements in magmatic and aqueous systems: evidence from Y/Ho, Zr/Hf and lanthanide tetrad effect. *Contributions to Mineralogy and Petrology*, 123, pp. 323-333.
- Bell, K. (1994).** Carbonatites and mantle evolution: a review. *Goldschmidt Conference*, Edinburgh, pp. 69.
- Bell, K. and Tillton, G. R. (2001).** Nd, Pb and Sr Isotopic Composition of East African Carbonatites: Evidence for Mantle Mixing and Plume Inhomogeneity, *Journal of Petrology*, 42, pp. 1927-1945.
- Bell, K. Blenkinsop, J., Cole, T. J. S. and Menagh, D. P. (1982).** Evidence from Sr isotopes for long-lived heterogeneities in the upper mantle. *Nature*, 298, pp. 251-253.
- Bhattacharya, C., Chakraborty, A. and Banerjee, P. K. (1991).** Petrology-Geochemistry of apatite-magnetite amphibolites and their role in phosphate mineralisation along the Southern Shear Zone, Purulia Dt., West Bengal. *Indian Journal of Earth Sciences*, 18, pp. 94-108.
- Bhattacharya, C., Chakraborty, A. and Banerjee, P. K., (1991).** Petrology-Geochemistry of apatite-magnetite amphibolites and their role in phosphate mineralisation along the Southern Shear Zone, Purulia District, West Bengal, *Indian Journal of Earth Sciences*, 18, pp. 94-108.
- Bhattacharya, D. K. and Dasgupta, S. (1992).** Apatite mineralisation around Beldih and its genetic control, District Purulia, West Bengal, *Journal of Geological Society of India*, 39, pp. 7-15.
- Bhattacharya, H. N. and Bandyopadhyaya, S. (1998).** Seismites in a Proterozoic tidal succession, Singhbhum, Bihar, India. *Sedimentary Geology*, 119, pp. 239-252.

- Bhattacharya, S. (1992).** Evolution of Singhbhum mobile belt by continental rifting and implications of the geochemistry of Purulia amphibolites. *Indian Journal of Earth Sciences*, 19, pp. 9-17.
- Bhattacharyya, C. and Chaudhuri, K. (1986).** Foid syenites and sodic schists from Sushina Hill, Purulia District, West Bengal, *Indian Journal of Earth Sciences*, 13(4), pp. 339-342.
- Blackburn, W. H. and Srivastava, D. C. (1994).** Geochemistry and tectonic significance of the Ongarbira metavolcanic rocks, Singhbhum district, India. *Precambrian Research*, 67, pp. 181-206.
- Borisov, A. B. (1985).** Mineralogy and genesis of benstonitic carbonatites of the Murun massif. Vestnik Leningradskogo Universiteta, Seriya 7. *Geologiya i Geografiya* 3, pp. 97-102 (in Russian).
- Bose, M. K. (1994).** Sedimentation pattern and tectonic evolution of the Proterozoic Singhbhum Basin in the eastern Indian shield. *Tectonophysics*, 231, pp. 325-346.
- Bose, M. K., Chakraborti, M. K. and Saunders, A. D. (1989).** Petrochemistry of the lavas from Proterozoic Dalma volcanic belt, Singhbhum, eastern India. *Geological Rundschau*, 78, pp. 633-648.
- Bose, P. K. and Chakraborty, P. P. (1994).** Marine to fluvial transition: Proterozoic Upper Rewa Sandstone, Maihar, India. *Sedimentary Geology*, 89, pp. 285-302.
- Bose, P. N. (1884).** Geology of lower Narbada Valley. *Memoir of Geological Society of India*, XXI, Part 1.
- Brassinnes, S., Balaganskaya, E. and Demaiffe, D. (2005).** Magmatic evolution of the differentiated ultramafic, alkaline and carbonatite intrusion of Vuoriyarvi (Kola Peninsula, Russia). A LA-ICP-MS study of apatite. *Lithos*, 85, pp. 76-92.
- Brooker, R. A. (1998).** The effect of CO₂ saturation on immiscibility between silicate and carbonate liquids: an experimental study, *Journal of Petrology*, 39, pp. 1905-1915.
- Bühn, B. (2008).** The role of the volatile phase for REE and Y fractionation in low-silica carbonate magmas: implications from natural carbonatites, Namibia. *Mineralogy and Petrology*, 92, pp. 403-470.
- Bühn, B., Schneider, J., Dulski, P. and Rankin, A. H. (2003).** Fluid–rock interaction during progressive migration of carbonatitic fluids, derived from small-scale trace-element and Sr, Pb isotope distribution in hydrothermal fluorite. *Geochimica et Cosmochimica Acta*, 67, pp. 4577-4595.
- Bühn, B., Wall F and Le Bas M. J. (2001).** Rare-earth element systematics of carbonatitic fluorapatites, and their significance for carbonatite magma evolution. *Contribution to Mineralogy and Petrology*, 141, pp. 572-591.

- Bulakh, A. G. (1965).** Amphibole group. In Kaledonskii kompleks ul'traosnovnykh, shchelochnykh porod i karbonatitov Kol'skogo Poluoostrova i severnoi Karelia, *In: Kukhareno, AA (ed.) Nedra*, Moscow, pp. 453-463.
- Carmichael, I. S. E. (1967).** The iron–titanium oxides of salic volcanic rocks and their associated ferromagnesian silicates, *Contribution to Mineralogy and Petrology*, 14, pp. 36–64.
- Chakhmouradian, A. R. (2006).** High-field-strength elements in carbonatitic rocks: Geochemistry, crystal chemistry and significance for constraining the sources of carbonatites, *Chemical Geology*, 235, pp. 138-160.
- Chakhmouradian, A. R. and Mitchell, R. H. (1999).** Primary, agpaitic and deuteritic stages in the evolution of accessory Sr, REE, Ba and Nb-mineralization in nepheline-syenite pegmatites at Pegmatite Peak, Bearpaw Mts., Montana. *Mineralogy and Petrology*, 67, pp. 85-110.
- Chakhmouradian, A. R. and Mitchell, R. H. (2002).** The mineralogy of Ba- and Zr-rich pegmatites from Gordon Butte, Crazy Mountains (Montana, USA): comparison between potassic and sodic agpaitic pegmatites. *Contributions to Mineralogy and Petrology*, 143, pp. 93-114.
- Chakhmouradian, A. R., Mumin, A. H., Demeney, A and Elliott, B. (2008).** Postorogenic carbonatites at Eden Lake, Trans-Hudson Orogen (northern Manitoba, Canada): Geological setting, mineralogy and geochemistry. *Lithos*, 103, pp. 503-526.
- Chakhmouradian, A. R., Reguir, E. P. and Mitchell, R. H. (2002).** Strontium-apatite: new occurrences, and the extent of Sr-for-Ca substitution in apatite-group minerals. *The Canadian Mineralogist*, 40, pp. 121-136.
- Chakrabarty, A. (2002).** Geochemical studies of Beldih carbonatite, Purulia, West Bengal. Unpublished M. Tech Dissertation, IIT Roorkee, Roorkee, India, pp. 1-84.
- Chakrabarty, A. (2005).** Geochronological Status of Carbonatite Intrusive at Purulia (West Bengal): Its Implication in Tectono-Magmatic Evolution of the East Indian Craton. *Abstract Volume, 14th Biennial Convention of IGC and National Conference on Earth Science: Its Relevance to Society*, pp. 10.
- Chakrabarty, A. and Sen, A. K. (2004).** Geochemistry of Carbonatite and Apatite-Magnetite Rock from Beldih Area, Purulia District, West Bengal. *Abstract Volume, National Seminar on "Role of fluids in the Crustal Evolution: Special Emphasis on the Himalayan Magmatism, Tectonism and Metallogeny"*, pp. 38.
- Chakrabarty, A. and Sen, A. K. (2007).** Amphibole Composition: A Pressure Indicator (?) During Carbonatite Intrusion along South Purulia Shear Zone, West Bengal. *Abstract Volume, National Seminar on Magmatism, Tectonism and Mineralization (MTM-2007) and X Convention of South Asian Association of Economic Geologists (SAAEG, India Chapter)*, pp. 143.
- Chakrabarty, A., Sen, A. K. and Ghosh, T. K. (2009).** Amphibole – A Key Indicator Mineral for Petrogenesis of Carbonatite from Purulia, West Bengal, India. *Mineralogy and Petrology*, 95, pp. 105-112.

- Chakraborti, M. K. (1980).** On the pyroclastic rocks of Dalma volcanic sequence, Singhbhum, Bihar. *Indian Journal of Earth Sciences*, 7, pp. 216-222.
- Chakraborti, M. K. and Bose, M. K. (1985).** Evaluation of the tectonic setting of Precambrian Dalma volcanic belt, eastern India using trace element data. *Precambrian Research*, 28, pp. 253-268.
- Chakraborty, K. L. (1996).** A comprehensive geological review of the Precambrian banded iron-formation (BIF) of Bihar and Orissa, Eastern India. *Indian Journal of Geology*, 68(4), pp. 211-236.
- Charles, R. W. (1975).** The phase equilibria of richterite and ferrichterite. *American Mineralogist*, 60, pp. 367-374.
- Chatterjee, N., Crowley, J. L. and Ghose, N. C. (2008).** Geochronology of the 1.55 Ga Bengal anorthosite and Grenvillian metamorphism in the Chotanagpur gneissic complex, eastern India. *Precambrian Research*, 161, pp. 303-316.
- Chatterjee, N., Crowley, J. L. and Ghose, N. C. (2008).** Geochronology of the 1.55 Ga Bengal anorthosite and Grenvillian metamorphism in the Chotanagpur gneissic complex, eastern India. *Precambrian Research*, 161, pp. 303-316.
- Chattopadhyay, N. and Hashimi, S. (1984).** The Sung Valley alkaline-ultramafic-carbonatite complex, East Khasi and Jaintia Hills district, Meghalaya. *Record of Geological Survey of India*, 113, point. 4, pp. 24-33.
- Cooper, A. F. and Reid, D. L. (2000).** The association of potassic trachytes and carbonatites at the Dicker Willem Complex, southwest Namibia: coexisting, immiscible, but not cogenetic magmas. *Contributions to Mineralogy and Petrology*, 139, pp. 570-583.
- Coulson, I. M. (1997).** Postmagmatic alteration in eudialyte from the North Qôroq centre, South Greenland. *Mineralogical Magazine*, 61, pp. 99-109.
- Cox, K. G., Bell, J. D. and Pankhurst, R. J. (1979).** The interpretation of Igneous Rocks. George Allen and Unwin, London.
- Crawford, A. R. (1969).** India, Ceylon and Pakistan: New age data and comparison with Australia. *Nature*, 223, pp. 380-384.
- Currie, K. L. (1976).** The alkaline rocks of Canada. *Geological Survey of Canada Bulletin*, 239.
- Currie, K. L. (1989).** New Ideas on an Old Problem: The Peralkaline Rocks. In: Alkaline Rocks, Leelanandam, C. (Ed), Geological Society of India, pp. 117-136.
- Currie, K. L., Knutson, J. and Temby, P. A. (1992).** The Mud Tank Carbonatite Complex, Central Australia – An Example of Metasomatism at Mid-Crustal Levels. *Contribution to Mineralogy and Petrology*, 109, pp. 326-339.
- Curtis, L. W. and Gittins, J. (1979).** Aluminous and titaniferous clinopyroxenes from regionally metamorphosed agpaite rocks in central Labrador. *Journal of Petrology*, 20, 165-186.

- Dasgupta, S. and Bhattacharya, D. K. (1992).** Apatite mineralization along Singhbhum and Purulia-Bankura Shear Zones: Their nature and physico-chemical characteristics. *Indian Minerals*, 46, 123-132.
- Dawson, J. B and Hinton, R. W. (2003).** Trace-element content and partitioning in calcite, dolomite and apatite in carbonatite, Phalaborwa, South Africa, *Mineralogical Magazine*, 67(5), pp. 921-930.
- De, A. (1964).** Precambrian Dalma Dhanjori volcanicity of E India and its stratigraphic significance. *Proceedings in International Geological Congress*, 10, pp. 59-70.
- Deans, T. and Powell, J. L. (1968).** Trace Elements and Strontium Isotopes in Carbonatites, Fluorites and Limestones from India and Pakistan. *Nature*, 218, pp. 750-752.
- Deans, T., Sukeshwala, R. N., Sethna, S. and Viladkar, S. G. (1973).** Discussion and contributions. *Trans. Inst. Minerals and Metallogeny, Section b*, 82, pp. 33-40.
- Deer, W.A., Howie, R. A. and Zussman, J. (1992).** An Introduction To The Rock Forming Minerals. ELBS, pp. 223-275.
- Deitrich, V. J., Carman, M. F., Wyttenbach, A. and McKee, E. H. (1984).** Geochemistry of basalts from Holes 519A, 520, 522B, and 524, Deep Sea Drilling Project Leg 73 (South Atlantic). *Institute Reports DSDP*, 7, pp. 579-601.
- DePaolo, D. J. and Wasserburg, G. J. (1976).** Nd isotopic variations and petrogenetic models. *Geophysical Research Letters*, 3, pp. 249-252.
- Dollase, W. A. and Thomas, W. M. (1978).** The crystal chemistry of silicarich, alkali-deficient nepheline. *Journal of Petrology*, 20, pp. 311-318.
- Droop, G.T.R. (1987).** A general equation for estimating Fe^{3+} concentrations in ferromagnesian silicate and oxides from microprobe analyses, using stoichiometric criteria, *Mineralogical Magazine*, 51, pp. 431-435.
- Duke, N. A. and Edgar, A. D. (1977).** Petrology of the Blue Mountain and Bigwood felsic alkaline complexes of the Grenville province of Ontario, *Canadian Journal of Earth Sciences*, 14 (4), pp. 515-538.
- Dunn, J. A. (1929).** Geology of north Singhbhum including parts of Ranchi and Manbhum districts. *Memoir Geological Survey of India*, 54, pp. 1-166.
- Dunn, J. A. and Dey, A. K. (1942).** The geology and petrology of eastern Singhbhum and surrounding areas. *Memoir Geological Survey of India*, 69, pp. 281-450.
- Dunworth, E. A. and Bell, K. (2001).** The Turiy massif, Kola Peninsula, Russia: isotopic and geochemical evidence for multi-source evolution. *Journal of Petrology*, 42, pp. 377-405.

Eby, G. N., Woolley, A. R., Din, V. and Platt, G. (1998). Geochemistry and Petrogenesis of Nepheline Syenites: Kausngu-Chipala, Ilomba, and Ulindi Nepheline Syenite Intrusions, North Nyasa Alkaline Province, Malawi. *Journal of Petrology*, 39, pp. 1405-1424.

Eriksson, P. G., Mazumder, R., Catuneanu, O., Bumby, A. J. and Ilondo, B. O. (2006). Precambrian continental freeboard and geological evolution: A time perspective. *Earth-Science Reviews*, 79, pp. 165-204.

Eriksson, P. G., Mazumder, R., Sarkar, S., Bose, P. K., Altermann, W. and van der Merwe. (1999). The 2.7-2.0 Ga. volcano sedimentary record of Africa, India and Australia: evidence for global and local changes in sea level and continental freeboard. *Precambrian Research*, 97, pp. 269-302.

Fabriés, J. (1978). Les types paragénetiques des amphiboles sodiques dans les roches magmatiques. *Bulletin de Minéralogie*, 101, pp. 155-165.

Faure, G. and Hurley, P. M. (1963). The isotopic composition of strontium in oceanic and continental basalts; application to the origin of igneous rocks. *Journal of Petrology*, 4, 31-50.

Fersman, A. (1929). Geochemische Migration der Elemente und deren wissenschaftliche und wirtschaftliche Bedeutung, erläutert an vier Mineralvorkommen: Chibina-Tundren-Samaragdgruben-Uran-Grube-Tuja-Mujun-Wüste Karakumy. *Abh. prakt. Geol. BergwLehre*, 18, pp. 1-116.

Floor, P. (1974). Alkaline gneisses. In *The alkaline rocks* (H. Sørensen, Ed.), John Wiley and Sons, London, pp. 124-141.

Foster M. D. (1960). Interpretation of the composition of trioctahedral micas. *United States Geological Professional Paper*, 354B, pp. 1149.

Fuhrman, M. L. and Lindsley, D. L. (1988). Ternary-feldspar modeling and thermometry. *American Mineralogist*, 73, pp. 201-215.

Ghose, N. C., Shmakin, B. M. and Smirnov, V. N. (1973). Some geochronological observations on the Precambrians of Chhotanagpur. Bihar. *Geological Magazine*, 110, pp. 481-484.

Ghosh Roy, A. K. and Sengupta, P. R. (1988). Alkalic-carbonatitic magmatism and associated mineralisation along Porapahar-Tamar lineament in the Proterozoics of Purulia Dt., West Bengal, India. *Abstract, International Conference on Metallogeny Related to Tectonics of the Proterozoic Mobile Belts*, I.G.C.P., 247, pp. 38.

Ghosh, S. K., Sarkar, S. C. and Sengupta, S. (1985). A field guide for Ghatshila and neighbouring mineral belt COSIP-ULP in geology. Kolkata 7 Jadavpur University, pp. 87.

Giret, A., Bonin, B. and Leger, J. M. (1980). Amphibole compositional trends in oversaturated and understaturated alalaine plutonic ring-complexes. *Canadian Mineralogist*, 18, pp. 481-495.

Gittins, J. (1988). The origin of carbonatites. *Nature*, 335, pp. 295-296.

Gittins, J., Beckett, M. F. and Jago, B. C. (1990). Composition of the fluid phase accompanying carbonatite magma: a critical examination. *American Mineralogist*, 75, pp. 1106-1109.

Goldschmidt, V. M. (1930). Elemente und Minerale pegmatitischer Gesteine. *Nachr. Gesellsch. Wiss. Göttingen. Math. Phys. Kl.*, pp. 370-387.

Gomes, C. de B., Moro, S. L. and Dutra, C. V. (1970). Pyroxenes from the alkaline rocks of Itapirapua, 56o Paulo, Brazil. *American Mineralogist*, 55, pp. 224-230.

Goswami, J. N., Mishra, S., Wiedenbeck, M., Ray, S. L. and Saha, A. K. (1995). 3.55 Ga old zircon from Singhbhum-Orissa iron ore Craton, Eastern India. *Current Science*, 69, pp. 1008-1011.

Green, T. H. (1995). Significance of Nb/Ta as an indicator of geochemical processes in the crust-mantle system. *Chemical Geology*, 120, pp. 347-359.

Günther, D., Audétat, A., Frischknecht, R., and Heinrich C. A. (1998). Quantitative analysis of major, minor and trace elements in fluid inclusions using laser ablation inductively coupled plasma mass spectrometry. *Journal of Analytical Atomic Spectrometry*, 13(4), pp. 263-270.

Gupta, A. and Basu, A. (1991). Evolutionary trend of the mafic-ultramafic volcanism in the Proterozoic North Singhbhum mobile belt. *Indian Minerals*, 45, pp. 273-83.

Gupta, A. and Basu, A. (1991). Evolutionary trend of the mafic-ultramafic volcanism in the Proterozoic North Singhbhum mobile belt. *Indian Mineral*, 45, pp. 273-283.

Gupta, A. and Basu, A. (2000). North Singhbhum Proterozoic mobile belt Eastern India-a review. *Special Publication*, Geological Survey of India, 55, pp. 195-226.

Gupta, A., Basu, A. and Ghosh, P. K. (1980). The Proterozoic ultramafic and mafic lavas and tuffs of the Dalma greenstone belt, Singhbhum, eastern India. *Canadian Journal of Earth Sciences*, 17, pp. 210-231.

Gupta, A., Basu, A. and Ghosh, P. K. (1982). Ultramafic volcanoclastics of the Precambrian Dalma volcanic belt, Singhbhum, Eastern India. *Geological Magazine*, 119, pp. 505-510.

Gupta, A., Basu, A. and Singh, S. K. (1985). Stratigraphy and petrochemistry of Dhanjori Greenstone belt, Eastern India. *Quaternary Journal of Geology*, Min Metall Soc India, 57, pp. 248-263.

Hamilton, D. L. (1961). Nephelines as crystallization temperature indicators. *Journal of Geology*, 69, pp. 321-329.

Hammarstrom, J. M. and Zen, E. (1986). Aluminium in hornblende: An empirical igneous geobarometer. *American Mineralogist*, 71, pp. 1297-1313.

Hanson, G. N. (1980). Rare Earth Elements in Petrogenetic Studies of Igneous Systems. *Annual Reviews*, Earth Planetary Sciences, 8, pp. 371-406.

Hart, S. R. (1988). Heterogeneous mantle domains: signatures, genesis and mixing chronologies. *Earth and Planetary Science Letters*, 90, 273-296.

Heaman, L. M., Robert, B. and Crocket, J (1990). The chemical composition of igneous zircon suites: Implications for geochemical tracer studies. *Geochimica Cosmochimica Acta*, 54, pp. 1597-1607.

Heinrich, C. A., Pettke, T., Halter, W. E., Aigner-Torres, M., Audétat, A., Günther, D., Hattendorf, B., Bleiner, D., Guillong, M., and Horn, I. (2003). Quantitative multi-element analysis of minerals, fluid and melt inclusions by laser-ablation inductively-coupled-plasma mass-spectrometry. *Geochimica Cosmochimica Acta*, 67, pp. 3473-3497.

Heinrich, E. W. (1966). The Geology of Carbonatites. Rand McNally, Chicago, Illinois.

Heinrich, E. W. (1985). Infinite variations on a fenite theme. *Indian Mineral*, Sukheswala Vol., pp. 151-162.

Heinrich, E. W. M. (1966). The geology of carbonatites. Rand McNally and Company, Chicago, pp. 555.

Hogarth, D. D. (1989). Pyrochlore, apatite and amphibole: distinctive minerals in carbonatite. *In: Bell, K (ed.) Carbonatites: Genesis and Evolution.* Unwin Hyman Ltd., London, pp. 105-148.

Hogarth, D. D., Chao, G. Y. and Townsend, M. G. (1987). Potassium and Fluorine-Rich Amphiboles From The Gatineau Area, Quebec. *Canadian Mineralogist*, 25, pp. 739-753.

Holland, T. and Blundy, J. (1994). Non-ideal interactions in calcic amphiboles and their bearing on amphibole-plagioclase thermometry. *Contribution to Mineralogy and Petrology*, 116, pp. 433-447.

Hollister, L. S., Grissom, G. C., Peters, E. K., Stowell, H. H and Sisson, V. B. (1987). Confirmation of the empirical correlation of Al in hornblende with pressure of solidification of calc-alkaline plutons. *American Mineralogist*, 72, pp. 231-239.

Holm, R. F. (1971). Some garnets, pyroxenes, and amphiboles from nepheline gneisses in Ghana. *American Mineralogist*, 56, pp. 2111-2122.

Holmes, A. (1950). Age of uraninite from a pegmatite near Singar, Gaya district, India. *American Mineralogist*, 35, pp. 19.

Holmes, A. (1955). Dating the Precambrian of Peninsular India and Ceylon. *Proceedings of Geological Association Canada*, 7, pp. 81-106.

Hoskin, P. W. O. and Schaltegger, U. (2003). The composition of zircon and igneous and metamorphic petrogenesis. *In Zircon (J.M. Hanchar and P.W.O. Hoskin, Eds.). Mineralogical Society of America, Reviews in Mineralogy and Geochemistry*, 53, pp. 27-62.

Hytönen, K. (1959). On the petrology and mineralogy of some alkaline volcanic rocks of Toror Hills, Mt. Moroto, and Morulinga in Karamoja, Northeastern Uganda. *Bull. Comm. géol. Finl.*, 184, pp. 75-137.

- Iwasaki, M. (1960).** Clinopyroxenes intermediate between jadeite and aegirine from Suberi-dani, Tokushima Prefecture. *Journal of Geological Society of Japan*, 66, pp. 334-340.
- Iyengar, S. V. P. and Banerjee, S. (1964).** Magmatic phases associated with the Precambrian tectonics of Mayurbhanj district, Orissa, India. *Report 22nd International Geological Congress*, Point 10, pp. 515-538.
- Iyengar, S. V. P. and Murthy, Y. G. K. (1982).** The evolution of the Archean Proterozoic crust in parts of Bihar and Orissa, eastern India. *Record of Geological Survey of India*, 112(3), pp. 1-5.
- Jago, B. C. and Gittins, J. (1991).** The role of fluorine in carbonatite magma evolution. *Nature*, 349, pp. 56-58.
- Johnsen, O. and Grice, J. D. (1999).** The crystal chemistry of the eudialyte group. *Canadian Mineralogist*, 37, pp. 865-891.
- Jones, H. C. (1934).** The iron ore deposits of Bihar and Orissa. *Memoir Geological Survey of India*, 63(2), pp. 167-302.
- Kapustin, Yu. L. (1980).** Mineralogy of carbonatites. D. K. Biswas (trans.), Amerind, New Delhi, India.
- Keller, J. and Spettel, B. (1995).** Trace element composition and petrogenesis of natrocarbonatite. In: *Bell, K (ed.) Carbonatites: Genesis and Evolution*. Unwin Hyman Ltd., London, pp. 105-148.
- Kent, R. W., Pringle, M. S., Muller, R. D., Saunders, A. D. and Ghose, N. C. (2002).** ⁴⁰Ar/⁴⁰Ar Geochronology of the Rajmahal basalts, India, and their relationship to the Kerguelen Plateau. *Journal of Petrology*, 43, pp. 1141-1153.
- Keppler, H. and Wyllie, P. J. (1991).** Partitioning of Cu, Sn, Mo, W, U, and Th between melt and aqueous fluid in the systems haplogranite–H₂O–HCl and haplogranite–H₂O–HF. *Contributions to Mineralogy and Petrology*, 109, pp. 139–150.
- Khomyakov, A. P. (1990).** Mineralogy of hyperagpaitic alkaline rocks. Moscow, Nauka, 195 pp. (in Russian).
- Khomyakov, A. P. (1995).** Mineralogy of hyperagpaitic alkaline rocks. Oxford Scientific Publications. Clarendon Press, Oxford, pp. 222.
- King, B. C. (1949).** The Napak area of Southern Karamoja, Uganda. *Geological Survey of Uganda, Memoir V*, 57.
- Kjarsgaard, B. A. (1998).** Rare Earth Elements in Sövitic Carbonatites and their Mineral Phases. *Journal of Petrology*, 39, pp. 2105-2121.
- Kjarsgaard, B. A., Hamilton, D. L. and Peterson, T. D. (1995).** Peralkaline nephelinite/carbonatite liquid immiscibility: comparison of phase composition in experiments and natural lavas from Oldoinyo Lengai. In: *Bell, K. and Keller, J. (Eds.), Carbonatite Volcanism:*

Oldoinyo Lengai and the Petrogenesis of Natrocarbonatites. IAVCEI Proceedings in Volcanology 4, pp. 163-190.

Known, S. T., Tilton, G. R. and Grünenfelder, M. H. (1989). Laed isotope relationships in carbonatites and alkalic complexes: An overview. In: *Bell, K. (Ed.), Carbonatites: Genesis and Evolution*. Unwin Hyman, London: 360-387.

Kornprobst, J., Cantagrel, J-M., Fabriès, J., Lasserre, M., Rollet, M. and Soba, D. (1976). Existence, au Cameroun, d'un magmatisme alcalin panafrican ou plus ancien, la syénite nephélinique à mboziite de Nkonglong – com-paraison avec les roches alcalines connues dans la même région. *Bull. Soc. Geol. France*, 18, pp. 1295-1305.

Koster van Groos, A. F. and Wyllie, P. J. (1963). Experimental data bearing on the role of liquid immiscibility in the genesis of carbonatites, *Nature*, 199, pp. 801-802.

Kresten, P. (1988). The chemistry of fenitization: Examples from Fen, Norway. *Chemical Geology*, 68, pp. 329-349.

Krishnamurthy, P. (1988). Carbonatites of India, *Exploration and Research for Atomic Minerals I*, pp. 81-115.

Kumar, M. N., Das, N. and Das Gupta, S. (1985). Gold and mineralisation along the northern shear zone, Purulia district, West Bengal – an up-to-date appraisal. *Record of Geological Survey of India*, 113(3), pp. 25-32.

Larsen, L. M. (1976). Clinopyroxenes and coexisting mafic minerals from the alkaline Ilimaussaq intrusion, South Greenland. *Journal of Petrology*, 17, pp. 258-90.

Le Bas, M. J. (1977). Carbonatite–Nephelinite Volcanism. John Wiley and Sons, London, U.K.

Le Bas, M. J. (1987). Nephelinites and carbonatites. In: *Fitton, J. G., Upton, B. G. J. (Eds.), Alkaline Igneous Rocks. Special Publication*, Geological Society of London, 30, pp. 53-83.

Le Bas, M. J. (2008). Fenites associated with carbonatites. *The Canadian Mineralogist*, 46. pp. 915-932.

Le Bas, M. J., Keller, J., Kejie, T., Wall, F., Williams, C. T. and Peishan, Z. (1992). Carbonatite dykes at Bayan Obo, Inner Mongolia, China. *Mineralogy and Petrology*, 46, pp. 195-228.

Le Bas, M. J. and Streckeisen, A. L. (1991). The IUGS systematics of igneous rocks. *Journal of Geological Society of London*, 148, pp. 825-833.

Le Bas, M. J., Subbarao, K. V. And Walsh, J. N. (2002). Metacarbonatite or marble? – the case of the carbonate, pyroxenite, calcite-apatite rock complex at Borra, Eastern Ghats, India. *Journal of Asian Earth Sciences*, 20, pp. 127-140.

Leake, B. E., Woolley, A. R., Birch, W. D., Burke, E. A. J., Ferraris, G., Grice, J. D., Hawthorne, F. C., Kisch, H. J., Krivovichev, V. G., Schumacher, J. C., Stephenson, N. C. N.

and Whittaker, E. J. W. (2004). Nomenclature of amphiboles: additions and revisions to the International Mineralogical Associations amphibole nomenclature. *Mineralogical Magazine*, 68 (1), pp. 209-215.

Leake, B. E. (1978). Nomenclature of amphiboles. *Mineralogical Magazine*, 42, pp. 533-563.

Leake, B. E., Woolley, A. R., Arps, C. E. S., Birch, W. D., Gilbert, M. C., Grice, J. D., Hawthorne, F. C., Kato, A., Kisch, H. J., Krivovichev, V. G., Linthout, K., Larid, J., Mandarino, J. A., Maresch, W. V., Nickel, E. H., Rock, N. M. S., Schumacher, J. C., Smith, D. C., Stephenson, N. C. N., Ungaretti, L., Whittaker, E. J. W. and Youzhi, G. (1997). Nomenclature of Amphiboles: Report of the Subcommittee on Amphiboles of the International Mineralogical Association, Commission on New Minerals and Mineral Names. *Canadian Mineralogist*, 35, pp. 219-246.

Liferovich, R. P. and Mitchell, R. H. (2006). Apatite-group of minerals from nepheline syenite, Pilansberg alkaline complex, South Africa. *Mineralogical Magazine*, 70, pp. 463-484.

Ludwig, K. R. (2003). Isoplot 3.0-a geochronological toolkit for Microsoft Excel. Berkeley Geochronology Center, *Special Publication*, 4, pp. 71.

Lumbers, S. B. (1976). Omphacite-bearing nepheline-syenite in an anorthositic complex, Grenville Province of Ontario. Geological Association of Canada-Mineralogical Association of Canada, *Abstract*, 1, pp. 73.

Mahadevan, T. M. (2002). Geology of Bihar and Jharkhand. *Text Book Series*, Geological Society of India.

Maji, A. K., Goon, S., Bhattacharya, A., Mishra, B., Mahato, S. and Bernhardt, H. J. (2008). Proterozoic polyphase metamorphism in the Chhotanagpur Gneissic Complex (India), and implication for trans-continental Gondwanaland correlation. *Precambrian Research*, 162, pp. 385-402.

Mallik, A. K., Gupta, S. N. and Ray Barman, T. (1991). Dating of early Precambrian granite-greenstone complex of the Eastern Indian Precambrian shield with special reference to the Chotanagpur granite gneiss complex. *Record of Geological Survey of India*, 124 (2), pp. 20-21.

Markl, G. (2001). A new type of silicate liquid immiscibility in peralkaline nepheline syenites (lujavrites) of the Illimaussaq complex, South Greenland. *Contributions to Mineralogy and Petrology*, 141, pp. 458-472.

Markl, G. and Baumgartner, L. (2002). pH changes in peralkaline late-magmatic fluids. *Contribution to Mineralogy and Petrology*, 144, pp. 331-346.

Marks, M. and Markl, G. (2003). Ilímaussaq 'en miniature': closed-system fractionation an agpaitic dyke rock from the Gardar Province, South Greenland (contribution to the mineralogy of Ilímaussaq no. 117). *Mineralogical Magazine*, 67, pp. 893-919.

- Mazumder, R. (2002).** Sedimentation history of the Dhanjori and Chaibasa Formations, eastern India and its implications. *PhD thesis (unpublished)*, Jadavpur University, Kolkata, India, pp. 119.
- Mazumder, R. (2003).** Correlations between the Eastern Block of the North China Craton and the South Indian Block of the Indian Shield: an Archaean to Palaeoproterozoic link—comment. *Precambrian Research*, 127, pp. 379-380.
- Mazumder, R. (2005).** Proterozoic sedimentation and volcanism in the Singhbhum crustal province, India and their implications, *Sedimentary Geology*, 176, pp. 167-193.
- Mazumder, R. and Arima, M. (2004).** Proterozoic events in the Singhbhum crustal province. Extended abstract, *Gondwana Research*, 7(45), pp. 1343-1345.
- Mazumder, R. and Sarkar, S. (2004).** Sedimentation history of the Palaeoproterozoic Dhanjori Formation, Singhbhum, eastern India. *Precambrian Research*, 130, pp. 269-289.
- Mazumder, R., Bose, P. K. and Sarkar, S. (2000).** A commentary on the tectono-sedimentary record of the pre-2.0 Ga continental growth of India vis-à-vis a possible pre-Gondwana Afro-Indian supercontinent. *Journal of African Earth Sciences*, 30(2), pp. 201-217.
- McKie, D. (1966).** Fertilization. In *Carbonatites* (O.F. Tuttle & J. Gittins, eds.). Interscience, New York, N.Y. pp. 261-294.
- Mishra, S., Deomurari, M. P., Widenbeck, M., Goswami, J. N., Ray, S. L. and Saha, A. K. (1999).** $^{207}\text{Pb}/^{206}\text{Pb}$ zircon ages and the evolution of the Singhbhum craton, eastern India: an ion microprobe study. *Precambrian Research*, 93, pp. 139-151.
- Mishra, S., Deomurari, M. P., Widenbeck, M., Goswami, J. N., Ray, S. L. and Saha, A. K. (1999).** $^{207}\text{Pb}/^{206}\text{Pb}$ zircon ages and the evolution of the Singhbhum craton, eastern India: an ion microprobe study. *Precambrian Research*, 93, pp. 139-151.
- Mitchell, R. H. (1980).** Pyroxenes of the Fen alkaline complex, Norway. *American Mineralogist*, 65, pp. 45-54.
- Mitchell, R. H. (1990).** A review of the compositional variation of amphiboles in alkaline plutonic complexes. *Lithos*, 26, pp. 135-156.
- Mitchell, R. H. and Liferovich, R. P. (2006).** Subsolidus deuteric/hydrothermal alteration of eudialyte in lujavrite from the Pilansberg alkaline complex, South Africa. *Lithos*, 91, pp. 352-372.
- Mitchell, R. H. and Platt, R. G. (1978).** Mafic mineralogy of ferroaugite syenite from the Coldwell alkaline complex, Ontario, Canada. *Journal of Petrology*, 19, pp. 627-651.
- Mitchell, R. H. and Platt, R. G. (1979).** Nepheline-bearing rocks from the Poohbah Lake complex, Ontario: malignites and malignites. *Contribution to Mineralogy and Petrology*, 69, pp. 255-264.

Moecher, D. P., Anderson, E. D., Cook, C. A. and Mezger, K. (1997). The petrogenesis of metamorphosed carbonatites in the Grenville Province, Ontario. *Canadian Journal of Earth Sciences*, 34, pp. 1185-1201.

Moorbath, S., Taylor, P. N. and Jones, N. W. (1986). Dating the oldest terrestrial rocks - facts and fiction. *Chemical Geology*, 57, pp. 63-86.

Moralev, V. M., Voronovski, S. N. and Borodin, L. S. (1975). New findings about the age of carbonatites and syenites from southern India. *U.S.S.R. Academy of Science*, 222, pp. 46-48.

Morimoto, N., Fabries, J., Ferguson, A. K., Ginzburg, I. V., Ross, M., Seifert, F. A., Zussman, J., Aoki, K. and Gottardi, G. (1988). Nomenclature of pyroxenes. *Mineralogical Magazine*, 52, pp. 535-550.

Morogan, V. and Woolley, A. R. (1988). Fertilization at the Alno carbonatite complex, Sweden; distribution, mineralogy and genesis. *Contribution to Mineralogy and Petrology*, 100, pp. 169-182.

Mukhopadhyaya, D. (1984). The Singhbhum Shear Zone and its place in the Evolution of the Precambrian mobile belt of North Singhbhum. Proceedings seminar on Crustal evolution of the Indian Shield and its bearing on metallogeny. *Indian Journal of Earth Sciences*, pp. 205-212.

Mukhopadhyaya, D. (2001). The Archaean nucleus of Singhbhum: the present state of knowledge. *Gondwana Research*, 4, pp. 307-318.

Mukhopadhyaya, D., Ghosh, A. K. and Bhattacharya, S. (1975). A reassessment of the Structures in the Singhbhum shear zone. *Bull Geol Min Metall Soc India*, 48, pp. 49-67.

Nagpaul, K. K. and Mehta, P. P. (1975). Cooling history of south India as revealed by fission tracks studies. *American Journal of Science*, 275, pp. 753-762.

Naha, K. (1965). Metamorphism in relation to stratigraphy, structure and movements in parts of east Singhbhum, Eastern India. *Quaternary Journal of Geology*, *Min Metall Soc India*, 37, pp. 41-88.

Naha, K. and Ghosh, S. K. (1960). Archaean palaeogeography of E and N Singhbhum. *Geological Magazine*, 97, pp. 436-439.

Nash, W. P. (1972). Mineralogy and petrology of the Iron Hill carbonatite complex, Colorado. *Bulletin of Geological Society of America*, 83, pp. 1361-1382.

Natarajan, M., Bhaskar Rao, B., Parthasarathy, R., Kumar, A. and Gopalan, K. (1994). 2.0 Ga pyroxenite-carbonatite complex of Hogenakal, Tamil Nadu, South India. *Precambrian Research*, 65, pp. 167-181.

Neil, O. C., Muller, D. and Steinberger, B. (2003). Geodynamic implications of moving Indian Ocean hotspots. *Earth and Planetary Science Letters*, 215, pp. 151-168.

Nicholls, J. and Carmichael, I. S. E. (1969). Peralkaline acid Liquids: a petrological study. *Contribution to Mineralogy and Petrology*, 20, pp. 268-294.

- Nicholls, J. and Carmichael, I. S. E. (1969).** Peralkaline acid liquids: a petrological study. *Contributions to Mineralogy and Petrology*, 20, pp. 268-294.
- Nisbet, E. G., Deitrich, V. J. and Esenwein, A. (1979).** Routine trace element determination in silicate minerals and rocks by X-Ray Fluorescence. *Fortschr. Mineral*, 57(2), pp. 264-279.
- Olivo, G. R. and Williams-Jones, A. E. (1999).** Hydrothermal REE-rich eudialyte from the Pilansberg complex, South Africa. *Canadian Mineralogist*, 37, pp. 653-663.
- O'Nions, R.K., Hamilton, P.J. and Evensen, N.M. (1977).** Variations in (super 143) Nd/ (super 144) Nd and (super 87) Sr/ (super 86) Sr ratios in oceanic basalts. *Earth and Planetary Science Letters*, 34(1), pp. 13-22.
- Pandey, B. K., Gupta, J. N. and Lall, Y. (1986).** Whole rock and Rb–Sr isochron ages for the granites from Bihar mica belt of Hazaribagh, Bihar, India. *Indian Journal of Earth Sciences*, 12, pp. 157-162.
- Pandit, M. K., Sial, A. N., Sukumaran, G. B., Pimentel, M. M., Ramasamy, A. K. and Ferreira, V. P. (2002).** Depleted and enriched mantle sources for Paleo- and Neoproterozoic carbonatites of southern India: Sr, Nd, C-O isotopic and geochemical constraints, *Chemical Geology*, 189, pp. 69-89.
- Parthasarathy, R. and Sankar Das, M. (1976).** Thorium, uranium and lead contents of some Indian zircons and their ages. *Journal of Geological Society of India*, 17, pp. 262-271.
- Peiffert, C., Nguyen-Trung, C. and Cuney, M. (1996).** Uranium in granitic magmas: Part 2. Experimental determination of uranium solubility and fluid-melt partition coefficients in the uranium oxide-haplogranite-H₂O–NaX (X = Cl, F) system at 770°C, 2 kbar. *Geochimica et Cosmochimica Acta*, 60, pp. 1515–1529.
- Pell, J. and Höy, T. (1989).** Carbonatites in a continental margin environment – the Canadian Cordillera. In *Carbonatites: Genesis and Evolution* (K. Bell, ed.). Chapman & Hall, London, U.K. pp. 200-220.
- Perchuk, L. L. and Ryabchikov, I. D. (1968).** Mineral equilibria in the system nepheline - alkali feldspar – plagioclase and their petrological significance. *Journal of Petrology*, 9, pp. 123-167.
- Peytcheva, I., von Quadt, A., Georgiev, N., Ivanov, Zh., Heirich, C. A. and Frank, M. (2008, in press).** Combining trace-element compositions, U-Pb geochronology and Hf isotopes in zircons to unravel complex calcalkaline magma chambers in the Upper Cretaceous Srednogorie zone (Bulgaria). *Lithos*.
- Pupin, J. P. (1980).** Zircon and granite petrology. *Contribution to Mineralogy and Petrology*, 73, pp. 207-220.
- Rao, Y. J. and Murthy, I. S. N. (1974).** Nepheline as a Metasomatic Product. *American Mineralogist*, 59, pp. 690-693.

- Ray Barman, T. and Bishui, P. K. (1994).** Dating of Chotanagpur gneissic complex of eastern Indian Precambrian shield. *Record of Geological Survey of India*, 127 (pt. 2), pp. 25–27.
- Ray Barman, T., Bishui, P. K., Mukhopadhyay, K. and Ray, J. N. (1994).** Rb–Sr geochronology of the high grade rocks from Purulia, West Bengal, and Jamua-Dumka sector, Bihar. *Indian Minerals*, 48, pp. 45–46.
- Ray, J. S. and Pande, K. (1999).** Carbonatite alkaline magmatism associated with continental flood basalts at stratigraphic boundaries: cause for mass extinctions. *Geophysical Research Letter*, 26, pp. 1917-1920.
- Ray, J. S. and Pande, K. (2001).** ^{40}Ar - ^{39}Ar age of carbonatite-alkaline magmatism in Sung Valley, Meghalaya. *Indian Proceedings, Indian Academy of Science (Earth Planetary Science)* 110, pp. 185-190.
- Ray, K. K, Ghosh Roy, A. K. and Sengupta, S. (1996).** Acid volcanic rocks between the Dalma volcanic belt and the Chhotanagpur Gneissic Complex, East Singhbhum and Purulia districts of Bihar and West Bengal. *Indian Minerals*, 50, pp. 1-8.
- Rogers, J. J. W. (1996).** A history of continents in the past 3 billion years. *Journal of Geology*, 104, pp. 91-107.
- Romberger, S. B. (1984).** Transport and deposition of uranium in hydrothermal systems at temperatures up to 300°C: geological applications. In *Uranium Geochemistry, Mineralogy, Geology, Exploration and Resources* (DeVivo, B., Ippolito, F., Capaldi, G. & Simpson, P. R. Eds.). London: Institution of Mining and Metallurgy, pp. 12-17.
- Roy, A., Sarkar, A., Jeyakumar, S., Aggrawal, S. K. and Ebihara, M. (2002a).** Sm–Nd age and mantle characteristics of the Dhanjori volcanic rocks, Eastern India. *Geochemical Journal*, 36, 503-518.
- Roy, A., Sarkar, A., Jeyakumar, S., Aggrawal, S. K. and Ebihara, M. (2002b).** Mid-Proterozoic Plume-related thermal event in Eastern Indian Craton: evidence from trace elements, REE geochemistry and Sr–Nd isotope systematics of basic–ultrabasic intrusives from Dalma Volcanic Belt. *Gondwana Research*, 5, pp. 133-146.
- Rüdnick, R. L., McDonough, W. F. and Chappell, B. W. (1993).** Carbonatite metasomatism I northern Tanzanian mantle: petrographic and geochemical characteristics. *Earth and Planetary Science Letters*, 114, pp. 463-475.
- Saha, A. K. (1994).** Crustal evolution of Singhbhum-North Orissa, Eastern India. *Memoir Geol Society of India*, 27, pp. 341.
- Saha, A. K., Ray, S. L., Ghosh, S., Mukhopadhyay, K. and Dasgupta, D. (1984).** Studies in crustal evolution of the Singhbhum Orissa Iron Ore craton. *Monograph on Crustal evolution of parts of Indian Shield*. Indian Society of Earth Sciences, pp. 1-74.
- Samoylov, V. S, Gormasheva, G. S and Chernysheva, E. A. (1974).** Low-aluminum alkalic amphiboles of carbonatites. *Yearbook Institute of Geochemistry, Irkutsk*, pp. 189-193.

Samoylov, V. S. (1977). Karbonatity (fatsii i usloviya obrazovaniya). Nauka, Moscow (in Russian)

Samoylov, V. S. (1984). *Geochemistry of carbonatites*. Nauka Press, Moscow (in Russ.).

Samoylov, V. S. and Gormasheva, G. S. (1975). Alkali amphiboles of carbonatites and genetically related rocks. *Zapiski Vsesoyuznogo Mineralogicheskogo Obshchestva*, 104, pp. 145-159.

Sarkar, A. N. (1982). Precambrian Tectonic Evolution of Eastern India: A Model of Converging Microplates, *Tectonophysics*, 86, pp. 363-397.

Sarkar, A. N. (1988). Tectonic evolution of the Chhotanagpur plateau and the Gondwana basins in eastern India. In: D. Mukhopadhyay (ed), *Precambrian of the eastern Indian shield, Memoir 8*, geological Society of India, pp. 127-146.

Sarkar, S. C, Gupta, A. and Basu, A. (1992). North Singhbhum Proterozoic mobile belt, Eastern India: its character, evolution and metallogeny. In: *Sarkar SC, editor. Metallogeny related to Tectonics of the Proterozoic mobile belts*. New Delhi 7, Oxford & IBH, pp. 271-305.

Sarkar, S. N. (1968). Precambrian Stratigraphy and Geochronology of Peninsular India: a synopsis. *Dhanbad Pulications*, Dhanbad, pp. 1-33.

Sarkar, S. N. and Saha, A. K. (1962). A revision of the Precambrian stratigraphy and tectonics of Singhbhum and adjacent region. *Quaternary Journal of Geology*, Min Metall Soc India, 34, pp. 97-136.

Sarkar, S. N. and Saha, A. K. (1983). Structure and tectonics of the Singhbhum-Orissa Iron Ore Craton, eastern India. In: *Recent Researches in Geology: (Structure and tectonics of the Precambrian rocks)*, Hindusthan Publishing Corporation India, Delhi, 10, pp. 1-25.

Sarkar, S. N., Ghosh, D. and Lambert, R. J. (1986). Rb-Sr and lead isotopic studies on the soda granites from Mosaboni, Singhbhum Copper Belt, eastern India. *Indian Journal of Earth Sciences*, 13, pp. 101-116.

Schleicher, H., Kramm, U., Pernicka, E., Schidlowski, M., Schmidt, F., Subramanian, V., Todt, W. and Viladkar, S. G. (1998). Enriched Subcontinental Upper Mantle beneath Southern India: Evidence from Pb, Nd, Sr and C-O Isotopic Studies on Tamil Nadu Carbonatites. *Journal of Petrology*, 39, pp. 1765-1785.

Schleicher, H., Todt, W., Viladkar, S. G. and Schmidt, F. (1997). Pb/Pb age determinations on the Newania and Sevattur carbonatites of India: evidence for multi-stage histories, *Chemical Geology*, 140, pp. 261-273.

Schönenberger, J and Markl, G. (2008). The Magmatic and Fluid Evolution of the Motzfeldt Intrusion in Southy Greenland: Insights into the Formation of Agpaitic and Miaskitic Rocks. *Journal of Petrology*, 49, pp. 1549-1577.

- Scogings, A. J. and Forster, I. F. (1989).** Gneissose carbonatites in the Bull's Run complex, Natal. *South African Journal of Geology*, 92, pp. 1-10.
- Sengupta, S. and Mukhopadhyaya, P. K. (2000).** Sequence of Precambrian events in the eastern Indian craton. Proceedings Int Sem, Precambrian Crust in eastern and central India. *UNESCO-IUGS-IGCP 368*, Bhubaneswar 7, Geological Survey of India, pp. 49-56.
- Sengupta, S., Acharyya, S. K. and de Smith, J. B. (1997).** Geochemistry of Archaean volcanic rocks from Iron Ore Supergroup, Singhbhum, eastern India. *Proceedings of Indian Academy of Science, Earth Planetary Science*, 106, pp. 327-342.
- Sharma, M., Basu, A. R. and Ray, S. L. (1994).** Sm–Nd isotopic and geochemical study of the Archaean tonalite amphibolite association from the eastern Indian Craton. *Contribution to Mineralogy and Petrology*, 17, pp. 45-55.
- Singh, G. H., Suri Sastry, C., Tiwary, K. N., Shirke, V. G. and Chatterjee, B. D. (1977).** Status of exploration for atomic minerals in the Purulia district, West Bengal and future possibilities. *Journal of Minerals Metals and Fuels*, pp. 61-66.
- Singh, S. P. (1997).** Geochemistry of Acid volcanics of the Dalma Group, Singhbhum, Eastern India. *Journal of Geological Society of India*, 49, pp. 437-441.
- Singh, S. P. (1998).** Precambrian stratigraphy of Bihar. In: Paliwal BS, editor. *The Indian Precambrian*, Jodhpur, India 7 Scientific Publication, pp. 376-408.
- Sørensen, H. (1997).** The agpaitic rocks-an overview. *Mineralogical Magazine*, 61, pp. 485-498.
- Sørensen, H. (1974).** The Alkaline Rocks. John Wiley and Sons, New York.
- Speer, J. A. (1984).** Micas in igneous rocks. In Micas (S. W. Bailey, Ed.), *Reviews in Mineralogy*, 13, 299-356.
- Spencer, K. J. and Lindsley, D. H. (1981).** A solution model for coexisting iron titanium oxides. *American Mineralogist*, 66, pp. 1189-1201.
- Srivastava, R. K. and Sinha, A. K. (2004).** Early Cretaceous Sung Valley ultramafic-alkaline-carbonatite complex, Shillong Plateau, Northeastern India: petrological and genetic significance, *Mineralogy and Petrology*, 80, pp. 241-263.
- Srivastava, R., Heaman, L. M., Sinha, A. K. and Shihua, S. (2005).** Emplacement age and isotope geochemistry of Sung Valley alkaline-carbonatite complex, Shillong Plateau, northeastern India: implications for primary carbonate melt and genesis of the associated silicate rocks, *Lithos*, 81, pp. 33-54.
- Stacey, J. and Kramers, J. (1975).** Approximation of terrestrial lead isotope evolution by a two-stage model. *Earth and Planetary Science Letters*, 26, pp. 207-221.
- Stephenson, D. (1972).** Alkali clinopyroxenes from the nepheline syenites of the South Qôroq centre, south Greenland. *Lithos*, 5, pp. 187-201.

Streckeisen, A. (1980). Classification and nomenclature of volcanic rocks, lamprophyres, carbonatites and melilitic rocks. IUGS Subcommittee on the Systematics of Igneous Rocks. *Geologische Rundschau*, 69 pp. 194-207.

Strum, R. (2002). PX-NOM—an interactive spreadsheet program for the computation of pyroxene analyses derived from the electron microprobe. *Computer and Geosciences*, 28, pp. 473-483.

Subramaniam, A. P. and Parimoo, M. L. (1963). Fluorspar mineralization related to Deccan basalt volcanism at Ambadongar, Baroda district, India. *Nature*, 198, pp. 563-564.

Sukheswala, R. N. and Udas, G. R. (1963). Note on the carbonatite of Ambadongar and its economic potentialities. *Science and Cultivation*, 29, pp. 563-568.

Sun, S. S. and McDonough, W. F. (1989). Chemical and isotopic systematics of oceanic basalts: implications for mantle composition and processes. In: Saunders, A. D., Norry, M. J. (Eds.), *Magmatism in the Ocean Basins. Special Publication*, Geological Society of London, 42, pp. 313-345.

Tichomirowa, M., Grosche, G., Götze, J., Belyatsky, B. V., Savva, E. V, Keller, J., Todt, W. (2006). The mineral isotope composition of two Precambrian carbonatite complexes from the Kola Alkaline Province – Alteration versus primary magmatic signatures, *Lithos*, 91, pp. 229-249.

Tilley, C. E. (1957). Problems of alkali rock genesis. *Quaternary Journal of Geological Society of London*, 113, pp. 323-60.

Tilley, C. E., (1954). Nepheline-alkali feldspar parageneses. *American Journal of Science*, 252, pp. 65-75.

Treiman, A. H. and Essene, E. J. (1992). Composition of the fluid phase accompanying carbonatite magma: a critical examination –discussion. *American Mineralogist*, 77, pp. 663-665.

Tröger, W. E. (1969). *Optische Bestimmung der gesteinsbildenden Minerale. Teil 2. Auflage 2.* Published by: H. U. Bambauer, F. Taborszky and H. D. Trochim. E. Schweizerbart'sche Verlagsbuchhandlung Stuttgart, pp. 1-822.

Tuttle, O. F. and Gittins, J. (1966). Carbonatites. John Wiley & Sons, New York, N.Y.

Twyman, J. D. and Gittins, J. (1987). Alkalic carbonatite magmas: parental or derivative? In: Fitton, J. G., Upton, B. G. J. (Eds.), *Alkaline Igneous Rocks, Special Publication*, Geological Society of London, 30, pp. 85-94.

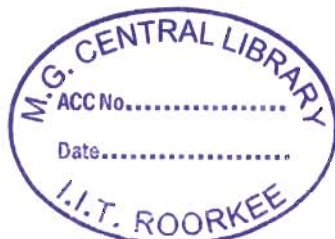
Tyler, R. C. and King, B. C. (1967). The pyroxenes of the alkaline igneous complexes of eastern Uganda. *Mineralogical Magazine*, 36, pp. 5-22.

Ussing, N. V. (1912). Geology of the country around Julianehaab, Greenland. *Meddr. GrOnland*, 38, pp. 1-426.

Vartiainen, H. and Woolley, A. R. (1976). The petrography, mineralogy and chemistry of the fenites of the Sokli carbonatite intrusion, Finland. *Geological Survey of Finland Bulletin*, 280.

- Veksler, I. V., Nielson, T. F. D and Sokolov, S. V. (1998).** Mineralogy of crystallized melt inclusions from Gardiner and Kovdor ultramafic alkaline complexes: implications for carbonatite genesis, *Journal of Petrology*, 39, pp. 2015-2031.
- Veksler, I.V., Petibon, C., Jenner, G. A., Dorfman, A. M. and Dingwell, D. B. (1998).** Trace element partitioning in immiscible silicate-carbonate liquid systems: an initial experimental study using a centrifuge autoclave. *Journal of Petrology*, 39, pp. 2095-2104.
- Venkatasubramanian, V. S. and Krishnan, R. S. (1960).** Radioactivity and geochronology of igneous and metamorphic rocks of the Precambrian Era of the Indian Peninsula. *Proceedings of National Institute of Science, Indian 26A, Supplementary II*, 89.
- Viladkar, D. G. and Subramanian, V. (1995).** Mineralogy and geochemistry of the carbonatite of the Sevathur and Samalpatti Complexes, Tamil Nadu. *Journal of the Geological Society of India*, 45, pp. 505-517.
- Vinogradov, A., Tugarinov, A., Zhykov, C., Stapanikova, N., Bibikova, E. and Khorre, K. (1964).** Geochronology of Indian Precambrian. *International Geological Congress Report, 22nd Session*, part 10, pp. 553-567.
- Von Quadt, A., Peytcheva, I., Kamenov, B., Fanger, L., Heinrich, C. and Frank, M. (2002).** The Elatsite porphyry copper deposit in the Panagyurishte ore district, Srednogie zone, Bulgaria: U-Pb zircon geochronology and isotope geochemical investigations of magmatism and ore genesis. In: Blundell, D., Neubauer, F., von Quadt, A. (Eds.), *The Timing and Location of Major Ore Deposits in an Evolving Orogen. Special Publications*, 204, Geological Society of London, pp. 119-135.
- Wallace, G. M., Whanlen, J. B. and Martin, R. F. (1990).** Agpaitic and miaskitic nepheline syenites of the McGerrigle Plutonic Complex, Gaspé, Quebec: An unusual petrological association. *Canadian Mineralogist*, 28, pp. 251-266.
- Wallace, M. E and Green D. H. (1988).** An experimental determination of primary carbonatite magma composition, *Nature*, 335, pp. 343-346.
- Wasserburg, G. J., Albee, A. L. And Lanphere, M. A. (1964).** Migration of Radiogenic Strontium during Metamorphism. *Journal of Geophysical Research*, 69 (20), pp. 4395-4401.
- Welman, T. R. (1970).** The stability of sodalite in a synthetic syenite plus aqueous chloride fluid system. *Journal of Petrology*, 11, pp. 49-71.
- Wilkinson, J. F. G. (1965).** Some feldspars, nephelines and analcimes from the Square Top intrusion, Nundle, N.S.W. *Journal of Petrology*, 6, pp. 420-444.
- Wilkinson, J. F. G. and Hensel, H. D. (1994).** Nephelines and analcimes in some alkaline igneous rocks. *Contribution to Mineralogy and Petrology*, 118, pp. 79-91.

- Wones, D. R. and Eguster, H. P. (1965).** Stability of biotite: experiment, theory and application. *American Mineralogist*, 50, pp. 1228-1272.
- Wooley, A. R. and Kempe, D. R. C. (1989).** Carbonatites: nomenclature, average chemical compositions, and element distribution. In: Bell, K. (Ed.), *Carbonatites: Genesis and Evolution*. Unwin Hyman, London: 1-14.
- Woolley, A. R. (1982).** A discussion of carbonatite evolution and nomenclature, and the generation of sodic and potassic fenites. *Mineralogical Magazine*, 46, pp. 13-7.
- Woolley, A. R. and Church, A. A. (2005).** Extrusive carbonatites: A brief review, *Lithos*, 85, pp. 1-14.
- Woolley, A. R. and Kjarsgaard, B. A. (2008).** Paragenetic types of carbonatite as indicated by the diversity and relative abundances of associated silicate rocks: evidence from a global database. *The Canadian Mineralogist*, 46, pp. 741-752.
- Woolley, A. R. and Platt, R. G. (1986).** The mineralogy of nepheline syenite complexes from the northern part of the Chilwa Province, Malawi. *Mineralogical Magazine*, 50, pp. 597-610.
- Woolley, A. R., Platt, R. G. and Eby, G. N. (1996).** Relatively aluminous alkali pyroxenes in nepheline syenites from Malawi: mineralogical response to metamorphism/metasomatism in alkaline rocks. *Canadian Mineralogist*, 34, pp. 423-434.
- Wyllie, P. J. and Huang, W. L. (1975).** Peridotite, kimberlite and carbonatite explained in the system CaO-MgO-SiO₂-CO₂, *Geology*, 3, pp. 621-624.
- Wyllie, P. J. and Lee, W.-J. (1998).** Model system controls on conditions for formation of magnesiocarbonatite and calciocarbonatite magmas from the mantle, *Journal of Petrology*, 39, pp. 1885-1893.
- Xu, Ch., Huang, Zh., Liu, C., Qi, L., Li, W., and Guan, T. (2003).** Geochemistry of carbonatites in Maoniuping REE deposit, Sichuan Province, China. *Science in China (Series D)*, 46, pp. 246-256.
- Yagi, K. (1953).** Petrochemical studies of the alkalic rocks of the Morotu district, Sakhalin. *Bulletin of Geological Society of America*, 64, pp. 769-810.
- Yusuf, S. and Saraswat, A. C. (1977).** A preliminary note on the carbonatites in Wah Sung Valley of Jaintia Hills district, Meghalaya. *Current Science*, 46, pp. 703-704.
- Zindler, A. and Hart, S. (1986).** Chemical geodynamics. *Annual Reviews, Earth and Planetary Science*, 14, 493-571.



ANSWER TO THE QUERIES OF EXAMINER

CHAPTER 1 & 2

Found satisfactory by the examiner and no specific change is suggested

CHAPTER 3

- (a) Textural relationships between the constituting minerals: necessary changes have been made in the respective sections.
- (b) The textural relationship between the amphibole and other constituting minerals: required explanations are added in the respective section.
- (c) Amphibole calculation is done manually. No software is used for the same. However as far as calculation given by Leake et al. (1997) is concerned the calculation of these amphiboles have rechecked and found to be correct. As per IMA classification given by Leake et al. (1997), in magnesio-arfvedsonite Na_B should be greater than 1.5 ($Na_B > 1.50$) where as in all the amphiboles of carbonatite (as well as alkali-pyroxenite) $Na_B < 1.50$ and do not satisfy the criteria to become a sodic amphibole of magnesio-arfvedsonite type.
- (d) The problem with Nb and U concentration is due to extreme variation in concentration of these elements within analyzed samples. Two samples give Nb and U concentration ~ 120 ppm and ~ 45 ppm and other two the Nb and U concentration is $\sim 10-15$ ppm and $\sim 4-7$ ppm respectively. The high concentration of Nb and U in two samples of carbonatite is explained by possible presence of Nb-U bearing mineral phase such as pyrochlore. But no pyrochlore grain could be identified during petrographic study. Possible reason may be extreme fine size and highly dispersed distribution of this phase. The presence of pyrochlore is not conclusive, it is speculative.
- (e) All the pyroxenes of the alkali-pyroxenite have recalculated as per suggestion by the examiner and the whole section is re-written.
- (f) This part has been completely revised following the suggestions given by the examiner. The suggested literatures have been consulted before re-phrasing this part of the thesis. New EPMA analysis of few critical mineral phases have also been carried out and incorporated.
- (g) Suggested changes have been made in the Tables of Chapter 3.

CHAPTER 4

- (a) Information about the error limits of the XRF and LA-ICP MS methods have been given as per suggestion of the examiner.
- (b) The necessary explanation is given an earlier part of the reply [Chapter 3(b)].
- (c) Geochemical and isotopic work presented in the thesis were carried out at ETH Zurich during my stay at ETH Zurich under ESKAS Fellowship programme for 12 months, including 3 months for language learning course. The major aim of the work was to find out the age of the Syenites and Carbonatite. To achieve the same zircon were separated from all the studied rocks and subsequently geochemistry were done for those samples. Unfortunately zircon could not be yielded from the strongly banded syenite gneiss and further geochemical work was not pursued. This work could not be taken up at the end of the tenure also due to lack of available time and funding. It is true that this unit of the gneiss package should not have been excluded. I honestly feel further work is needed on this particular unit of gneiss. To bridge this gap, major emphasis is given on the petrography of this rock while re-writing the thesis.
- (d) Necessary changes have been made in the relevant section of the revised thesis.
- (e) The 'spider diagrams' have been used for mainly for comparison of rocks and some critical minerals. In the revised version of the thesis apatite data were more methodically and properly interpreted in order to understand its formation in relation to the change of the alkalinity during autometasomatism of the nepheline syenites (Section 6.2.3). A more rigorous work on the apatites of the carbonatite and alkali-pyroxenite is also incorporated in the new version of the thesis (Section 6.1.3).

CHAPTER 5 and CHAPTER 6

All the recommended suggestions and corrections have been incorporated in these two chapters. Interpretation of the isotopic data is carried out as per suggestions of the examiner in view of the post magmatic deformational activity related to metamorphism and metasomatism. A rigorous revision in interpreting the zircon data is done and incorporated in the Chapter 5.

Unfortunately no facility is available for U-Pb and Th-Pb systematics in India. Hence, this part can not be included in the revised version of the thesis.

Chapter 6 is completely re-written and all the genetic speculations are omitted. This chapter has been divided into two parts: carbonatite-pyroxenite association and nepheline syenite(s). As mentioned earlier a major emphasis is given on the petrography and mineralogy of the nepheline syenites and this chapter is given a completely new shape with more recent literature reviews, comparison with respect to other reported nepheline syenites world wide and most importantly response of the syenite in relation to the post magmatic alterations processes: metamorphism and metasomatism.

CHAPTER 7

In view of the above modifications in Chapter 3-6, the Chapter 7 is re-written keeping in view the suggestions made by the examiner.

I personally thank the examiner for his critical examination of the earlier version of the thesis. I tried my best to follow his suggestions to improve the quality of the thesis.